ACS SYMPOSIUM SERIES 1051

# Advances in Silicones and Silicone-Modified Materials

EDITED BY

Stephen J. Clarson, Michael J. Owen,
Steven D. Smith, and Mark E. Van Dyke

Downloaded by 89.163.35.42 on June 23, 2012 | http://pubs.acs.org
Publication Date (Web): November 9, 2010 | doi: 10.1021/bk-2010-1051.fw001

# Advances in Silicones and Silicone-Modified Materials

In Advances in Silicones and Silicone-Modified Materials; Clarson, S., et al.;
ACS Symposium Series; American Chemical Society: Washington, DC, 2010.

Downloaded by 89.163.35.42 on June 23, 2012 | http://pubs.acs.org
Publication Date (Web): November 9, 2010 | doi: 10.1021/bk-2010-1051.fw001

Downloaded by 89.163.35.42 on June 23, 2012 | http://pubs.acs.org
Publication Date (Web): November 9, 2010 | doi: 10.1021/bk-2010-1051.fw001

ACS SYMPOSIUM SERIES **1051**

# Advances in Silicones and Silicone-Modified Materials

**Stephen J. Clarson**, Editor
*Department of Chemical and Materials Engineering*
*University of Cincinnati*

**Michael J. Owen**, Editor
*Michigan Molecular Institute*

**Steven D. Smith**, Editor
*Procter & Gamble*

**Mark E. Van Dyke**, Editor
*Wake Forest University School of Medicine*
*Wake Forest Institute for Regenerative Medicine*

**Sponsored by the**
**ACS Division of Polymer Chemistry, Inc.**

American Chemical Society, Washington, DC

Downloaded by 89.163.35.42 on June 23, 2012 | http://pubs.acs.org
Publication Date (Web): November 9, 2010 | doi: 10.1021/bk-2010-1051.fw001

**Library of Congress Cataloging-in-Publication Data**

Advances in silicones and silicone-modified materials / Stephen J. Clarson, editor ... [et al.].
p. cm. -- (ACS symposium series ; 1051)
"Sponsored by the ACS Division of Polymer Chemistry."
Includes bibliographical references and index.
ISBN 978-0-8412-2559-6 (alk. paper)
1. Silicones--Congresses. I. Clarson, Stephen J.
QD383.S54A38 2010
668.4'227--dc22
2010040807

The paper used in this publication meets the minimum requirements of American National Standard for Information Sciences—Permanence of Paper for Printed Library Materials, ANSI Z39.48n1984.

Copyright © 2010 American Chemical Society

Distributed by Oxford University Press

All Rights Reserved. Reprographic copying beyond that permitted by Sections 107 or 108 of the U.S. Copyright Act is allowed for internal use only, provided that a per-chapter fee of $40.25 plus $0.75 per page is paid to the Copyright Clearance Center, Inc., 222 Rosewood Drive, Danvers, MA 01923, USA. Republication or reproduction for sale of pages in this book is permitted only under license from ACS. Direct these and other permission requests to ACS Copyright Office, Publications Division, 1155 16th Street, N.W., Washington, DC 20036.

The citation of trade names and/or names of manufacturers in this publication is not to be construed as an endorsement or as approval by ACS of the commercial products or services referenced herein; nor should the mere reference herein to any drawing, specification, chemical process, or other data be regarded as a license or as a conveyance of any right or permission to the holder, reader, or any other person or corporation, to manufacture, reproduce, use, or sell any patented invention or copyrighted work that may in any way be related thereto. Registered names, trademarks, etc., used in this publication, even without specific indication thereof, are not to be considered unprotected by law.

PRINTED IN THE UNITED STATES OF AMERICA

Downloaded by 89.163.35.42 on June 23, 2012 | http://pubs.acs.org
Publication Date (Web): November 9, 2010 | doi: 10.1021/bk-2010-1051.fw001

# Foreword

The ACS Symposium Series was first published in 1974 to provide a mechanism for publishing symposia quickly in book form. The purpose of the series is to publish timely, comprehensive books developed from the ACS sponsored symposia based on current scientific research. Occasionally, books are developed from symposia sponsored by other organizations when the topic is of keen interest to the chemistry audience.

Before agreeing to publish a book, the proposed table of contents is reviewed for appropriate and comprehensive coverage and for interest to the audience. Some papers may be excluded to better focus the book; others may be added to provide comprehensiveness. When appropriate, overview or introductory chapters are added. Drafts of chapters are peer-reviewed prior to final acceptance or rejection, and manuscripts are prepared in camera-ready format.

As a rule, only original research papers and original review papers are included in the volumes. Verbatim reproductions of previous published papers are not accepted.

**ACS Books Department**

Downloaded by 89.163.35.42 on June 23, 2012 | http://pubs.acs.org
Publication Date (Web): November 9, 2010 | doi: 10.1021/bk-2010-1051.pr001

# Preface

The fourth *Silicones and Silicone-Modified Materials* symposium was held September 10 - 14, 2006 at the American Chemical Society (ACS) National Meeting in San Francisco, California. The three full-day symposium consisted of 44 oral presentations and an evening poster session of 20 presentations. The summaries of the contributions to the symposium can be found in Polymer Preprints, Volume 47, Number 2, 2006. This book has contributions from the symposium and also some invited chapters in the same overall subject area as the symposium.

Although I am usually the one that comes up with names and titles, our chosen title this time was suggested by Mike Owen. The cover is again based on an original computer simulation carried out at the University of Cincinnati by David Rigby and Stephen Clarson. It depicts a low energy conformation of the $D_{11}$ dimethylsiloxane ring and the image was photographed from the Silicon Graphics monitor by our good friend and colleague Jay Yocis. This volume was acquired and kindly moved towards publication by Tim Marney, Bob Hauserman, Sherry Weisgarber and Pamela Kame of ACS Books.

The three books from our earlier *Silicones and Silicone-Modified Materials* symposia in Dallas (1998), San Diego (2001) and Anaheim (2004) are, respectively: Silicones and Silicone-Modified Materials: edited by S. J. Clarson, J. J. Fitzgerald, M. J. Owen and S. D. Smith; ACS Symposium Series 729; American Chemical Society: Washington, D. C.; ISBN 0-8412-3613-5, Synthesis and Properties of Silicones and Silicone-Modified Materials, edited by S. J. Clarson, J. J. Fitzgerald, M. J. Owen, S. D. Smith and M. E. Van Dyke; ACS Symposium Series 838; American Chemical Society: Washington, D. C.; ISBN 0-8412-3804-9 and Science and Technology of Silicones and Silicone-Modified Materials, edited by S. J. Clarson, J. J. Fitzgerald, M. J. Owen, S. D. Smith and M. E. Van Dyke; ACS Symposium Series 964; American Chemical Society: Washington, D. C.; ISBN 978-0-8412-3943-2. Fortunately, the American Chemical Society and Oxford University Press have kept these books in press for all of us to enjoy.

From the American Chemical Society Division of Polymer Chemistry (POLY) we thank President Kathleen Havelka, Program Chair Christine Landry-Coltrain and Treasurer Rigoberto Advincula for their invaluable help and assistance. We also thank Procter and Gamble and the American Chemical Society for kindly providing financial support and thus making it possible for many of our presenters to be able to attend the San Francisco symposium. We look forward to seeing you all again for *Silicones and Silicone-Modified Materials VI* in Philadelphia, USA in 2012.

In Advances in Silicones and Silicone-Modified Materials; Clarson, S., et al.;
ACS Symposium Series; American Chemical Society: Washington, DC, 2010.

**Stephen J. Clarson**
BA DPhil FRSC CChem

Professor of Chemical and Materials Engineering
550 Engineering Research Center
University of Cincinnati
Cincinnati, OH 45221-0012, USA
513-556-5430 (telephone)
Stephen.Clarson@UC.Edu (e-mail)

Downloaded by 89.163.35.42 on June 23, 2012 | http://pubs.acs.org
Publication Date (Web): November 9, 2010 | doi: 10.1021/bk-2010-1051.pr001

In Advances in Silicones and Silicone-Modified Materials; Clarson, S., et al.;
ACS Symposium Series; American Chemical Society: Washington, DC, 2010.

# Dedication

This book is dedicated to our spouses or “better halves”: Marie, Christine, Bonnie, and LoriAnne who kindly “tolerate” our tendency to visit distant locations around the globe to engage our colleagues, friends and collaborators in discussions about all things related to the fabulous element silicon.

Downloaded by 89.163.35.42 on June 23, 2012 | http://pubs.acs.org
Publication Date (Web): November 9, 2010 | doi: 10.1021/bk-2010-1051.pr002

In Advances in Silicones and Silicone-Modified Materials; Clarson, S., et al.;
ACS Symposium Series; American Chemical Society: Washington, DC, 2010.

Downloaded by 89.163.35.42 on June 23, 2012 | http://pubs.acs.org
Publication Date (Web): November 9, 2010 | doi: 10.1021/bk-2010-1051.ch001

## Chapter 1

# Advanced Materials Containing the Siloxane Bond

**Stephen J. Clarson**[*]

**Department of Chemical and Materials Engineering and the Polymer Research Centre, University of Cincinnati, Cincinnati, OH 45221-0012, USA**
**[*]E-mail: Stephen.Clarson@UC.Edu**

Silicon, silica and silicones are all related and each of them have important but separate technological roles to play for mankind in this millennium. All three have the element silicon (Si) in common but they have unique and distinctive chemistries, properties and applications. This overview describes some of the themes that continue to attract the attention of those of us with an interest in advanced materials which are based on the siloxane bond (Si-O). Materials based on the siloxane bond have been the main theme of the various ACS 'Silicones and Silicone-Modified Materials Symposia' and the resulting books that have been our pleasure to assemble from them. The siloxane bond is therefore the common factor that threads through this overview.

## Introduction

Silicon and oxygen are highly abundant, and it has been reported that together they make up between 74 and 78% of the Earth's crust (*1*, *2*). The silica and silicates on Earth are slowly dissolving into water and one therefore finds silicon in the form of silicic acid $Si(OH)_4$ both in freshwater and in seawater. Paasche has stated that silicon concentrations in the oceans are generally lower than in many freshwater environments (*3*). Seawater has been reported to contain 3-150μM of dissolved silicon (*4*). For surface water the concentration is often below 3 μM (*5*). Each and every day organisms such as diatoms actively uptake 'silicon' in vast quantities and then bioprocess it into useful biosilica structures such as species specific exoskeletans or frustules. After a diatom dies, the frustule settles

In Advances in Silicones and Silicone-Modified Materials; Clarson, S., et al.;
ACS Symposium Series; American Chemical Society: Washington, DC, 2010.

Downloaded by 89.163.35.42 on June 23, 2012 | http://pubs.acs.org
Publication Date (Web): November 9, 2010 | doi: 10.1021/bk-2010-1051.ch001

to the bottom of a pond, lake, river or ocean in the form of a siliceous sediment. Such sediments are therefore useful indicators of the environments in which these organisms have lived. In this materials cycle ‘silicon’ is therefore very much a ‘green’ or renewable resource (*6*, *7*).

Silicon is one of the required trace elements for human life. It has been estimated that we ingest 30mg silicon per day, with 60% coming from cereals and 20% from water and drinks. In human blood 138 μmol/l of silicate has been reported (*8*). The combined amount of silicon in the human body has been calculated to be around 5 to 10 grams. While the exact role of silicon in the human body is still unknown, it is thought that the interactions between aluminum and silicon are of vital importance (*9–11*). For example, restrictions of the absorption of aluminum in the human gut by silicic acid has been experimentally demonstrated (*12*).

As stated above silica and silicates are widely abundant materials. Silica is well known to have three common polymorphs with α-quartz being the most stable. Amorphous silica exists in many forms including vitreous silica, silica gel, diatomaceous silica, precipitated silica and colloidal silica. These silica forms find a wide variety of applications in personal care products, chromatographic media and elastomer reinforcing agents.

In terms of commercial polymeric materials, the most successful polymers having an inorganic backbone are the silicones. As with silica, the siloxane bond Si-O is the basis of these polymeric materials. Silicones have annual sales of around $10 billion and these have steadily grown to this level since the commercialization of silicones in the 1940’s (*13–15*). Despite many new developments over past several decades, the workhorse of the silicones industry remains poly(dimethylsiloxane) (PDMS).

$$\textbf{-[(CH}_3\textbf{)}_2\textbf{SiO]}_y\textbf{-}$$

Silicones may have various physical forms such as fluids, gels, elastomers and resins and these will be discussed below.

## Nomenclature

An overview of silicone nomenclature has been presented elsewhere by Teague (*16*). It was noted in the Macromolecular Nomenclature Note that the various CAS databases do not use the M (monofunctional), D (difunctional), T (trifunctional) and Q (tetrafunctional) notation that is widely accepted in the silicones community. Thus a trimethylsilyl terminated linear chain with four dimethylsiloxane units

$$\textbf{(CH}_3\textbf{)}_3\textbf{SiO-[(CH}_3\textbf{)}_2\textbf{SiO]}_4\textbf{-Si(CH}_3\textbf{)}_3$$

is designated $MD_4M$ and octamethylcyclotetrasiloxane, which is the most common cyclic silicone monomer, is denoted $D_4$.

## Silicone Homopolymers

The ring-opening polymerization of octamethylcyclotetrasiloxane ($D_4$) is readily achieved by acid or base catalysis. If one wishes to have non-functional chains then termination by trimethylchlorosilane leads to $MD_yM$ chains. These are the basis of the silicone fluid products described below. If one wishes to have functional chains then the growing chains can then be terminated with a source of protons (water or acid) to give α,ω-silanol terminated materials. The end-functional silicone chains can then act as network precursor chains and they can be crosslinked using a variety of crosslinking agents - a common example being tetraethoxysilane (TEOS). These components are the condensation cured to give elastomeric materials. These functional precursor chains are widely used in products such as liquid gaskets or sealants. In academic laboratories they can yield "model networks" of highly controlled structure.

## Silicone Copolymers

High molar mass silicones typically do not mix well with other high molar mass silicones nor indeed do they mix with other organic polymers. There are just a few studies of siloxane-siloxane blends reported in the literature. One system that was investigated by Clarson and Kuo was binary blends of poly(dimethylsiloxane) with poly(methylphenylsiloxane) (*17–20*). This system was studied in terms of molar mass, composition, type of end-group and cyclic content. Lower critical temperature solution (LCST) behavior was seen for the various PDMS–PMPS blends.

The various low molar mass cyclic silicone monomers are often miscible and hence there are a wide variety of copolymers that are available wherein low molar mass cyclic siloxanes having different substituent groups can be copolymerized into chains (*21*). A good example of this is the incorporation of vinyl functionalities as pendent groups when methylvinylsiloxane rings are copolymerized with dimethylsiloxane rings. Such vinyl functional systems can then be easily crosslinked using either peroxide cure or hydrosilation cure chemistries (see below).

## Architecture and Topology of Silicones

Silicones have been made in most of the macromolecular architectures and topological structures. Linear polymers and network polymers dominate the silicone product market in the form of fluids, gels, elastomers and resins. Some of their properties will be reviewed below. Other silicone systems include cyclics, dendrimers, branches, stars and brushes. In terms of more complex topologies, silicone rings have been threaded onto network chains. The catenanes and rotaxanes remains largely wide open for development for silicones.

Downloaded by 89.163.35.42 on June 23, 2012 | http://pubs.acs.org
Publication Date (Web): November 9, 2010 | doi: 10.1021/bk-2010-1051.ch001

Downloaded by 89.163.35.42 on June 23, 2012 | http://pubs.acs.org
Publication Date (Web): November 9, 2010 | doi: 10.1021/bk-2010-1051.ch001

## Silicone Fluids

Broadly speaking, silicone fluids are either non-functional, as typified by the linear $MD_yM$ materials, or functional. The non-functional fluids have properties that depend on their molar masses. Thus bulk properties such as density and glass transition temperatures asymptote with molar mass, whereas viscosity increases with molar mass and even more markedly so above the critical entanglement molecular weight. Silicone fluids have many properties that show a much lower temperature dependence than organic (carbon backbone) chains.

PDMS fluids have excellent thermal properties with a glass transition temperature around -120°C, a melting temperature of around -40°C and an onset of thermally induced bond rearrangements about 350°C. Thus PDMS has the one of the widest working temperature ranges of the commercial polymers.

## Silicone Elastomers

One can use peroxide, gamma or e-beam methods to randomly link together silicone chains that are either functional or non-functional. Using condensation cure chemistry one can link silanol groups to crosslinking agents such as TEOS and thus use the molar mass of the precursor chains to control the crosslink density. The familiar room temperature vulcanization (RTV) silicones are typically single component cure formulations that involve hydrolysis and condensation reactions of acetoxy functional silicones.

Hydrosilation reactions involve the following addition reaction

$$\mathbf{Si\text{-}CH{=}CH_2 \ + \ H\text{-}Si}$$

are catalyzed by a wide variety of platinum species. Commercial formulations are typically stabilized as two components for a long shelf life at room temperature and then the two liquid precursor components are mixed prior to carrying out curing at elevated temperatures to form silicone elastomers.

High extents of cure are seen for commercial silicone elastomers and low sol fractions (extractable materials) are seen. As the mechanical properties are often somewhat lower than some of the organic elastomers, it is common to see silicones highly filled by mechanically blending in silica ($SiO_2$) and titania ($TiO_2$) prior to cure. Silicone elastomers exhibit rubbery behaviour and they are hydrophobic but oleophilic (they are seen to swell in solvents such as toluene at room temperature).

## Silicone Gels

Silicones are able to form hydrophobic gels having a wide range of properties that depend on the composition, extent of cure chemistry and processing parameters. For example, linear non-functional PDMS can be incorporated into a network formulation prior to cure and the material remains single phase. After cure or partial cure the linear non-functional silicone remains within the silicone network but is unattached to the silicone network by covalent bonds. Addition of $MD_yM$ fluid is one example of how one can then vary the composition of the silicone gel to control the final material properties.

## Silicone Resins

Using a combination of T and Q functional silicones and/or silanes one can prepare a wide variety of silicone resins by varying the composition and extent of cure. Such materials have resin like character due to being highly crosslinked species. One major application of silicone resins is as tough and durable high performance coatings.

## Silicone-Modified Organic Systems

Downloaded by 89.163.35.42 on June 23, 2012 | http://pubs.acs.org
Publication Date (Web): November 9, 2010 | doi: 10.1021/bk-2010-1051.ch001

Silicones have been copolymerized with organic monomers in many different chemistries and structures. Segmented, block, graft, and dendritic copolymers are among the many examples that have been reported in the literature.

In terms of block copolymers, growing anions can typically initiate ring-opening polymerization of strained silicone rings (such as $D_3$). Thus one can prepare diblocks of highly controlled molar mass and low polydispersity by the living anionic polymerization of styrene which can undergo a change of mechanism over to a ring-opening polymerization for the silicone (*22*). These resulting polymeric materials are multiphase due to the differences in solubility parameter of the two blocks and associated chi parameter effects. Another feature of such silicone containing diblock copolymers is that they show marked surface segregation of the silicone to surfaces and interfaces when blended into the parent organic homopolymer due to the large differences in surface energies of the respective blocks. Such segregation effects are useful for wetting, friction, flammability and mold release properties.

## Silicone-Modified Inorganic Systems

One can approach silicone-modified inorganic systems from either end of the composition range. Thus silicones can be incorporated into ceramic systems to improve toughness. On the other hand inorganic fillers can be incorporated in silicone systems to improve modulus and tear strength. The most common filler for silicones is silica ($SiO_2$), although other fillers are used such at titania ($TiO_2$) and calcium carbonate ($CaCO_3$). For some medical applications it is desirable to be able to image the silicone in the body and hence barium compounds can be incorporated for high contrast with X-Rays.

## Polyhedral Oligomeric Silsesquioxanes POSS

The nanoscale hybrid nature of polyhedral oligomeric silsesquioxanes POSS has attracted much scientific and technological interest (*23*, *24*). When incorporated or copolymerized into organic polymer systems then marked improvements in mechanical, thermal and dielectric properties have been reported. Trisilanol-POSS derivatives show novel properties based on surface activity. Indeed trisilanolphenyl-POSS forms Langmuir-Blodgett multilayer films by Y-type deposition. Mabry and coworkers have reported that a fluorinated POSS compound $FD_8T_8$ is the most hydrophobic lowest surface tension crystalline substance reported to date with a water contact angle of 154°.

Downloaded by 89.163.35.42 on June 23, 2012 | http://pubs.acs.org
Publication Date (Web): November 9, 2010 | doi: 10.1021/bk-2010-1051.ch001

## Silica, Biosilica and Bioinspired Silica

Fumed silica and precipitated silica are widely used in the commercial applications of silicones. To cite two examples, incorporating silica into elastomers improves their mechanical properties and adsorption of silicones onto silica supports give excellent separation media for gas chromatography.

As stated above, Nature also bioprocesses ‘silicon’ and we are beginning to understand the mechanisms by which ‘silicon’ is transported across cell membranes and is then built into elaborate and hierarchically controlled silica structures within organisms such as diatoms, sponges and grasses.

The fact that silica can be chemically dissolved by acid or base treatments, has allowed for the isolation of the ‘organic matrix’ from these complex biosilica structures which are organic-inorganic hybrids. The biomacromolecles isolated from the ‘organic matrix’ to date have included the silacateins and silaffins. When the protein molecules are then exposed to silica precursors *in vitro*, silica precipitation is seen from aqueous buffered solutions.

Knowledge from the behaviour of these biomacromolecules has led to bioinspired materials whereby natural, genetically generated and synthetic macromolecules have been utilized to generate new silica structures and forms. Furthermore the bioinpsired routes can be carried out under the mild conditions that one sees ‘silicon’ bioprocessed in Nature.

## Biocatalytic Routes to Silicones

Another area that is crying out for development is enzymatic routes to silicones and silicone copolymers. Enzyme mediated chemistries that are of interest currently include the use of various hydrolase enzymes to prepare segmented and block silicone copolymers linked by ester, amide and carbonate groups. So far enzymatic routes to aliphatic silicone polyesters (*25*), aromatic silicone polyesters (*26*), silicone polylactones (*27*), silicone polyethers (*28*), silicone polyamides (*29*) and silicone polysaccharides (*30*) have been reported in the literature.

## Future Perspectives

We have seen tremendous developments in silicon-based materials over the past century and yet clearly there is still much potential for new advanced materials based on the siloaxne bond. With the high abundance of silicon and oxygen on Earth, we are probably working with the most sustainable and "green" materials if we adopt the correct materials chemistry, materials processing, materials recovery and materials reuse strategies.

## References

1. Phillips, C. S. G.; Williams, R. J. P. *Inorganic Chemistry*; Clarendon Press: Oxford, 1965; Volume I, p 476.
2. Thomas, J. *Silicon*; Marshall Cavendish Books: New York, 2002.
3. Paasche, E. In *The Physiological Ecology of Plankton*; Morris, I., Ed.; University of California Press: Berkeley, CA, 1980; pp 262−269.
4. Kennish, M. J. *Practical Handbook of Marine Science*; CRC Press: Boca Raton, FL, 1994.
5. Nelson, D. M.; Treguer, P.; Brezinski, M. A.; Leynaert, A.; Queguiner, B. *Global Biochem. Cycles* **1995**, *9*, 359–372.
6. Leng, M. J.; Swann, G. E. A.; Hodson, M. J.; Tyler, J. J.; Patwardhan, S. V.; Sloane, H. J. *Silicon* **2009**, *1* (2), 65–75.
7. Struyf, E.; Van Damme, P.; Meire, P.; Conley, D. J. *Silicon* **2010**, *1* (4), 207–213.
8. *Wissenschaftliche Tabellan Giegy*; CIBA-Geigy Ltd.: Basel, Switzerland, 1979; Volume II, pp 1−331.
9. Birchall, J. D. *Chem. Soc. Rev.* **1995**, *24*, 351.
10. Perry, C. C.; Keeling-Tucker, T. *J. Inorg. Biochem.* **1998**, *69*, 181.
11. Birchall, J. D.; Exley, C.; Chappell, J. S.; Phillips, M. J. *Nature* **1989**, *338*, 146.
12. Edwardson, J. A.; Moore, D. B.; Ferrier, I. N.; Lilley, J. S.; Newton, G. W. A.; Barker, J.; Templar, J.; Day, J. P. *Lancet* **1994**, *342*, 211.
13. Liebhafsky, H. A. *Silicones Under the Monogram*; Wiley-Interscience: New York, 1978.
14. Warrick, E. L. *Forty Years of Firsts: The Recollections of a Dow Corning Pioneer*; McGraw Hill: New York, 1990.
15. *Siloxane Polymers*; Clarson, S. J., Semlyen, J. A., Eds.; Prentice Hall: Englewoods Cliffs, NJ, 1993.
16. Teague, S. J. *Polym. Prepr.* **2001**, *42* (1), xviii–xxiii.
17. Kuo, C. M.; Clarson, S. J. *Macromolecules* **1992**, *2*, 2192–2195.
18. Kuo, C. M.; Clarson, S. J. *Eur. Polym. J.* **1993**, *29*, 661–664.
19. Kuo, C. M.; Clarson, S. J.; Semlyen, J. A. *Polymer* **1994**, *35*, 4623–4626.
20. Kuo, C. M.; Clarson, S. J. *Polymer* **2000**, *41*, 5993–6002.
21. Kennan, J. J. In *Siloxane Polymers*; Clarson, S. J., Semlyen, J. A., Eds.; Prentice Hall: Englewoods Cliffs, NJ, 1993; pp 72−134.
22. Selby, C. E.; Stuart, J. O.; Clarson, S. J.; Smith, S. D.; Sabata, A.; van Ooij, W. J.; Cave, N. G. *J. Inorg. Organomet. Polym.* **1994**, *4* (1), 85.
23. Esker, A. R.; Vastine, B. A.; Deng, J.; Ferguson, M. K.; Morris, J. R.; Satija, S. K.; Viers, B. D. *Polym. Prepr.* **2004**, *45* (1), 644–645.
24. Mabry, J. M.; Vij, A.; Viers, B. D.; Grabow, W. W.; Marchant. D.; Iacona, S. T.; Ruth P. N.; Vij, I. In *Science and Technology of Silicones and Silicone-Modified Materials*; Clarson, S. J., Fitzgerald, J. J., Owen, M. J., Smith, S.

Downloaded by 89.163.35.42 on June 23, 2012 | http://pubs.acs.org
Publication Date (Web): November 9, 2010 | doi: 10.1021/bk-2010-1051.ch001

D., Van Dyke, M. A., Eds.; ACS Symposium Series 964; American Chemical Society: Washington, DC, 2007; pp 290−300.

25. Poojari, Y.; Palsule, A. S.; Cai, M.; Clarson, S. J.; Gross, R. A. *Eur. Poly. J.* **2008**, *44*, 4139–4145.
26. Poojari, Y.; Clarson, S. J. *Chem. Commun.* **2009**, 6834–6835.
27. Poojari, Y.; Clarson, S. J. *Silicon* **2009**, *1* (3), 165–172.
28. Poojari, Y.; Clarson, S. J. *Inorg. Organomet. Polym.* **2010**, *20*, 46–52.
29. Poojari, Y.; Clarson, S. J. *Macromolecules* **2010**, *43*, 4616–4622.
30. Bishwabhusan, S.; Brandstadt, K. F.; Lane, T. H.; Gross, R. A. *Org. Lett.* **2005**, *18*, 3857–3860.

Downloaded by 89.163.35.42 on June 23, 2012 | http://pubs.acs.org
Publication Date (Web): November 9, 2010 | doi: 10.1021/bk-2010-1051.ch001

Downloaded by STANFORD UNIV GREEN LIBR on June 23, 2012 | http://pubs.acs.org
Publication Date (Web): November 9, 2010 | doi: 10.1021/bk-2010-1051.ch002

## Chapter 2

# Properties and Applications of Silicones

**Michael J. Owen***

**Michigan Molecular Institute, Midland, MI 48640**
***michaelowen01@chartermi.net**

As part of the fourth Silicones and Silicone-Modified Materials symposium, it is useful to reflect on the properties of the mainstay of the silicone industry, polydimethylsiloxane (PDMS), and how these properties relate to the varied applications of this exceptional polymer.

## Applications of PDMS

List 1 shows some selected applications of PDMS. This list could be very much longer but has been limited to these nine selections to illustrate some fundamental points regarding the symbiotic relationship of polymer properties and applications. Firstly, they fall into three groups representing the familiar broad categories of silicone applications; additives, coatings and bulk cross-linked materials. Secondly, some of these applications have been chosen because of their familiarity and importance to the industry throughout its over sixty year history. These examples, one from each broad category, are antifoams, release coatings, and sealants. Thirdly, some are listed because they represent newer growth opportunities. One such application is high voltage insulation as indeed also is the newest generation of silicone contact lens materials. Primarily, however, these particular selections have been made because they present various apparent paradoxes worthy of discussion. For example, the antifoam and foam stabilizer applications, and the wetting agent and water repellency areas. Release coatings and sealants are a less obvious paradoxical pair until it is recalled that a prime requirement of any sealant should be good substrate adhesion. The least obvious paradox, that of high voltage insulation and contact lens materials, is elucidated in the subsequent discussion.

In Advances in Silicones and Silicone-Modified Materials; Clarson, S., et al.;
ACS Symposium Series; American Chemical Society: Washington, DC, 2010.

**List 1: Chosen Applications of PDMS**

- Antifoams
- Wetting agents
- Polyurethane foam stabilizers
- Release coatings
- Water repellent coatings
- Architectural coatings
- Sealants
- High voltage insulation
- Contact lens material

Downloaded by STANFORD UNIV GREEN LIBR on June 23, 2012 | http://pubs.acs.org
Publication Date (Web): November 9, 2010 | doi: 10.1021/bk-2010-1051.ch002

# Properties of PDMS

List 2 summarizes a number of important characteristics of PDMS relevant to our consideration of structure/property/application relationships.

**List 2: Some Important Characteristics of PDMS**

- Low intermolecular forces between methyl groups
- Unique flexibility of siloxane backbone
- High bond energy of siloxane bond
- Partial ionic nature of siloxane bond
- Low surface energy
- Hydrophobic/oleophilic
- Low solubility parameter
- High free volume
- Low glass transition temperature
- High gas permeability
- Liquid nature to high molecular weight
- Presence of low molecular weight component
- Versatile cross-linking chemistry
- Low toxicity
- UV stability

The first four of these characteristics of polydimethylsiloxane are the more fundamental and essentially provide the underlying explanation for the other physical and chemical attributes listed in List 2. Quantitative data pertinent to these attributes are shown in Table I. Characteristic pressure is perhaps the least familiar of these quantities. It is a measure of the mean intermolecular energy per unit volume corrected for the density of packing in the liquid state.

# Discussion

## Antifoams

Also known as defoamers, these materials are available in considerable product variety as fluids, compounds i.e. synergistic combinations of carrier fluid and hydrophobic solid, emulsions, and encapsulated products e.g. for detergent foam control. Their particular advantages comprise a broad range of applicability, thermal stability (e.g. in petrochemical processing) and FDA approval for applications such as antiflatulents. Perceived disadvantages include limitations on longevity of action and occasional impact on subsequent processes such as paintability. The key characteristics in this application include low surface energy, to enable entering and spreading at foaming lamellae, high siloxane bond energy (in its relationship to high thermal stability) and low toxicity.

## Surfactants

Silicone surfactants come in a variety of product types including the so-called trisiloxane "superwetters", silicone-polyether rake copolymers as used in polyurethane foam stabilization, and novel water-in-oil and oil-in-water emulsifiers. There is a pronounced preponderance of nonionic products, unlike hydrocarbon and fluorocarbon based surfactants. The primary advantage of silicone surfactants is their ability to wet low energy surfaces such as plastics, skin, hair, plant surfaces, etc. and to lower the surface tension of organic fluids such as the polyols that are polyurethane precursors. The main disadvantage is a limited stable pH range of 4 – 9. Note that for a PDMS monolayer on water this stable pH range is wider, 2.5 – 11, presumably due to the more limited two-dimensional exposure to water of a spread film as opposed to the three-dimensional exposure of a dissolved surfactant. The spreading advantage accrues from the lower aqueous surface tension of PDMS surfactants, typically *ca* 20 mN/m above the critical micelle concentration, compared to hydrocarbon surfactants which typically have corresponding values of *ca* 30 mN/m. The disadvantage is the result of the partially ionic siloxane backbone rendering it susceptible to nucleophilic or electrophilic attack at extremes of pH.

## Water-Repellent Coatings

These are available as cross-linkable emulsions, liquid silicone elastomers, and filled materials that exploit the "lotus effect" – enhancement of high contact angle by controlled roughness. A disadvantage is that oleophobicity is sometimes required as well as hydrophobicity. Fluorosilicones can be advantageously employed in such situations. Breathability, an important comfort factor for textiles, is best when individual fibers are treated but even a continuous PDMS elastomer film will transmit water vapor. The high contact angle of water, greater than 90 degrees, is significant. The oleophilic nature is a direct consequence of the methyl groups present along the chain of this semi-inorganic polymer.

There are two apparent paradoxes in these applications. That between antifoaming and urethane foam stabilization is simply a reflection of solubility. The prerequisites of antifoaming are insolubility and surface activity whereas for foaming it is solubility and surface activity, explaining why polyurethane foam stabilizers are copolymers of PDMS with polyol-soluble polyethers. Given the inherent insolubility of PDMS in water, it is axiomatic that all aqueous silicone surfactants will also have a hydrophilic entity, usually as a silicone-polyether

Downloaded by STANFORD UNIV GREEN LIBR on June 23, 2012 | http://pubs.acs.org
Publication Date (Web): November 9, 2010 | doi: 10.1021/bk-2010-1051.ch002

copolymer. The paradox between wetting agents and water repellency arises because of confusion between “wetting of” and “wetting by”. A low surface tension is required for a liquid to wet a substrate. A water-repellent coating also needs to be of low surface energy to repel wetting by water. Thus in both cases low surface tension is the key. The wetting agent’s low surface tension aids in its spreading and wetting “of” a substrate; the water-repellent coating’s low surface energy resists wetting “by” water.

## Release Coatings

These products are available as cross-linkable materials based on either condensation or hydrosilylation addition chemistry, in the form of water-based emulsions, solvent dispersions, or neat, solventless materials. Non-reactive release products are also widely available. The advantages of the coatings are that they are effective on a broad range of substrates, permit slippage during peeling of pressure-sensitive adhesives, and offer a range of controlled release force by the use of high release additives. A disadvantage in certain processes is that transfer of free PDMS can affect subsequent surface treatment of the released articles. Low surface energy and low glass transition temperature are the key characteristics of importance in this application.

## Sealants

Sealants are available as one or two part, room temperature or heat curing systems dependent on the cross-linking chemistry utilized. Condensation cure materials, particularly those producing acetic acid as an *in-situ* etchant, have excellent adhesion to a variety of substrates. Others based on hydrosilylation addition cure might require the incorporation of adhesion promoters such as silane coupling agents. Applicational advantages include a low viscosity before curing, facile displacement of leaving groups due to the high permeability of PDMS, and the low surface tension promoting easy spreading. Fungal growth, resulting from the oleophilic nature, can be a problem if products are not formulated with fungicides.

## Architectural Coatings

These coatings are supplied as a water-based paint. Their advantages include environmental inertness and longevity. They are also useful on poorly adherent surfaces. Disadvantages include staining from organic material in the environment and difficulty in recoating with other paint systems. The key characteristics are UV stability, low surface energy (wets substrates well; poorly wetted by other materials), elastomeric nature and oleophilicity.

The release coating/sealant adhesion conundrum is a further example of the wetting “by” and “of” confusion described earlier. Low surface tension is part of the explanation of good sealant adhesion by promoting good wetting of the substrate and repelling wetting of a release coating by an adhesive. The inconsistency in architectural coatings seems to be staining of such a low surface

Downloaded by STANFORD UNIV GREEN LIBR on June 23, 2012 | http://pubs.acs.org
Publication Date (Web): November 9, 2010 | doi: 10.1021/bk-2010-1051.ch002

energy material. In this case it seems it is the oleophilic nature of the polymer, with two methyl groups on every silicon, that triumphs over the release characteristic. The presence of low molecular weight material that might solubilize organic contaminants at the coating surface is also a contributory factor.

### High Voltage Insulation and Contact Lens Materials

These very different applications are not self-evidently contradictory. This aspect results from the hydrophobic recovery behavior of silicones. It turns out to be beneficial for high voltage insulation but a detriment to contact lens materials. Plasma treatment has been used to increase the wettability of contact lenses by tears. Corona discharge will inadvertently do this to high voltage insulation. In the contact lens case hydrophobic recovery is an unwanted attribute; in high voltage insulation it is very much desired.

Silicone high voltage insulation products are available as composite insulators, elastomer dispersions, and grease-like coatings. Their advantages over porcelain are light weight, vandal resistance and resistance to salt contamination. The advantage over other polymers is the facile hydrophobic recovery. Algal growth is one disadvantage; a few cases of rodent damage in storage and bird damage by pecking when installed have been reported. Key attributes are low surface energy, low glass transition and the presence of low molecular weight material, the diffusion of which to the surface is the prime reason for subsequent hydrophobic recovery.

A PDMS elastomer lens has long been used in eye surgery on young children. New organosilicon-containing copolymers and hydrogels have also recently been introduced. Contact lenses based on PDMS continue to appeal, primarily because of the unrivalled oxygen transmission to the cornea. This is offset by poor wettability by the tears necessitating copolymerization with hydrophilic monomers or some other type of wettability enhancement treatment. Lipid uptake can also present difficulties. The fundamental factors involved in this application are the low surface energy (low intermolecular forces), high oxygen permeability (chain flexibility, low $T_g$, high free volume), and oleophilicity. Note that oleophobic fluorosilicone intra-ocular lenses are available.

## Summary

Our objective in this paper has been to shed light on the fundamental characteristics of PDMS (*6*, *7*) and how they relate to its applications. Some apparently contradictory applications have been examined to show that in each case the same set of fundamental attributes is operating and that, expectedly, the paradox is illusory. Polydimethylsiloxane's most fundamental features are its low intermolecular forces between the methyl groups, unique backbone flexibility, high siloxane bond energy and the partial ionic nature of the siloxane bond. As the varied contributions to this series of symposia amply attest, research in silicone polymers is expanding continuously and there is every reason to expect

Downloaded by STANFORD UNIV GREEN LIBR on June 23, 2012 | http://pubs.acs.org
Publication Date (Web): November 9, 2010 | doi: 10.1021/bk-2010-1051.ch002

**Table I. Fundamental Properties of PDMS**

| *Property* | *Value* | *Unit* | *Ref* |
|---|---|---|---|
| Characteristic pressure | 341 | J $cm^{-3}$ | (*1*) |
| Energy of backbone rotation | ~0 | kJ/mol | (*2*) |
| Glass transition temperature | 150 | K | (*3*) |
| Siloxane bond energy | 445 | kJ/mol | (*4*) |
| Siloxane bond polar character. | 41 | % | (*5*) |

that this set of attributes will enable the historic growth of silicones to continue for a further sixty years.

## References

1. Shih, H.; Flory, P. J. *Macromolecules* **1972**, *5*, 758.
2. Tobolsky, A. V. *Properties and Structures of Polymers*; John Wiley and Sons: New York, 1960; p 67.
3. Lee, C. L.; Johannson, O. K.; Flaningam, O. L.; Hahn, P. *Polym. Prepr.* **1969**, *10* (2), 1311.
4. Beezer, A. E.; Mortimer, C. T. *J. Chem. Soc. A* **1966**, 514.
5. Pauling, L. *J. Phys. Chem.* **1952**, *56*, 361.
6. For those requiring more quantitative data on the properties of PDMS, Kuo has provided an excellent comprehensive compilation. (a) Kuo, A. C. M. In *Polymer Data Handbook*; Mark, J. E., Ed.; Oxford University Press: New York, 1999; p 41. (b) Kuo, A. C. M. In *Polymer Data Handbook*, 2nd ed.; Mark, J. E., Ed.; Oxford University Press: New York, 2009; p 539.
7. For more extensive information concerning PDMS and related polymers see (a) Jones, R. G.; Ando, W.; Chojnowski, J. *Silicon-Containing Polymers*; Kluwer Academic Publishers: Dordrecht, The Netherlands, 2000. (b) Clarson, S. J.; Semlyen, J. A. *Siloxane Polymers*; PTR Prentice Hall: Englewood Cliffs, NJ, 1993.

Downloaded by STANFORD UNIV GREEN LIBR on June 23, 2012 | http://pubs.acs.org
Publication Date (Web): November 9, 2010 | doi: 10.1021/bk-2010-1051.ch002

Downloaded by PENNSYLVANIA STATE UNIV on June 25, 2012 | http://pubs.acs.org
Publication Date (Web): November 9, 2010 | doi: 10.1021/bk-2010-1051.ch003

## Chapter 3

# Polymorphs of Octaphenylcyclotetrasiloxane

**Abhilasha M. Baruah, Anirban Karmakar, and Jubaraj B. Baruah***

**Department of Chemistry, Indian Institute of Technology Guwahati,
Guwahati 781 039 Assam, India
*email: juba@iitg.ernet.in**

Three polymorphs of octaphenylcyclotetrasiloxane are described in order to show an uncommon type of polymorphism in which the number of symmetry independent molecules are sequentially increased. The C-H··π interactions play a crucial role in the stability of the polymorphs and in these polymorphs two different types of end-to-face hydrogen bonding interactions play a crucial role in the packing pattern.

## Introduction

In order to understand the polymorphism occurring from variation of the number of symmetry independent molecules per unit cell (*1*) it is essential to identify suitable systems that exhibit polymorphism (*2*). It has been already shown that hydrogen bonding interactions are responsible for holding multiple numbers of symmetry nonequivalent units (*3*) in the unit cell. However, there are systems in which weak interactions such as C-H•••π interactions (*4*) becomes prominent which may also lead to polymorphs. It is already reported that polymorphism in siloxanes plays a major role in understanding their physical properties (*5*). In this study we have chosen a phenyl substituted cyclic siloxane, namely octaphenylcyclotetrasiloxane, (**A**) for understanding the role of C-H•••π interactions in polymorphs as this molecule has several phenyl groups oriented in different directions with a relatively simple structure and it can be easily prepared by different methods (*6*).

In Advances in Silicones and Silicone-Modified Materials; Clarson, S., et al.;
ACS Symposium Series; American Chemical Society: Washington, DC, 2010.

Downloaded by PENNSYLVANIA STATE UNIV on June 25, 2012 | http://pubs.acs.org
Publication Date (Web): November 9, 2010 | doi: 10.1021/bk-2010-1051.ch003

# Experimental

The crystallographic details and synthetic procedure for polymorph **I** and **II** of octaphenylcyclotetrasiloxane are also available in reference (*6*).

## The Synthesis of Polymorph III of Octaphenylcyclotetrasiloxane

A solution of diphenylsilane (0.18 gm, 1mmol) in ethanol/ allyl alcohol (3ml, 1:1mixture) were stirred with catalytic amount of tetramethylammoinum-borohydride (0.088gm, 0.1mmol) 80°C for five minutes. The solution was cooled and kept standing for three days; white crystals of octaphenyl-cyclotetrasiloxane (30%). Crystal data for polymorph **III**: CCDC number 634266: Colorless blocks (0.48 x 0.32 x 0.20mm$^3$), $C_{48}H_{40}O_4Si_4$, 793.16, Triclinic (P-1), $a$=10.7494(9)Å, $b$=20.969(2)Å, $c$=21.3035(19)Å, $\alpha$ = 66.788(5)°, $\beta$ = 75.973(5)°, $\gamma$ = 89.359(5)°, Z = 4,V = 4262.4(7)Å (*3*), $\rho_{calcd}$ = 1.236 Mgm$^{-3}$, $\mu$ (Mo$_{K\alpha}$) = 0.101mm$^{-1}$, Goof = 0.972, Final R1 = 0.0879 for 20205 reflections of $I > 2\sigma(I)$, R1 = 0.1693, wR2 = 0.2196 for all data.

# Results

A base catalyzed hydrolytic reaction of diphenylsilane leads to octaphenylcyclotetrasiloxane (**A**) (see Equation 1). The formation of different polymorphs (**I-III** as illustrated in Figure 1) of **A** is governed by the solvent used in the crystallization as well as reaction medium. For example the hydrolytic reaction of diphenylsilane in aqueous methanol gives polymorph **II**. The polymorph **II** is formed when such hydrolytic reaction and crystallization is carried out from mixture of allyl alcohol and ethanol. Similar reaction in aqueous acetonitrile (5%) gives the polymorph **I**.

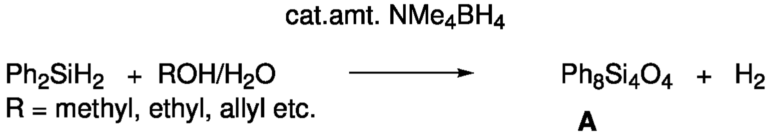

$$\underset{\text{R = methyl, ethyl, allyl etc.}}{Ph_2SiH_2 + ROH/H_2O} \xrightarrow{\text{cat.amt. } NMe_4BH_4} \underset{\mathbf{A}}{Ph_8Si_4O_4} + H_2$$

**Equation 1**

Downloaded by PENNSYLVANIA STATE UNIV on June 25, 2012 | http://pubs.acs.org
Publication Date (Web): November 9, 2010 | doi: 10.1021/bk-2010-1051.ch003

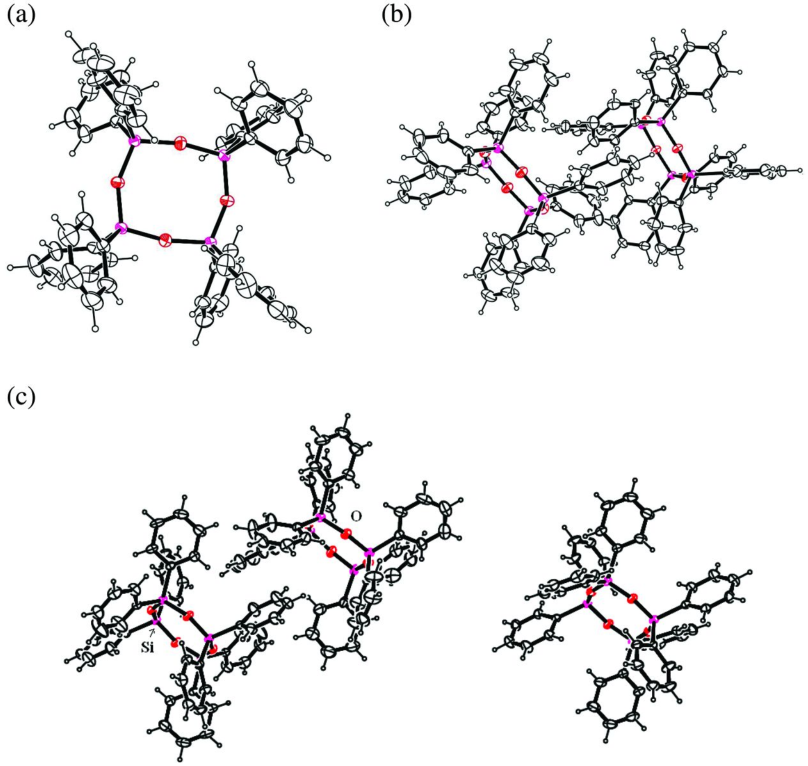

*Figure 1. The ORTEP of polymorphs of octaphenylcyclotetrasiloxane: polymorph (a)* ***I*** *(b)* ***II*** *and (c)* ***III*** *each are drawn with a 20% thermal ellipsoid. (Red = oxygen atoms; Pink = silicon atoms).*

Two polymorphs of compound **A** were reported earlier (*7*), but these polymorphs were not being discussed in detail. We have observed that by variation of the reaction medium and crystallization from different solvents, three polymorphs of octaphenylcyclotetrasiloxane can be obtained. The two already known polymorphs of octaphenylcyclotetrasiloxane crystallizes in a monoclinic, P2(1)/c (polymorph **I**) or a triclinic, P-1 (polymorph **II**) space group (*7*). Whereas the third polymorph reported here is also triclinic, P-1 (polymorph **III**) but has a different crystal dimension. The polymorph **I**, **II** and **III** have one, two and three symmetry independent molecules respectively, in their unit cells as illustrated in Figure 1. However, each of the polymorphs has characteristic features, for example the siloxane ring in the polymorph **I** has one type of rings that have two distinct types of Si-O-Si bond angles of 167.2° and 152.8° making the ring slightly distorted. In the polymorph **II**, the two rings of the two molecules are not equivalent. One of the rings is relatively symmetric with Si-O-Si bond angles 158.9° and 157.5°, whereas the other ring is distorted having two sets of Si-O-Si bond angles 165.4° and 152.5° respectively. The polymorph **III** has three symmetry independent cyclic units per unit cell; of which two rings resemble the rings of polymorph **II**; each ring having Si-O-Si bond angles 158.1°, 157.5° and

160.9°, 152.9° respectively; whereas the third ring has a set of bond angles 159.3° and 153.6°. Thus, it may be imagined that the polymorph **III** is arising from a combination of polymorph **II** and **III**. In all the three cases the cyclic siloxane molecules are held together by weak C-H··π interactions, but the orientation of the siloxane rings in the lattice makes the C-H groups of phenyl groups to orient in different manner in each lattices; making the packing pattern distinguishable. Among these the polymorph **II** is the most stable and upon recrystallisation from different solvents of **I** and **III** leads to formation of **II**. The crystal packing in each case is basically governed by end-face C-H··π interactions and two different types of such interactions are observed as illustrated in Figure 2. Linear chain like structures in the case of polymorph **I** are held by end-face interactions of the type 1 as illustrated in Figure 2. By such interactions a helical assembly is formed as shown in Figure 3a. In the case of polymorph **II** these interactions leads to three dimensional structure; whereas in the case of the polymorph **III** the molecules are held in multiple number of chains which incidentally crosses at certain point in a cross-wise fashion and thereby provide stability to the lattice. The weak interactions involved in the lattice are illustrated in Figure 3c. In the case of polymorph **II** the three dimensional network is formed by both the types of end-face C-H··π interactions shown in Figure 2. The three dimensional growth makes the system thermodynamically more favorable and is readily formed during crystallization and this polymorph is commonly observed during crystallisation. The polymorph **III** is governed by end-face C-H··π interactions of type 1 as shown in figure 2 and these interactions results in two dimensional structure. Since rings in some system are disordered we prefer to discuss it qualitatively. The IR spectra of the three polymorphs are indistingushable and is illustrated in Figure 4(i). The X-ray powder pattern of polymorphs of **A** formed from different crystallisation from different solvent such as aqeous methanol, ethanol, ethanol/allylalcohol mixture and also from acetonitrile are shown in Figure 4(ii)-(v). It is clear that the solvent has a significant role in the polymoph formation. In the case of methanol as solvent only polymorph **I** is formed, whereas the mixed solvent of ethanol and allyl alcohol leads to the formation of polymorph **III** as the major product, crystallisation from acetonitrile leads to **I** as major polymorph, whereas from ethanol a mixture of **II** and **III** are formed.

Downloaded by PENNSYLVANIA STATE UNIV on June 25, 2012 | http://pubs.acs.org
Publication Date (Web): November 9, 2010 | doi: 10.1021/bk-2010-1051.ch003

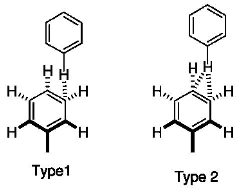

*Figure 2. Two types of end-face C-H··π interactions*

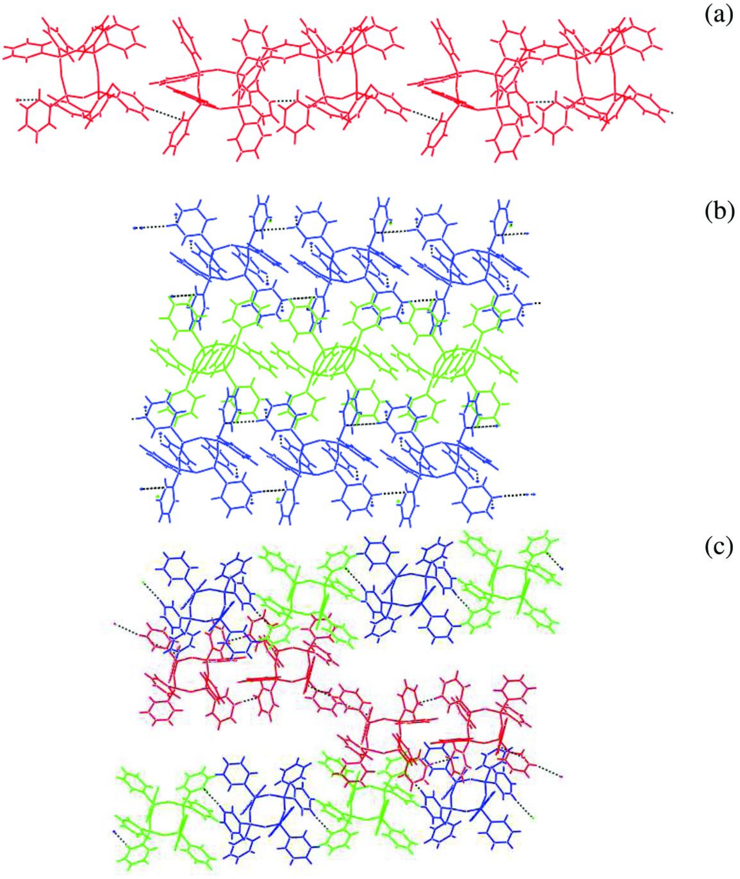

*Figure 3. Packing in the part of the lattice of the polymorphs (a)* ***I*** *(b)* ***II*** *(c)* ***III*** *showing the weak interactions (black dashed lines) associated in packing. (see color insert)*

Downloaded by PENNSYLVANIA STATE UNIV on June 25, 2012 | http://pubs.acs.org
Publication Date (Web): November 9, 2010 | doi: 10.1021/bk-2010-1051.ch003

Downloaded by PENNSYLVANIA STATE UNIV on June 25, 2012 | http://pubs.acs.org
Publication Date (Web): November 9, 2010 | doi: 10.1021/bk-2010-1051.ch003

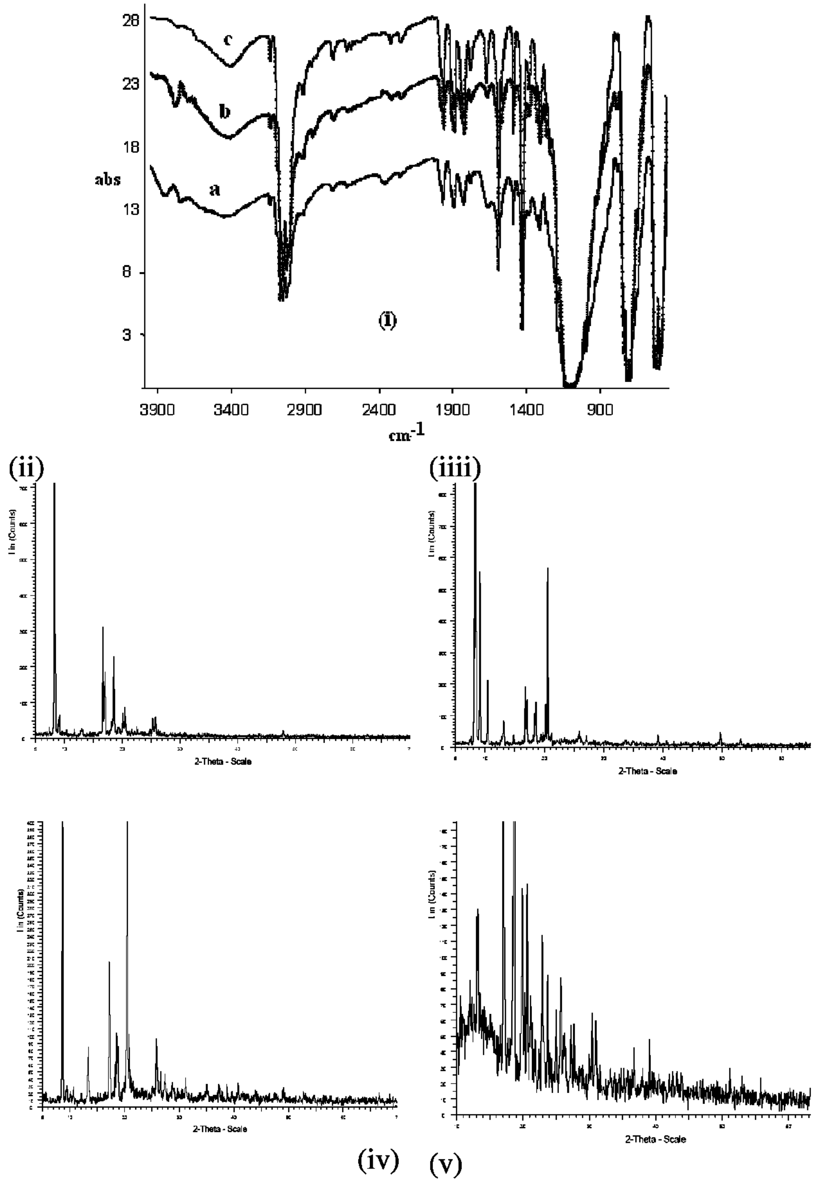

*Figure 4. (i) IR spectra of polymorphs (a)* ***I****, (b)* ***II****, (c)* ***III*** *in KBr (cm$^{-1}$). The X-ray powder diffraction pattern from the octaphenylcyclotetrasiloxane obtained from (ii) methanol (iii) from ethanol (iii) mixed solvent of allylalcohol and ethanol (1:1) and (v) acetonitrile.*

Downloaded by PENNSYLVANIA STATE UNIV on June 25, 2012 | http://pubs.acs.org
Publication Date (Web): November 9, 2010 | doi: 10.1021/bk-2010-1051.ch003

## Conclusions

In conclusion we have described here three polymorphs of octaphenylcyclotetrasiloxane arising from packing differences in the numbers of symmetry independent molecules in a unit cell having slight conformational difference in the rings.

## Acknowledgments

We thank the Department of Science and Technology, New Delhi, India for the X-ray diffraction facility used in this research.

## References

1. Desiraju, G. R. *CrystEngComm* **2007**, *9*, 91.
2. Anderson, K. M.; Afarikia, K.; Yu, H.; Goeta, A. E.; Steed, J. W. *Cryst. Growth Des.* **2006**, *6*, 2109.
3. Das, D.; Banerjee, R.; Mondal, R.; Howard, J. A. K.; Boese, R.; Desiraju, G. R. *Chem. Commun.* **2006**, 555.
4. (a) Nishio, M.; Hirota, M.; Umezawa, Y. *The CH/π Interaction: Evidence, Nature and Consequences*; Wiley: New York, 1998. (b) Nishio, M.; Hirota, M. *Tetrahedron* **1989**, *45*, 7201. (c) Takahashi, H.; Tsuboyama, S.; Umezawa, Y.; Honda, K.; Nishio, M. *Tetrahedron* **2000**, *56*, 6185. (d) Nishio, M. *CrystEngComm* **2004**, *6*, 130.
5. Molenberg, A.; Moller, M. *Macromolecules* **1997**, *30*, 8332.
6. Deka, K.; Sarma, R. J.; Baruah, J. B. *Inorg. Chem. Commun.* **2005**, *8*, 1082.
7. (a) Hensen, K.; Gebhardt, F.; Kettner, M.; Pickel, P.; Bolte, M. *Acta Crystallogr., Sect. C: Cryst. Struct. Commun.* **1997**, *C53*, 1867. (b) Ovchinnikov, Y. E.; Shklover, V. E.; Struchkov, Y. T.; Demeńtev, V. V.; Frunze, T. M. *Metalloorganicheskaya Khimiya* **1988**, *1*, 1117. (c) Braga, D.; Zanotti, G. *Acta Crystallogr., Sect. B* **1980**, *B36*, 950. (d) Hossain, M. A.; Hursthouse, M. B.; Malik, K. M. A. *Acta Crystallogr., Sect. B* **1979**, *B35*, 522. (e) Burkhard, C. A.; Decker, B. F.; Harker, D. *J. Am. Chem. Soc.* **1945**, *67*, 2174.

Downloaded by UNIV OF DELAWARE MORRIS LIB on June 23, 2012 | http://pubs.acs.org
Publication Date (Web): November 9, 2010 | doi: 10.1021/bk-2010-1051.ch004

## Chapter 4

# Synthesis and Characterization of Cycloaliphatic Siloxanes Copolymers

**Ruby Chakraborty and Mark D. Soucek***

**Department of Polymer Engineering, The University of Akron,**
**Akron, OH 44311-0301**
***msoucek@uakron.edu**

Both random and block siloxane copolymers were synthesized with methyl, and cyclopentyl, or cyclohexyl substituents. Random copolymers were obtained by hydrolytic condensation of dimethyldichlorosilane and dicyclopentyldichlorosilane or dicyclohexanedichlorosilane. Block polymers were prepared using cyclic oligomers via a ring opening polymerization (ROP). Amberlyst-15 was used as the catalyst for ROP. The synthesized polymers were characterized by $^{1}$H-NMR, $^{13}$C-NMR, $^{29}$Si-NMR, FT-IR, and GPC. The glass transition temperatures of the siloxanes were measured using DSC and DMA. The random and block structures were identified via NMR. As expected, The $T_g$ of the copolymers were intermediate between those of the homopolymers.

## Introduction

Silicones have a unique combination of properties (*1*). These properties include extremely low $T_g$, excellent thermal, oxidative, and UV-stability. Some other benefits of methylsiloxane are high gas permeability (*2*), hydrophobicity (*3*), interfacial activity (*4*) and excellent atomic oxygen resistance (*5*). A variety of reactive end groups on siloxanes has led to a wide range of chemical, physical, thermal and mechanical properties (*6–8*). In addition, many different backbone substituents have been reported from numerous academic laboratories (*9–11*). The predominant siloxanes used commercially with same substituents along the backbone are polydimethylsiloxane (PDMS) and polydiphenylsiloxane (PDPhS) (*12*, *13*). PDMS is mechanically very weak and shows cold flow at high molecular

In Advances in Silicones and Silicone-Modified Materials; Clarson, S., et al.;
ACS Symposium Series; American Chemical Society: Washington, DC, 2010.

weight. Also, PDMS has crystallization properties at low temperatures, which can be disrupted by introduction of other siloxane segments having different backbone substitutions such as alkyl, cycloaliphatic or aromatic groups, thus keeping the siloxanes amorphous over a much wider temperature range than homopolymers (*14*). Although, the PDPhS has a higher glass transition temperature, the poor photo-oxidative stability of the aromatic groups compared to systems having no unsaturations, limits the usage of the aromatics specially for outdoor applications (*15*, *16*).

A diverse variety of linear, random, graft and block polymers have been synthesized during the last 40 years by either ring opening polymerization or anionic polymerization (*17*). Block copolymers are synthesized through reactions between organofunctionally terminated siloxanes or by ring opening of cyclic siloxanes. The block polymers are useful for compatabilizing inorganic and organic polymers (*18*, *19*). The majority of copolymer synthesis involving siloxane polymers centers on siloxane-organic block copolymers which can be utilized as surfactants and compatibilizers (*20*, *21*).

Due to the ionic nature of siloxane (Si-O) bond, both acidic and basic catalysts can be used for ring opening of cyclic siloxanes (*22*, *23*). The catalyst cleaves the siloxane bonds in both the cyclic and linear species (*24*). The overall process leads to ring-chain equilibrium or redistribution reactions (*25*, *26*). On account of redistribution reactions, the development of block copolymers of polysiloxanes has been neglected. These types of polymers are relatively rare due to the requirements for a specific reactivity of monomers or oligomeric precursors.

An important approach to the synthesis of siloxane containing block or segmented copolymers is the step growth or condensation reactions involving reactive, telechelic siloxane oligomers with organic difunctional monomers or oligomers (*27*). Siloxane oligomers are generally synthesized via anionic or cationic ring opening polymerization of cyclic siloxane monomers, such as octamethylcyclotetrasiloxane ($D_4$) in the presence of functionally terminated disiloxanes which act as end-blockers (*28*, *29*). Ring opening polymerization (ROP) is another way of synthesizing reactive oligomers or block copolymers (*30*, *31*). This is due to the availability of a wide range of cyclic monomers, versatility of the initiation/termination systems and mechanisms and also to some extent to the ease of the control of the end group functionalization (*29*).

Hydrolytic condensation of dimethyl, dicyclopentyl and dicyclohexyl dichlorosilanes was performed to obtain the corresponding homopolymers. Random copolymers were obtained by hydrolytic condensation of dimethyldichlorosilane with dicyclopentyldichlorosilane or dicyclohexanedichlorosilane. Cyclic oligomers were used as precursors for ring opening polymerization (ROP) of cyclic oligomers to obtain block copolymers. Amberlyst-15 was used as the catalyst for ROP. Spectroscopic characterization of $^{1}$H, $^{13}$C-NMR, FTIR was used to identify either block or random structure of the copolymers. The glass transition temperature was obtained using DSC and rheological measurements.

Downloaded by UNIV OF DELAWARE MORRIS LIB on June 23, 2012 | http://pubs.acs.org
Publication Date (Web): November 9, 2010 | doi: 10.1021/bk-2010-1051.ch004

Downloaded by UNIV OF DELAWARE MORRIS LIB on June 23, 2012 | http://pubs.acs.org
Publication Date (Web): November 9, 2010 | doi: 10.1021/bk-2010-1051.ch004

# Experimental

## Materials

Octamethylcyclotetrasiloxane ($D_4$), dimethyldichlorosilane and dichlorosilane were purchased from Gelest, Inc, (Morrisville, PA). Cyclopentene, cyclohexene, chloroform-D, Amberlyst 15 ion- exchange resin, platinum(0)-1,3-divinyl-1,1,3,3 –tetramethyl disiloxane (Karstedt catalyst), 3 wt % solution in xylenes were obtained from Aldrich (Milwaukee, Wisconsin). Sodium bicarbonate, sodium sulfate, dichloromethane, potassium hydroxide and toluene were purchased from EMD chemicals (Gibbstown, NJ).

# Instruments and Characterization

Fourier transform infrared spectroscopy was obtained on a Nicolet 380 FT-IR instrument (Thermo Electron Corp). $^1$H-NMR and $^{13}$C-NMR spectra were acquired on a Varion Unity plus 300- MHz Spectrometer in $CDCl_3$. $^{29}$Si-NMR was acquired on **a** 400 MHz Mercury instrument. TMS was used as internal standard. The glass transition temperatures were measured by differential scanning calorimetry (DSC) on a TA instrument, DSC (Model-29210). The specimens were heated at a scanning rate of 5 °C/min, from -150 °C to 100 °C. An Advanced Rheometric Expansion System (ARES, TA Instruments) was also used in the oscillatory mode with a parallel plate fixture (25 mm diameter). Dynamic temperature sweep experiments were performed at an angular frequency 1(*ö*) rad/s. All experiments were conducted under a nitrogen atmosphere. Gel Permeation Chromatography (GPC) measurements were performed on a Waters GPC instrument equipped with a series of six Styragel columns (HR 0.5, HR 1, HR 3, HR 4, HR 5 and HR 6) calibrated with narrow-MWD polystyrene standards. A refractive-index (RI) detector (Optilab, Wyatt Technology), a dual-ultraviolet absorbance detector (Waters 2487), and a laser light scattering detector (Minidawn, Wyatt Technology) were used to obtain number- average molecular weights ($\overline{M}_w$), weight- average molecular weights ($\overline{M}_w$) and polydispersity index (PDI). Tetrahydrofuran was used as the eluent at the flow rate of 1 mL/min. All molecular weights are reported relative to polystyrene standards.

## Synthesis of Cyclic Oligomer of Polydicyclopentyl Siloxane(PDPS) (1) and Polydicyclohexyl Siloxane (PDHS) (2)

To a three neck round bottom flask, equipped with a reflux condenser, nitrogen inlet/outlet, and dropping funnel was added aqueous potassium hydroxide solution. A solution of dicyclopentyl dichlorosilane (15 g, 0.06 mol) or dicyclohexyl dichlorosilane (15.92 g, 0.06 mol) was taken in the round bottom flask and aqueous potassium hydroxide solution was added via a dropping funnel and the solution was allowed to stir for several min at 35 °C. This was continued until effervescence (HCl evolution) stops. The aqueous and organic layer were separated using a separatory funnel after removing the precipitated KCl by decanting the liquid reaction mixture. The organic layer was dried using sodium sulfate. From the organic layer, diethyl ether was removed under vacuum to yield a clear yellow oily liquid in the case of the cyclopentyl derivative, 10 g (66 % yield) and a clear oily liquid in the case of the cyclohexyl derivative, 8.2 g (54 % yield). For the cyclic oligomer of PDPS, the number average molecular weight as obtained by GPC is 1200 dalton. FT-IR ($cm^{-1}$): 1010- 1147 (Si-O-Si), 2848-2942 (-$CH_2$-), 2929-2980 (-$CH_3$ -); $^1$H NMR ($CDC_{l3}$) $\delta$ (ppm): 0.01 ( Si – $CH_3$), 1.25-1.7 (-$CH_2$-), 1.8-2.5 (-CH-).

For the cyclic oligomer of PDPS, the number average molecular weight as obtained by GPC is 1500 dalton. FT-IR ($cm^{-1}$): 1016- 1122 (Si-O-Si), 2835-2887 (-$CH_2$-), 2895-2990 (-$CH_3$ -); $^1$H NMR ($CDC_{l3}$) $\delta$ (ppm): -0.05 ( Si – $CH_3$), 1.0-1.25 (-$CH_2$-), 1.6-2.0 (-CH-).

## Activation of Ion Exchange Resin

Amberlyst-15, ion exchange resin is activated before use (*32*). The Amberlyst catalyst (100 g) was activated by placing in a 1000 mL Erlenmeyer flask with 500 mL of THF and stirring it for 18 h. Then the resin is filtered off and air dried. The catalyst was then placed in a 1000 mL Erlenmeyer flask with 400 mL of 0.1 N HCl. This mixture was stirred for 3 h, and then the acid solution was decanted. The resin was washed with distilled water (3 x 100 mL) until a neutral pH is obtained, and this resin was air dried. The acid capacity of the resin increases by this operation. The resin becomes more resistant to deactivation as the number of acidic sites increases (*33*).

## Synthesis of Block Copolymer of PDMS with PDPS (PDMS-*block*-PDPS) (3) and PDHS (PDMS-*block*-PDHS) (4)

A 300 mL three neck round bottom flask was fitted to a condenser and a nitrogen inlet valve. To the flask, octamethylcyclotetrasiloxane (10 g, 0.034 mol) and cyclic oligomers of PDPS (30 g, 0.034 mol) or cyclic oligomers of PDHS (35.7 g, 0.034 mol) and 2 g of activated Amberlyst catalyst were added. The reaction mixture was heated in an oil bath at 60 °C for 15 h to enable ring opening and then condensation of the cyclic oligomers and then filtered to remove the amberlyst resin. The final reaction product was a clear viscous fluid. viscous fluid. PDMS-*block*-PDPS *(3)*, FT-IR ($cm^{-1}$): 1020-1090 (Si-O-Si), 796 (C-H stretching), 2950 ($CH_3$ asymmetrical stretch). $^1$H-NMR $\delta$ (ppm): 0.01-0.16 (Si-$CH_3$), 1.34-1.80 (-$CH_2$-), 1.80-1.96 (-CH-).

PDMS-*block*-PDHS*(4)*, FT-IR of ($cm^{-1}$): 987-1090 (Si-O-Si), 795 (C-H stretching), 2960 ($CH_3$ asymmetrical stretch). $^1$H-NMR $\delta$ (ppm): 0.0-0.22 (Si-$CH_3$), 1.09-1.41 (-$CH_2$-), 1.66-1.93 (-CH-).

## Synthesis of Homopolymers of PDMS (5), PDPS (6) and PDHS (7)

A 500 mL three neck flask was fitted with a condenser and nitrogen inlet valve. Either dimethyl dichlorosilane (0.12 mol, 15.48 g), dicyclopentyl dichlorosilane (0.12 mol, 28.5 g) or dicyclohexyl dichlorosilane (0.12 mol, 31.8 g) was charged

In Advances in Silicones and Silicone-Modified Materials; Clarson, S., et al.;
ACS Symposium Series; American Chemical Society: Washington, DC, 2010.

Downloaded by UNIV OF DELAWARE MORRIS LIB on June 23, 2012 | http://pubs.acs.org
Publication Date (Web): November 9, 2010 | doi: 10.1021/bk-2010-1051.ch004

Downloaded by UNIV OF DELAWARE MORRIS LIB on June 23, 2012 | http://pubs.acs.org
Publication Date (Web): November 9, 2010 | doi: 10.1021/bk-2010-1051.ch004

into the flask. 100 g of toluene was added to the flask. With stirring at 60 °C, KOH (4.4 g, 0.24 mol) was added dropwise over 30 min, and then the reaction mixture was aged 6 h at 60 °C. The reaction mixture was then cooled to 30 °C and $NaHCO_3$ (20.16 g, 0.24 mol) was added. Stirring was continued for 3 more hours at 30 °C. The reaction mixture was filtered off to remove inorganic salt present at the flask bottom. The organic layer was washed with distilled water (3x, 300 mL) till the pH is neutral. Toluene was then removed under vacuum to give a viscous oily hydroxyl functional PDMS **(5)**, PDPS **(6)** and PDHS **(7)**.

Homopolymer of PDPS *(6)*. FT-IR of ($cm^{-1}$): FT-IR ($cm^{-1}$): 1000-1100 (Si-O-Si), 791-868 (C-H stretching). $^1H$-NMR $\delta$ (ppm): 1.31-1.74 ($-CH_2-$), 1.74-1.96(-CH-).

Homopolymer of PDHS *(7)*: FT-IR of ($cm^{-1}$): 989-1110 (Si-O-Si), 845 (C-H stretching). $^1H$-NMR $\delta$ (ppm): 1.08-1.44 ($-CH_2-$), 1.66-1.94(-CH-).

### Synthesis of Random Copolymer of PDMS with PDPS (PDMS-*ran*-PDPS) (8) and PDHS (PDMS-*ran*-PDHS) (9)

A 500 mL three neck flask was fitted with a condenser and a nitrogen inlet valve. Dimethyl dichlorosilane (0.084 mol, 10.8 g) and dicyclopentyl dichlorosilane (0.084 mol, 20 g) or dicyclohexyl dichlorosilane (0.084 mol, 22.3 g) were charged into the flask. 200 g of toluene was added dropwise to the flask with stirring at 60 °C, (3 g, 0.17 mol) over 30 min, and then the reaction mixture was aged 6 h at 60 °C. The reaction mixture was then cooled to 30 °C and $NaHCO_3$ (14.1 g, 0.17 mol) was added. Stirring was continued for 3 more hours at 30 °C. The reaction mixture was filtered off to remove inorganic salt present at the flask bottom. The organic layer was washed with distilled water (3x, 300 mL) till the pH is neutral. Toluene was then removed in *vacuo* to give a viscous oily hydroxyl functional. PDMS-*ran*-PDPS *(8)*, FT-IR of ($cm^{-1}$): 997-1090 (Si-O-Si), 775-812 (C-H stretching), 2954 ($CH_3$ asymmetrical stretch). $^1H$-NMR $\delta$ (ppm): 0.03-0.22 ($Si-CH_3$), 0.88-1.09 ($Si-CH_2$), 1.37-1.70 ($-CH_2$), 1.70-1.89 (-CH-).

PDMS- *ran* -PDHS*(9)*, FT-IR of ($cm^{-1}$): 993-1080 (Si-O-Si), 777-818 (C-H stretching), 2965 ($CH_3$ asymmetrical stretch). $^1H$-NMR $\delta$ (ppm): 0.04-0.25 ($Si-CH_3$), 0.65-0.88 ($Si-CH_2$), 1.13-1.37 ($-CH_2$), 1.65-1.89 (-CH-).

## Results and Discussion

Usually the **routes** for synthesizing random block copolymers are through the mutually reactive hydroxyl end groups under non-equilibrium kinetic conditions. Synthesis of hydroxyl terminated polysiloxane has never been straightforward, since both acid or base catalysis leads to side reactions involving the terminal hydroxyl group (*34*, *35*). This leads to loss of end group functionality and in turn to loss of molecular weight control. Although NMR spectroscopy is one of the most frequently used tools for the structural analysis of copolymers, assigning the spectrum is complicated for the configurational sequences of multiple monomers (*36*). Siloxane homopolymers having the cyclopentyl and cyclohexyl groups were synthesized to be used as controls for comparison with the copolymers.

Downloaded by UNIV OF DELAWARE MORRIS LIB on June 23, 2012 | http://pubs.acs.org
Publication Date (Web): November 9, 2010 | doi: 10.1021/bk-2010-1051.ch004

In this study, there was an attempt to prepare both random and block copolymers of polydimethylsiloxanes with cyclopentyl or cyclohexyl siloxanes. The copolymers were compared to homopolymers of the corresponding cycloaliphatic siloxanes through NMR and FTIR data. The glass transition temperatures of the polymers were also compared through DSC and rheological measurements. Hydrolytic condensation of organoalkoxysilanes and/or oligomers is the usual methodology to prepare polyorganosiloxane resins. Scheme 1, shows the synthetic route to the homopolymers and copolymers. By adding a weakly acidic compound to the reaction mixture to adjust the reaction mixture to pH 2-5, the alcohol by-product can be distilled off from the reaction mixture without altering the polyorganosiloxane resins.

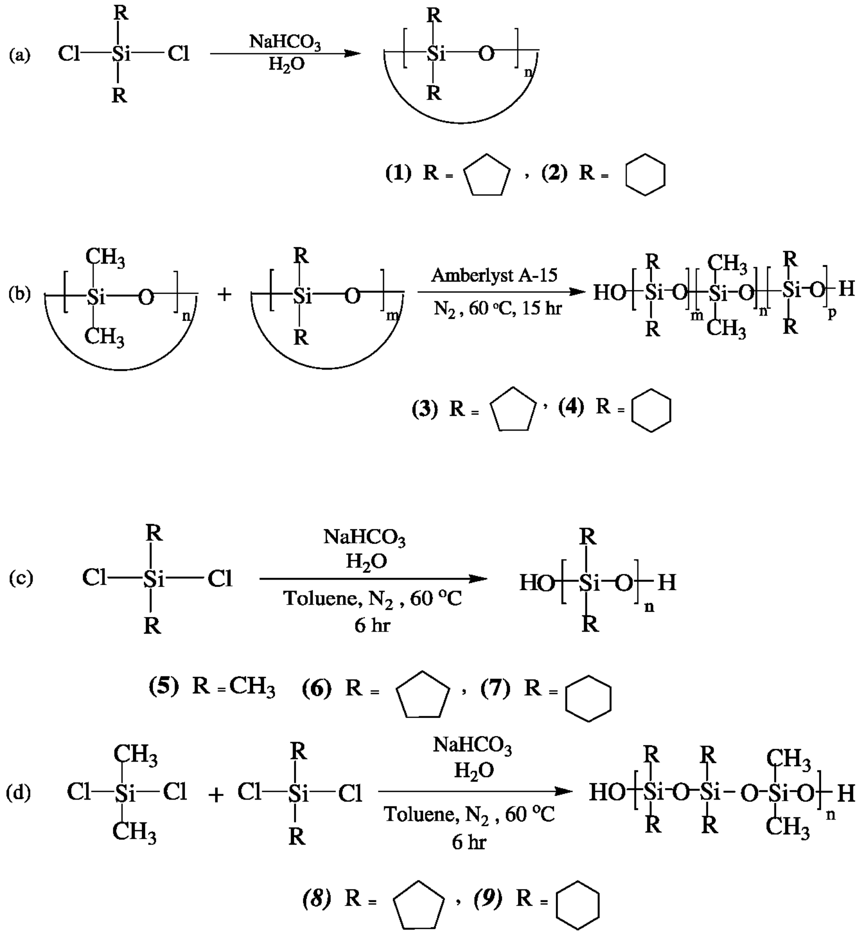

*Scheme 1. Route for synthesis of homopolymers and copolymers **(a)**Cyclic oligomer synthesis by hydrolytic condensation of dichlorosilanes, **(b)** Block copolymer synthesis by ROP of cyclic oligomers **(c)** Homopolymer synthesis by condensation of di substituted dichlorosilane **(d)** Random copolymer synthesis by condensation of two different di substituted dichlorosilanes*

Downloaded by UNIV OF DELAWARE MORRIS LIB on June 23, 2012 | http://pubs.acs.org
Publication Date (Web): November 9, 2010 | doi: 10.1021/bk-2010-1051.ch004

## Characterization

The cyclic oligomers of polydicyclopentylsiloxane (PDPS) and polydicyclohexylsiloxane (PDHS) are a clear yellow and a white oily liquid, respectively. Figure 1 shows the FTIR of homopolymers and copolymers of polydicyclohexylsiloxane (PDHS).

The three main stretching peaks in the FT-IR spectra of cyclic oligomers present at 1000- 1100 cm$^{-1}$ are due to the siloxane (Si-O-Si) bond stretching. The C-H alkylene group of the cycloaliphatic moiety occurs at 2800 cm$^{-1}$, and the C-H stretch of the methyl group occurs around 300 cm$^{-1}$. A sharp absorption can be found at 795 cm$^{-1}$ for copolymers. It is due to the C-H stretching vibrations of the methyl group of PDMS present in either the random or block copolymer with PDHS. In PDHS homopolymer, due to the absence of the $CH_3$-Si bond, this absorbtion is absent. At 2960 cm$^{-1}$, there is an absorption in the random and block copolymers which is absent in the PDHS homopolymer. This is due to asymmetrical stretching of the methyl group ($\upsilon_{as}$ $CH_3$) group of PDMS present in the copolymers, which is absent in the PDHS homopolymer. The corresponding spectrum for polydicyclopentylsiloxane is very similar and hence is not shown.

Figure 2 gives $^1$H-NMR spectra of homopolymers and copolymers of polydicyclohexyl- siloxane (PDHS). The random and block copolymers were synthesized from equimolar proportions of PDHS and PDMS.

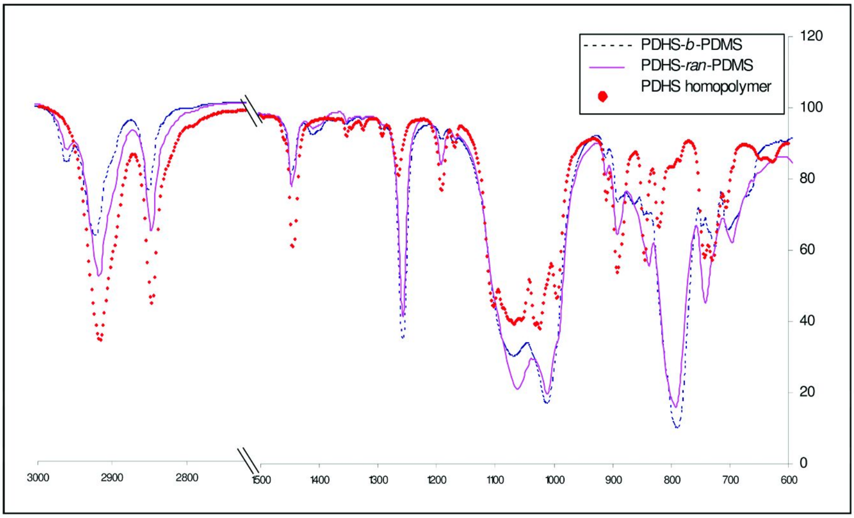

*Figure 1. FT-IR of homopolymer and copolymer of polydicyclohexylsiloxane (PDHS)*

Downloaded by UNIV OF DELAWARE MORRIS LIB on June 23, 2012 | http://pubs.acs.org
Publication Date (Web): November 9, 2010 | doi: 10.1021/bk-2010-1051.ch004

In the block copolymer of PDHS and PDMS, i.e. PDHS-b-PDMS, the ratio of integration of three protons of methyl to eleven protons of cyclohexyl group is 3.3, the theoretical value being 3.6. Spectral differences between homopolymers, block and random copolymers are good and clear indications for distinguishing between the polymers. The NMR spectra of block copolymers are expected to be almost the superimposition of the spectra of the corresponding homopolymers. In functionally terminated polymers, the block copolymers can be distinguished from the mixture of the corresponding homopolymers by the resonances of the end groups, even though the predominant part of the spectra of the block copolymer and homopolymer mixture is the same. But in this case since the block copolymers are not end capped the $^{1}$H-NMR spectra are indistinguishable from homopolymer mixtures (*36*).

In random copolymer PDMS-random-PDHS, there is an appearance of additional resonance such as at $\delta$ 0.71 and $\delta$ 2.39 due to random distribution of cyclohexyl and methyl groups along the backbone. Methylene and methine units of cycloaliphatic group showed complicated splitting around the methyl (Si-$\underline{CH_3}$) resonance ($\delta$ 0.04 to 0.25 ppm) owing to the presence of different types of monomer sequences. Similarly in Figure 2(b), the proton NMR spectra of block copolymer of PDPS and PDMS, is a superimposition of spectra of homopolymer of PDMS and PDPS, respectively. An additional resonance at 1.0 and 2.37 ppm is present.

Figure 3 gives $^{13}$C-NMR spectra of homopolymers and copolymers of polydicyclohexylsiloxane (PDHS). As in the case of the $^{1}$H-NMR spectrum, $^{13}$C-NMR spectrum of the block copolymer is indistinguishable from the superposition of the two homopolymers PDMS and PDHS in Figure 3(b). The PDHS homopolymer $^{13}$C-NMR spectrum consists of four resonances appearing at $\delta$ 26.25, 26.63, 27.51 and 28.69 ppm. The four resonances correspond to the four types of carbon in dicyclohexylsiloxane. In the random copolymer of PDHS and PDMS complicated splitting of cyclohexyl and methyl carbon resonances occurs with the appearance of additional resonances at $\delta$ 37.8, 39.5, 51.0, and 53.6 ppm. The carbon NMR spectra of homopolymers and copolymers of PDPS, show a similar trait.

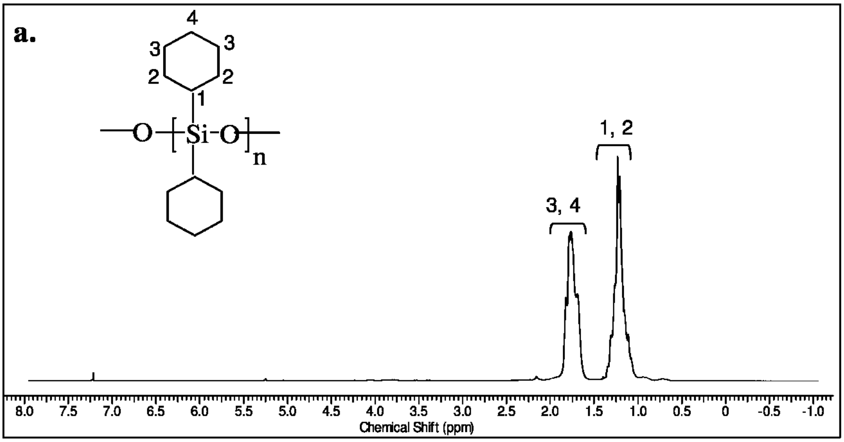

Downloaded by UNIV OF DELAWARE MORRIS LIB on June 23, 2012 | http://pubs.acs.org
Publication Date (Web): November 9, 2010 | doi: 10.1021/bk-2010-1051.ch004

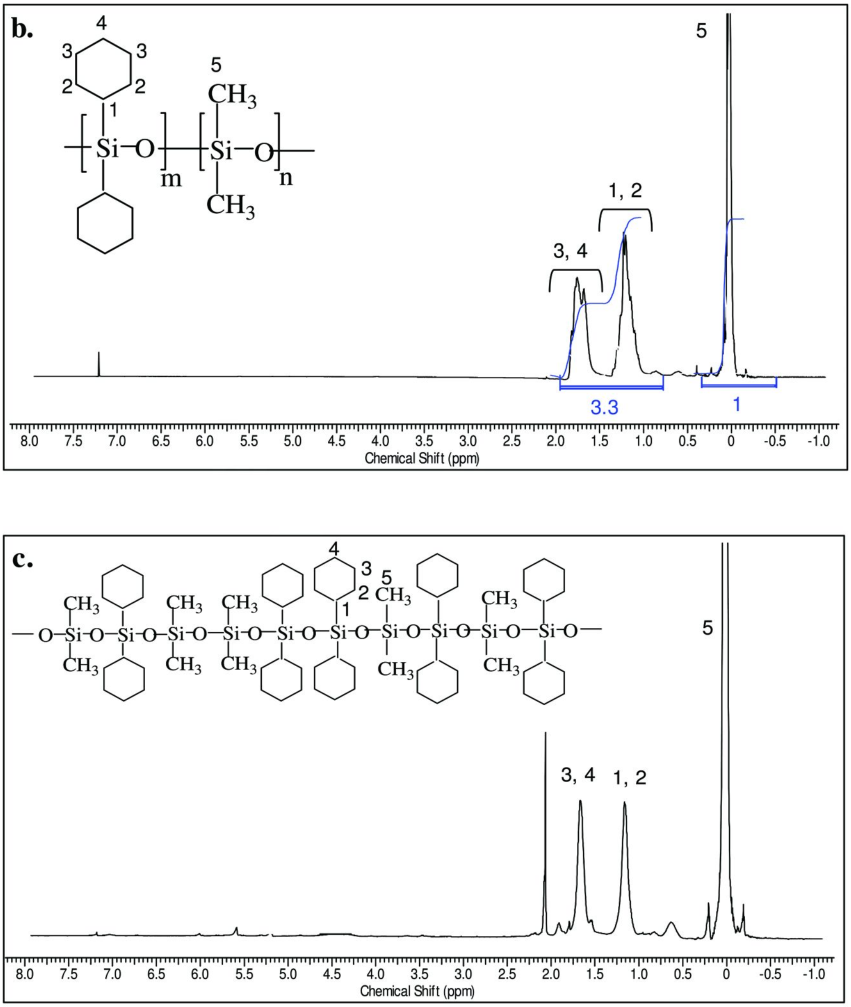

*Figure 2. ¹H-NMR spectra of (a) polydicyclohexylsiloxane (PDHS) homopolymers, (b) block copolymer of PDHS and PDMS, (c) random copolymer of PDHS and PDMS*

Downloaded by UNIV OF DELAWARE MORRIS LIB on June 23, 2012 | http://pubs.acs.org
Publication Date (Web): November 9, 2010 | doi: 10.1021/bk-2010-1051.ch004

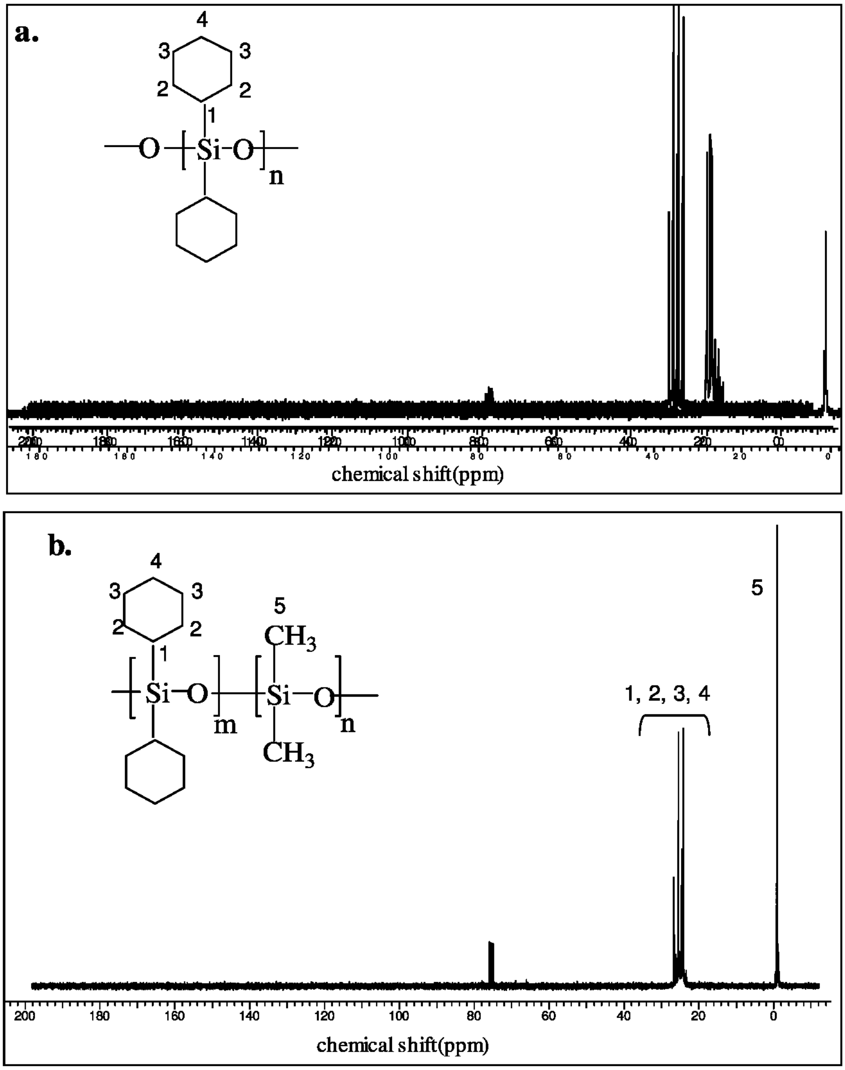

Downloaded by UNIV OF DELAWARE MORRIS LIB on June 23, 2012 | http://pubs.acs.org
Publication Date (Web): November 9, 2010 | doi: 10.1021/bk-2010-1051.ch004

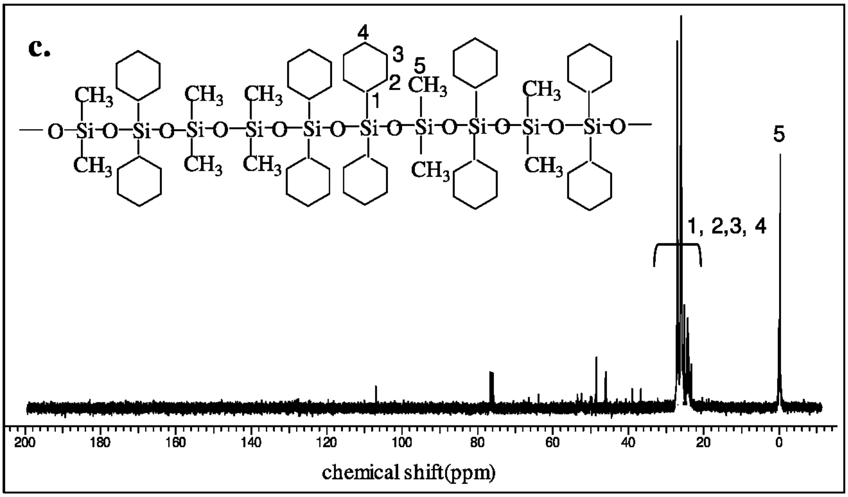

*Figure 3. ${}^{13}$C-NMR of of (a) polydicyclohexylsiloxane (PDHS) homopolymers, (b) block copolymer of PDHS and PDMS, (c) random copolymer of PDHS and PDMS*

Figure 4 gives the ${}^{29}$Si-NMR spectra of homopolymers and copolymers of polydicyclohexylsiloxane (PDHS). The resonance at δ 0 ppm is due to the TMS standard. The Si resonance due to dicyclopentyl in PDHS homopolymer appears at δ -39.5 ppm. The Si-NMR spectrum of the block copolymer, shows no splitting of resonance due to the Si atom of PDMS. The random copolymer shows complicated splitting around PDMS Si (-20 ppm ) and PDHS Si (-39.5 ppm), due to random monomer sequences.

The differential scanning calorimetry thermograms of homo, block, and random copolymers of PDHS and PDPS are given in Figures 5(a), (b), and (c) respectively. Since PDMS is completely miscible with PDPS and PDHS, the DSC curves show a single and narrow glass transition temperature ($T_g$). The $T_g$ (-65 °C) of random copolymer PDHS-*ran*-PDMS was found to be very close to the $T_g$ (-56 °C) of homopolymer PDHS. The bulky cyclohexyl group of PDHS dominates over the thermal transition of the constituent PDMS in the random copolymer and hence the $T_g$ of the random copolymer and the homopolymer of PDHS are very close. The $T_g$ of the block copolymer PDHS-*b*-PDMS is (-82°C ) intermediate between those of the homopolymers but is much nearer to the PDHS value than the PDMS value.

Downloaded by UNIV OF DELAWARE MORRIS LIB on June 23, 2012 | http://pubs.acs.org
Publication Date (Web): November 9, 2010 | doi: 10.1021/bk-2010-1051.ch004

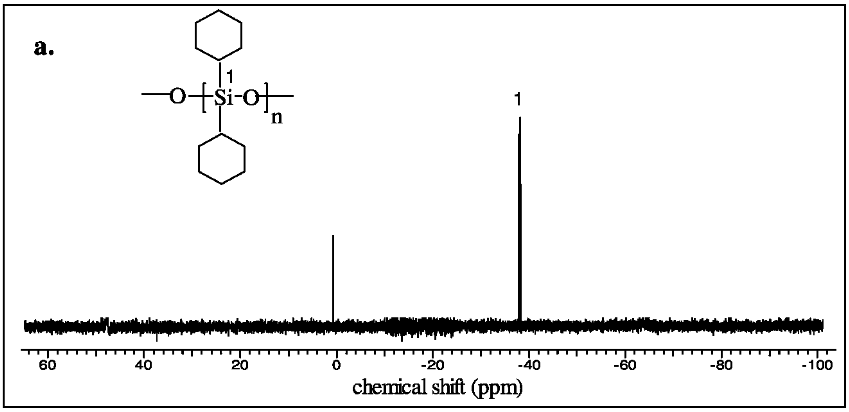

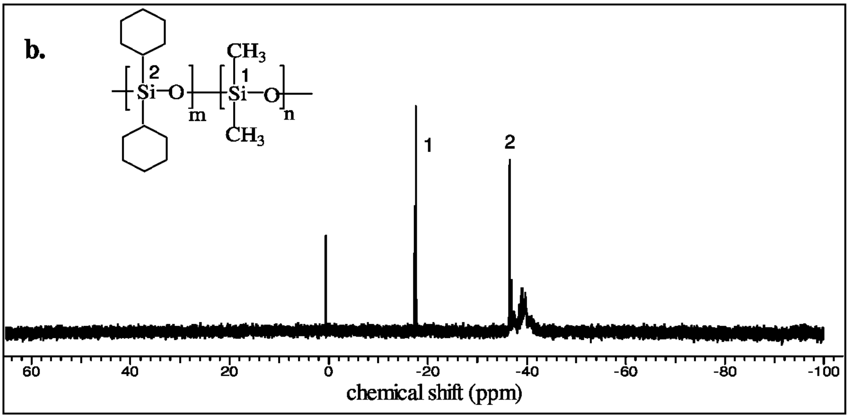

Downloaded by UNIV OF DELAWARE MORRIS LIB on June 23, 2012 | http://pubs.acs.org
Publication Date (Web): November 9, 2010 | doi: 10.1021/bk-2010-1051.ch004

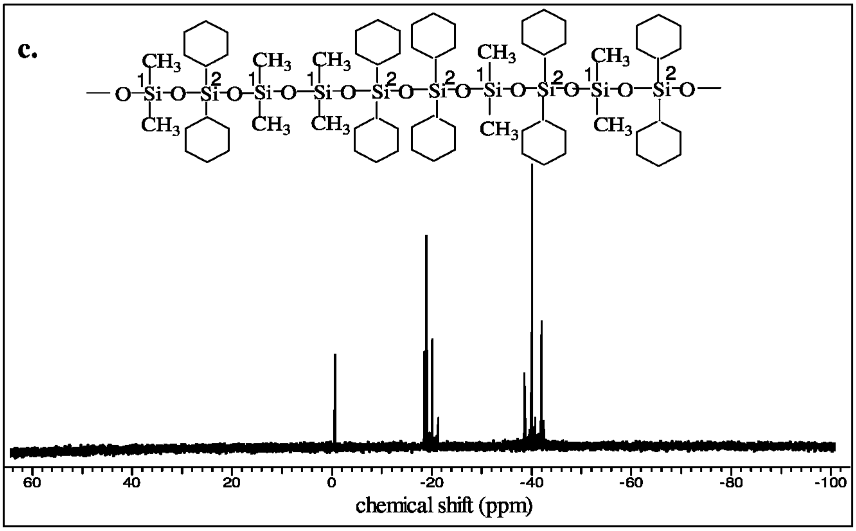

*Figure 4. $^{29}$Si-NMR of (a) polydicyclohexylsiloxane (PDHS) homopolymers, (b) block copolymer of PDHS and PDMS, (c) random copolymer of PDHS and PDMS*

The Advanced Rheometric Expansion System (ARES, TA Instruments) was used at a constant angular frequency of 1 rad/s for dynamic temperature sweep experiments. The $T_g$ was obtained as the maximum of tan δ. Figures 6 (a), (b), and (c) show the glass transition temperature of (a) homopolymers (b) block copolymers, (c) random copolymers of polydicyclohexylsiloxane (PDHS) and polydicyclopentylsiloxane (PDPS) obtained from DMA respectively. As can be observed by comparing Figure 5(a) with 6 (a) or Figure 5 (b) with 6 (b), the trend of increase of $T_g$ remains the same irrespective of the measurement techniques used.

Downloaded by UNIV OF DELAWARE MORRIS LIB on June 23, 2012 | http://pubs.acs.org
Publication Date (Web): November 9, 2010 | doi: 10.1021/bk-2010-1051.ch004

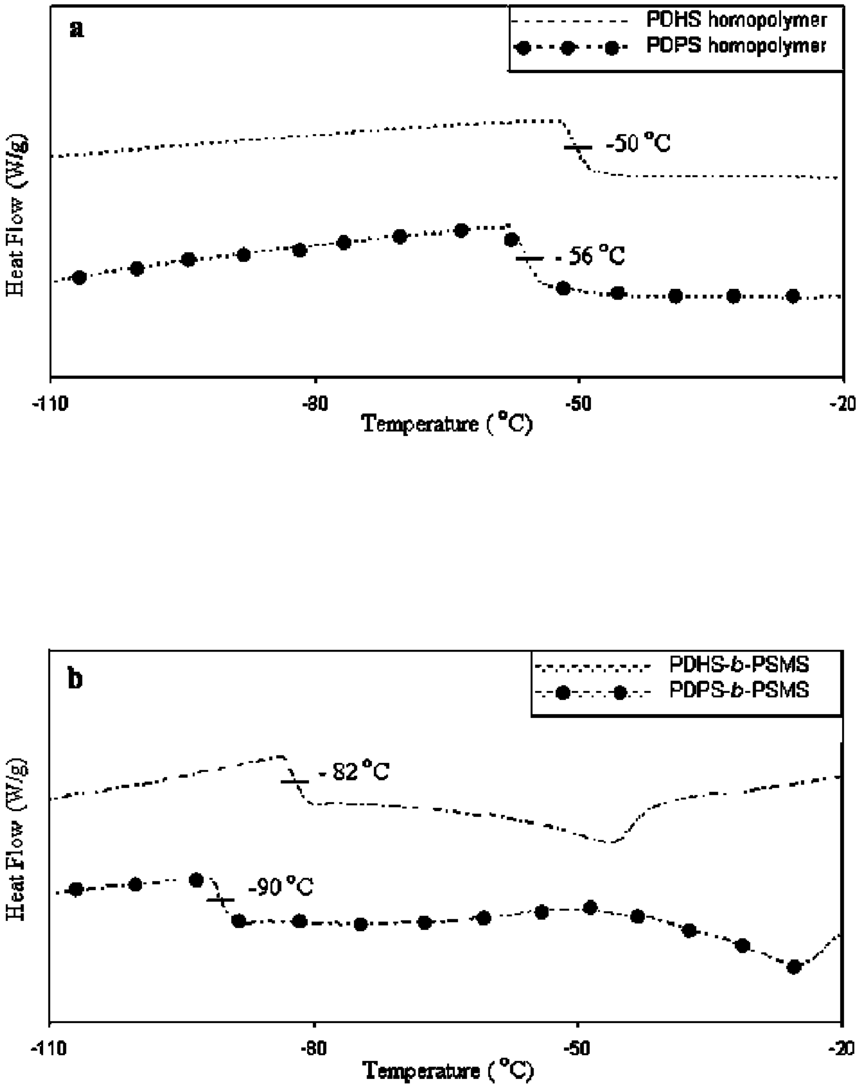

Downloaded by UNIV OF DELAWARE MORRIS LIB on June 23, 2012 | http://pubs.acs.org
Publication Date (Web): November 9, 2010 | doi: 10.1021/bk-2010-1051.ch004

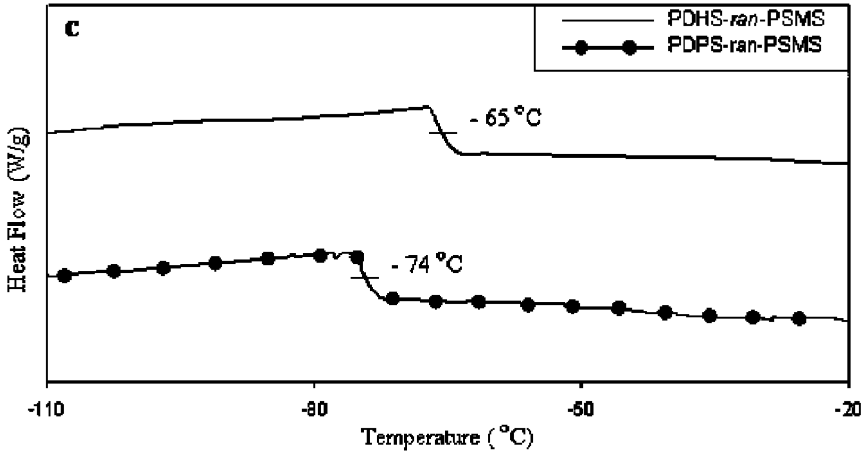

*Figure 5. DSC curves of (a) homopolymers, (b) block copolymers, (c) random copolymers Polydicyclohexylsiloxane (PDHS) and Polydicyclopentylsiloxane (PDPS)*

The relationship between the $T_g$ of random and block copolymers of polydimethylsiloxane (PDMS) with polydicyclopentylsiloxane (PDPS) and polydicyclohexyl siloxane (PDHS) was compared to the homopolymers using Fox equation (*37*). The Fox equation is based on free-volume concepts and can be expressed as follows:

$$\frac{1}{T_g} = \sum \frac{w_i}{T_{gi}} \qquad (1)$$

where $w_i$ is the weight fraction of monomer i and $T_{gi}$ and $T_g$ are the glass transition temperatures of homopolymers i and the copolymers, respectively. It is observed that the $T_g$ values predicted by the Fox equation are in good agreement with the experimental $T_g$ values of the block copolymers found by DSC measurements but not for the random copolymers (Table 1).

Downloaded by UNIV OF DELAWARE MORRIS LIB on June 23, 2012 | http://pubs.acs.org
Publication Date (Web): November 9, 2010 | doi: 10.1021/bk-2010-1051.ch004

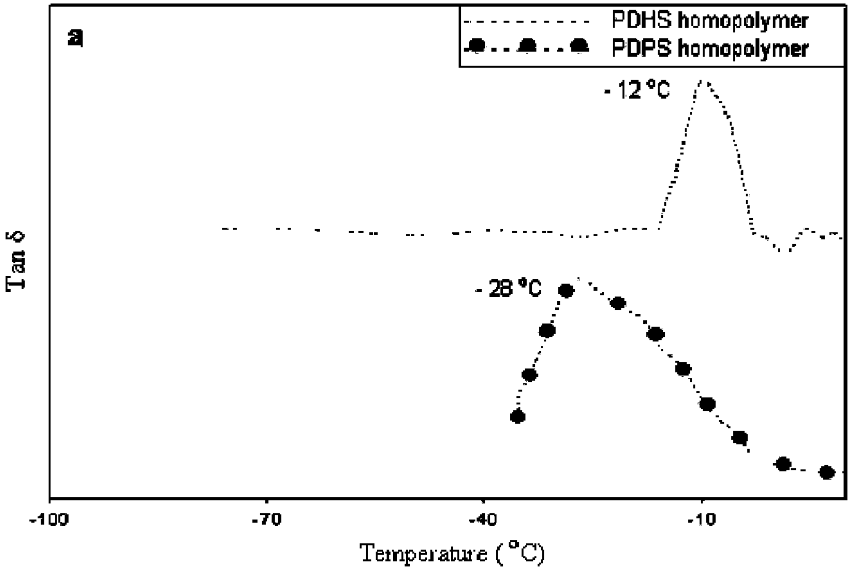

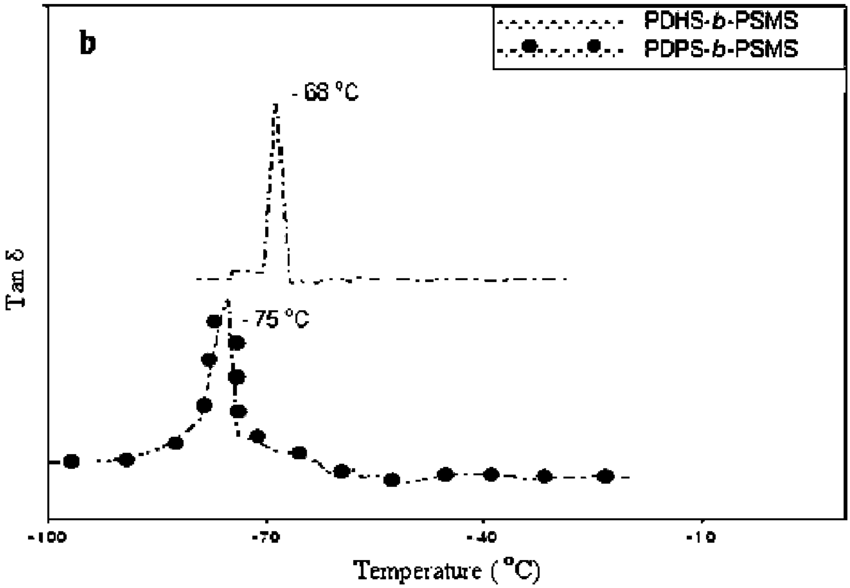

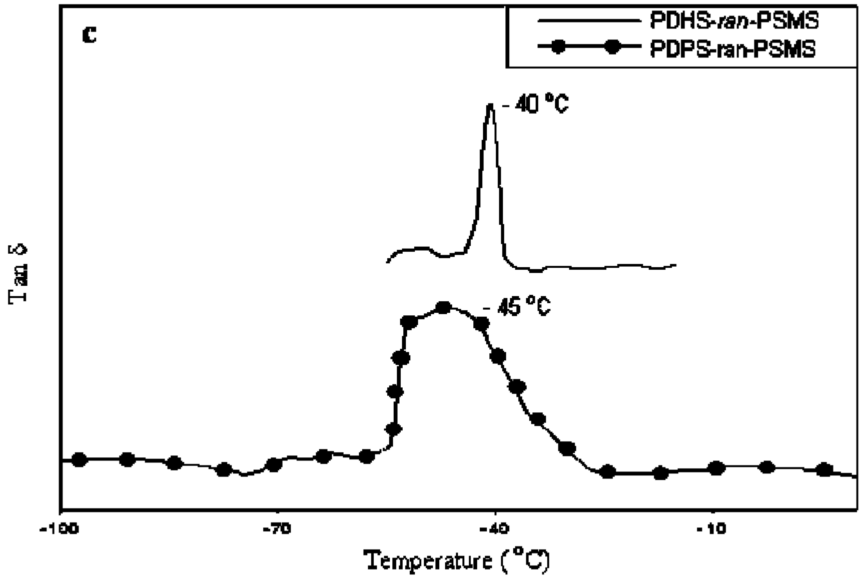

*Figure 6. Glass transition temperature (α-transition) of (a) homopolymers, (b) block copolymers, (c) random copolymers of polydicyclohexylsiloxane (PDHS) and polydicyclopentylsiloxane (PDPS) from DMA*

**Table 1. Comparison of Tg values obtained experimentally and predicted by the Fox equation**

| *Sample Name* | *Weight Fractions* | *$T_g$ (°C)* | |
|---|---|---|---|
| | | *Experimental (DSC)* | *Calculated by Fox $eq^n$* |
| PDPS-*b*-PDMS | 0.75 : 0.25 | -90 | -94 |
| PDHS-*b*-PDMS | 0.78 : 0.22 | -82 | -86 |
| PDPS-*ran*-PDMS | 0.65 : 0.35 | -50 | -95 |
| PDHS-*ran*-PDMS | 0.67 : 0.33 | -56 | -88 |

Hydroxy terminated polysiloxanes are of great importance due to their reactivities towards isocyantes and carboxylic acids (and their derivatives) (*38*, *39*). This reactivity allows for subsequent synthesis of segmented polyurethanes, polyesters and polycarbonates (*40–42*). Block copolymers seem to be particularly interesting because of an unusually high mobility of the silicon-oxygen chain (*43*, *44*). These polymers are soluble in various organic solvents making siloxanes useful in many applications (*45*, *46*) as additives for solvent-containing and also low-solvent finishes (*47*), surface coatings and pastes, textile coatings (*48*) and paper (tissues) (*49*), as starting materials for cross-linking reactions (*50*), as

Downloaded by UNIV OF DELAWARE MORRIS LIB on June 23, 2012 | http://pubs.acs.org
Publication Date (Web): November 9, 2010 | doi: 10.1021/bk-2010-1051.ch004

Downloaded by UNIV OF DELAWARE MORRIS LIB on June 23, 2012 | http://pubs.acs.org
Publication Date (Web): November 9, 2010 | doi: 10.1021/bk-2010-1051.ch004

antifoams (*51*), as emulsifiers (*52*), as additives in cosmetic formulations (*53*) etc. The linkage of different siloxane blocks in one molecule has unusual and surprising effects in various application tests. The various siloxane blocks can be linked to one another via coupling agents (*54*, *55*). The blocks may differ from one another in polarities (*56*), hydrophilic / hydrophobic balance (*52*, *57*), or in the proportions of reactive groups (*58*).

## Conclusion

Synthesis of random and block copolymers of PDMS was accomplished with either PDPS and PDHS. Control of copolymerization can be achieved for copolymers of dimethyl dicycloaliphatic groups. The synthesized polymers were characterized and compared using $^{1}$H-NMR, $^{13}$C-NMR, $^{29}$Si-NMR, FT-IR, DSC and ARES techniques. The $T_g$ of random copolymers were found to be higher than the corresponding block copolymer $T_g$. There was very little difference in $T_g$ of homopolymers PDPS and PDHS from the $T_g$ of the corresponding random copolymers synthesized with PDMS i.e PDPS-*ran*-PDMS and PDHS-*ran*-PDMS.

## References

1. Yilgor, I.; Steckle, W. P.; Yilgor, E.; Freelin, R. G.; Riffle, J. S. *J. Polym. Sci., Part A: Polym. Chem.* **1989**, *27* (11), 3673.
2. Gomes, D.; Peinemann, K. V.; Nunes, S. P.; Kujawski, W.; Kozakiewicz, J. *J. Membr. Sci.* **2006**, *281* (1−2), 747.
3. Amin, M.; Akbar, M.; Amin, S. *Rev. Adv. Mater. Sci.* **2007**, *16* (1−2), 10.
4. Sangermano, M.; Bongiovanni, R.; Malucelli, G.; Roppolo, I.; Priola, A. *Prog. Org. Coat.* **2006**, *57* (1), 44.
5. Connell, J. W.; Crivello, J. V.; Bi, D. *J. Appl. Polym. Sci.* **1995**, *57* (10), 1251.
6. Park, S. J.; Jin, F. L.; Park, J. H.; Kim, K. S. *Mater. Sci. Eng. A* **2005**, *399* (1−2), 377.
7. Yilgor, I.; McGrath, J. E. *Polym. Prepr.* **1985**, *26* (1), 57.
8. Angelopoulos, M.; Ariram, A.; Guarnieri, R. C.; Huang, W. S.; Kwong, R.; Moreau, W. M. European Patent 1,521,797, 2005.
9. Hale, P. D.; Inagaki, T.; Karan, H. I.; Okamoto, Y.; Skotheim, T. A. *J. Am. Chem. Soc.* **1989**, *111* (9), 3482.
10. Thomas, J.; Choi, S. B.; Fjeldheim, R.; Boudjouk, P. *Biofouling* **2004**, *20* (4−5), 227.
11. Antonen, R. C.; Kookootsedes, G. J.; Field, A. J. U.S. Patent 3,703,562, 1972.
12. Greubel, P. W. U.S. Patent 3,221,650, 1965.
13. Goyel, S. K. U.S. Patent 4,961,840, 1990.
14. Chou, C.; Yang, M. H. *J. Therm. Anal.* **1993**, *40* (2), 657.
15. Kushibiki, N.; Takeuchi, K.; Kobayashi, H.; Masatomi, T.; Yoshinaga, K.; Hashimoto, Y.; Nishida, S. European Patent 7,71,805, 1997.

16. Meszaros, O.; Schmidt, P.; Pospisil, J.; Nespurek, S. *J. Polym. Sci., Part A: Polym. Chem.* **2004**, *42* (3), 714.
17. Noshay, A.; McGrath, J. E. *Block Copolymers: Overview and Critical Survey*; Academic Press: New York, 1977.
18. Landry, C. J. T.; Coltrain, B. K.; Teegarden, D. M.; Long, T. E.; Long, V. K. *Macromolecules* **1996**, *29* (13), 4712.
19. Ochi, M.; Takemiya, K.; Kiyohara, O.; Nakanishi, T. *Polymer* **1999**, *41* (1), 195.
20. Kuo, C. M.; Clarson, S. J. *PMSE Polym. Prepr.* **1991**, *32* (3), 183.
21. Gee, R. P.; Keil, J. W. U.S. Patent 4,122,029, 1978.
22. Liu, Q.; Shi, W.; Babonneau, F.; Interrante, L. V. *Chem. Mater.* **1997**, *9* (11), 2434.
23. Nye, S. A.; Riccio, D. A.; Wutzer, B. S. U.S. Patent 5,698,654, 1997.
24. Kopylov, V. M.; Kovjazin, V. A. Investigation of Organosiloxane Equilibrium Reactions. In *Polymer Yearbook 16*; Pethrick R. A., Ed.; CRC Press, Inc.: Boca Raton, FL, 1999.
25. Graiver, D.; Fearon, G. Polysiloxanes: Direction of Applications and Perspectives. In *Silicon-Containing Polymers*; Jones, R. G., Ando, W., Chojnowski, J., Eds.; Kluwer Academic Publishers: Boston, 2000.
26. Kricheldorf, H. R. *Handbook of Polymer Synthesis, Part B*; Marcel Dekker: New York, 1991; p 1148.
27. Steckle, W. P.; Yilgor, E.; Riffle, J. S.; Spinu, M.; Yilgor, I.; Ward, R. S. *Polym. Prepr.* **1987**, *28* (1), 254.
28. Noll, W. *Chemistry and Technology of Silicones*; Academic Press: New York, 1968.
29. Mazurek, M. Silicone Copolymer Networks and Interpenetrating Polymer Networks. In *Silicon-Containing Polymers*; Jones, R. G., Ando, W., Chojnowski, J., Eds.; Kluwer Academic Publishers: Boston, 2000.
30. Rempp, P. F.; Franta, E. *Adv. Polym. Sci.* **1984**, *58*, 1.
31. Goethals, E. J. *Telechelic Polymer: Synthesis and Applications*; CRC Press, Inc.: Boca Raton, FL, 1989.
32. Kunzler, J. F.; Seelye, D. E. U.S. Patent 6,891,010, 2005.
33. Yoon, J. W.; Jhung, S. H.; Kim, T. J.; Lee, H. D.; Jang, N. H.; Chang, J. S. *Bull. Korean Chem. Soc.* **2007**, *28* (11), 2075.
34. Kojima, K.; Gore, C. R.; Marvel, C. S. *J. Polym. Sci., Part A: Polym. Chem.* **1966**, *4* (9), 2325.
35. Speier, J. L.; David, M. P.; Eynon, B. A. *J. Org. Chem.* **1960**, *25*, 1637.
36. Kitayama, T.; Ute, K.; Yamamoto, M.; Fujimoto, N.; Hatada, K. *Polym. Bull.* **1991**, *25* (6), 683.
37. Fox, T. G. *Bull. Am. Phys. Soc.* **1956**, *1*, 123.
38. Nitzsche, S.; Wick, M. U.S. Patent 3,070,566, 1959.
39. Homrighausen, C. L.; Keller, T. M. *J. Polym. Sci., Part A: Polym. Chem.* **2001**, *40* (1), 88.
40. Chun, Y. C.; Kim, K. S.; Shin, J. S.; Kim, K. H. *Polym. Int.* **1992**, *27* (2), 177.
41. Matzner, M.; Noshay, A.; Barclay, R. U.S. Patent 3,701,815, 1972.
42. Buechner, W.; Noll, W.; Bressel, B. U.S. Patent 3,819,744, 1973.

Downloaded by UNIV OF DELAWARE MORRIS LIB on June 23, 2012 | http://pubs.acs.org
Publication Date (Web): November 9, 2010 | doi: 10.1021/bk-2010-1051.ch004

43. Tyagi, D.; Wilkes, G. L.; Yilgor, I.; McGrath, J. E. *Polym. Bull.* **1982**, *8* (11−12), 543.
44. Nagaoka, K.; Naruse, H.; Shinohara, I.; Watanaba, M. *J .Polym. Sci., Part C: Polym. Lett.* **1984**, *22* (12), 659.
45. Auner, N.; Weis, J. *Organosilicon Chemistry IV: From Molecules to Materials*; Wiley-VCH: New York, 2000; p527.
46. Scibiorek, M.; Gladkova, N. K.; Chojnowski, J. *Polym. Bull.* **2000**, *44* (4), 377.
47. Brock, T.; Mischke, P.; Groteklaes, M. *European Coatings Handbook*; Vincentz Network GmbH & Co. KG: Hanover, Germany, 2000; p 156.
48. Schindler, W. D.; Hauser, P. J. *Chemical Finishing of Textiles*; Woodhead Publishing: Cambridge, U.K., 2004; p 169.
49. Klofta, T. J.; Warner, A. V. WO Patent 9,535,411, 1995.
50. Marko, O. W. U.S. Patent 4,360,687, 1982.
51. Holmberg, K. *Novel Surfactants: Preparation, Applications, and Biodegradability*; Marcel Dekker, Inc.: New York, 2003; p 601.
52. Hill, R. M. *Silicone Surfactants*; Marcel Dekker, Inc.: New York, 1999.
53. Elliott, T. J.; Ford, D. I. U.S. Patent 4,246,257, 1981.
54. Smaihi, M.; Schrotter, J. C.; Lesimple, C.; Prevost, I.; Guizard, C. *J. Membr. Sci.* **1999**, *161* (1−2), 157.
55. Hoxmeier, R. J. U.S. Patent 5,276,095, 1994.
56. Szycher, M. *Szycher's Handbook of Polyurethanes*; CRC Press, Inc.: Boca Raton, FL, 1999.
57. Yosomiya, R. M. *Adhesion and Bonding in Composites*; Marcel Dekker, Inc.: New York, 1990; p 156.
58. Burkhart, G.; Langenhagen, R. D.; Weier, A. U.S. Patent 6,730,749, 2004.

Downloaded by UNIV OF DELAWARE MORRIS LIB on June 23, 2012 | http://pubs.acs.org
Publication Date (Web): November 9, 2010 | doi: 10.1021/bk-2010-1051.ch004

Downloaded by CORNELL UNIV on June 25, 2012 | http://pubs.acs.org
Publication Date (Web): November 9, 2010 | doi: 10.1021/bk-2010-1051.ch005

## Chapter 5

# Trypsin-Catalyzed Cross-Linking of α,ω-Triethoxysilyl-Terminated Polydimethylsiloxane: An Experimental and Computational Approach

**Paul M. Zelisko,* Travis Dudding,† Karen R. Arnelien, and Heidi Stanisic**

**Department of Chemistry, Brock University, 500 Glenridge Ave.,**
**St. Catharines, Ontario, Canada L2S 3A1**
***Corresponding author. Tel: +1-905-688-5550 ext. 4389,**
**Fax: +1-905-682-9020, E-mail: pzelisko@brocku.ca**
**†E-mail: tdudding@brocku.ca**

Dibutyltin dilaurate is typically employed as a catalyst to bring about the hydrolysis, and subsequent condensation, of silicones to form cross-linked networks in the room temperature vulcanization (RTV) process. However, given the interest in using silicones as biomaterials, sealants, and lubricants, potentially toxic tin-based catalysts can limit the use of silicones in these applications. This study describes the use of enzymes as catalysts for the cross-linking of silicones in place of the more toxic catalyst systems such as those based on tin. The results indicate that trypsin effectively catalyzes the cross-linking of α,ω-(triethoxysilyl)ethyl-polydimethylsiloxane (TES-PDMS), similar to dibutyltin dilaurate; $^{29}$Si-NMR experiments revealed little difference between the products of the dibutyltin dilaurate- and trypsin-catalyzed systems. Computational methods are being employed to determine the mechanism occurring within the enzymes' active site during the RTV process. The computational studies have demonstrated that the enzyme-catalyzed cross-linking mechanism displays components of both natural trypsin chemistry as well as solution-phase silicon chemistry. The use of these techniques

In Advances in Silicones and Silicone-Modified Materials; Clarson, S., et al.;
ACS Symposium Series; American Chemical Society: Washington, DC, 2010.

Downloaded by CORNELL UNIV on June 25, 2012 | http://pubs.acs.org
Publication Date (Web): November 9, 2010 | doi: 10.1021/bk-2010-1051.ch005

in the development of enzyme-based methodologies for performing "green" silicone reactions will be discussed.

# Introduction

Silicon is one of the most abundant elements in the Earth's crust. As a result, perhaps not surprisingly, the juxtaposition of silica, the principal form of natural inorganic silicon, with biological systems including proteins, is not a novel concept (*1*). Nature has made use of silica in biological environments both as an essential nutrient and as the skeleton of certain marine organisms (*1*, *2*). Controlled silica formation has even been accomplished *in vitro* using mammalian digestive enzymes (*3*). Although enzymes have been used to form carbohydrate-modified silicones, to the best of our knowledge the cross-linking of silicone polymers using enzymes has not been examined (*4*).

Tin catalysts are often employed in the cross-linking of silicones, however, given the interest in using silicones as biomaterials, the use of potentially toxic tin compounds as catalysts can be limiting in this regard (*5*, *6*). Silicones and proteins are not incompatible species (*5c*, *7*). Research conducted by both Morse *et al.* and Bassindale *et al.* has demonstrated the ability of silicatein and trypsin, respectively, to catalyze the hydrolysis and subsequent condensation of tetramethoxy- and tetraethoxysilanes (*3*, *8*). However, to date these experiments have focused almost exclusively on the ability of enzymes/proteins to generate inorganic silica species.

Enzymes are commonly employed to perform chemical reactions in many synthetic applications (*9*). Concomitant with using enzymes to perform chemical reactions is the need to fully understand the mechanism by which the substrate is processed by the enzyme. Given the complex nature of enzymes it is often beneficial to study the reaction mechanisms *in silico* using computational chemistry (*10*). However, even with computational methodologies studying enzymes can be unwieldy. In order to make the enzyme more manageable, theozymes are studied in place of the entire enzyme. Theozymes are truncated active site constructs for modeling enzyme catalysis from a first principles approach (*11*). This approach allows one to focus the calculation on the enzyme active site without having to worry about extraneous amino acid residues.

The focus of this paper is to examine the ability of trypsin to perform chemistry on alkoxysilyl-modified silicone polymers and to study the mechanistic details of this chemistry within the enzymes active site using computational methods.

# Experimental Section

## Reagents

Tetraethoxysilane (TEOS), vinytriethoxysilane, hydride terminated polydimethylsiloxane (H-PDMS-H) (n = ~7-8, 2-3 cSt, $M_n$ = ~580 g/mol and n = ~270, 1000 cSt, $M_n$ = ~24000 g/mol), platinum divinyl-tetramethyldisiloxane complex (3-5% platinum concentration, Karstedt's catalyst) in vinyl-terminated polydimethylsiloxane (PDMS), and dibutyltin dilaurate were purchased from

Aldrich. Bovine pancreatic trypsin (EC 3.4.21.4) was supplied by Sigma. Dichloromethane (DCM, $CH_2Cl_2$) was obtained from Caledon. Distilled water ($dH_2O$) was used in all aqueous preparations. Scanning electron micrograph (SEM) images were acquired using an AMRAY 1600T scanning electron microscope and nuclear magnetic resonance (NMR) spectra were acquired using a Bruker AV600.

### Synthesis of α,ω-(Triethoxysilyl)ethyl-polydimethylsiloxane (TES-PDMS)

A low molecular weight TES-PDMS ($TES\text{-}PDMS_{580}$) and a high molecular weight TES-PDMS ($TES\text{-}PDMS_{24000}$) were used independently in the cross-linking experiments. The synthesis of TES-PDMS is described in detail elsewhere (*12*).

Downloaded by CORNELL UNIV on June 25, 2012 | http://pubs.acs.org
Publication Date (Web): November 9, 2010 | doi: 10.1021/bk-2010-1051.ch005

### Preparation of the Trypsin Catalyst System

Trypsin was added to the reaction system either as a solution in $dH_2O$ or as a suspension in $CH_2Cl_2$. In both instances the trypsin was added to the appropriate solvent and placed in a sonicator for 1-2 min.

### Formulation of Cross-Linked Silicone Polymers

The general formulation of the cross-linked silicone involved combining commercially available TEOS ($(H_3CH_2CO)_4Si$) with either $TES\text{-}PDMS_{580}$ or $TES\text{-}PDMS_{24000}$ in a sample vial and mixed vigorously by inversion. Immediately upon the cessation of mixing, the tin catalyst dibutyltin dilaurate or a trypsin catalyst was added to the sample vial containing the silicon-based compounds. The vial was subsequently capped and the contents mixed for a further 5 min by inverting the vial end-over-end. Once the mixing cycle was complete, the contents were poured into either a small (3.5 cm diameter) Petri dish or a separate sample vial and were left uncovered for 30 min. The dish or vial cap was then replaced and the reaction was left covered on the lab bench at either ambient temperature or in an incubator at 37° Celsius. The exact amounts for the reagents used in the cross-linking experiments are outlined in Table 1. The formation of a macroscopically homogeneous solid inside the Petri dish or the sample vial was taken as evidence for cross-linking. Formulations containing both water and dichloromethane were also examined (Table 1). The cross-linking experiments were performed at both 21°C and 37°C.

### Imaging of Cross-Linked Silicone Systems

In order to prepare the samples for SEM imaging, the sample was adhered to the SEM stub using a carbon adhesive. Once the sample was adhered to the stub, a conductive layer of gold and palladium was applied to the sample using a POLARON SC500 sputter coater. The samples were subsequently imaged using an AMRAY 1600T scanning electron microscope.

Downloaded by CORNELL UNIV on June 25, 2012 | http://pubs.acs.org
Publication Date (Web): November 9, 2010 | doi: 10.1021/bk-2010-1051.ch005

**Table 1. Formulations used in silicone cross-linking experiments**

| | *Reagents* | | | | | | | |
|---|---|---|---|---|---|---|---|---|
| *Entry* | *Trypsin (g)* | *TEOS (g)* | *TES-PDMS-1*[a] *(g)* | *TES-PDMS-2*[b] *(g)* | *Sn*[c] *(g)* | *$H_2O$ (mL)* | *DCM (mL)* | *Temp (°C)* |
| *1* | - | 0.28 | 0.44 | - | - | - | - | 21 |
| *2* | - | 0.26 | 0.40 | - | 0.06 | - | - | 21 |
| *3* | 0.26 | 0.34 | 0.41 | - | - | 1.5 | - | 21 |
| *4* | 0.26 | 0.25 | - | 0.40 | - | - | 1.0 | 21 |
| *5* | 0.26 | 0.26 | - | 0.42 | - | 1.0 | 1.0 | 21 |
| *6* | - | 0.28 | 0.50 | - | 0.08 | 1.0 | 1.0 | 21 |
| *7* | - | 0.27 | 0.41 | - | - | 1.0 | - | 21 |
| *8* | - | 0.26 | 0.41 | - | - | 1.0 | 1.0 | 21 |
| *9* | 0.05 | 0.08 | 0.18 | - | - | 1.0 | - | 37 |
| *10* | 0.05 | - | - | - | - | 1.0 | - | 37 |
| *11* | 0.05 | 0.08 | 0.17 | - | - | 1.0 | 3.0 | 37 |

[a] TES-PDMS$_{580}$. [b] TES-PDMS$_{24000}$. [c] dibutyltin dilaurate.

### $^{29}$Si Solid-State NMR Analysis of the Cross-Linked Elastomers

NMR spectra of the silicone elastomers were acquired using a Bruker AV 600 spectrometer with a 4 mm MAS broadband probe. The silicone elastomers were cooled using liquid nitrogen and crushed using a mortar and pestle prior to being added to a zirconium oxide rotor. The sample was spinning at 7000 Hz within the NMR probe. A delay (D1) of 10.0 s and a pulse with a 30° flip angle were employed. A total of 40 960 scans were collected for each sample at 298 K.

### Computational Modeling

Computational studies using density functional theory (DFT) employing the gradient-corrected (B3LYP) hybrid functional of Becke-Lee-Yang and Parr (*13*) with a double zeta-potential 6-31G(d) (*14*) basis set as implemented by Gaussian 03 have been utilized to examine the chemistry within the enzymes' active site.

## Results and Discussion

When the TEOS and TES-PDMS were combined in the absence of either dibutyltin dilaurate or trypsin (Table 1), no cross-liking was observed after a period of 2.5 months – only liquid was present; there was no evidence of elastomer or glass formation. Conversely, the addition of dibutyltin dilaurate to a solution of TEOS and TES-PDMS (Table 1, Entry 2) yielded a translucent solid in approximately 2-3 h. Even when water was added to $CH_2Cl_2$ and the mixture introduced into the formulations (Table 1, Entry 6), cross-linking of the silicone system was observed through the production of a translucent solid.

Substituting trypsin for dibutyltin dilaurate in the cross-linking experiments (Table 1) resulted in cross-linking of the TEOS/TES-PDMS system being observed in approximately 48 h at 21°C and approximately 18-20 h at 37°C. The increased rate of reaction at the elevated temperature was not unexpected given that the enzyme operates at 37°C *in vivo* (*15*). Given that the TEOS/TES-PDMS system cure time is on the order of months in the absence of any added rate-enhancing compounds, it is unlikely that this "background" rate is responsible for the accelerated cure rate observed with the systems containing trypsin. Trypsin is therefore believed to expedite the hydrolysis and subsequent condensation of the alkoxysilyl moieties. This conclusion is further supported by experiments that utilized trypsin in the production of inorganic silica (*3*).

Although the dibutyltin dilaurate- and trypsin-catalyzed systems appeared to be macroscopically homogeneous, SEM imaging of the samples revealed gross surface morphologies that differed from one sample to the other when the tin- and enzyme-catalyzed systems were compared (Figure 1). The exact cause for these differences in the surface morphologies is unclear.

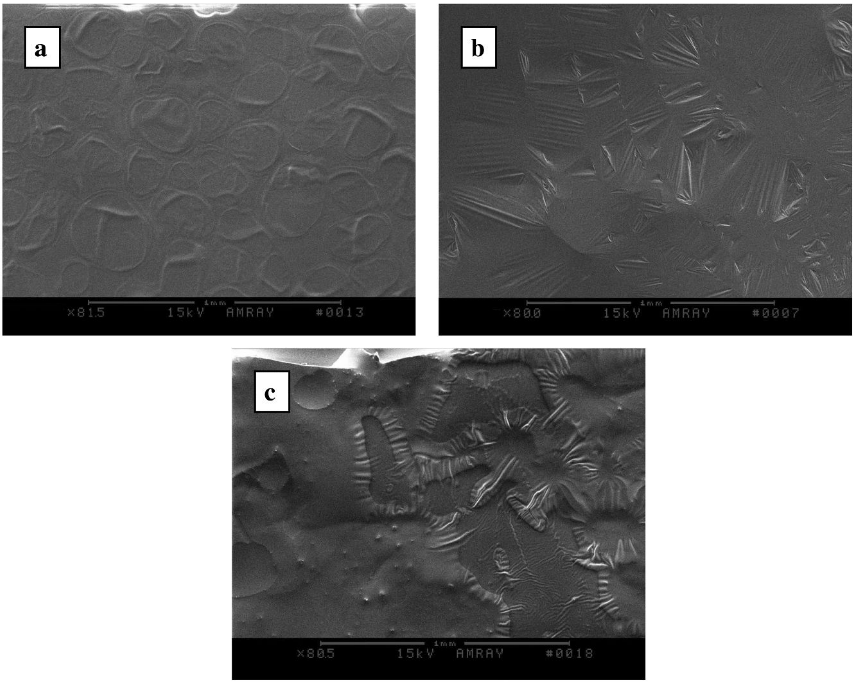

*Figure 1. SEM images of a cross-linked silicone system consisting of (a) TES-PDMS$_{580}$, TEOS, and dibutyltin dilaurate, (b) TEOS, TES-PDMS$_{24000}$, and trypsin, and (c) TEOS, TES-PDMS$_{580}$, and trypsin.*

Downloaded by CORNELL UNIV on June 25, 2012 | http://pubs.acs.org
Publication Date (Web): November 9, 2010 | doi: 10.1021/bk-2010-1051.ch005

Downloaded by CORNELL UNIV on June 25, 2012 | http://pubs.acs.org
Publication Date (Web): November 9, 2010 | doi: 10.1021/bk-2010-1051.ch005

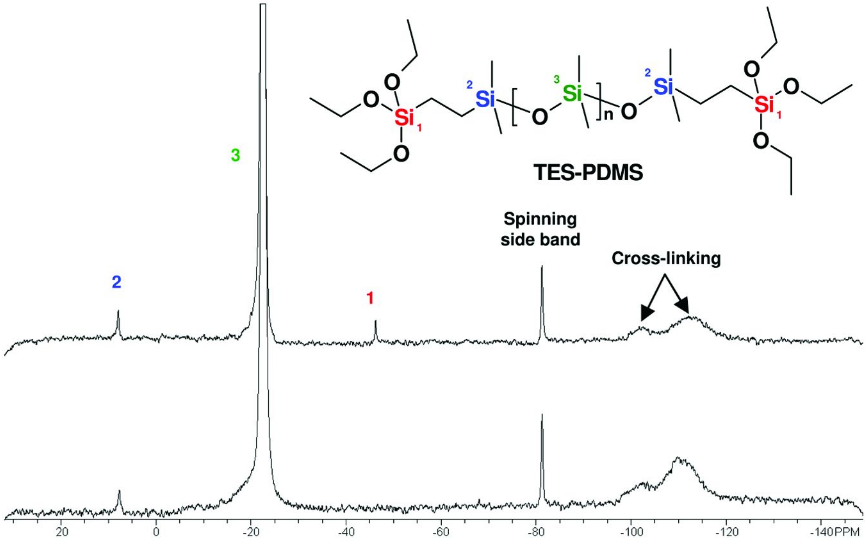

*Figure 2. The solid-state $^{29}$Si-NMR spectra of a trypsin cross-linked silicone elastomer (21°C) (top) and a dibutyltin dilaurate cross-linked silicone elastomer (bottom).*

A comparison of the $^{29}$Si solid-state NMR spectra of the dibutyltin dilaurate- and trypsin-catalyzed silicone elastomers demonstrated striking similarities between the two systems (Figure 2). In both instances a marked decrease in the resonance corresponding to the triethoxysilyl silicon atom and the evolution of signals indicative of cross-linking were observed. Based on the NMR experiments the trypsin-catalyzed system did not appear to be as efficient as the dibutyltin dilaurate-catalyzed system at room temperature based on the relative abundance of the triethoxysilyl silicon resonance (Figure 2). The presence of a spinning side-band in the NMR spectra was confirmed by altering the frequency at which the sample was spinning.

Targeting a long-term program grounded in the development of enzyme-mediated biosynthetic methodologies for the production of designer polymeric silicon materials, we are currently investigating the reaction mechanisms of trypsin-promoted silicone polymerizations computationally to assist on-going experimental efforts. It is noteworthy that, aside from a single conceptual proposal put forth by Morse and co-workers for the *in vitro* production of silica networks from alkoxysilyl precursors, a mechanistic rationale for silicatein and related trypsin and chymotrypsin serine protease-catalyzed silicone polymerization remains unsecured and certainly unaddressed within the context of accurate computation (*16*).

Upon examination of the trypsin catalytic triad (Figure 3) it became apparent that two possible mechanisms could be used to account for the cross-linking of the TEOS/TES-PDMS by the serine protease:

Downloaded by CORNELL UNIV on June 25, 2012 | http://pubs.acs.org
Publication Date (Web): November 9, 2010 | doi: 10.1021/bk-2010-1051.ch005

1. Initial formation of a serine-silicon bond – an analogue of traditional trypsin chemistry (Figure 4) (*15*)
2. Initial formation of a histidine-silicon bond – an analogue of solution-phase silicon chemistry (Figure 4) (*17*)

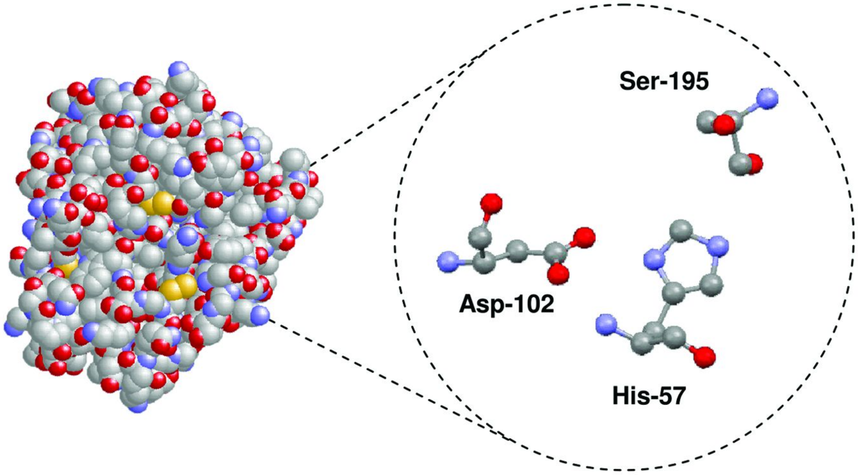
Ser-195
Asp-102
His-57

*Figure 3. The structure of bovine pancreatic trypsin and its catalytic triad (serine, histidine, and aspartic acid).*

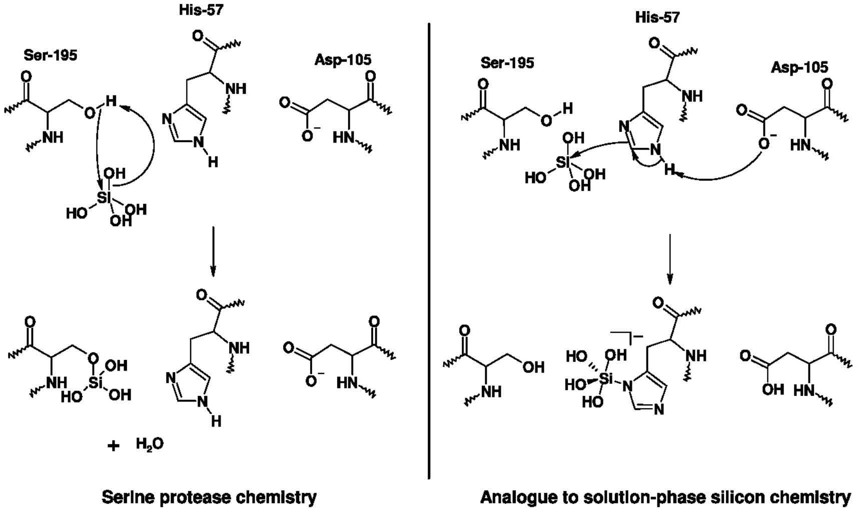
His-57
Ser-195
Asp-105
+ H₂O
Serine protease chemistry
His-57
Ser-195
Asp-105
Analogue to solution-phase silicon chemistry

*Figure 4. Two potential reaction pathways for the trypsin-catalyzed cross-linking of TEOS and TES-PDMS.*

Downloaded by CORNELL UNIV on June 25, 2012 | http://pubs.acs.org
Publication Date (Web): November 9, 2010 | doi: 10.1021/bk-2010-1051.ch005

As a first principles approach toward addressing these fundamental mechanistic questions, our preliminary theoretical studies have taken advantage of Houk's implementation of theozymes as truncated active site constructs for modeling enzyme catalysis (*11*). To facilitate this work electronic structure calculations using density functional theory employing the gradient-corrected (B3LYP) hybrid functional of Becke-Lee-Yang and Parr (*13*) with a double zeta-potential 6-31G(d) (*14*) basis set as implemented in Gaussian 03 have been utilized (*18*). For the purposes of these studies silicic acid ($Si(OH_4)$) was used as a model compound as Bassindale *et al.* have demonstrated that the hydrolysis of the alkoxysilyl moieties to silanols occurs on the surface of the enzyme, while the condensation of the silanols occurs within the active site (*3*).

The transition states for histidine addition (analogous to solution-phase silicon chemistry) (Figure 5) and serine addition (serine protease mechanism) (Figure 6) to the silicon atom have both been modeled (*15*, *17*). Preliminary computational results suggest that serine and histidine addition are mechanistically rate determining. Analysis of the transition state energies for both possible mechanisms within a trypsin theozyme revealed that the addition of the serine residue is 3.72 kcal/mol (15.56 kJ/mol) more stable than the addition of the histidine residue, suggesting that serine addition to silicon is the preferred reaction mode for this condensation.

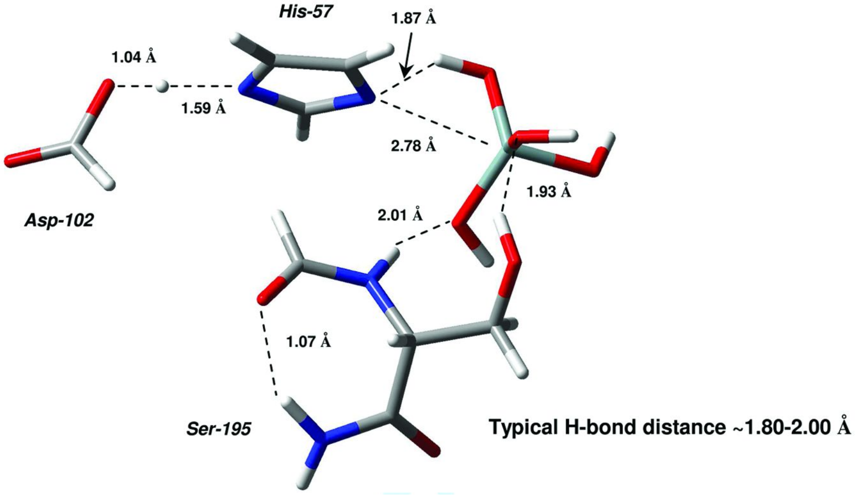

*Figure 5. A computational model of histidine addition to silicic acid in a trypsin theozyme. Reprinted from Journal of Molecular Catalysis B: Enzymatic, Frampton et al., The enzymatic cleavage of Si–O bonds: A kinetic analysis of the biocatalyzed hydrolysis of phenyltrimethoxysilane, pages 1818-1825. Copyright 2010, with permission from Elsevier.*

Downloaded by CORNELL UNIV on June 25, 2012 | http://pubs.acs.org
Publication Date (Web): November 9, 2010 | doi: 10.1021/bk-2010-1051.ch005

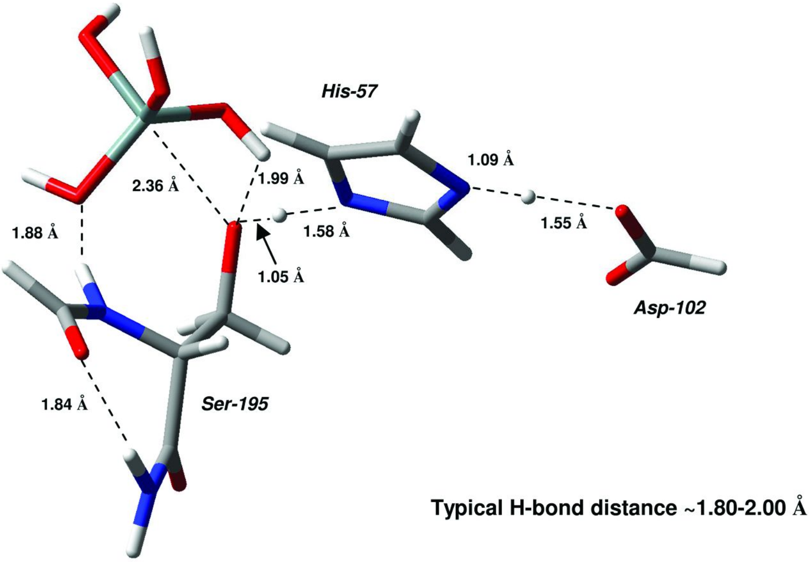

*Figure 6. A computational model of serine addition to silicic acid in a trypsin theozyme. Reprinted from Journal of Molecular Catalysis B: Enzymatic, Frampton et al., The enzymatic cleavage of Si–O bonds: A kinetic analysis of the biocatalyzed hydrolysis of phenyltrimethoxysilane, pages 1818-1825. Copyright 2010, with permission from Elsevier.*

The latter observation is consistent with known Si-O (536 kJ/mol, 128 kcal/mol) versus Si-N (401 kJ/mol, 96 kcal/mol) bond strengths (Figure 6) (*19*). Taken together the highlighted bond strengths and relative transition state energies suggest that the serine addition pathway is the operative mechanistic mode of catalysis. Perhaps the most interesting feature of the serine addition model is the Brønsted activation of the approaching silicic acid unit toward nucleophilic hydroxyl addition as a result of favorable (N-H···O) hydrogen bonding with the serine carboxy amide fragment (Figure 6). As such it would appear that amide-hydroxyl hydrogen bond activation plays a critical role in facilitating silanol condensation. Also, the well defined position of the histidine residue proximal to the serine hydroxyl group allows for rapid proton transfer from serine to histidine after nucleophilic addition. Continuing efforts are focusing on the calculation of the complete reaction pathway for the trypsin-catalyzed cross-linking of alkoxysilyl-modified silicones and a full detailed account will be reported in due course.

## Conclusions

It is possible to use enzymes as a means of cross-linking silicone polymers. The ability to generate cross-linked silicone systems using enzymes rather than potentially toxic heavy metal catalysts has a great deal of potential in silicone chemistry, both from synthetic and environment vantage points. Trypsin provides an alternative to dibutyltin dilaurate in the cross-linking of alkoxysilyl-modified silicone polymers. The mechanism for this process has analogies to both serine protease chemistry and solution-phase silicon chemistry. In spite of processing an unnatural substrate, namely a silicone, the same basic machinery and processes used on natural substrates are applied by the enzyme. Enzymes have the potential to act as "green" catalysts in the synthesis of silicone-based materials.

## Acknowledgments

We are grateful to the Brock University Faculty of Mathematics and Science and to the Natural Sciences and Engineering Research Council (NSERC) of Canada for their financial support of this work, and to Razvan Simionescu for assistance with the NMR experiments and Glenda Hooper for assistance with the SEM.

Downloaded by CORNELL UNIV on June 25, 2012 | http://pubs.acs.org
Publication Date (Web): November 9, 2010 | doi: 10.1021/bk-2010-1051.ch005

## References

1. Brook, M. A. *Silicon in Organic, Organometallic, and Polymer Chemistry*; John Wiley & Sons, Inc.: New York, 2000.
2. (a) Kong, L.; Beattie, J. K.; Hunter, R. J. *Colloids Surf., B*, **2003**, *27*, 11−21. (b) Peters, G. H. *Colloids Surf., B* **2002**, *26*, 84−101. (c) Simpson, T. L., Volcani, B. E., Eds.; *Silicon and Siliceous Structures in Biological Systems*; Springer Verlag: New York, 1981. (d) Kröger, N.; Lorenz, S.; Brunner, E.; Sumper, M. *Science* **2002**, *298*, 584−586. (e) Kinrade, S. D.; Gilson, A. M. E.; Knight, C. T. G. *J. Chem. Soc., Dalton Trans.* **2002**, 307−309.
3. Bassindale, A. R.; Brandstadt, K. F.; Lane, T. H.; Taylor, P. G. *J. Inorg. Biochem.* **2003**, *96*, 401–406.
4. Sahoo, B.; Brandstadt, K. F.; Lane, T. H.; Gross, R. A. In *Polymer Biocatalysis and Biomaterials*; Cheng, H. N., Gross, R. A., Eds.; ACS Symposium Series 900; American Chemical Society: Washington, DC, 2005; pp 182−190.
5. (a) Deyrail, Y.; Zydowicz, N.; Cassagnau, P. *Polymer* **2004**, *45*, 6123−6131. (b) Park, J. H.; Bae, Y. H. *Biomaterials* **2002**, *23*, 1797−1808. (c) Brook, M. A.; Zelisko, P. M.; Walsh, M. J.; Crowley, J. *Silicon Chem.* **2002**, *1*, 99−106. (d) Wang, Q.; Gao, W.; Xie, Z. *J. Appl. Polym. Sci.* **2003**, *89*, 2397−2399. (e) Tang, Y.; Tsiang, R. *Polymer* **1999**, *40*, 6135−6146.
6. (a) Thayer, J. S. Toxicity of Tin in Humans. In *Handbook of Metal-Ligand in Biological Fluids: Bioinorganic Medicine*; Berthon, G., Ed.; Marcel Dekker, Inc.: New York, 1995; Vol. 2, pp 726−789.
7. (a) Liu, M.; Pacard, E.; Ragheb, A. M.; Zelisko, P. M.; Brook, M. A. Stabilisation of Protein-Containing Water-in-Oil Emulsions. In *Cahiers de Formulation*; Lanteri, P., Bordes, C., Eds.; EDP Sciences: Les Ulis, France, 2004; Vol. 11, pp 1542−162. (b) Zelisko, P. M.; Coo-Ranger, J. J.; Brook, M. A. *Polym. Prepr.* **2004**, *45*(1), 604−605. (c) Coo-Ranger, J. J.; Zelisko, P. M.; Brook, M. A. *Polym. Prepr.* **2004**, *45*(1), 674−675. (d) Liu, M.; Ragheb, A.; Zelisko, P.; Brook, M. A. Preparation and Applications of Silicone Emulsions Using Biopolymers. In *Colloidal Biomolecules, Biomaterials,*

Downloaded by CORNELL UNIV on June 25, 2012 | http://pubs.acs.org
Publication Date (Web): November 9, 2010 | doi: 10.1021/bk-2010-1051.ch005

*and Biomedical Applications*; Elaïssari, A., Ed.; Marcel Dekker, Inc.: New York, 2003; Chapter 11, pp 309−329. (e) Brook, M. A.; Bartzoka, V.; Zelisko, P.; Walsh, M. Silicone-Protein Copolymers: Controlling Interfacial and Protein Stabilization. In *Organosilicone Chemistry V: From Molecules to Materials*; Auner, N., Weis, J., Eds.; Wiley-VCH: Weinheim, Germany, 2003; pp 606−611. (f) Zelisko, P. M.; Bartzoka, V.; Brook, M. A. Exploiting Silicone-Protein Interactions: Stabilization against Denaturation at Interfaces. In *Synthesis and Properties of Silicones and Silicone-Modified Materials*; ACS Symposium Series 838; Clarson, S. J., Fitzgerald, J. J., Owen, M. J., Smith, S. D., Van Dyke, M. E., Eds.; American Chemical Society: Washington, DC, 2003; Chapter 19, pp 212−221. (g) Zelisko, P. M.; Brook, M. A. *Langmuir* **2002**, *18*(23), 8982−8987.

8. (a) Zhou, Y.; Shimizu, K.; Cha, J. N.; Stucky, G. D.; Morse, D. E. *Angew. Chem., Int. Ed.* **1999**, *38*, 779−782. (b) Cha, J. N.; Shimizu, K.; Zhou, Y.; Christiansen, S. C.; Chmelka, B. F.; Stucky, G. D.; Morse, D. E. *Proc. Natl. Acad. Sci. U.S.A.* **1999**, *96*, 361−365.
9. (a) Butt, S.; Roberts, S. M. *Nat. Prod. Rep.* **1986**, *3*, 489−503. (b) Turner, N. J. *Nat. Prod. Rep.* **1989**, *6*, 625−644. (c) Turner, N. J. *Nat. Prod. Rep.* **1994**, *11*, 1−15. (d) Davis, B. G.; Boyer, V. *Nat. Prod. Rep.* **2001**, *18*, 618−640.
10. Antoniou, D.; Basner, J.; Núñez, S.; Schwartz, S. D. *Chem. Rev.* **2006**, *106*, 3170–3187.
11. (a) Tantillo, D. J.; Chen, J.; Houk, K. N. *Curr. Opin. Chem. Biol.* **1998**, *2*, 743−750. (b) Ujaque, G.; Tantillo, D. J.; Hu, Y.; Houk, K. N.; Hotta, K.; Hilvert, D. *J. Comput. Chem.* **2003**, *24*, 98−110.
12. Bartzoka, V.; Chan, G.; Brook, M. A. *Langmuir* **2000**, *16*, 4589–4593.
13. (a) Becke, A. D. *J. Chem. Phys.* **1993**, *98*, 1372−1377. (b) Becke, A. D. *J. Chem. Phys.* **1993**, *98*, 5648−5652. (c) Lee, C.; Yang, W.; Parr, R. G. *Phys. Rev. B.* **1998**, *37*, 785−789.
14. (a) Ditchfield, R.; Hehre, W. J.; Pople, J. A. *J. Chem. Phys.* **1971**, *54*, 724−728. (b) Here, W. J.; Ditchfield, R.; Pople, J. A. *J. Chem. Phys.* **1972**, *56*, 2257−2261. (c) Hariharan, P. C.; Pople, J. A. *Theor. Chim. Acta* **1973**, *28*, 213−222.
15. (a) Brown, W.; Wold, F. *Biochemistry* **1973**, *12*, 828−834. (b) Brown, W.; Wold, F. *Biochemistry* **1973**, *12*, 835−840.
16. (a) Zhou, Y.; Shimizu, K.; Cha, J. N.; Stucky, G. D.; Morse, D. E. *Angew. Chem., Int. Ed.* **1999**, *38*, 779−782. (b) Cha, J. N.; Shimizu, K.; Zhou, Y.; Christiansen, S. C.; Chmelka, B. F.; Stucky, G. D.; Morse, D. E. *Proc. Natl. Acad. Sci. U.S.A.* **1999**, *96*, 361−365.
17. Chuit, C.; Corriu, R. J. P.; Reye, C.; Young, J. C. *Chem. Rev.* **1993**, *93*, 1371–1448.
18. Frisch, M. J., et al. *Gaussian 03*, rev. B; Gaussian, Inc.: Pittsburgh, PA, 2003.
19. (a) Becerra, R.; Walsh, R. Thermochemistry. In *The Chemistry of Organic Silicon Compounds*; Rappoport, Z., Apeloig, Y., Eds.; Wiley: Chichester, U.K., 1998; Vol. 2, p 153. (b) Walsh, R. Thermochemistry. In *The Chemistry of Organic Silicon Compounds*; Patai, S., Rappoport, Z., Eds.; Wiley: Chichester, U.K., 1998; Vol. 1, p 371.

Downloaded by UNIV OF GUELPH LIBRARY on June 23, 2012 | http://pubs.acs.org
Publication Date (Web): November 9, 2010 | doi: 10.1021/bk-2010-1051.ch006

## Chapter 6

# Viscoelastic Behavior of Polydimethylsiloxane Stabilized Magnetite Magnetic Nanoparticle Complexes

**Wen Yin, Qiongdan Xie, Jianjun Deng, Jonathan D. Goff, Timothy P. Vadala, Judy S. Riffle, and Alan R. Esker***

**Department of Chemistry and the Macromolecules and Interfaces Institute, Virginia Polytechnic Institute and State University, Blacksburg, VA 24061**
***aesker@vt.edu**

Magnetic materials, especially magnetic nanoparticles (MNPs), have attracted considerable interest because of their potential application in biomedical fields like separations, biosensing, targeted drug delivery, hyperthermia based cancer treatments, etc. This study examines the interfacial viscoelastic properties of polydimethylsiloxane stabilized magnetic nanoparticle complexes (PDMS-MNPs) via surface light scattering (SLS) and the Wilhelmy plate technique at the air/water (A/W) interface. Trimethylsilyl-terminated polydimethylsiloxane (PDMS) and tricarboxylic acid-terminated polydimethylsiloxane (PDMS-Stabilizer) provide suitable reference compounds for comparative studies. Results show that PDMS, PDMS-Stabilizer, and PDMS-MNPs are ideal systems for SLS studies. The SLS data show that PDMS and PDMS-MNPs have similar phase transitions and viscoelastic behavior from the gaseous state through bilayer formation. In contrast, the viscoelastic properties of the PDMS-Stabilizer show marked differences starting in the collapsed regime. The differences between PDMS-Stabilizer and PDMS-MNPs are consistent with complete coupling of the carboxylic acid groups to the magnetite surfaces in PDMS-MNPs.

In Advances in Silicones and Silicone-Modified Materials; Clarson, S., et al.;
ACS Symposium Series; American Chemical Society: Washington, DC, 2010.

## Introduction

Magnetic materials have attracted considerable interest for modifying the optical properties of films (*1*) and as catalyst carriers (*2*). Recently, magnetic nanoparticles (MNPs) have enabled additional potential applications in biomedical fields like separations, biosensing, targeted drug delivery, magnetic resonance imaging contrast agents, and hyperthermia based cancer treatments (*3–7*). For all of these potential applications, stabilizers are required to prevent MNP aggregation in solution. The polymers should contain at least two segments: a functionalized segment that adheres to the metal or metal oxide surface of the MNP, and at least one flexible segment that prevents MNP aggregation through steric stabilization. There are numerous studies on the stabilization of MNPs in aqueous fluids using poly(methacrylic acid) (*8*), dextran (*9*), poly(vinyl alcohol) (*9*), carboxylic acid-functionalized poly(ethylene oxide) (*10–13*), sodium poly(oxyalkylene diphosphonate)s (*14*), block copolymer stabilizers like poly(ethylene oxide-b-methacrylic acid) (*15*), and graft copolymers such as poly(alkylene oxide-g-acrylic acid) (*16*). In addition, silicone stabilizers have been considered for direct use inside the eye for treating detached retinas (*17–20*). For other non-polar fluids, oleic acid is probably the most common stabilizer (*21*, *22*). Interestingly, many of these stabilizers render the particles surface active at the air/water (A/W) interface.

Molecules forming Langmuir films at the A/W interface are amphiphilic and contain hydrophobic tails and hydrophilic heads. The study of Langmuir films at the A/W interface has attracted considerable interest in the fields of chemistry, physics, and life sciences (*23–26*). In particular, the smooth water substrate with two controllable thermodynamic variables: temperature (T) and surface area per molecule (A), make Langmuir films at the A/W interface model two-dimensional (2D) systems for studying phase transitions and ordering (*27*), and 2D templates for studying bioreactions (*28*). The reduction of one dimension in 2D Langmuir films vs. three-dimensional (3D) bulk systems can sometimes simplify model theoretical calculations (*29*). With the introduction of Brewster angle microscopy (BAM) (*30–37*), fluorescence microscopy (FM) (*38*, *39*), ellipsometry (*40*), grazing incidence X-ray diffraction (GIXD) (*41*), etc. (*42*, *43*) numerous thermodynamic and structural studies of Langmuir monolayers now exist.

Another area of interest for Langmuir films is their rheological properties. The rheology of surfactant monolayers is critical for film formation and the dynamic stability of gas/liquid and liquid/liquid interfaces. Materials design of polymeric surfactants crucially hinges on their interfacial rheology, in complete parallel with polymeric systems in bulk or concentrated solution. The static and dynamic behavior of a fair number of polymeric and small molecule surfactant monolayers is available from techniques that include mechanically generated waves (*44*), electrocapillary wave diffraction (ECWD) (*45–49*), surface light scattering (SLS) (*50–62*), canal viscometry (*63–65*), interfacial stress rheometry (ISR) (*66–68*), and even surface pressure relaxation studies (*69*). In this study, SLS serves as a non-invasive optical technique that is ideally suited for low viscosity polydimethylsiloxane (PDMS) films (*54*, *55*, *70–72*).

Downloaded by UNIV OF GUELPH LIBRARY on June 23, 2012 | http://pubs.acs.org
Publication Date (Web): November 9, 2010 | doi: 10.1021/bk-2010-1051.ch006

Downloaded by UNIV OF GUELPH LIBRARY on June 23, 2012 | http://pubs.acs.org
Publication Date (Web): November 9, 2010 | doi: 10.1021/bk-2010-1051.ch006

SLS probes the propagation characteristics of spontaneously formed capillary waves on liquid surfaces that arise from density fluctuations within the underlying liquid subphase. The amplitudes and wavelengths (λ) of the relevant fluctuations are 3-5 Å for water (*73*) and a few 100 μm, respectively. Most SLS instruments utilize a transmission diffraction grating (*74*) to detect scattered light through heterodyne beating. Subsequent analysis normally takes one of two paths: (1) direct fitting of the heterodyne intensity correlation functions (*50–53*), or (2) a Lorentzian fit of the power spectrum for the scattered light (*54–62*). For the second approach (used in this study), the power spectrum yields a frequency shift ($f_s$) and an experimental full-width at half-maximum intensity ($\Delta f_s$). Normally, the experimental full-width is corrected for the Gaussian beam profile of the laser (*74*):

$$\Delta f_{s,c} = \Delta f_s - \frac{\Delta f_i^2}{\Delta f_s} \qquad [1]$$

where the instrumental full-width at half-maximum intensity for the i<sup>th</sup> diffraction order of the transmission diffraction grating is defined as

$$\Delta f_i = \sqrt{2}\left(\frac{\Delta u_i \cos\theta_i}{R\lambda}\right)\left(\frac{d\omega_o}{dk}\right) \qquad [2]$$

Here, $\Delta u_i$ is the full-width at half-maximum intensity of the Gaussian laser beam profile for the ith diffraction order of the transmission diffraction grating, $\theta_i$ is the incident angle, k is the spatial wavevector, and R is the distance from the interface to the detector. $f_s$ is proportional to the capillary wave propagation rate ($\omega_o = 2\pi f_s$) and $\Delta f_{s,c}$ is related to the capillary wave damping coefficient ($\alpha = \pi\Delta f_{s,c}$). $\omega_o$ and $\alpha$ can then be used to solve the Lucassen-Reynders-Lucassen dispersion relation for a monomolecular film at the A/W interface (*75*):

$$[\eta(k - m^*)]^2 = \left(\frac{\varepsilon^* k^2}{i\omega^*} + \eta(k + m^*)\right)\left(\eta(k + m^*) + \frac{\sigma^* k^2}{i\omega^*} + \frac{g\rho}{i\omega^*} - \frac{\omega^* \rho}{ik}\right) \qquad [3]$$

where the ε*, σ*, ω*, and m* correspond to the complex dilational modulus, complex surface tension, complex frequency, and the complex wavevector in the z-direction, respectively. These complex quantities correspond to Eqs. 4 through 7, respectively.

$$\varepsilon^* = \varepsilon_d + i\omega^* \kappa \qquad [4]$$

$$\sigma^* = \sigma_d + i\omega^* \mu \qquad [5]$$

$$\omega^* = \omega_o + i\alpha \qquad [6]$$

Downloaded by UNIV OF GUELPH LIBRARY on June 23, 2012 | http://pubs.acs.org
Publication Date (Web): November 9, 2010 | doi: 10.1021/bk-2010-1051.ch006

$$m^* = \left(k^2 + \frac{i\omega^* \rho}{\eta}\right)^{1/2}, \mathrm{Re}(m^*) > 0 \qquad [7]$$

In Eq. 3 through 7, $\varepsilon_d$ is the dynamic dilational elasticity, $\kappa$ is the dilational viscosity, $\sigma_d$ is the dynamic surface tension, $\mu$ is the transverse viscosity, g is acceleration due to gravity, and $\rho$ and $\eta$ are the density and viscosity of the subphase (water), respectively. In principle, $\varepsilon_d$ and $\kappa$ also contain a shear component, although this seems to be negligible (*76*). The solution of Eq. 3 is complicated by the fact that only two quantities are measured, $f_s$ and $\Delta f_{s,c}$, but four parameters, $\varepsilon_d$, $\kappa$, $\sigma_d$, and $\mu$, need to be determined. For the case of direct analysis of the correlation function, these terms serve as fitting parameters. Whereas, during the analysis of the power spectra, $\mu$ is normally assumed to be zero (*76*) and $\sigma_d$ is replaced by the static surface tension ($\sigma_s$), which can be measured simultaneously by the Wilhelmy plate technique. Hence, $\varepsilon_d$ and $\kappa$ become the obtainable parameters.

In this study, SLS is used to probe the viscoelastic properties of a trimethylsilyl-terminated polydimethylsiloxane (PDMS), a tricarboxylic acid-terminated PDMS stabilizer (PDMS-Stabilizer, Figure 1A), and PDMS stabilized magnetite magnetic nanoparticle complexes (PDMS-MNPs, Figure 1B) at the A/W interface. This study shows that differences in viscoelastic behavior between PDMS and PDMS-Stabilizer during collapse change when the PDMS-Stabilizer is coupled to magnetite MNPs to form the PDMS-MNPs.

## Experimental

### Materials

Trimethylsilyl-terminated PDMS (PDMS, number average molar mass, $M_n = 7.5$ kg·mol$^{-1}$, and polydispersity index, $M_w/M_n = 1.09$), initiated with sec-butyl lithium was obtained from Polymer Source, Inc. and was used without further purification. The PDMS-Stabilizer and PDMS-MNPs were synthesized following published procedures (*20*). $^1$H-NMR yielded $M_n = 2.5$ kg·mol$^{-1}$ for the PDMS-Stabilizer. For the PDMS-MNPs, the graft density of PDMS chains calculated from transmission electron microscopy (10 nm diameter particles) and thermal gravimetric analysis (50 wt% magnetite) was 1.25 PDMS-Stabilizers per nm$^2$. Spreading solutions were prepared with nominal concentrations of ~0.5 mg·mL$^{-1}$ in HPLC grade chloroform. All aqueous subphases were Millipore water (Milli-Q Gradient A-10, 18.2 MΩ, < 10 ppb organic impurities).

### Surface Pressure – Area per Dimethylsiloxane Repeat Unit ($\Pi$-$A_{DMS}$) Isotherms

Chloroform solutions were spread onto the surface of a standard Langmuir trough (700 cm$^2$, 601BAM, Nima Technology, Ltd.) filled with Millipore water maintained at 22.5 °C in a Plexiglas box with a relative humidity of ~70-75%. The surface of the water was further cleaned by suctioning off potential impurities from

Downloaded by UNIV OF GUELPH LIBRARY on June 23, 2012 | http://pubs.acs.org
Publication Date (Web): November 9, 2010 | doi: 10.1021/bk-2010-1051.ch006

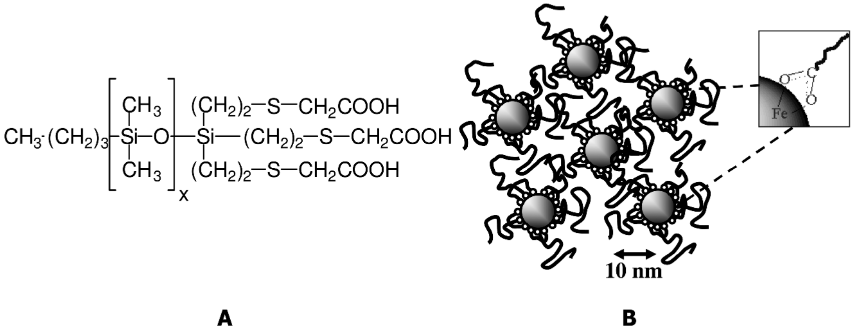

*Figure 1. (A) Molecular structure of the PDMS-Stabilizer (x = 28). (B) A schematic depiction of PDMS-MNPs. The dots symbolize carboxylic acid groups and squiggly lines represent PDMS chains. The inset shows carboxylic acid binding to the magnetite surface.*

the interface. Successive additions were used to control the surface concentration. For this approach, pre-determined volumes were spread onto the water surface using a Hamilton gas-tight syringe. Surface concentrations are expressed in terms of area per monomer where monomer is short for dimethylsiloxane repeat unit ($A_{DMS}$). A minimum of 15 minutes was allowed to ensure the complete evaporation of chloroform before the surface pressure ($\Pi$) was measured by using a paper Wilhelmy plate to ±0.1 $mN \cdot m^{-1}$.

### Surface Light Scattering (SLS)

A homemade SLS instrument was constructed based on the design of Sano, *et al.* (*77*) that incorporated the advances made by Hård and Neuman (*78*). The instrument uses a 17 mW He:Ne laser with a wavelength of 632.8 nm, an incident angle of $\theta_i = 66.00°$ and a distance of R = 3.40 m from the air/liquid interface to the detector. The transmission diffraction grating generated different diffraction orders that serve as reference beams for heterodyne detection. Water calibration was used to determine the wavevectors of the 6th through 10th diffraction orders: 353.7, 404.3, 459.0, 512.6, and 572.6 $cm^{-1}$, respectively. For SLS, the solutions were spread onto the surface of a home built Langmuir trough (174 $cm^2$) maintained at 22.5 °C and $\Pi$ was measured simultaneously by the Wilhelmy plate technique. The surface concentration is controlled by successive additions of chloroform solution and SLS measurements commenced after attaining a stable $\Pi$ value ($\Delta\Pi < 0.1$ $mN \cdot m^{-1}$ over a 5 minute period), with a minimum waiting time of 15 minutes to ensure spreading solvent evaporation.

## Results and Discussion

### Compression Isotherms for PDMS, PDMS-Stabilizer, and PDMS-MNPs

Figure 2 shows $\Pi$-$A_{DMS}$ isotherms for PDMS, PDMS-Stabilizer, and PDMS-MNPs. Here $A_{DMS}$ represents the area per dimethylsiloxane repeat

Downloaded by UNIV OF GUELPH LIBRARY on June 23, 2012 | http://pubs.acs.org
Publication Date (Web): November 9, 2010 | doi: 10.1021/bk-2010-1051.ch006

unit (monomer for short). For the case of the PDMS-MNPs, the $A_{DMS}$ values only reflect the silicone component in the complex (i.e., if there was 1 g of PDMS-MNPs on the surface, 0.5 g was used for the calculation of $A_{DMS}$ because the MNPs are 50 wt% magnetite). The PDMS isotherm in Figure 2 exhibits the four classical regimes originally reported by Fox, *et al.* (*79*): (A) $A_{DMS} > A_{lift\text{-}off,DMS}$ = 18 $Å^2 \cdot monomer^{-1}$ (where Π starts to increase) corresponding to the end of the submonolayer regime ($\Pi = 0$ $mN \cdot m^{-1}$). In this regime, PDMS films are biphasic with the coexistence of gaseous and liquid-like domains (*80*); (B) 14 $Å^2 \cdot monomer^{-1} < A_{DMS} <$ 18 $Å^2 \cdot monomer^{-1}$ corresponding to a PDMS monolayer with adsorbed oxygen and silicon atoms from the repeating unit; (C) ~ 8 $Å^2 \cdot monomer^{-1} < A_{DMS} <$ 14 $Å^2 \cdot monomer^{-1}$, the first plateau regime ($\Pi \approx 8.0$ $mN \cdot m^{-1}$) where it was postulated that PDMS underwent progressive coiling into helical structures; and (D) $A_{DMS} <$ ~ 8 $Å^2 \cdot monomer^{-1}$, the second plateau ($\Pi \approx 9.0$ $mN \cdot m^{-1}$), where the helical structures undergo collapse. While the interpretation of Regime A and B is widely accepted, newer measurements have suggested that the plateaus correspond to the formation of bilayers and multilayers as PDMS spreads easily upon the underlying hydrated PDMS monolayer and the films can be heterogeneous (*80*, *81*).

Qualitatively, the isotherm for the PDMS-Stabilizer is similar to PDMS in Regimes A and B, with a few quantitative differences. First, $A_{lift\text{-}off}$ shifts from 18 to ~ 17 $Å^2 \cdot$(monomer$^{-1}$ for the PDMS-Stabilizer reflecting the fact that the end groups make a more significant contribution to the calculation of $A_{DMS}$ for the 2.5 $kg \cdot mol^{-1}$ PDMS-Stabilizer than the 7.5 $kg \cdot mol^{-1}$ PDMS. The second difference is a bigger plateau pressure ($\Pi \approx 8.7$ $mN \cdot m^{-1}$) for the PDMS-Stabilizer in Regime C. Third, there is a steeper upturn in the PDMS-Stabilizer isotherm starting at the end of what is Regime C for PDMS. The upturn in Π out of Regime C has been reported previously for other polar terminated silicone oligomers (*82*), and reflects a more traditional surfactant like structure as the collapsing polymer starts to "stand" on the hydrophilic anchor. The isotherm for PDMS-MNPs is identical to the PDMS-Stabilizer through Regime A and most of Regime B. This result suggests that grafting flexible PDMS-Stabilizer to the magnetite surfaces at densities of the order ~1.25 per $nm^2$ has little effect on the ability of the dimethylsiloxane repeating units to interact with water, a likely consequence of the relatively long linking group (Figure 1A). Interestingly, the PDMS-MNPs' isotherm agrees with PDMS in Regime C. Apparently, tethering the polar portion of the PDMS-Stabilizer to the magnetite core causes the PDMS-MNPs to behave more like the hydrophobically terminated PDMS during collapse. In Regime D, the PDMS-MNPs exhibit behavior that lies between PDMS and PDMS-Stabilizer. As the polar end groups of the stabilizer are not available for anchoring PDMS to the A/W interface, one interpretation would be that the PDMS-MNPs do not undergo multilayer formation as easily as hydrophobic PDMS. The subsequent discussion of viscoelastic behavior will make use of the regimes defined in Figure 2.

In Advances in Silicones and Silicone-Modified Materials; Clarson, S., et al.;
ACS Symposium Series; American Chemical Society: Washington, DC, 2010.

Downloaded by UNIV OF GUELPH LIBRARY on June 23, 2012 | http://pubs.acs.org
Publication Date (Web): November 9, 2010 | doi: 10.1021/bk-2010-1051.ch006

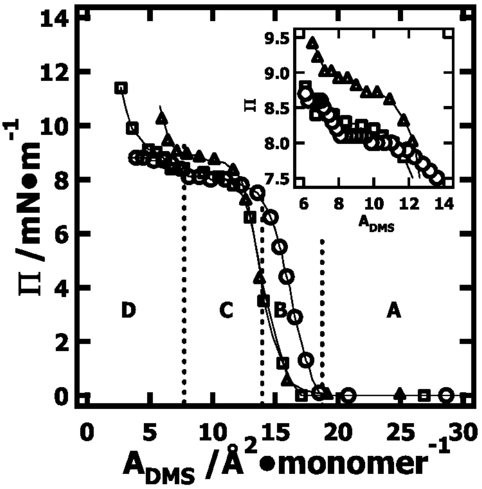

*Figure 2. Π-$A_{DMS}$ isotherms (T = 22.5 °C) for PDMS (circles), PDMS-Stabilizer (triangles), and PDMS-MNPs (squares). The solid lines between points are only trend lines. Transitions in the PDMS isotherm define the boundaries (vertical dotted lines) for Regimes A through D. The inset expands Regime C, the first plateau.*

## SLS Results for PDMS, PDMS-Stabilizer, and PDMS-MNPs

Esker, *et al.* (*56*, *61*) recently noted that in the absence of frequency dependent viscoelastic behavior, it is convenient to reduce all viscoelastic data down to a common reference state. The approach is essentially the same one used by Hård and Neuman (*70*). One starts by measuring $f_s$, $\Delta f_{s,c}$, and $\sigma_s$, and uses Eq. 3 to calculate the viscoelastic parameters $\varepsilon_d$ and $\kappa$. Next, the values of $\varepsilon_d$, $\kappa$, and $\sigma_s$ are used along with Eq. 3 to calculate the equivalent values of the frequency shift ($f_{s,eq}$) and corrected full-width at half-maximum intensity ($\Delta f_{s,c,eq}$) at an arbitrary reference state. For this study, the reference state is chosen to correspond to water at 25 °C ($k = 324.3$ cm$^{-1}$, $\sigma_d = 71.97$ mN·m$^{-1}$, $\mu = 0$, $\rho = 997.0$ kg·m$^{-3}$, and $\eta = 0.894$ mPa·s). Figure 3 shows $f_{s,eq}$ plotted as a function of Π for PDMS, PDMS-Stabilizer, and PDMS-MNPs. The assignment of the regimes in Figure 4 is in accord with the regimes of Figure 2 for PDMS. Figure 4 provides similar data for $\Delta f_{s,c}$ as a function of Π. The use of logarithmic x-axes for Π < 1 mN·m$^{-1}$ and linear scales for Π > 1 mN·m$^{-1}$ in Figures 3 and 4 provides a convenient way to plot the data and has no physical significance. The data points in Figures 3 and 4 represent an average for five wavevectors (6th through 10th diffraction orders) with one standard deviation error bars.

Downloaded by UNIV OF GUELPH LIBRARY on June 23, 2012 | http://pubs.acs.org
Publication Date (Web): November 9, 2010 | doi: 10.1021/bk-2010-1051.ch006

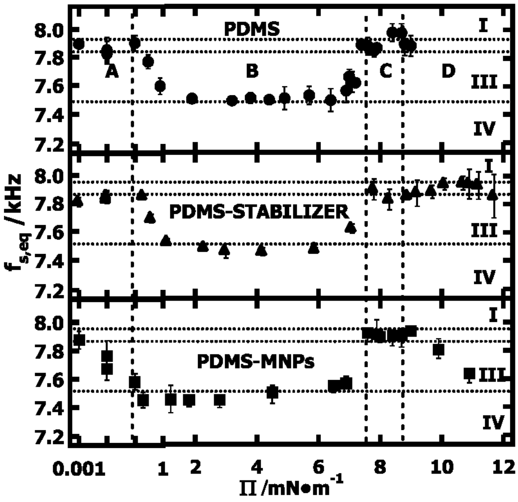

*Figure 3. $f_{s,eq}$–$\Pi$ for PDMS (circles), PDMS-Stabilizer (triangles), and PDMS-MNPs (squares). The x-axis uses a logarithmic scale for $\Pi < 1$ mN·m$^{-1}$, and a linear scale for $\Pi > 1$ mN·m$^{-1}$. Data points represent an average of five wavevectors with one standard deviation error bars. Data points at $\Pi = 0.001$ mN·m$^{-1}$ correspond to water ($\Pi = 0$), while points at $\Pi = 0.01$ mN·m$^{-1}$ correspond to submonolayer films that do not have a detectable $\Pi$ ($\Pi < 0.1$ mN·m$^{-1}$). Vertical dotted lines indicate Regimes A through D defined in Figure 2. The three horizontal dotted lines correspond to limiting behavior of the dispersion relation: (I) pure liquid limit, (III) the maximum damping coefficient for a perfectly elastic surface film, and (IV) the minimum velocity limit for a perfectly elastic surface film.*

Plotting the data as done in Figures 3 and 4 facilitates easy comparisons between the experimental data and important limiting behavior of the dispersion equation (*56*, *61*). There are six important limiting cases for the viscoelastic behavior of Langmuir films at the A/W interface: (I) Pure liquid behavior ($\varepsilon^*$ and $\mu = 0$), purely elastic surface films ($\kappa = 0$ and $\mu = 0$) which yield – (II) the maximum velocity limit, (III) the maximum damping coefficient, and (IV) the minimum velocity limit, (V) films with an infinite lateral modulus ($\varepsilon^* \rightarrow \infty$), and (VI) the maximum damping coefficient for a purely viscous surface film ($\varepsilon_d = 0$ and $\mu = 0$). As PDMS forms perfectly elastic surface films, the three most important limits are (I), (III), and (IV). These limits are included on Figures 3 and 4.

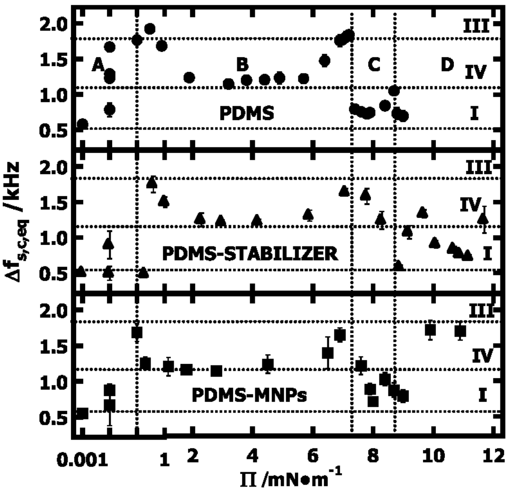

*Figure 4. $\Delta f_{s,c,eq}$-$\Pi$ for PDMS (circles), PDMS-Stabilizer (triangles), and PDMS-MNPs (squares). The x-axis uses a logarithmic scale for $\Pi < 1$ mN·m$^{-1}$, and a linear scale for $\Pi > 1$ mN·m$^{-1}$. Data points represent an average of five wavevectors with one standard deviation error bars. Data points at $\Pi = 0.001$ mN·m$^{-1}$ correspond to water ($\Pi = 0$), while points at $\Pi = 0.01$ mN·m$^{-1}$ correspond to submonolayer films that do not have a detectable $\Pi$ ($\Pi < 0.1$ mN·m$^{-1}$). Vertical dotted lines indicate Regimes A through D defined in Figure 2. The three horizontal dotted lines correspond to limiting behavior of the dispersion relation: (I) pure liquid limit, (III) the maximum damping coefficient for a perfectly elastic surface film, and (IV) the minimum velocity limit for a perfectly elastic surface film.*

In Regime A – submonolayer coverage, as seen in Figures 3 and 4, PDMS behaves as a pure liquid (I). With increasing concentration, the monolayer forms, $\Pi \sim 0$, leading to a sharp drop in $f_{s,eq}$ and a sharp increase in $\Delta f_{s,c,eq}$. Figure 4, clearly shows that as the monolayer forms the damping of the PDMS monolayer is consistent with the maximum damping coefficient of a perfectly elastic surface film (III) and indicates that $\varepsilon_d/\sigma_s \sim 0.17$ (*59*, *61*). In the middle of Regime B, the global minimum in $f_{s,eq}$, and the local minimum in $\Delta f_{s,c,eq}$ indicate the viscoelastic properties of the film are similar to those of a perfectly elastic surface film in the minimum velocity limit (IV). Such a film is characterized by intermediate $\varepsilon_d \sim 30 - 50$ mN·m$^{-1}$ and negligible $\kappa$. At the high $\Pi$ end of Regime B, $f_{s,eq}$ starts to rise, and $\Delta f_{s,c,eq}$ shows another maximum that is in agreement with the maximum damping coefficient for a perfectly elastic surface film (III). The appearance of a second maximum indicates that as the film collapses, $\varepsilon_d/\sigma_s$ is again ~ 0.17 and more importantly that $\varepsilon_d$ is decreasing in the collapsing film. In Regimes C and D, the viscoelastic properties are essentially those of a pure liquid (I), except for a small enhancement of viscoelastic behavior at the boundary between Regimes C and D.

It is interesting to note how the PDMS-Stabilizer and PDMS-MNPs differ from PDMS in Figures 3 and 4. In Regime A, all systems are roughly the same. As the monolayer forms during compression ($\Pi \sim 0$), the behavior is similar as all

Downloaded by UNIV OF GUELPH LIBRARY on June 23, 2012 | http://pubs.acs.org
Publication Date (Web): November 9, 2010 | doi: 10.1021/bk-2010-1051.ch006

the films are essentially perfectly elastic, and the maximum in $\Delta f_{s,c,eq}$ occurs at $\Pi \sim 0$. This observation is consistent with the facts that $\varepsilon_d/\sigma_s \sim 0.17$ at the maximum (*59*) and the A/W interface is a poor solvent for PDMS (*71*). The behavior of the PDMS-Stabilizer starts to depart from that of PDMS and PDMS-MNPs at the high Π end of Regime B. As seen in Figure 4, the second maximum in $\Delta f_{s,c,eq}$ shifts to a higher Π value. This feature is likely due to a different collapse mechanism as the hydrophilic tricarboxylic acid end group inhibits PDMS-Stabilizer multilayer formation by the same mechanism as PDMS. Differences become even more apparent when the PDMS-Stabilizer fails to exhibit a local maximum in $\Delta f_{s,c,eq}$ at the boundary between Regimes C and D. Again, this feature shifts to higher Π. It is notable that PDMS-MNPs exhibit essentially PDMS behavior in Regimes A through C. Given the isotherms in Figure 2, it is not surprising that PDMS, PDMS-Stabilizer, and PDMS-MNPs exhibit the largest differences in Regime D. In Regime D, PDMS-Stabilizer and PDMS-MNPs exhibit different $f_{s,eq}$ and $\Delta f_{s,c,eq}$ that do not conform to any particular limiting behavior, thereby warranting an analysis of the surface viscoelastic parameters through the dispersion equation.

## Surface Viscoelastic Parameters for PDMS, PDMS-Stabilizer, and PDMS-MNPs

$\varepsilon_d$ probed by SLS is a high frequency (kHz) analog to the static dilational modulus (0 Hz, a 2D analog to the bulk modulus):

$$\varepsilon_s = C_s^{-1} = -A_{DMS}\left(\frac{\partial \Pi}{\partial A_{DMS}}\right)_T \qquad [8]$$

where $C_s$ is the surface compressibility, the 2D analog to the isothermal compressibility in 3D. Figure 5 shows $\varepsilon_s$ obtained from Figure 2 and Eq. 8, and $\varepsilon_d$ (an average of the five different wavevectors) plotted as a function of Π for PDMS, PDMS-Stabilizer, and PDMS-MNPs. For PDMS, there is excellent agreement between $\varepsilon_d$ and $\varepsilon_s$ throughout the entire range of Π. This behavior is consistent with negligible κ. Figure 6 shows, κ vs. Π for PDMS, PDMS-Stabilizer, and PDMS-MNPs. κ is indeed small for PDMS and is nearly zero within experimental error. This result is consistent with previous studies (*54*, *55*, *70*, *72*). Furthermore, Esker, *et al.*, noted that $\varepsilon_s = z\Pi$, where z is the scaling exponent (*61*). For PDMS, the initial slope yields z = 28, i.e. the A/W interface is a poor solvent for PDMS (*71*). Another important feature of Figure 5, is that the maximum $\varepsilon_d \sim 30$ mN·m$^{-1}$ occurs in the center of Regime B as expected. Finally, $\varepsilon_d$ shows a small peak at the boundary between Regimes C and D for PDMS. One interpretation is the collapse of a helical monolayer (*79*), although a bilayer to multilayer transition is more probable (*80*, *81*). These observations are all consistent with the discussion of Figures 3 and 4.

Downloaded by UNIV OF GUELPH LIBRARY on June 23, 2012 | http://pubs.acs.org
Publication Date (Web): November 9, 2010 | doi: 10.1021/bk-2010-1051.ch006

Downloaded by UNIV OF GUELPH LIBRARY on June 23, 2012 | http://pubs.acs.org
Publication Date (Web): November 9, 2010 | doi: 10.1021/bk-2010-1051.ch006

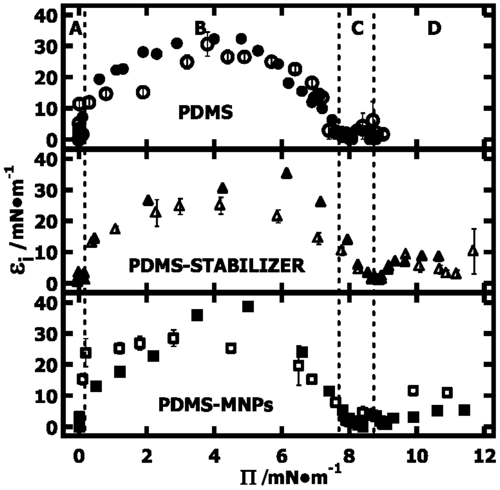

*Figure 5. Plots of $\varepsilon_i$-$\Pi$ for PDMS (circles), PDMS-Stabilizer (triangles), and PDMS-MNPs (squares). Figure 2 and Eq. 8 yield $\varepsilon_s$ values (filled symbols). $\varepsilon_d$ values (open symbols) represent the average of 5 different wavevectors with one standard deviation error bars. The dotted vertical lines indicate the boundaries of the regimes defined in Figure 2.*

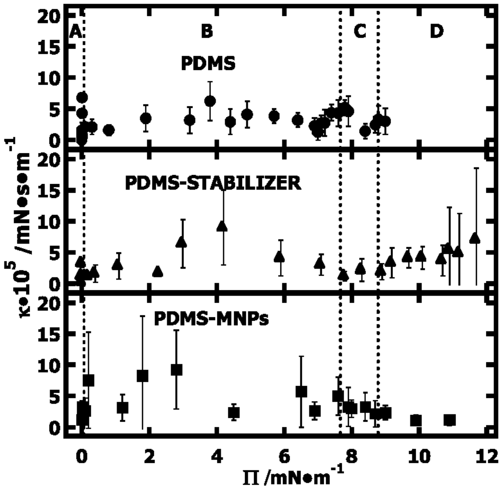

*Figure 6. Plots of $\kappa$-$\Pi$ for PDMS (circles), PDMS-Stabilizer (triangles), and PDMS-MNPs (squares). $\kappa$ values represent the average of 5 different wavevectors with one standard deviation error bars. The dotted vertical lines indicate the boundaries of the regimes defined in Figure 2.*

As seen in Figures 5 and 6, the viscoelastic behavior of the PDMS-Stabilizer and PDMS-MNPs are nearly identical to PDMS up to the end of Regime B. The first key difference is that PDMS-Stabilizer, does not exhibit $\varepsilon_d = 0$, until $\Pi \sim 9$ mN·m$^{-1}$ during the initial collapse of the film. Moreover, Regime C is essentially absent for the PDMS-Stabilizer. This feature must arise from stronger anchoring of the PDMS-Stabilizer to the subphase by the hydrophilic tricarboxylic acid terminal group (*82*). Interestingly, Regime C is present for PDMS-MNPs after the stabilizer is coupled to the magnetite surface and film collapse as measured by the point where $\varepsilon_d$ returns to zero is the same as PDMS ($\Pi \sim 8$ mN·m$^{-1}$). The other main differences all occur in Regime D. For PDMS, pure liquid behavior is observed in Regime D ($\varepsilon_d = 0$ and $\kappa = 0$). In contrast, both PDMS-Stabilizer and PDMS-MNPs exhibit non-zero $\varepsilon_d$ and $\kappa$ in Regime D. Moreover, the PDMS-Stabilizer film is more viscous than the PDMS-MNPs in Regime D. This enhancement in the film's viscosity is attributed to multilayer formation for PDMS-MNPs, similar to PDMS, whereas collapse in PDMS-Stabilizer leads to chains standing on their hydrophilic anchor.

Downloaded by UNIV OF GUELPH LIBRARY on June 23, 2012 | http://pubs.acs.org
Publication Date (Web): November 9, 2010 | doi: 10.1021/bk-2010-1051.ch006

## Conclusions

As already known, PDMS exhibits four distinct regimes at the A/W interface (schematically depicted in Figure 7). In Regime A, PDMS films can be heterogeneous (*80*, *81*), representing a coexistence of liquid-like PDMS and gas domains. In Regime A, PDMS chains should have 2D coil conformations. The addition of the polar end group (PDMS-Stabilizer), or the tethering of the PDMS-Stabilizer to the magnetite to form PDMS-MNPs should have little effect on the observed behavior in Regime A relative to PDMS. In Regime B, a semi-dilute 2D liquid-like film forms at low $\Pi$ and scaling behavior is consistent with poor solvent behavior for the A/W interface. As expected for a semi-dilute solution, PDMS, PDMS-Stabilizer and PDMS-MNPs all exhibit similar behavior. During film collapse in Regime C, we favor bilayer formation (depicted in Figure 7) (*80*, *81*) for both PDMS and PDMS-MNPs rather than the elaborate coil to helix transition model (*79*). However, the tricarboxylic acid end group of the PDMS-Stabilizer leads to a different collapse mechanism. As depicted in Figure 7, the PDMS chains can now stand on end during further compression yielding a viscoelastic film (*82*). Consequently, Regime C and Regime D are essentially one and the same for the PDMS-Stabilizer. In contrast, both PDMS and PDMS-MNPs should be forming multilayers in Regime D. For PDMS, the absence of viscoelastic behavior or an increase in $\Pi$ indicates there is no energy penalty for forming thicker PDMS layers. In contrast, SLS clearly shows that the PDMS-MNPs are less able to form multilayers during compression with both a rise in $\Pi$ and viscoelastic responses from the film. Hence, even though PDMS-Stabilizer shows deviation from PDMS-like behavior in Regime C, PDMS-MNPs behave like PDMS from Regime A through Regime C and only deviate in Regime D. This response to film compression is consistent with complete anchoring of the carboxylic acid end groups to the magnetite cores of the PDMS-MNPs.

Downloaded by UNIV OF GUELPH LIBRARY on June 23, 2012 | http://pubs.acs.org
Publication Date (Web): November 9, 2010 | doi: 10.1021/bk-2010-1051.ch006

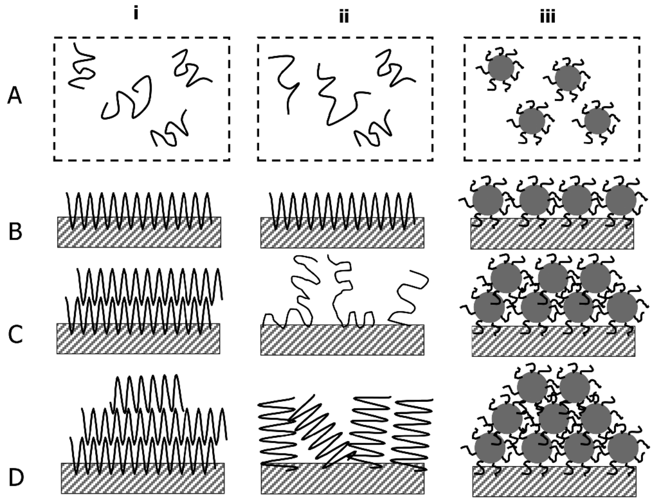

*Figure 7. Schematic depictions of conformations within Regimes A (top views) and B through D (side views) for (i) PDMS, (ii) PDMS-Stabilizer, and (iii) PDMS-MNPs.*

## Acknowledgments

The authors are grateful for financial support from the National Science Foundation (CHE-0239633, DMR-0312046, and DMR-0552661) and the Virginia Tech Aspires Program.

## References

1. Sohn, B. H.; Cohen, R. E. *Chem. Mater.* **1997**, *9*, 264–269.
2. Tamai, H.; Sakurai, H.; Hirota, Y.; Nishiyama, F.; Yasuda, H. *J. Appl. Polym. Sci.* **1995**, *56*, 441–449.
3. Bulte, J. W.; Brooks, R. A.; Moskowitz, B. M.; Bryant, L. H., Jr; Frank, J. A. *Magn. Reson. Med.* **1999**, *42*, 379–384.
4. Ivkov, R.; DeNardo, S. J.; Daum, W.; Foreman, A. R.; Goldstein, R. C.; Nemkov, V. S.; DeNardo, G. L. *Clin. Cancer Res.* **2005**, *11*, 7093–7103.
5. Vorotnikova, E.; Ivkov, R.; Foreman, A. R.; Tries, M.; Braunhut, S. J. *Int. J. Radiat Biol.* **2006**, *82*, 549–559.
6. Kondo, A.; Fukuda, H. *J. Ferment. Bioeng.* **1997**, *84*, 337–341.
7. Needham, D.; Mclntosh, T. J.; Simon, S. A.; Zhelev, D. *Curr. Opin. Colloid Interface Sci.* **1998**, *3*, 511–517.
8. Mendenhall, G. D.; Geng, Y.; Hwang, J. *J. Colloid Interface Sci.* **1996**, *184*, 519–526.
9. Pardoe, H.; Chua-anusorn, W.; St. Pierre, T. G.; Dobson, J. *J. Magn. Magn. Mater.* **2001**, *225*, 41–46.
10. Harris, L. A.; Goff, J. D.; Carmichael, A. Y.; Riffle, J. S.; Harburn, J. J.; St. Pierre, T. G.; Saunders, M. *Chem. Mater.* **2003**, *15*, 1367–1377.

Downloaded by UNIV OF GUELPH LIBRARY on June 23, 2012 | http://pubs.acs.org
Publication Date (Web): November 9, 2010 | doi: 10.1021/bk-2010-1051.ch006

11. Liu, X.; Kaminski, M. D.; Riffle, J. S.; Chen, H.; Torno, M.; Finck, M. R.; Taylor, L.; Rosengart, A. J. *J. Magn. Magn. Mater.* **2007**, *311*, 84–87.
12. Woodward, R. C.; Heeris, J.; St. Pierre, T. G.; Saunders, M.; Gilbert, E. P.; Rutnakornpituk, M.; Zhang, Q.; Riffle, J. S. *J. Appl. Crystallogr.* **2007**, *40*, 495–500.
13. Zhang, Q.; Thompson, M. S.; Carmichael-Baranauskas, A. Y.; Caba, B. L.; Zalich, M. A.; Lin, Y.-N.; Mefford, O. T.; Davis, R. M.; Riffle, J. S. *Langmuir* **2007**, *23*, 6927–6936.
14. Dumazet-Bonnamour, I.; Le Perchec, P. *Colloids Surf., A* **2000**, *173*, 61–71.
15. Wormuth, K. *J. Colloid Interface Sci.* **2001**, *241*, 366–377.
16. Moeser, G. D.; Roach, K. A.; Green, W. H.; Laibinis, P. E.; Hatton, T. A. *Ind. Eng. Chem. Res.* **2002**, *41*, 4739–4749.
17. Mefford, O. T.; Woodward, R. C.; Goff, J. D.; Vadala, T. P.; St. Pierre, T. G.; Dailey, J. P.; Riffle, J. S. *J. Magn. Magn. Mater.* **2007**, *311*, 347–353.
18. Rutnakornpituk, M.; Thompson, M. S.; Harris, L. A.; Farmer, K. E.; Esker, A. R.; Riffle, J. S.; Connolly, J.; St. Pierre, T. G. *Polymer* **2002**, *43*, 2337–2348.
19. Stevenson, J. P.; Rutnakornpituk, M.; Vadala, M.; Esker, A. R.; Charles, S. W.; Wells, S.; Dailey, J. P.; Riffle, J. S. *J. Magn. Magn. Mater.* **2001**, *225*, 47–58.
20. Wilson, K. S.; Goff, J. D.; Riffle, J. S.; Harris, L. A.; St. Pierre, T. G. *Polym. Adv. Technol.* **2005**, *16*, 200–211.
21. Sahoo, Y.; Pizem, H.; Fried, T.; Golodnitsky, D.; Burstein, L.; Sukenik, C. N.; Markovich, G. *Langmuir* **2001**, *17*, 7907–7911.
22. Sun, S.; Zeng, H. *J. Am. Chem. Soc* **2002**, *124*, 8204–8205.
23. Kaganer, V. M.; Möhwald, H.; Dutta, P. *Rev. Mod. Phys.* **1999**, *71*, 779–819.
24. Knobler, C. M.; Desai, R. C. *Annu. Rev. Phys. Chem.* **1992**, *43*, 207–236.
25. McConnell, H. M. *Annu. Rev. Phys. Chem.* **1991**, *42*, 171–195.
26. Möhwald, H. *Annu. Rev. Phys. Chem.* **1990**, *41*, 441–476.
27. Dutta, P. In *Studies in Interface Science*; Dietmar, M., Reinhard M., Eds.; Elsevier Press: New York, 2002; Vol. 16, pp 1−12.
28. Debreczeny, M. P.; Svec, W. A.; Wasielewski, M. R. *Science* **1996**, *274*, 584–587.
29. Cantor, R. S.; Dill, K. A. *Langmuir* **1986**, *2*, 331–337.
30. Hénon, S.; Meunier, J. *Rev. Sci. Instrum.* **1991**, *62*, 936–939.
31. Hönig, D.; Möbius, D. *J. Phys. Chem.* **1991**, *95*, 4590–4592.
32. Deng, J.; Farmer-Creely, C. E.; Viers, B. D.; Esker, A. R. *Langmuir* **2004**, *20*, 2527–2530.
33. Deng, J.; Hottle, J. R.; Polidan, J. T.; Kim, H.; Farmer-Creely, C. E.; Viers, B. D.; Esker, A. R. *Langmuir* **2004**, *20*, 109–115.
34. Deng, J.; Polidan, J. T.; Hottle, J. R.; Farmer-Creely, C. E.; Viers, B. D.; Esker, A. R. *J. Am. Chem. Soc.* **2002**, *124*, 15194–15195.
35. Hottle, J. R.; Kim, H.; Deng, J.; Farmer-Creely, C. E.; Viers, B. D.; Esker, A. R. *Macromolecules* **2004**, *37*, 4900–4908.
36. Kim, H.; Deng, J.; Lalli, J. H.; Riffle, J. S.; Viers, B. D.; Esker, A. R. *Langmuir* **2005**, *21*, 1908–1916.
37. Ni, S.; Lee, W.; Li, B.; Esker, A. R. *Langmuir* **2006**, *22*, 3672–3677.

38. Bercegol, H.; Gallet, F.; Langevin, D.; Meunier, J. *J. Phys. (Paris)* **1989**, *50*, 2277–2289.
39. Moy, V. T.; Keller, D. J.; Gaub, H. E.; McConnell, H. H. *J. Phys. Chem.* **1986**, *90*, 3198–3202.
40. Sauer, B. B.; Yu, H.; Yazdanian, M.; Zografi, G.; Kim, M. W. *Macromolecules* **1989**, *22*, 2332–2337.
41. Dutta, P.; Peng, J. B.; Lin, B.; Ketterson, J. B.; Prakash, M.; Georgopoulos, P.; Ehrlich, S. *Phys. Rev. Lett.* **1987**, *58*, 2228–31.
42. Ulman, A. *An Introduction to Ultrathin Organic Films: From Langmuir−Blodgett to Self-Assembly*; Elsevier Press: New York, 1991.
43. Petty, M. C. *Langmuir−Blogett Films*; Cambridge University Press: London, 1996.
44. Garrett, W. D.; Zisman, W. A. *J. Phys. Chem.* **1970**, *74*, 1796–1805.
45. Seo, Y.; Skarlupka, R.; Yu, H. *Polym. Eng. Sci.* **1998**, *38*, 741–748.
46. Skarlupka, R.; Seo, Y.; Yu, H. *Polymer* **1997**, *39*, 387–392.
47. Sohn, D.; Yu, H.; Nakamatsu, J.; Russo, P. S.; Daly, W. H. *J. Polym. Sci., Part B: Polym. Phys.* **1996**, *34*, 3025–3034.
48. Fang, K.; He, P. *Huaxue Tongbao* **2001**, 608–613.
49. Gau, C. S.; Yu, H.; Zografi, G. *J. Colloid Interface Sci.* **1994**, *162*, 214–221.
50. Earnshaw, J. C.; Grattan, M. W. D.; Lunkenheimer, K.; Rosenthal, U. *J. Phys. Chem. B* **2000**, *104*, 2709–2713.
51. Earnshaw, J. C.; McGivern, R. C.; McLaughlin, A. C.; Winch, P. J. *Langmuir* **1990**, *6*, 649–660.
52. Earnshaw, J. C.; Nugent, C. P.; Lunkenheimer, K. *Langmuir* **1997**, *13*, 1368–1370.
53. Earnshaw, J. C.; Sharpe, D. J. *J. Chem. Soc., Faraday Trans.* **1996**, *92*, 611–618.
54. Runge, F. E.; Yu, H.; Woermann, D. *Ber. Bunsen-Ges. Phys. Chem.* **1994**, *98*, 1046–1055.
55. Runge, F. E.; Yu, H. *Langmuir* **1993**, *9*, 3191–3199.
56. Esker, A. R.; Zhang, L.-H.; Olsen, C. E.; No, K.; Yu, H. *Langmuir* **1999**, *15*, 1716–1724.
57. Sauer, B. B.; Chen, Y. L.; Zografi, G.; Yu, H. *Langmuir* **1988**, *4*, 111–117.
58. Sauer, B. B.; Kawaguchi, M.; Yu, H. *Macromolecules* **1987**, *20*, 2732–2739.
59. Kawaguchi, M.; Sauer, B. B.; Yu, H. *Macromolecules* **1989**, *22*, 1735–1743.
60. Kim, C.; Yu, H. *Langmuir* **2003**, *19*, 4460–4464.
61. Esker, A. R.; Zhang, L. H.; Sauer, B. B.; Lee, W.; Yu, H. *Colloids Surf., A* **2000**, *171*, 131–148.
62. Kim, C.; Esker, A. R.; Runge, F. E.; Yu, H. *Macromolecules* **2006**, *39*, 4889–4893.
63. Sacchetti, M.; Yu, H.; Zografi, G. *Rev. Sci. Instrum.* **1993**, *64*, 1941–1946.
64. Sacchetti, M.; Yu, H.; Zografi, G. *Langmuir* **1993**, *9*, 2168–2171.
65. Sacchetti, M.; Yu, H.; Zografi, G. *J. Chem. Phys.* **1993**, *99*, 563–566.
66. Naumann, C. A.; Brooks, C. F.; Fuller, G. G.; Knoll, W.; Frank, C. W. *Langmuir* **1999**, *15*, 7752–7761.
67. Brooks, C. F.; Fuller, G. G.; Frank, C. W.; Robertson, C. R. *Langmuir* **1999**, *15*, 2450–2459.

Downloaded by UNIV OF GUELPH LIBRARY on June 23, 2012 | http://pubs.acs.org
Publication Date (Web): November 9, 2010 | doi: 10.1021/bk-2010-1051.ch006

68. Deng, J.; Viers, B. D.; Esker, A. R.; Anseth, J. W.; Fuller, G. G. *Langmuir* **2005**, *21*, 2375–2385.
69. Monroy, F.; Ortega, F.; Rubio, R. G.; Ritacco, H.; Langevin, D. *Phys. Rev. Lett.* **2005**, *95*, 1–4.
70. Hård, S.; Neuman, R. D. *J. Colloid Interface Sci.* **1987**, *120*, 15–29.
71. Granick, S. *Macromolecules* **1985**, *18*, 1597–1602.
72. Jarvis, N. L. *J. Phys. Chem.* **1966**, *70*, 3027–3033.
73. Braslau, A.; Deutsch, M.; Pershan, P. S.; Weiss, A. H.; Als-Nielsen, J.; Bohr, J. *Phys. Rev. Lett.* **1985**, *54*, 114–117.
74. Hård, S.; Hamnerius, Y.; Nilsson, O. *J. Appl. Phys.* **1976**, *47*, 2433–2442.
75. Lucassen-Reynders, E. H.; Lucassen, J. *Adv. Colloid Interface Sci.* **1970**, *2*, 347–395.
76. Langevin, D. *J. Colloid Interface Sci* **1981**, *80*, 412–475.
77. Sano, M.; Kawaguchi, M.; Chen, Y. L.; Skarlupka, R. J.; Chang, T.; Zografi, G.; Yu, H. *Rev. Sci. Instrum.* **1986**, *57*, 1158–1162.
78. Hård, S.; Neuman, R. D. *J. Colloid Interface Sci.* **1981**, *83*, 315–334.
79. Fox, H. W.; Taylor, P. W.; Zisman, W. A. *Ind. Eng. Chem.* **1947**, *39*, 1401–1409.
80. Mann, E. K.; Henon, S.; Langevin, D.; Meunier, J. *J. Phys. II (France)* **1992**, *2*, 1683–1704.
81. Mann, E. K.; Langevin, D. *Langmuir* **1991**, *7*, 1112–1117.
82. Lenk, T. J.; Lee, D. H. T.; Koberstein, J. T. *Langmuir* **1994**, *10*, 1857–1864.

Downloaded by UNIV OF GUELPH LIBRARY on June 23, 2012 | http://pubs.acs.org
Publication Date (Web): November 9, 2010 | doi: 10.1021/bk-2010-1051.ch006

Downloaded by STANFORD UNIV GREEN LIBR on June 25, 2012 | http://pubs.acs.org
Publication Date (Web): November 9, 2010 | doi: 10.1021/bk-2010-1051.ch007

## Chapter 7

# Characterization of Complex Engineering Silicones by $^1$H Multiple Quantum NMR and Large Scale Molecular Dynamics Simulations

**Robert S. Maxwell,* Richard H. Gee, Theodore Baumann,
Naida Lacevic, Julie L. Herberg, and Sarah C. Chinn**

**Lawrence Livermore National Laboratory, 7000 East Ave.,
Livermore, CA 94550, USA
*maxwell7@llnl.gov**

Static $^1$H Multiple Quantum Nuclear Magnetic Resonance (MQ-NMR) and large scale Molecular Dynamics (MD) simulations have been used to understand structure property relationships in silicone networks with bi- and tri-modal topology and with both micro- and nano-scale inorganic fillers. The MQ-NMR method characterizes the residual dipolar couplings of the silicone chains that depend on the average molecular weight between physical or chemical constraints. The MQ-NMR experiments allow for quantitative characterization of network structure in these crosslinked and filled systems. Large scale MD simulations have allowed for the characterization of structural perturbations due to the presence of filler particles and the effect of such particles on the composite elastomer's response to strain. Specifically, the polymer-filler network is shown to mitigate the risk of cavitation in the network under tensile strain.

It is generally accepted that the properties of polymeric materials are controlled by the network structure and the reactions by which they have been constructed (*1*). These properties include the bulk moduli at creation, but also the properties as a function of age during use. In order to interpret mechanical

In Advances in Silicones and Silicone-Modified Materials; Clarson, S., et al.;
ACS Symposium Series; American Chemical Society: Washington, DC, 2010.

Downloaded by STANFORD UNIV GREEN LIBR on June 25, 2012 | http://pubs.acs.org
Publication Date (Web): November 9, 2010 | doi: 10.1021/bk-2010-1051.ch007

properties and predict the time dependent changes in these properties, detailed knowledge of the effect of structural changes must be obtained.

In this paper, we provide an overview of our ongoing work using large scale Molecular Dynamics (MD) calculations combined with Mulitple Quantum NMR (MQ-NMR) measurements to gain further insight into some of the structural motifs of filled silicone elastomers and to evaluate the influence of the network structure on the physical and chemical properties of the elastomers, including material performance in severe environments (high temperature, high strains, high radiation fluxes). The ability of MD methods to uncover structural motifs and dynamics at the atomistic scale is well know. In polymer systems, however, the relationship to bulk material properties can be somewhat tenuous due to the often limited number of atoms and short time durations that can be studied. Extending these MD simulations to large assemblies of atoms and extending them to longer times using state of the art computational resources has allowed us to probe some useful relationships. Here, we use MD to study the structural and dynamic changes in bulk PDMS melts under stress. MD provides static and dynamic properties for a collection of particles that allow atomic scale insights that are difficult to gain otherwise. Additionally, static $^1$H MQ-NMR spectroscopy has shown the ability to provide more reliable and quantitative information regarding the elastomer network structure and heterogeneities (*2–6*). $^1$H MQ-NMR methods allow for the measurement of absolute residual dipolar couplings ($<\Omega_d>$) and segmental/cooperative dynamics Thus, the MQ-NMR method allows for the direct measure of network topology and in many cases, filler-particle interactions.

## Experimental

MQ-NMR experiments were performed on filled silicone networks, described elsewhere (*2–6*). The gum stocks for all formulations were endlinked networks of PDMS chains of variable length. The silicones were reinforced with fillers of various sizes (Cab-o-Sil d ~ 200 Å, Polyhedral Oligomeric Silesquioxane (POSS) and meta-carborane, d ~ 10 Å) and crosslinked with standard organotin curing agents.

All MQ-NMR experiments were performed on a Bruker Avance 400 MHz spectrometer equipped with a 5mm Bruker TBI probe. The pulse sequence used is described in detail elsewhere (*2*). MQ growth curves were obtained generally by incrementing the base MQ preparation sequence. Further details are described elsewhere (*2*, *6*). Insight was obtained on the network structure from the distributions of the residual dipolar couplings extracted from the MQ growth curves using a fast Thikonov regularization (FTIKREG) algorithm (*7*). Correlation to network structure were obtained by using the well established relationship between the dynamic order parameter, $S_b$, the residual dipolar coupling, and the number of statistical segments between chemical or physical constraints:

$$S_b = \frac{1}{P_2(\cos\alpha)} \frac{\langle \Omega_d \rangle}{\langle \Omega_d \rangle_{static}} = \frac{3r^2}{5N} \tag{1}$$

Downloaded by STANFORD UNIV GREEN LIBR on June 25, 2012 | http://pubs.acs.org
Publication Date (Web): November 9, 2010 | doi: 10.1021/bk-2010-1051.ch007

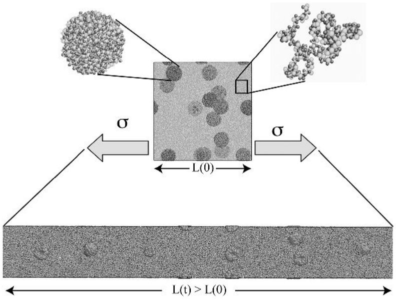

*Figure 1. Illustration of the filled PDMS system under uniaxial tension.*

The MD simulations of PDMS and silica-filled/PDMS composites were carried out on a variety of bulk amorphous ensembles using three-dimensional periodic boundary conditions. In the simulations, the PDMS polymer chains are each composed of repeating silicon-oxygen bonds along the polymer chain backbone,[1] and two methyl ($CH_3$) moieties (treated here as united-atoms) pendent to the Si atoms along the polymer backbone. The united-atom model representation treats each carbon and its bonded hydrogen atoms as a single united particle, whereas Si and O atoms are each represented as individual particles. The chemical structure of the PDMS molecule is $[\text{-O-Si}(CH_3)_2\text{-}]_n$, where $n$ is the number of repeat units or monomers; where $n = 120$ for all PDMS chains used in this work. Thus, the molecular weight of our PDMS chains is $M_w = 8{,}880$ *g/mol*, where the molecular weight between entanglements for PDMS has been determined to be $M_e \sim 8{,}100$ *g/mol* (*8*, *9*), thus, our PDMS melts are weakly entangled, since $M_c < M_w$.

The bulk *pure* PDMS (unfilled) ensembles consisted of 1,331 unbranched PDMS polymer chains. The silica-filled/PDMS composite consisted of 1,280 unbranched PDMS polymer chains and 16 spherical *fused* silica nanoparticles (80/1 polymer/filler ratio; ~6 weight percent, where the diameter of the nanoparticles are ~40 Å). Further, the number of surface hydroxyl groups was ~4OH/100 Å$^2$, consistent with experiment (*10*). The nanocomposites simulations employed the force field parameter set of Frischknecht *et al.* (*11*) to describe the PDMS atom pair interactions, as well as the PDMS valence terms. The valence terms and atomic pair interactions of the silica nanoparticle employed the CFF91 force field parameter set (*12*, *13*). All valence degrees of freedom were explicitly treated and unconstrained. Further, all unlike atom pairs were determined using the 6th order combination law (*14*). In all simulations, a standard Nose-Hoover thermostat and barostat (*15*) was used and the applied constant pressure in the extension direction ranged from 10-80 *MPa*. All computations were carried out with LAMMPS (*14*, *16*). An illustration of the composite ensembles used in the simulations are shown in in Figure 1. Further details of the MD simulations reported here can be found elsewhere (*17*).

Downloaded by STANFORD UNIV GREEN LIBR on June 25, 2012 | http://pubs.acs.org
Publication Date (Web): November 9, 2010 | doi: 10.1021/bk-2010-1051.ch007

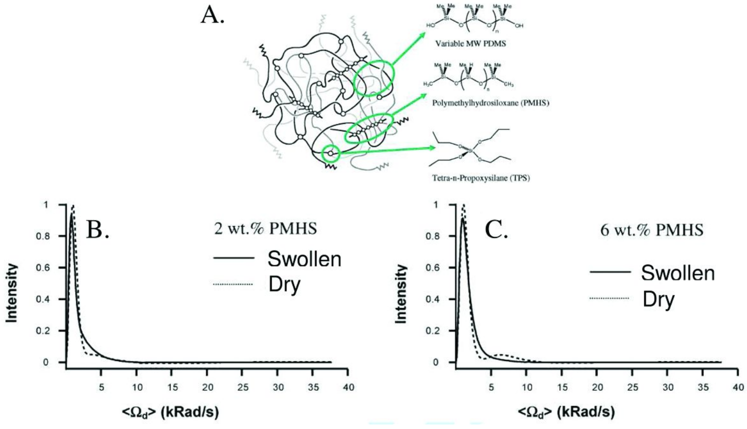

*Figure 2. (A) Schematic of network structure of typical engineering silicone with both short and long chain constituents and standard four site crosslinking species and highly functional crosslinking sites; (B) Distributions of $<\Omega_d>$ for low PMHS content network; (C) Distributions of $<\Omega_d>$ for high PMHS content networks.*

# Results and Discussion

## MQ NMR Characterization of Multicomponent Silicone Materials

Typical filled silicone composites for engineering applications are often constructed from end-linking of polymer chains of multiple lengths (i.e. bimodal and trimodal networks), highly functional crosslinking sites (providing > 4 site junctions), and inorganic fillers of multiple size scales and incorporation (e.g. functionalized, blended, bonded). A cartoon of a typical structure is shown in Figure 2A. Upon formation of the network, a detailed picture of the structure is inferred from knowledge of the starting materials. We have used MQ-NMR to characterize the distributions of residual dipolar couplings, $<\Omega_d>$, and thus the amplitude of the segmental dyamics and via equation (1), the MW between crosslinks in a series of synthesized model networks. The results of regularization of the MQ NMR growth curves for two trimodal PDMS networks formed with the highly functional crosslinker Polymethylhydrosiloxane (PMHS) in the dry and swollen state are shown in Figure 2B and 2C. The distribution of the residual dipolar couplings, $<\Omega_d>$, observed for both samples in the dry state are characterized by near Gaussian distributions centered at 1 krad/sec and 6 krad/sec. The distributions are surprisingly narrow, as has been observed in other formuations and is discussed in detail elsewhere (*6*). Using the relationship between $<\Omega_d>$ and 1/N in Equation (1), we can convert these probability curves to curves representing the probability distrbituions of monomers between crosslinks, MW between crosslinks, or crosslink density (1/MW) as shown in Figure 3. The partitioning and the mean MW between crosslinks compares favorably with what would be expected from the entanglement MW and the MW of the short chains, as is discussed in more detail in ref (*3*). Upon swelling, the distributions of $<\Omega_d>$ smear out and begin to gain more resemblance to a Gamma distribution

Downloaded by STANFORD UNIV GREEN LIBR on June 25, 2012 | http://pubs.acs.org
Publication Date (Web): November 9, 2010 | doi: 10.1021/bk-2010-1051.ch007

expected form Gaussian chain statistics. These changes have been ascribed to heterogeneities in interchain interactions with increasing PMHS content (*3*).

Results of regularization of MQ-NMR growth curves for a bimodal network filled with increasing amounts of a high surface area micro-filler (unmodified Cab-o-sil) are shown in Figure 4A. The distributions show that the addition of inorganic filler increases the average $<\Omega_d>$ and increases the width of the distribution and thus decreases the segmental mobility via reduction of the effective crosslink density. This increase in the effective crosslink density is expected due to the formation of a large number of interfacial hydrogen bonds and van der Waals interactions that constrain the polymer motion, particularly at fill levels greater than 10 wt.%. Though the effects are observed in both the low and high molecular weight chains, the high molecular weight chains are perturbed to a greater extent, likely due to the increased mobility of these chains and the increased amount of free volume that the fillers can occupy in these domains.

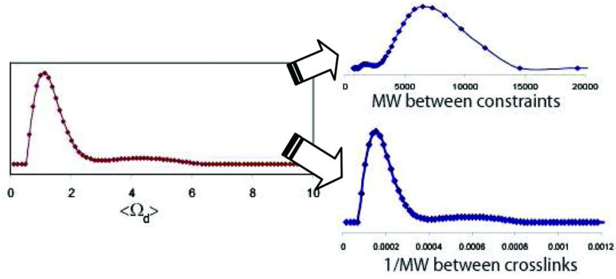

*Figure 3. Conversion of MQ-NMR derived probability distributions into distributions of MW and crosslink density using equation (1).*

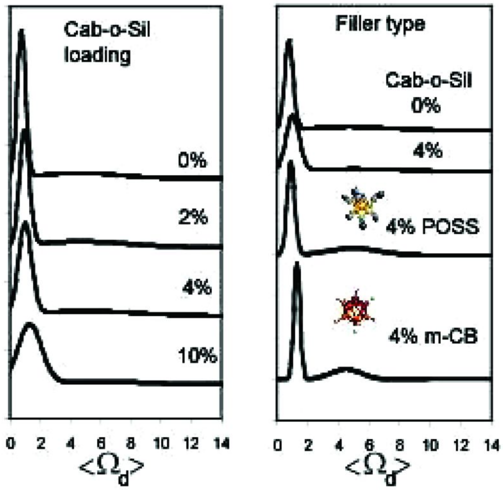

*Figure 4. Effect of fillers on segmental dynamics in bimodal PDMS networks as determined by MQ-NMR: A) increasing wt.% of Cab-o-Sil; B) effect of nanometric fillers compared to microfillers.*

We have also applied the MQ-NMR approach to samples synthesized from the same bimodal network, but filled with low amounts of nanoscale inorganic fillers, in this case meta-carborane and octamethyl-POSS. The results of regularization are shown in Figure 4B. We observe similar perturbations of the segmental dynamics in the case of these fillers. In the case of these nanometric fillers, the degree of surface interactions is unknowns since the size of the filler is on the order of the radius of gyration of the polymer chains. We postulate that the decrease in the segmental dynamics in this case is arising from overlapping effects of decreased free volume via occupation by the filler and the formation of transient filler-polymer interactions (*8*).

Downloaded by STANFORD UNIV GREEN LIBR on June 25, 2012 | http://pubs.acs.org
Publication Date (Web): November 9, 2010 | doi: 10.1021/bk-2010-1051.ch007

## MD Simulation of Effect of Filler Content to Structural Changes in Filled Silicone Materials

As illustrated by the changes observed in segmental dynamics observed by NMR, above, and by a number of other experimental and computational studies, it is known that polymer chains next to the confining surfaces form sorbed layers. In contrast to molecular liquids, polymer molecules usually participates in a few different layers, as illustrated in Fig. 5. The chains that form layered structures have very low mobilities or are even immobilized. If we define the interfacial layer as the region where local polymer density oscillates, then both our earlier simulation and integral equation data (*18*, *19*) and present simulation results (see Fig. 6b) are within the range of experimental observations (*20–22*). Polymer chains neighboring the layered region still do not represent 'bulk' polymer, since some of the chains from this region are parts of the immobile polymer. It has been observed that as the distance between filler particles increases, further layers of polymer are identified (*19*). In particular, we can see that local density distribution shown in Fig. 6 indicates very high probability for the polymer to be adsorbed on the silica surface.

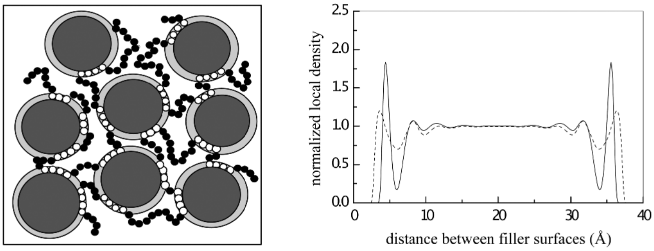

*Figure 5. Illustration of polymer bridging between embedded filler particles in a polymer/filler composint (a). (b) Structural perturbations due to presence of filler (Si-solid curve; $CH_3$-dotted curve).*

Downloaded by STANFORD UNIV GREEN LIBR on June 25, 2012 | http://pubs.acs.org
Publication Date (Web): November 9, 2010 | doi: 10.1021/bk-2010-1051.ch007

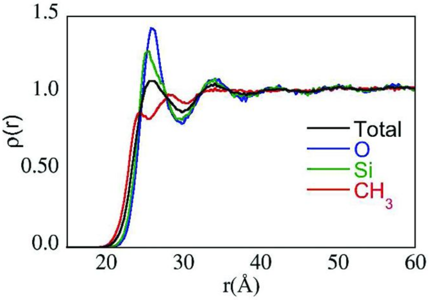

*Figure 6. PDMS local density profile next to a silica nano-filler 'surface' at 550 K; the filler particle has an effective diameter of ~40 Å (see color insert)*

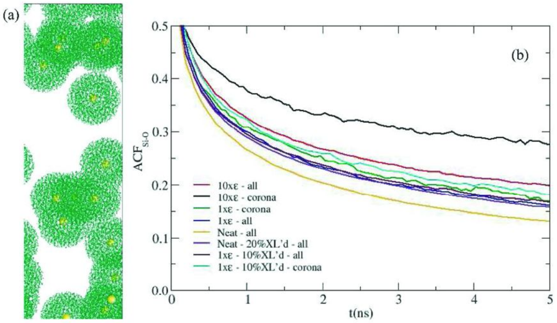

*Figure 7. (a) Illustration of the "bound" PDMS polymer interfacial layer (green; labeled as the 'corona') around the silica filler (represented as yellow sphere); white space is the "bulk" polymer matrix. (b) Si-O bond autocorrelation function for a variety of PDMS ensembles; filled ensembles have a volume fraction of* $\phi = 0.26$*. The "bound" polymer layer ('corona' layer) is chosen as the polymer layer ~30 Å from the surface of the filler. The cross-link number density and polymer/filler interaction strengths are labeled. (see color insert)*

An illustration of the interfacial layer from an MD simulation with a 0.26 filler volume fraction is shown in Figure 7a, where the ~40 Å silica filler is represented as the 'yellow' sphere, and the surrounding interfacial layer (chosen as a ~30 Å region about the filler surface) is shown in green. The mobility of the PDMS polymer in the composite was determined by computing the relaxation times of the Si-O bond vector via a time-dependent autocorrelation function, given as,

$$ACF_{Si-O}(t) = \frac{\left\langle \mathbf{d}_{Si-O}(0) \cdot \mathbf{d}_{Si-O}(t) \right\rangle}{\left\langle \mathbf{d}_{Si-O}(0)^2 \right\rangle}, \qquad (2)$$

where $\mathbf{d}_{Si-O}$ is the Si-O bond vector, and $\langle\ \rangle$ is the ensemble average. The results show that: (i) relaxation times are slower for crosslinked networks (as expected), (ii) relaxation times of filled systems are slower than unfilled systems (as expected), (iii) relaxation times are slower near the filler surface (~0-30 Å)

Downloaded by STANFORD UNIV GREEN LIBR on June 25, 2012 | http://pubs.acs.org
Publication Date (Web): November 9, 2010 | doi: 10.1021/bk-2010-1051.ch007

as compared to the bulk, and (iv) relaxation times are dramatically slowed by increased polymer/filler interaction strength. The crosslink number density and polymer/filler interaction strengths are labeled as follows: $\varepsilon$ is the polymer/filler interaction strength and XL's refers to the percent crosslinking; e.g., $10\text{x}\varepsilon$- corona refers to the $ACF_{Si-O}(t)$ computed for only those Si-O bond vectors within 0-30 Å region of the filler particle with an interaction strength between polymer and filler which is 10 times that of the original CFF91 energy term in the Lennard-Jones 9-6 potential between the filler and polymer atoms (*12*, *13*).

Our simulations show that in the immediate vicinity of the particle surface there is a shell around filler particles formed by an adsorbed polymer. The thickness of this shell does not exceed ~1.5 nm; the shell is strongly adsorbed to the surface of filler particle and may result in the limiting of the mobility of adsorbed molecules (see previous discussion). This agrees well with the experimental evidence, which suggest that the restriction of the chains mobility does not extend throughout the material but affects only the chains within a few nanometers of the filler surface. To further understand the effects of the silica filler in the PDMS composites, MD simulations were performed with varying degrees of silica filler loadings. In these MD simulations, The filled and unfilled ensembles were uniaxially extended, and the degree of cavitation was determined (illustrative simulation cells are shown in Fig. 8 at a strain of $\lambda = 4$). The appearance of cavities, which may lead to mechanical failure, are diminished at increased filler loading and require a larger imposed stress to manifest.

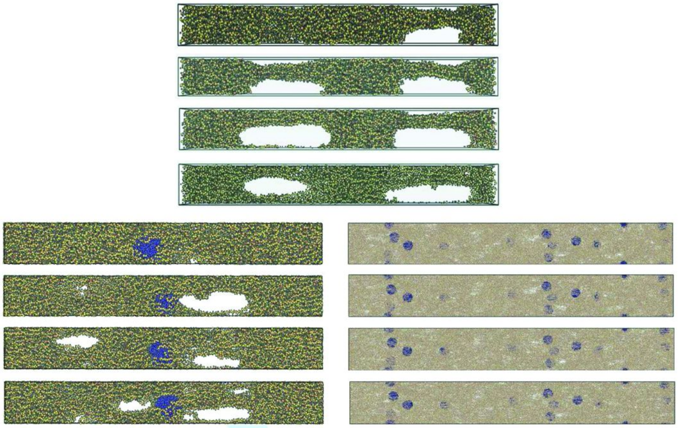

*Figure 8. Snapshots of the filled and unfilled systems at* $\lambda = 4$*. The imposed 'stress' along the y-axis is 50, 60, 70, and 80 MPa (from top to bottom, respectively). (see color insert)*

Downloaded by STANFORD UNIV GREEN LIBR on June 25, 2012 | http://pubs.acs.org
Publication Date (Web): November 9, 2010 | doi: 10.1021/bk-2010-1051.ch007

**Table 1. Elastic constants obtained from MD. The bulk modulus, *($B_o$)* and Young's modulus, *(E)* obtained from MD simulations at 298 K. The shear modulus, *(G)* and Poisson's ratio, *($\nu$)* are computed the equations above**

| *Ensemble*[a] | *$B_o$ (GPa)*[b] | *E(MPa)*[c] | *G(MPa)* | $\nu$ |
|---|---|---|---|---|
| Unfilled | 0.80 | 1.6 | 0.53 | 0.50 |
| Unfilled 10% XL'd | 0.80 | 4.5 | 1.5 | 0.50 |
| Unfilled 20% XL'd | 0.80 | 6.0 | 2.0 | 0.50 |
| 6% Filled 10% XL'd | 0.80 | 5.0<br>0.2-9.4[d] | 3.8 | 0.50 |
| 6% Filled 20% XL'd | 0.80 | 80.0 | 27.0 | 0.48 |

[a] XL'd ≡ Crosslinking number density. [b] $B_o$ is obtained by fitting the isothermal *PV* data Sun equation-of-state (*23*). [c] Experimental values for PDMS range from 0.2-1 MPa. [d] Callow et al., *Biofouling* **2008**, *21*, 41.

To further characterize the PDMS/silica filler model, the bulk modulus, $B_o$, derived from simulated isothermal PV simulations, and the Young's modulus, $E$, obtained by fitting the linear region of the stress-strain curve were determined; the shear modulus, $G = {}^{3B_oE}\!/_{9B_o-E}$, and Poisson's ratio, $\nu = {}^{3B_o-E}\!/_{6B_o}$, are thus computed from the computationally derived quantities, $B_o$ and $E$. The computed bulk modulus, $B_o$, were obtain by fitting to the Sun equation-of-state (see ref. (*23*)). The results of the MD simulations are tabulated in Table 1. The computed modular properties are found to agree well with experiment.

## Conclusions

We are employing studies of the role of network topology and filler content on the segmental dynamics and polymer structure and ordering using Multiple Quantum NMR and large scale Molecular Dynamics calculations. MQ_NMR methods allow for the selective characterization of dynamics in individual domains in multimodal silicone networks. The effect of fillers, both micro and nanoscale, were characterized. Results of MD simulations of filled silicones indicates surface adsorbtion and layering. Polymer chains sorbed to the inorganic surface are motionally retarded. This reduction in the segmental dynamics, however, is not isolated to the sorbed layer, but extends into the "bulk" network. Further MD simulations have characterized the role of filler particles on the resistance of filled composites to tensile failure through cavitation.

## Acknowledgments

This work performed under the auspices of the U.S. Department of Energy by Lawrence Livermore National Laboratory under Contract DE-AC52-07NA27344. Part of this work was supported by the LLNL Laboratory Directed Research and Development (LDRD) program (tracking number: 06-SI-005).

# References

1. Brook, M. A. *Silicon in Organic, Organometallic, and Polymer Chemistry*; John Wiley & Sons: New York, 2000.
2. Saalwächter, K. *J. Am. Chem. Soc.* **2003**, *125*, 14684.
3. Maxwell, R. S.; Chinn, S. C.; Solyom, D.; Cohenour, R. *Macromolecules* **2005**, *38*, 7026.
4. Gjersing, E.; Chinn, S.; Maxwell, R. S.; Giuliani, J. R.; Herberg, J.; Eastwood, E.; Bowen, D.; Stephens, T. *Macromolecules* **2007**, *40*, 4953.
5. Giuliani, J. R.; Gjersing, E. L.; Chinn, S. C.; Jones, T. V.; Wilson, T. M.; Alviso, C. A.; Herberg, J. L.; Pearson, M. A.; Maxwell, R. S. *J. Phys. Chem B* **2007**, *111*, 12977.
6. Saalwächter, K. *Prog. NMR Spectrosc.* **2007**, *51*, 1.
7. Honerkamp, J.; Weese, J. Fast Tikhonov Regularization (FTIKREG) © Freiburger Materialforschunszentrum F.M.F. *Comput. Phys. Commun.* **1992**, *69*, 99.
8. Lewicki, J. P.; Maxwell, R. S.; Patel, M.; Herberg, J. L.; Swain, A. C.; Liggat, J. J.; Pethrick, R. A. *Macromolecules* **2008**, *41*, 9179.
9. Graessly, W. W. *Adv. Polym. Sci.* **1974**, *16*, 1.
10. Bordeaux, D.; Cohen-Addad, J. P. *Polymer* **1990**, *31*, 743.
11. Frischknecht, A. L.; Curro, J. G. *Macromolecules* **2003**, *36*, 2122.
12. Maple, J. R.; Dinur, U.; Hagler, A. T. *Proc. Natl. Acad. Sci. U.S.A.* **1988**, *85*, 5350.
13. Maple, J. R.; Hwang, M. J.; Stockfisch, T. P.; Dinur, U.; Waldman, M.; Ewig, C. S.; Hagler, A. T. *J. Comput. Chem.* **1994**, *15*, 162.
14. Waldman, M.; Hagler, A. T. *J. Comput. Chem.* **1993**, *14*, 1077.
15. Nose, S. *Mol. Phys.* **1984**, *52*, 255.
16. Plimpton, S. J. *J. Comp. Phys.* **1995**, *117*, 1.
17. Lacevic, N. M.; Maxwell, R. S.; Saab, A.; Gee, R. H. *J. Phys. Chem. B* **2006**, *110*, 3588.
18. Gee, R. H.; Maxwell, R. S.; Balazs, B. *Polymer* **2004**, *45*, 3885.
19. Henderson, D.; Trokhymchuk, A.; Kalyuzhnyi, Y. V.; Gee, R. H.; Lacevic, N. *J. Phys. Chem. C* **2007**, *111*, 15625.
20. Arrighi, V.; Higgins, J. S.; Burgess, A. H.; Floudas, G. *Polymer* **1998**, *39*, 6369.
21. Kirst, K. U.; Kremer, F.; Litvinov, V. M. *Macromolecules* **1993**, *26*, 975.
22. Litvinov, V. M.; Spiess, H. *Macromol. Chem. Phys.* **1991**, *192*, 3005.
23. Sun, Z. H.; Mo, S.; Yan, Z. T. *Polymer* **1992**, *33*, 328.

Downloaded by STANFORD UNIV GREEN LIBR on June 25, 2012 | http://pubs.acs.org
Publication Date (Web): November 9, 2010 | doi: 10.1021/bk-2010-1051.ch007

Downloaded by UNIV OF DELAWARE MORRIS LIB on June 24, 2012 | http://pubs.acs.org
Publication Date (Web): November 9, 2010 | doi: 10.1021/bk-2010-1051.ch008

## Chapter 8

# Characterization of a Biomedical Grade Silica-Filled Silicone Elastomer Using Ultrasound

**Alexander R. Anim-Mensah,[1] Jeffrey E. Franklin,[1] Aniruddha S. Palsule,[1] Luis A. Salazar,[2] Christopher W. Widenhouse,[3] David B. Mast,[4] James E. Mark,[5] William B. Krantz,[1] and Stephen J. Clarson*,[1]**

**[1]Department of Chemical and Materials Engineering,
University of Cincinnati, Cincinnati, OH 45221, USA
[2]Department of Biomedical Engineering, University of Texas,
Austin, TX 78712, USA
[3]Ethicon Endo-Surgery, Inc., 4545 Creek Road, Cincinnati, OH 45242, USA
[4]Department of Physics, University of Cincinnati,
Cincinnati, OH 45221, USA
[5]Department of Chemistry, University of Cincinnati,
Cincinnati, OH 45221, USA
*E-mail: Stephen.Clarson@UC.Edu**

Silicone gels and elastomers are often used in environments where it is desirable to be able to measure their properties *in-situ*. Examples include implanted biomaterials, assembled membrane modules, engineering seals and engineering gaskets. In this investigation, the properties of a biomedical grade silica-filled poly(dimethylsiloxane) (PDMS) elastomeric membrane have been investigated non-invasively using real-time Ultrasonic Time-Domain Reflectometry (UTDR). Water was used to apply pressure to one side of a silicone elastomer which was contained within a steel membrane module. The water pressure was applied: (i) in a constant mode but with increasing and decreasing pressure and (ii) in a pulsed or cyclic mode at two average pressure values. The flow rate of the water through the sealed membrane cell was 140 ml/min. It has been widely reported in the literature that filled

In Advances in Silicones and Silicone-Modified Materials; Clarson, S., et al.;
ACS Symposium Series; American Chemical Society: Washington, DC, 2010.

Downloaded by UNIV OF DELAWARE MORRIS LIB on June 24, 2012 | http://pubs.acs.org
Publication Date (Web): November 9, 2010 | doi: 10.1021/bk-2010-1051.ch008

silicone systems exhibit compression set. In this investigation, hysteresis was observed in the mechanical properties for the 1 mm thick biomedical grade silica-filled silicone elastomer upon increasing and then decreasing the transmembrane pressure over the range 0 to 450 psi (3.11 MPa). The biomedical grade silica-filled silicone elastomer was also placed under a pulsatile transmembrane pressure mode of 100 psi (0.69 MPa) with a transmembrane pressure amplitude of ± 18 psi (± 0.12 MPa) and of 150 psi (1.04 MPa) and with a transmembrane pressure amplitude of ± 12 psi (± 0.08 MPa). The silicone elastomer was studied over time and an increase in membrane compaction was seen up to constant values for the two pulse modes of 16.6 and 27.0 microns, respectively. It was noted that no water permeation through the silicone membrane was detected under the conditions employed. This approach provides an experimental method for determining the mechanical properties *in-situ* of polymers in various applications. Hence it is possible to realistically monitor the performance of polymeric films and membranes, in this case elastomeric PDMS, for applications involving separation, purification, discrimination (as in sensors), drug delivery and for the selective transport of solutes. The ability to characterize the properties of a membrane within an assembled module or device is a very useful way of monitoring its performance.

## Introduction

We describe herein a method for determining the mechanical properties of nonporous polymeric membranes noninvasively using ultrasound. The performance of elastomeric membranes can be monitored *in situ* under pressure with or without water permeation using Ultrasonic Time-Domain Reflectometry (UTDR). In particular, poly(dimethylsiloxane) (PDMS) elastomers and various siloxane-containing materials are of interest to us in the form of dense films (*1*–*3*).

Applications of siloxane polymers (silicones) and siloxane-containing polymers range from implants to membranes for separations. Silicones were found to be one of the first types of commercial biocompatible synthetic polymeric materials (*4*, *5*) and they have been used in many biomedical products outside the human body, on the human body and in the human body (*3*). Silicones have also been used as membranes where they can separate, purify, discriminate, deliver and selectively transport some molecules relative to others. One of the applications in membrane technology is to separate or purify organics from aqueous solutions (*6*, *7*). Silicones can also provide discrimination in sensors (*8*) and in fuel cell applications, where they allow only a particular target molecule to pass through a membrane (*9*, *10*).

In addition, PDMS and related silicone-containing polymers are found in drug-delivery devices such as transdermal drug patches (*11*). Applications involving selective transport (*12*) are seen in contact lenses (*13*) where they allow molecular oxygen to get to the eye and water molecules to diffuse out. The same principle is also seen in some miniature optical components (*14*) as well as in membrane lung oxygenators. Some other applications of PDMS and related polymers are seen in silicon wafer interconnectors for mechanical stability (*15*) as well as in spring materials found in accelerometers (*16*). They have also been used as the top elastomer on a perceptible sensor (*17*) because of their ability to avoid affecting the sensitivity of these devices. Moreover, they are used as flexible encapsulation material for the mechanical and chemical decoupling of sensors from their environment (*18*).

PDMS has a low glass transition temperature (150 K) (*19*) and is widely used as an elastomer when covalently cross-linked (*20*). It is physically and chemically stable, and a typical silicone elastomer has been reported to possess a shear elastic modulus of about 250 kPa (*20*). PDMS also has a low temperature dependence of its shear elastic modulus (1.1 kPa/°C) and a high compressibility (*20*). Other properties of PDMS include ease of processing, low curing temperature, high flexibility, the option of changing functional groups and low variation of properties with time and temperature (*20*). The properties of PDMS (especially the small change of properties with time and temperature) make it suitable for a variety of applications that includes micro-fabrication into mechanical and chemical sensors. However, the creep behavior of PDMS could negatively impact its performance (including flux and selectivity or separation factor, depending on the support and clamping system) when used in pressure-driven membrane separations or in implants that require subjection to the beat of the heart and other applications that put the PDMS under stress. The above applications of PDMS and related silicone-containing polymers indicate that the mechanical properties of these materials need to be determined for proper materials selection, failure prevention and device optimization for a given task. Moreover, these mechanical properties are used to predict the response of these materials under stress.

There is a need to evaluate the mechanical properties of polymeric materials in real time under either static, ramped or periodic loading. Applications of polymers including implants that are exposed to heart beats need to be assessed reliably in a timely manner without surgery. Membrane materials with permeation under different driving forces need to be analyzed in real time to realistically determine the effects of change in mechanical properties with time and to enhance the development of a mechanically stable selective layer or support and also to understand the effect of compaction on membrane performance.

The application of ultrasound presents a noninvasive technique to determine the tensile strength, the compressive strength, the yield strength, the Young's modulus, the flexural stiffness and the inelastic deformations of polymeric materials in real time. Thus, ultrasound is useful for monitoring the performance and change in mechanical properties of polymers with time *in situ*.

Downloaded by UNIV OF DELAWARE MORRIS LIB on June 24, 2012 | http://pubs.acs.org
Publication Date (Web): November 9, 2010 | doi: 10.1021/bk-2010-1051.ch008

Downloaded by UNIV OF DELAWARE MORRIS LIB on June 24, 2012 | http://pubs.acs.org
Publication Date (Web): November 9, 2010 | doi: 10.1021/bk-2010-1051.ch008

## Theory of UTDR

The underlying principles of UTDR are based upon a change in the velocity or energy of a sound wave as it passes through different media that are in contact with each other. When sound waves contact a material, the energy is partitioned between transmission, absorption and reflection. The reflected waves are of interest for this particular application. The energy partitioning depends on the acoustic impedance difference between the media in contact, the thicknesses of the media and the surface roughness. The acoustic impedance ($z$) is obtained as the product of the density of the medium ($\rho$) and the velocity (c) of sound through the medium by the following equation (*21–23*)

$$z = \rho c \tag{1}$$

It is worth noting that materials which strongly absorb the sound waves will not be good candidates for UTDR applications since the weakly reflected waves are likely to register a very small undefined (or absent) reflection peak.

The acoustic (compression) wave velocity that propagates through solid materials is also related to material properties such as the Young's modulus (E) and the density of the medium, as well as the nature of the support. By utilizing the Poisson's ratio ($\upsilon$) at a specific temperature the following equation is obtained (*21–23*)

$$c = \sqrt{\frac{E}{\rho}\left(\frac{(1-\upsilon)}{(1+\upsilon)(1-2\upsilon)}\right)} \tag{2}$$

The velocity of sound waves travelling through liquid media can also be estimated from a knowledge of the bulk modulus (β) and the density using the following equation (*21–23*)

$$c = \sqrt{\frac{\beta}{\rho}} \tag{3}$$

In principle, the contact between two materials having large differences in acoustic impedance results in a discrete boundary where a large fraction of the acoustic energy is reflected or absorbed depending on the arrangement shown in Figures 1 and 2. Figure 1 shows an arrangement where the sound energy travels from a less dense medium (1) to a denser medium (2). In this case one is likely to encounter a large reflected wave from the interface with a large echo signal since the sound wave is traveling from a low impedance ($z_1$) to a high impedance ($z_2$) medium.

Figure 2 shows an arrangement where the sound energy travels from a denser medium through to a less dense medium. Since the impedance of medium 2 is higher than medium 1, this arrangement will likely result in lower amplitude reflected waves from the interface.

When the incident waves are perpendicular to the media, the amplitude (A) of the reflected wave relative to the incident wave is given by the following equation (*20*)

Downloaded by UNIV OF DELAWARE MORRIS LIB on June 24, 2012 | http://pubs.acs.org
Publication Date (Web): November 9, 2010 | doi: 10.1021/bk-2010-1051.ch008

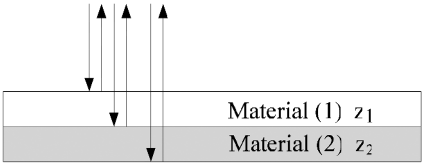

*Figure 1. Acoustic wave traveling from a less dense (1) to a more dense (2) material*

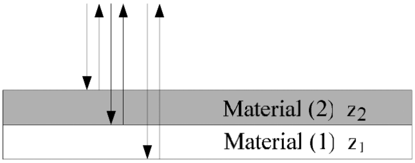

*Figure 2. Acoustic wave traveling from a denser (2) to a less dense (1) material*

$$A=\frac{z_1-z_2}{z_1+z_2} \quad (4)$$

Sound energy can have characteristics whereby the reflected wave is not significantly attenuated and this results in the transducer detecting waves from each distinct interface.

In our experiments, an acoustic transducer with a pulser/receiver emits and receives the sound waves. The time delay for the emitted waves to travel through the media and back to the transducer (known as the “time of flight” or the “arrival time”) is used to calculate the location of the interfaces or the change in thickness from a known reference point. The position of each interface registers a different time response and is used to monitor the position of the interface relative to a reference. It is known that the change in the arrival time ($\Delta t$) is proportional to the distance of the interfaces from a reference point at any time (t) as per the following equation (*21–26*)

$$\Delta l=\frac{c\Delta t}{2} \quad (5)$$

Here, $\Delta l$ is the distance from a reference point or change in thickness. The percent compaction is calculated using Equation (6):

$$\text{Percent Compaction}=\frac{\Delta l}{l}\times 100\% \quad (6)$$

Below we will describe the application of UTDR to characterize a biomedical grade silica-filled poly(dimethylsiloxane) (PDMS) elastomeric membrane within an assembled membrane module.

Downloaded by UNIV OF DELAWARE MORRIS LIB on June 24, 2012 | http://pubs.acs.org
Publication Date (Web): November 9, 2010 | doi: 10.1021/bk-2010-1051.ch008

# Experimental

## Materials

The material used for these investigations was a 1 mm thick sheet of a commercial biomedical grade silica-filled silicone elastomer. The silicone samples were kindly provided by Ethicon Endo-Surgery, Inc., Cincinnati, OH, USA (MED-4850 and MED-4854 Nusil Silicone Technology, Carpinteria, CA, USA). The biomedical grade silica-filled silicone elastomer is used for implantable medical devices (*27*). The silica loading of the elastomer was 30% $SiO_2$. The eluent was 18 M Ω Millipore deionized water and was applied to one side of the silicon elastomer (see Figure 3).

As described above, the UTDR-permeation studies involve determining the mechanical properties of porous and non-porous polymeric membranes and films used for separation, delivery, discrimination (sensing) and medical devices that require non-invasive and non-destructive determination of the mechanical properties under both static and dynamic conditions in real-time. The UTDR apparatus used for the present investigation is shown in Figure 3. The two main aspects of the procedure relate to the characterization process and to the ultrasound measurements. The process apparatus consisted of a permeation cell, a back pressure regulator (BPR, TESCOM Model 54-2164d24), a rotameter (505 ml/min max, Cole-Parmer), a surge tank, a feed tank, a weighing scale and a positive displacement pump (Alpha Laval, Model 7901-SEF). The acoustic measurement apparatus consisted of an acoustic transducer (5 MHz, Panametrics 5/0.5), an oscilloscope (HP 500 MHz, 1GSa/s) and a pulser/receiver (Model 5052PR) which can give measurements with a resolution of ± 0.01 microns. Depending on the mechanical properties of interest, the membrane can be supported in different configurations. In this investigation, both the non-pulsatile and pulsatile measurements were conducted with the silicone elastomer supported on a sintered stainless steel plate.

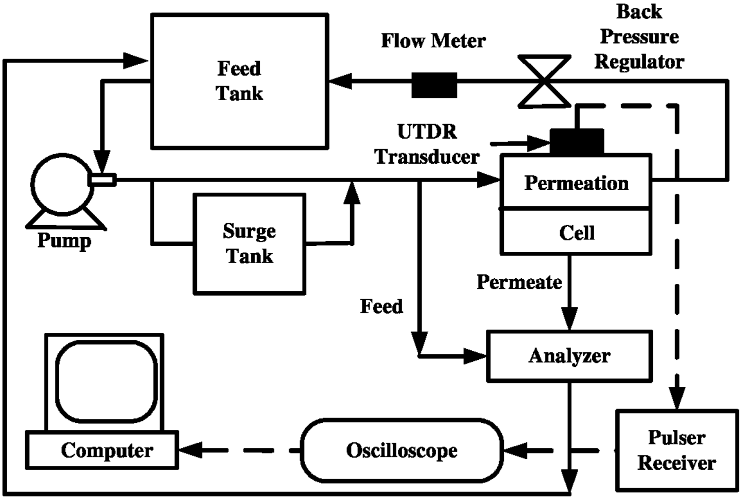

*Figure 3. Permeation process flow loop with attached UTDR apparatus*

Downloaded by UNIV OF DELAWARE MORRIS LIB on June 24, 2012 | http://pubs.acs.org
Publication Date (Web): November 9, 2010 | doi: 10.1021/bk-2010-1051.ch008

## Characterization Protocol

The experimental procedure involved cutting a three-inch diameter PDMS sample, placing it in the permeation cell on the porous support and securing it with a Teflon O-ring (McMaster) after which the cell was clamped shut. The arrangement is shown in Figure 4. The compacting fluid, which was water in this case, was circulated through the system using a positive displacement pump to bleed off any air trapped within the system (seen as bubbles in the rotameter) and also to prevent the transducer reading fluctuations due to any air bubbles. The rotameter and BPR permitted fixing the required flow rate and transmembrane (compressive) pressure, respectively. A flow rate of 140 ml/min and transmembrane pressure ranges of 0 to 450 psi (3.11 MPa) were used. The transmembrane pressure was increased and decreased in steps of 100 psi (0.69 MPa) and then 50 psi (0.35 MPa) within the transmembrane pressure range at the same feed rate. The positive displacement pump was used to provide the pressure for the system whereas the surge tank was used to eliminate pulsations from the pump. The system was adjusted until steady-state conditions were achieved at each transmembrane pressure. The mechanical properties of the silicone elastomer were determined in the present case without water permeation - since we did not detect any permeate on the downstream side of the PDMS elastomer at the transmembrane pressures used in this study.

## Ultrasound Measurements

Figure 4 shows a cross-sectional view of the permeation cell with the attached UTDR transducer. The position of the test sample surfaces or interfaces and the amplitude of the reflected waves were assigned from the times (seconds) and volts (V), respectively as recorded on the oscilloscope traces.

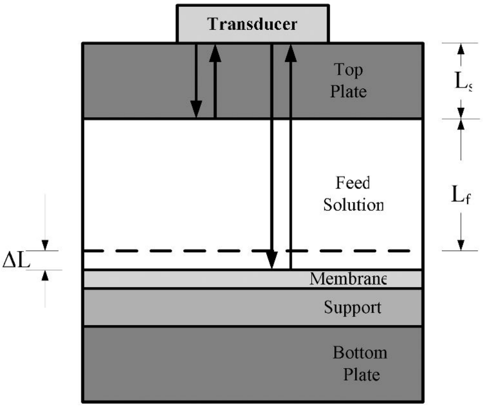

*Figure 4. Cross-sectional view of the permeation cell with mounted ultrasonic transducer*

Downloaded by UNIV OF DELAWARE MORRIS LIB on June 24, 2012 | http://pubs.acs.org
Publication Date (Web): November 9, 2010 | doi: 10.1021/bk-2010-1051.ch008

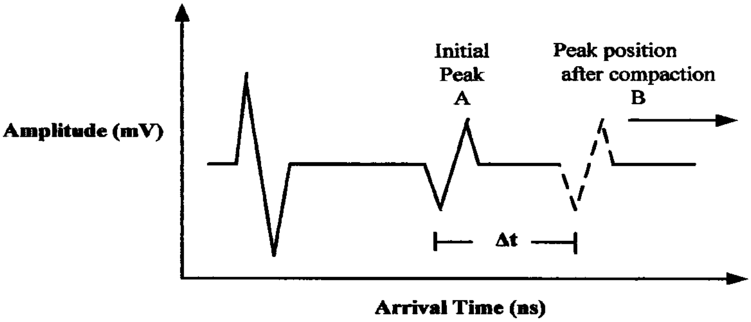

*Figure 5. Ultrasonic time-domain response as seen on the oscilloscope*

Equation (7) was used to determine the initial position of the sample surface as given by the peak time on the oscilloscope.

$$t_1 = 2\left[\frac{L_s}{V_s} + \frac{L_f}{V_f}\right] \tag{7}$$

This analysis requires a knowledge of the dimensions of the cell ($L_S$) and the depth of the fluid ($L_f$) above the test materials, as well as the velocity of sound $V_S$ and $V_f$ through the upper portion of the cell media and the fluid, respectively. The reflected acoustic wave needs to travel twice the distance from the acoustic transducer to the layer of interest. The UTDR response on the oscilloscope is shown in Figure 5 where "A" denotes the initial peak position (reference) of the test material as found on the oscilloscope (see equation (7)) and "B" is the position after compaction.

During compaction the fluid occupying the cavity between the lower and the upper portion of the cell is displaced since the lower and upper portions of the cell are fixed. The velocity of sound through water was 1500 m/s and the change in thickness as a result of compaction of the test material was calculated using the following equation

$$\Delta l(\mu m) = \frac{1500\Delta t(ns)}{2} \tag{8}$$

The accuracy of the measurement was found to be dependent on the resolution of the oscilloscope in measuring the response time, since it is proportional to the compaction.

Downloaded by UNIV OF DELAWARE MORRIS LIB on June 24, 2012 | http://pubs.acs.org
Publication Date (Web): November 9, 2010 | doi: 10.1021/bk-2010-1051.ch008

## Results and Discussion

Some properties of the biomedical grade silica-filled poly(dimethylsiloxane) (PDMS) elastomer are given in Table 1.

**Table 1. Properties of the biomedical grade silica-filled (30% $SiO_2$) poly(dimethylsiloxane) (PDMS) elastomer**

| *Property* | *Result* | *Metric Conv.* | *ASTM* |
|---|---|---|---|
| Specific Gravity | 1.15 | | D792 |
| Durometer - Type A | 50 | | D2240 |
| Tensile Strength | 1,400 psi | 9.7 MPa | D412, D882 |
| Elongation | 660% | | D412, D882 |
| Tear Strength | 230 ppi | 40.6 kN/m | D624 |
| Stress @ 200% Strain | 400 psi | 2.8 MPa | D412, D882 |

Hysteresis was observed upon applying and then removing pressure on one side of the silicone elastomer membrane with a compaction of 4.6 microns for the 1 mm thick filled PDMS elastomer after the compression / decompression cycle. Specifically, in Figure 6 the compaction in microns is plotted as a function of the transmembrane pressure for the PDMS elastomer. A sequence where the pressure was first increased to 100 psi (0.69 MPa) and then in steps of 50 psi (0.35 MPa) from 100 psi (0.69 MPa) to 450 psi (3.11 MPa) was followed. Each transmembrane pressure was held for approximately 20 minutes at a constant feed rate of 140.0 ml/min and then decreased in the same manner back to zero transmembrane pressure. No measurable permeation of water through the silicone membrane was detected under the conditions used.

Figure 7 shows the variation of the transmembrane pressure (compressive stress) with the instantaneous compressive strain for the PDMS elastomer upon increasing and then decreasing the transmembrane pressure. The increasing and decreasing pressures showed a compressive strain response that followed different paths associated with the observed hysterisis. The increasing pressure showed a higher compressive strain than the decreasing pressure. This was because compaction with the progressively increasing pressure caused the PDMS to lose some of its elasticity. The final strain recorded at zero pressure for the decreasing pressure represents a measure of the inelastic deformation.

Downloaded by UNIV OF DELAWARE MORRIS LIB on June 24, 2012 | http://pubs.acs.org
Publication Date (Web): November 9, 2010 | doi: 10.1021/bk-2010-1051.ch008

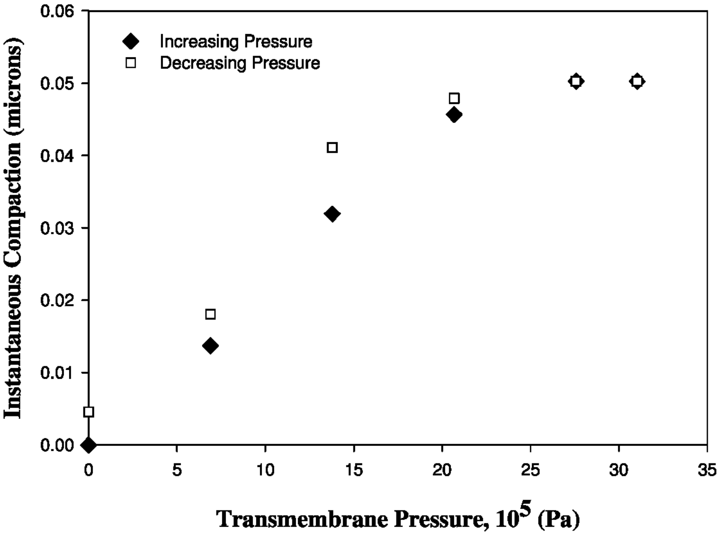

*Figure 6. The instantaneous compaction versus the transmembrane pressure for the silica-filled PDMS elastomer upon increasing and then decreasing the transmembrane pressure (non-pulsating pressures)*

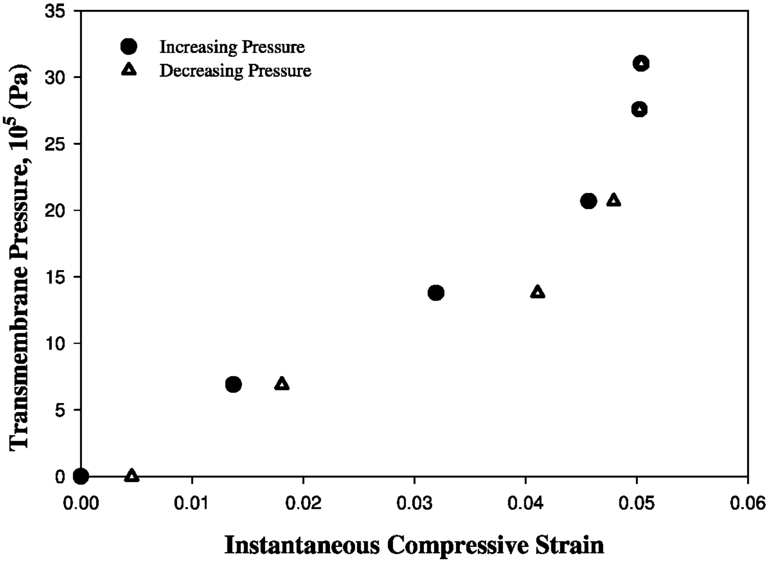

*Figure 7. The transmembrane pressure (compressive stress) versus the instantaneous strain for the silica-filled PDMS elastomer upon increasing and then decreasing the transmembrane pressure*

Downloaded by UNIV OF DELAWARE MORRIS LIB on June 24, 2012 | http://pubs.acs.org
Publication Date (Web): November 9, 2010 | doi: 10.1021/bk-2010-1051.ch008

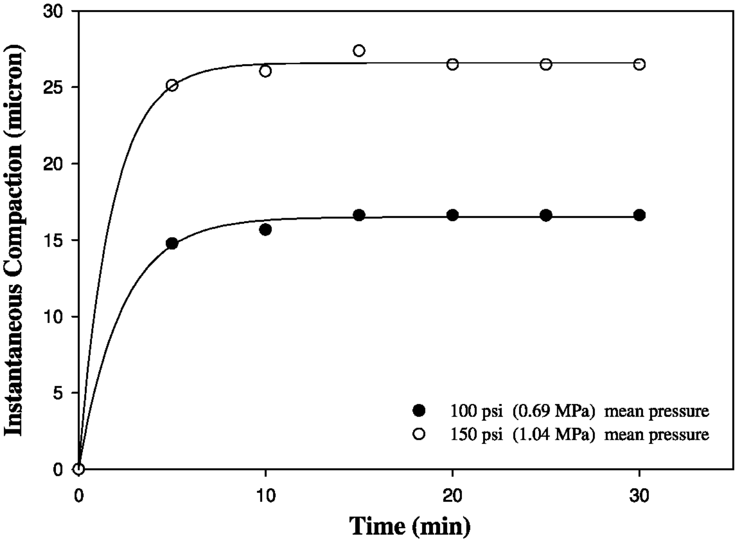

*Figure 8. The instantaneous compaction for the silica-filled PDMS elastomer with time for pulsating transmembrane pressure (pressure oscillating about the mean value by +18 psi (0.12 MPa) then -18 psi (0.12 MPa) for 100 psi (0.69 MPa) and +12 psi (0.08 MPa) then -12 (0.08 MPa) for 150 psi (1.04 MPa)*

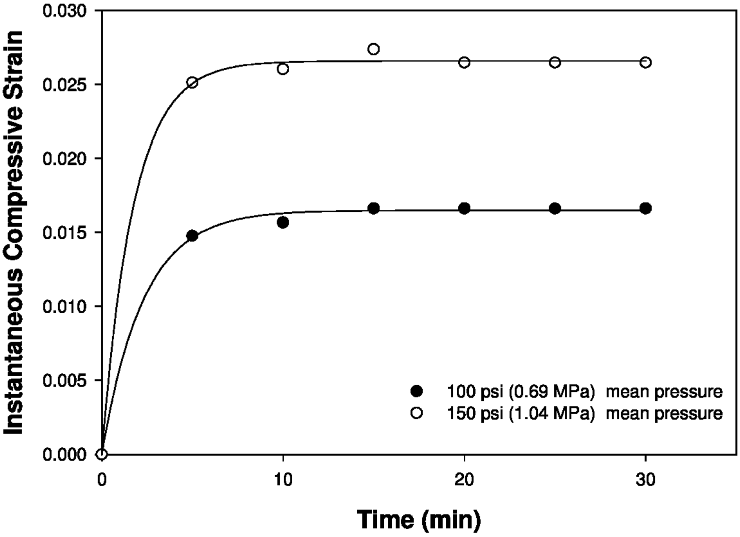

*Figure 9. The instantaneous compressive strain for the silica-filled PDMS elastomer with time for pulsating transmembrane pressure (pressure oscillating about the mean value by +18 psi (0.12 MPa) then -18 (0.12 MPa) for 100 psi (0.69 MPa) and +12 psi (0.08 MPa) then -12 (0.08 MPa) for 150 psi (1.04 MPa)*

Downloaded by UNIV OF DELAWARE MORRIS LIB on June 24, 2012 | http://pubs.acs.org
Publication Date (Web): November 9, 2010 | doi: 10.1021/bk-2010-1051.ch008

Figures 8 and 9 show the compaction and the strain as a function of time for PDMS under a pulsatile transmembrane pressure at two mean transmembrane pressures of 100 psi (0.69 MPa) and 150 psi (1.04 MPa) with transmembrane pressures amplitudes of ± 18 psi ( ± 0.12 MPa) and ± 12 psi ( ± 0.08 MPa), respectively.

Figure 8 shows the variation of compaction with time for PDMS at the two transmembrane pressures. Although the two pressures showed a similar trend for the compaction variation with transmembrane pressure, the higher pressure showed a higher strain relationship. The initial increase in compaction at the same pressure could be due to creep as the material densifies or reorients itself to accommodate the applied pressure.

Figure 9 shows the *instantaneous* compressive strain with time for PDMS at the two transmembrane pressures in a pulsating mode. A similar trend to that in Figure 8 was observed. This is a result of the increased pressure that causes an increased compaction and thereby an increased strain.

## Conclusions

The strain and the inelastic deformation were determined by UTDR for a 1 mm thick sheet of a biomedical grade silica-filled poly(dimethylsiloxane) (PDMS) elastomeric membrane under constant increasing and decreasing transmembrane pressure using water as the compacting fluid at a flow rate of 140 ml/min. The resulting strain and the inelastic deformation values were 0.05 and 4.6 microns, respectively. Pulsatile transmembrane pressures of 100 psi (0.69 MPa) and 150 psi (1.04 MPa) were applied with transmembrane pressure amplitudes of ± 18 psi (± 0.12 MPa) and ± 12 psi (± 0.08 MPa), respectively. This resulted in an increase in compression or compaction until it approaches the constant values of 16.6 and 27 microns that were observed at 100 psi (0.69 MPa) and 150 psi (1.04 MPa), respectively.

The UTDR method has been shown to provide a novel and flexible non-invasive way of assessing and monitoring the performance of polymers in devices and membrane modules under various real-time conditions. A particular advantage of the UTDR method is that it can be used to characterize the mechanical properties during permeation through polymeric membranes. As such UTDR can be used to infer whether factors such as the nature of the permeating solutes, concentration polarization and plasticization affect the mechanical properties of polymeric membranes and thereby the performance and lifetime of membranes.

## Acknowledgments

The authors gratefully acknowledge the financial support from the National Science Foundation Industry/University Cooperative Research Center (I/UCRC) for Membrane Applied Science and Technology (MAST) under Grants EEC-0120823 and EEC-0624148 and through the National Science Foundation

Research Experiences for Undergraduates REU Summer Program under Grant EEC-0139438.

## References

1. Clarson, S. J.; Semlyen, J. A. *Siloxane Polymers*; Prentice Hall: Englewood Cliffs, NJ, 1993.
2. Clarson, S. J.; Mark, J. E. In *The Polymeric Materials Encyclopedia*; Salamone, J. C., Ed.; CRC Press: Boca Raton, FL, 1996; Vol. 10, pp 7663−7677.
3. Van Dyke, M. E.; Clarson, S. J.; Arshady, R. In *Introduction to Polymeric Biomaterials*; Citus Books: London, 2003; pp 109−135.
4. Kurian, P.; Kasibhatla, B.; Daum, J.; Burns, C. A.; Moosa, M.; Rosenthal, K. S.; Kennedy, J. P. *Biomaterials* **2003**, *24*, 3493.
5. Park, J. H.; Allen, M. G.; Prausnitz, M. R. *J. Controlled Release* **2005**, *104*, 51.
6. Peng, F.; Pan, F.; Li, D.; Jiang, Z. *Chem. Eng. J.* **2005**, *114*, 123.
7. Zhang, X. K.; Poojari, Y.; Drechsler, L. E.; Kuo, C. M.; Fried, J. R.; Clarson, S. J. *J. Inorg. Organomet. Polym.* **2008**, *18*, 246–252.
8. Rego, R.; Caetano, N.; Mendes, A. *Sens. Actuators, B* **2005**, *111-112*, 150.
9. Shah, K.; Shin, W. C.; Besser, R. S. *J. Power Sources* **2003**, *123*, 172.
10. Shah, K.; Shin, W. C.; Besser, R. S. *Sens. Actuators, B* **2004**, *97*, 157.
11. Paranjape, M.; Garra, J.; Brida, S.; Schneider, T.; White, R.; Currie, J. *Sens. Actuators, A* **2003**, *104*, 195.
12. Pantoja, R.; Nagarah, J. M.; Strafe, D. M.; Melosh, N. A.; Blunck, R.; Bezanilla, F.; Heath, J. R. *Biosens. Bioelectron.* **2004**, *20*, 509–517.
13. Erdodi, G.; Kennedy, J. P. *J. Polym. Sci.* **2005**, *43*, 3491.
14. Parashar, V. K.; Sayah, A.; Pfeffer, M.; Schoch, F.; Gobrecht, J.; Gijs, M. A. M. *Microelectron. Eng.* **2003**, *67-68*, 710.
15. Arquint, P.; van der Wal, P. D.; van der Schoot, B. H.; deRooij, N. F. *Proc. Transducers '95*, Stockholm, 1995.
16. Lötters, J. C.; Olthuis, W.; Veltink, P. H.; Bergveld, P. *J. Micromech. Microeng.* **1996**, *6*, 52–54.
17. Chu, Z. *Flexible Package for a Tactile Sensor Array*, Proc. National Sensor Conference, The Netherlands, 1996.
18. Van Hal, R. E. G. Ph.D. Thesis, University of Twente, The Netherlands, 1994.
19. Lötters, J. C.; Olthuis, W; Veltink, P. H.; Bergveld, P. *J. Micromech. Microeng.* **1997**, *7*, 145–147.
20. Clarson, S. J.; Dodgson, K.; Semlyen, J. A. *Polymer* **1985**, *26*, 930–934.
21. Snyder, R. D.; Byars, E. F. *Engineering Mechanics: Static and Strength of Materials*; McGraw Hill: New York, 1973.
22. Ramaswamy, S.; Greenberg, A. R.; Peterson, M. L. *J. Membr. Sci.* **2004**, *239*, 143.
23. Aerts, P.; Greenberg, A. R.; Leysen, R.; Krantz, W. B.; Reinsch, V. E.; Jacobs, P. A. *Sep. Purif. Technol.* **2001**, *22-23*, 663.
24. Li, J.; Sanderson, R. D. *Desalination* **2002**, *146*, 169.

Downloaded by UNIV OF DELAWARE MORRIS LIB on June 24, 2012 | http://pubs.acs.org
Publication Date (Web): November 9, 2010 | doi: 10.1021/bk-2010-1051.ch008

25. Li, J.; Sanderson, R. D.; Jacobs, E. P. *J. Membr. Sci.* **2002**, *201*, 17.
26. Sanderson, R. D.; Li, J.; Koen, L. J.; Sorensen, L. *J. Membr. Sci.* **2002**, *207*, 105.
27. Palsule, A. S.; Clarson, S. J.; Widenhouse, C. W. *J. Inorg. Organomet. Polym.* **2008**, *18*, 207–221.

Downloaded by UNIV OF DELAWARE MORRIS LIB on June 24, 2012 | http://pubs.acs.org
Publication Date (Web): November 9, 2010 | doi: 10.1021/bk-2010-1051.ch008

## Chapter 9

# Fluorosilicones

**Michael J. Owen***

**Michigan Molecular Institute, Midland, MI 48640**
***michaelowen01@chartermi.net**

Downloaded by DUKE UNIV on June 25, 2012 | http://pubs.acs.org
Publication Date (Web): November 9, 2010 | doi: 10.1021/bk-2010-1051.ch009

Uses that relate to surface properties dominate the silicone industry. Since only aliphatic fluorocarbon-based materials have lower surface energies than conventional silicones such as polydimethylsiloxane (PDMS), it can be expected that fluorocarbon-modified silicones, i.e. fluorosilicones, would exhibit interesting and useful surface behavior. The fundamental characteristics of fluorosilicones are summarized. Significant properties such as surface energy and glass transition temperature are reviewed and related to important applications like release behavior. A particularly interesting subset of these fluorocarbon/silicone hybrids is the perfluoroether-modified silicones. Useful new fluorosilicone materials for release and other applications are a consequence of having both side-chains and backbone that are flexible, low-glass-transition entities.

Silicones can enhance fluorocarbon performance by improving properties such as softness, flexibility, low-temperature resistance, and better adherence to substrates (*1*). Conversely, fluorine incorporation can confer different attributes on silicones, particularly, lower surface energies than those of conventional methyl-based silicones such as polydimethylsiloxane (PDMS). Other familiar benefits of fluorine incorporation, namely higher thermal stability and enhanced chemical resistance, are not so important in the siloxane case as such polymers already have considerable thermal stability and any improvement in chemical stability is limited by the hydrolytic stability of the siloxane backbone at extremes of pH. Thus it is worthwhile to consider what such fluorine/silicone hybrids or fluorosilicones can bring to the important technological area of low-surface-energy materials. Note also that not all fluoropolymers have lower

In Advances in Silicones and Silicone-Modified Materials; Clarson, S., et al.;
ACS Symposium Series; American Chemical Society: Washington, DC, 2010.

Downloaded by DUKE UNIV on June 25, 2012 | http://pubs.acs.org
Publication Date (Web): November 9, 2010 | doi: 10.1021/bk-2010-1051.ch009

surface energies than PDMS so it is quite possible to use PDMS to lower the surface energy of certain fluoropolymers. A recent example of this is given by Baradie et al. (*2*) where the grafting of diisocyanate-terminated PDMS onto OH-functionalized poly(tetrafluoroethylene-*co*-vinyl acetate-*co*-vinyl alcohol) raised the water contact angle from 90° to 104°.

Traditional uses of silicones include thermally-stable elastomers, weather-resistant resins, organic pressure-sensitive adhesive (PSA) release liners, antifoams and wetting agents. Most of these applications depend on the surface properties of silicones. These are related to fundamental polymer characteristics such as intermolecular forces between polymer chains and polymer backbone flexibility. These factors also explain the growing interest in fluorosilicones as fuel-resistant elastomers, anti-graffiti and antifouling coatings and silicone PSA release liners. Fluorosilicone is a rather imprecise term. The term silicone usually implies an alternating silicon-oxygen (siloxane) backbone. The fluorine atoms cannot be usefully bonded directly to silicon as this Si-F functionality is too reactive and has utility only in reactive intermediates. Historically, fluorosilicones have incorporated fluorocarbon groups of structure $R_fX(CH_2)_n$ in place of methyl groups in PDMS into the pendent side-chains yielding siloxane polymer chain structures of the form $[R_fX(CH_2)_n](CH_3)SiO]_x$. Polymers with the $R_f$ substitution in the backbone such as $[Si(CH_2)_nR_f(CH_2)_nSi]$ also need to be considered particularly as they can form alternating structures with siloxanes. The original and most familiar fluorosilicone polymer is polymethyltrifluoropropylsiloxane (PMTFPS) with $CF_3 = R_fX$ and n=2 in the siloxane polymer formula above. This fluorosilicone was first commercialized in the 1950's.

## Fundamental Characteristics

The five fundamental characteristics of fluorosilicones that account for their physical and chemical behavior are:

- Low intermolecular forces
- Size of pendent group
- High siloxane chain flexibility
- High siloxane bond energy
- Partial ionic nature of siloxane bonds

The familiar order of increasing intermolecular forces between hydrocarbon and fluorocarbon moieties is $CF_3$- < -$CF_2$- < $CH_3$- < -$CH_2$-. Clearly, fluoropolymers with plentiful $CF_3$- groups will be preferred to those based on tetrafluoroethylene for further enhancing silicone surface activity. Note that the newer more highly fluorinated fluorosilicones, such as polymethyl-nonafluorohexylsiloxane [PMNFHS], contain all four fluorocarbon and hydrocarbon entities so prediction of surface energy from a simple structural perspective is not straightforward. Note also that the situation can become even more complex if mixed hydrocarbon/fluorocarbon groups such as $CF_2H$- and –CFH- are involved. The size of the pendent group is a trade-off between different attributes. As with all fluoropolymers, the longer $R_F$ groups result in lower surface energies but there is also an increased bulkiness that will reduce polymer chain flexibility and affect the temperature of the glass transition ($T_g$). High siloxane chain flexibility is important for low temperature applications and release. The high siloxane bond energy is a crucial part of the stability of silicones generally at elevated temperatures. The C-F bonds also have high bond energy but backbone integrity is more critical than side-chain stability. The partial ionic nature of the siloxane bond is the source of chemical attack at extremes of pH and is the “Achilles heel” of fluorosilicones in adverse environments.

Two decades ago (*3*), it appeared that the criteria for low surface energy polymers were:

- (i) A flexible linear backbone
- (ii) Sufficient pendent groups based on aliphatic hydrocarbon or fluorocarbon
- (iii) Linking groups between the backbone and pendent groups that introduce no additional adverse factors
- (iv) Combinations of these entities that are adequately stable and have no undesirable interactions

With the greatly increased variety of fluorosilicones and other fluoropolymers that have been studied in the last two decades, it is useful to reexamine these criteria. With the exception of the first one, these still appear to be necessary criteria. Clearly, the first criterion is not a critical one if sufficient pendent groups are present (second criterion). The lowest surface energy fluorosilicones, the fluoroPOSS materials are the most rigid polysiloxanes available. In general, the lower surface energy fluorosilicones have similar surface energies to the lowest surface energy fluoropolymers that do not contain siloxane linkages. That chain flexibility is not required for very low surface energy fluoropolymers has been well established by Tsibouklis and co-workers (*4*, *5*). Indeed, it is explicit in the seminal work of Pittman and Ludwig (*6*) where fluoroacrylates became less wettable as polymer crystallinity was increased. In the case of polymers such as polydimethylsiloxane that lack long side-chains whose alignment can dictate surface packing and orientation, we continue to assert that backbone flexibility is an important factor in surface configuration and resultant surface energy. Moreover, backbone flexibility is a critical attribute in various fluorosilicone applications, notably in the release area and at low temperatures contributing to the broad service temperature range of fluorosilicone elastomers.

One of the factors that has tended to keep fluorosilicones from achieving their potential for very low surface energy is the inclusion in many cases of a methyl group on the silicon atom as well as a fluorinated group. Why this has been so is worthy of comment. In part it results from the nature of PMTFPS being the first commercially successful fluorosilicone. There are considerable technological advantages in the production of such polymers. The presence of the methyl groups allows for a broader range of solvents to be used and enables higher molecular weights and lower cyclic formation to be achieved. Moreover, low surface tension was not the driving force in the development of these early fluorosilicones. This was a property that silicones already exhibited; the primary aim was to enhance

Downloaded by DUKE UNIV on June 25, 2012 | http://pubs.acs.org
Publication Date (Web): November 9, 2010 | doi: 10.1021/bk-2010-1051.ch009

Downloaded by DUKE UNIV on June 25, 2012 | http://pubs.acs.org
Publication Date (Web): November 9, 2010 | doi: 10.1021/bk-2010-1051.ch009

solvent resistance. Indeed fuel and solvent resistant aerospace and automotive applications still account for over 70% of fluorosilicone usage.

A good example of a linking group introducing an adverse factor is seen in the perfluoroether-modified siloxanes described by Thanawala and Chaudhury (*7*). The amide functionality of the fluoroether intermediate provided synthetic feasibility, however, the considerable contact angle hysteresis observed was an indication that these amide groups remained available for interfacial interaction despite being buried in the surface layer. More recent perfluoroether-modified siloxane studies make use of less polar linking entities (*8*).

In the same article as the criteria for low surface energies, we hypothesized that the $SF_5$- pendent group might be particularly effective in achieving very low surface energies. It is interesting to note that polymers containing such entities have recently become available (*9*). As yet their surface properties have not been disclosed but such studies must soon result. Presently, these new fluoropolymers do not contain silicon but the way is now open for such developments to occur.

## Properties and Applications

Fluorosilicone release coatings are needed for silicone-based adhesives and this is presently the most important use of more highly fluorinated fluorosilicones than PMTFPS such as polymethylnonafluorohexylsiloxane (PMNFHS). The conventional explanation for the efficacy of silicones as release coatings is their low surface energy. Some fluorosilicones are available with surface energies comparable to the lowest surface energy fluoropolymers yet reported. Table I summarizes some significant experimental data on surface energy of relevant fluoropolymers.

Detailed comparisons between surface energy values are only meaningful when the full details of measurement conditions, choice of contact angle test liquids, and interpretational methodology are taken into account. For these, readers are referred to the original citations. However, it is clear that some fluorosilicones are available with surface energies comparable to the lowest surface energy fluoropolymers yet reported. Water contact angles also shown in Table I are more directly comparable. The heptadecafluorodecylsilsesquioxane 154 deg value reported by Mabry et al. (*14*), also known as PF8T8, and the perfluoroethersilane/PDMS 140 deg value of Thanawala and Chaudhury (*7*) stand out as being significantly higher than that of the pure fluorocarbon, perfluoroeicosane ($C_{20}F_{42}$). This may seem anomalous but is most likely due to either physical or chemical surface heterogeneity. Mabry et al.'s silsequioxane derivatives (*14*) are also known as POSS (polyhedral oligomeric silsesquioxanes) compounds being based on cages, in this case a cubic $T_8$ cage, with a silicon atom at each corner, joined to each other via a SiOSi linkage and with the fluororadical occupying the other Si valency. There are thus eight fluorinated radicals on each cage, a highly substituted situation in line with their low surface energy and high hydrophobicity. Indeed, the fluoroPOSS materials of Mabry et al. have the highest molecular weight, highest density and lowest surface tension of any POSS compounds that have yet been produced. Note also that Kobayashi's

Downloaded by DUKE UNIV on June 25, 2012 | http://pubs.acs.org
Publication Date (Web): November 9, 2010 | doi: 10.1021/bk-2010-1051.ch009

**Table I. Fluoropolymer Surface Properties**

| *Polymer* | $\sigma_S$ *(mN/m)* | $\theta_a$ *(deg)* |
|---|---|---|
| Polyheptadecafluorodecyloxymethylstyrene (*10*) | 6 | - |
| Poly(heptadecalfluorodecylthiomethyl)oxyethylene (*11*) | 6.2 | 124 |
| $CF_3(CF_2)_7(CH_2)_2SiCl_3$ MAM (*12*) |  | 131 |
| Nonafluorohexylsilsesquioxane (*13*) | 6.6 | 122 |
| Heptadecafluorodecylsilsequioxane (*14*) | 8.7 | 154/124 |
| n-perfluoroeicosane (*15*) | 6.7 | 122 |
| Perfluoroethersilane/PDMS (*7*) | 8 | 140 |
| Polymethylpropenoxyfluoroalkylsiloxane (*16*) | 8.8 | 117 |
| Polymethylnonafluorohexylsiloxane [PMNFHS] (*17*) | 16.3 | 115 |
| Polymethyltrifluoropropylsiloxane [PMTFPS] (*18*) | 21.4 | 104 |
| Polydimethylsiloxane [PDMS] (*19*) | 22.7 | 108 |

nonafluorohexylsilsesquioxane (*13*) is not a POSS compound but rather is a more traditional, disordered silsesquioxane resin, a structural difference that needs to be considered when comparing the data in Table I.

That micro-heterogeneity can produce very large contact angles, a phenomenon also known as “superhydrophobicity” has been known for over half a century but received a new impetus in the late 90’s from a systematic study of the water repellency of plants by two German botanists (*20*) and is often referred to nowadays as the “lotus” effect. Clearly, fluorosilicones with their intrinsically low surface energies are prime candidates for such superhydrophobic coatings. A useful review of this active area of research is given by Callies and Quere (*21*). Mabry (*14*) recently reported at the Silicones and Silicone-Modified Materials IV symposium that the high 154 degree water contact angle for PF8T8 was due to micron scale roughness from the processing procedure. When this is removed by smoother deposition techniques leaving only the nanoscale roughness from the molecular structure, the water contact angle drops to 124 degrees. This compares quite well with the 122 degree value for *n*-perfluoroeicosane. Note that the 131 degree value reported by Crowe et al. (*12*) for a mechanically assembled fluorosilane monomer (MAM) is produced by attachment to a stretched PDMS surface that on relaxation squeezes the chains into densely populated arrays.

All the substrates in Table I are low energy surfaces. However, low surface energy alone does not guarantee excellent release performance. This is clearly illustrated in Table II where relatively poor release of the pressure-sensitive adhesive is evident from certain fluoropolymer surfaces that have lower surface energies than PDMS.

Downloaded by DUKE UNIV on June 25, 2012 | http://pubs.acs.org
Publication Date (Web): November 9, 2010 | doi: 10.1021/bk-2010-1051.ch009

Other factors such as interfacial dynamics and rheological considerations play an important role in this behavior. There are also reports of higher friction on fluorocarbon surfaces compared to hydrocarbons. Chaudhury and Owen (*23*) demonstrated that this was the case for a PDMS slider on fluorocarbon and hydrocarbon monolayers using the JKR contact mechanics methodology. Earlier studies of adhesion between thin monolayer films of fluorocarbon and hydrocarbon, supported on elastomeric PDMS by Chaudhury and Whitesides (*24*) had established that the adhesion hysteresis for the fluorocarbon monolayers was significantly higher than that of the hydrocarbon monolayers. Since friction between surfaces arises from the same types of dissipative processes as those that cause adhesion to be hysteretic, the two phenomena should be formally related. In practical terms of peeling an adhesive from a substrate, both phenomena will be manifest.

In these JKR sliding studies the values of the friction forces do not follow the trend of surface free energies. A polymer property that helps explain this observation is the glass transition temperature ($T_g$). Relevant $T_g$ values are summarized in Table III.

Fluorosilicone PSAs based on methyltrifluoropropylsiloxane (PMTFPS) have, somewhat unexpectedly, been reported to release from conventional PDMS-based release liners (*31*), despite the lower solid surface energy of the former. The liquid surface tension of PMTFPS is significantly higher than that of PDMS, so one possible explanation may be that the silicone PSA surface is more liquid-like in nature rather than solid-like.

Currently, there is concern about certain fluorocarbon-chain intermediates such as perfluorooctanoic acid (PFOA, also called C8) because of their persistence in the environment and toxicity issues. Presumably, the use of substantially longer or shorter side-chains should avoid this problem. However, the latter route to fluorosilicones such as PMNFHS also involves the shorter fluorocarbon-chain/higher surface energy trade-off common to all fluoropolymer systems including fluorosilicones. The use of branched rather than linear fluoroalkyl side-chains shorter than C8 should increase the ratio of $CF_3$- to –$CF_2$- for a given degree of fluorination and thereby enhance the chances of achieving low surface energy polymers. The increased bulkiness of the branched side-chain could be an adverse factor; however, interesting new polymers should result from this approach. The most common fluorosilicone, PMTFPS, is a relatively inert material under normal conditions. However, when exposed to elevated temperatures in air or when burnt, toxic fluorinated compounds such as 3,3,3-trifluoropropionaldehyde (TFPA) are produced. Such a decomposition product is unlikely with PMNFHS but this has yet to be established. In common with all methyl-containing silicones, generation of traces of formaldehyde at elevated temperatures is to be expected with PMNFHS.

Interestingly, both the $CF_3(CF_2)_3(CH_2)_2$silsesquioxane (*13*) and the $(CF_3)_2CHCH_2$silsesquioxane (*31*) have the same water contact angle, 122 deg., as the pure fluorocarbon *n*-perfluoroeicosane (*15*). This is significantly less than the exceptionally hydrophobic heptadececafluorodecylsilsesquioxane value (*13*) of 154 deg. but, nevertheless, indicates that as little as two $CF_3$ groups on one hydrocarbon entity are as effective in increasing hydrophobicity as a four-unit

Downloaded by DUKE UNIV on June 25, 2012 | http://pubs.acs.org
Publication Date (Web): November 9, 2010 | doi: 10.1021/bk-2010-1051.ch009

**Table II. Fracture Energy (G) on Release from Acrylic Adhesive (*22*)**

| *Substrate* | *G ($J/m^2$)* | *$\sigma_S$ (mN/m)* |
|---|---|---|
| Fluorocarbon monolayer | 29 | 11 |
| Polytetrafluoroethylene | 22 | 16 |
| Crystalline hydrocarbon monolayer | 12 | 21 |
| PDMS | 1 | 22 |
| Liquid-like hydrocarbon monolayer | 7 | 23 |
| Polystyrene | 63 | 40 |

**Table III. Fluoropolymer Glass Transition Temperatures**

| *Polymer* | *$T_g$ (K)* |
|---|---|
| Polydimethylsiloxane (PDMS) (*25*) | 150 |
| Polymethyltrifluoropropylsiloxane (PMTFPS) (*26*) | 203 |
| Polymethylnonafluorohexylsiloxane (PMNFHS) (*17*) | 198 |
| Polyoxyhexafluoropropylene (PHFPO) (*27*) | 195-219 |
| Copoly(oxytetrafluoroethylene-oxydifluoromethylene) (*28*) | ~140 |
| Polytetrafluoroethylene (PTFE) (*29*) | 399 (α) |
| | 292 (β) |

linear perfluorocarbon substituent and indicates the potential of shorter, branched perfluorocarbon side-chains.

## Perfluoroethersiloxanes

A combination of low $T_g$ fluoropolymer side-chains on the flexible siloxane backbone offers a fruitful way forward in the design of new fluorosilicone release and other coating substrates. The lowest $T_g$ fluoropolymers are the polyperfluoroethers. Thanawala and Chaudhury (*7*) began research in this novel direction. They modified the surface properties of a PDMS elastomer by reacting up to a few parts per hundred of a perfluoroether allylamide (PFE) into the composition. This reacted with the network and segregated to the air/polymer interface. This segregation was established by x-ray photoelectron spectroscopy (XPS) and contact angle measurements. Peel tests were conducted with an acrylic PSA. Interestingly, incorporation of the PFE significantly increased the release force. One explanation could be interaction between the high energy amide linkage functionality and the PSA. Marked contact angle hysteresis effects were attributed to this factor.

The way forward to enhanced anti-soiling, water repellency, and release behavior is to eliminate the polar amide linkage as shown by Itami et al. (*8*) Commercial products based on perfluoropolyether substituted silanes and siloxanes are available such as antireflective ophthalmic lens coatings (e.g.

In Advances in Silicones and Silicone-Modified Materials; Clarson, S., et al.;
ACS Symposium Series; American Chemical Society: Washington, DC, 2010.

Daikin's Optool™ DSX). In view of the importance of both low surface energy and low $T_g$ it is not surprising that such products have emerged for silicone PSA release liners (e.g. Shin-Etsu's Silfel™). Incorporating fluoroethers into the fluorosilicone backbone rather than the side-chains should also be a fruitful approach. According to Ameduri and Boutevin (*32*) materials such as $Q(C_nF_{2n}O)_p$-Q-$(MeSiRO)_q$ have been claimed in patents. Because of the particular chemistry employed, Q is not a simple hydrocarbon linking group but a rather more complex spacer, e.g. it can be -PhNMeCO-$R_f$-OCMeNPh-. This would be rather rigid and would detract from the flexibility advantage of copolymerizing fluoroethers and siloxanes but is a good indication of very interesting new materials on the horizon.

# Conclusion

In summary, there has been extensive development and expansion of fluorosilicone polymers in recent years resulting in a world-wide market that is presently of the order of 250 million $US. Significant trends can be summarized as follows:

- Increasing interest in more-highly fluorinated silicones than PMTFPS
- Greater variety of synthetic strategies to incorporate fluorine
- Increasing diversity in the nature of the fluorinated moiety
- Variations in the polymer backbone providing a variety of (fluorosiloxane – other fluoropolymer) copolymers.
- Use of small amounts of fluorosilicone in conventional PDMS matrices
- Emergence of fluoroether-siloxane polymers
- Appearance of other fluoropolymer/silicone hybrids, for example, interpenetrating networks and PTFE-filled PDMS.
- Broadening of application areas particularly in the fields of surface protection, personal care, medical materials and release applications.

Dvornic and Tomalia (*33*) classify macromolecular architecture into four categories, linear, cross-linked, branched and dendritic. Even with the great diversity of fluorosilicone polymers that have now been investigated, it is still the case that most fluorosilicones fall into the first two categories. Examples of linear polymer architecture applications include antifoams, lubricants and personal care materials. Examples of cross-linked architectures are elastomers and sealants, release coatings and interpenetrating networks (IPNs). However, there are also a growing number of examples of branched and dendritic structures. The most familiar branched materials are silane self-assembling monolayers (SAMs). Silane SAMs are usually considered as cross-linked assemblies but they can also be classified as a branched, brush-like architecture. The polyhedral oligomeric silsesquioxanes (POSS) materials are essentially the extreme, closed-cage example of branching in silicones. This is an area of great scientific and technological interest currently, for example, the low surface energy heptadecylfluorodecylPOSS discussed earlier by Mabry et al. (*14*). Carbosilane dendrimers and hyperbranched polymers containing fluorocarbon substituents

Downloaded by DUKE UNIV on June 25, 2012 | http://pubs.acs.org
Publication Date (Web): November 9, 2010 | doi: 10.1021/bk-2010-1051.ch009

have been reported by Krska and co-workers (*34*) and Muzafarov et al. (*35*) but as yet there appear to be no dendritic fluorosiloxanes where the siloxane backbone is the dominant branching component. For instance, in the case of the dendrimers investigated by Muzafarov et al. (*35*), a dendritic polycarbosiloxane interior is surrounded by a -$(CH_2)_3Me_2SiOSi(CH_2CH_2CF_3)_3$ fluorosiloxane exterior.

The development of copolymers of fluorosiloxanes and other fluoropolymers is an obvious, major expansion of the field. To this point these are alternating rather than long block copolymers, so their full potential in creating novel very-low-surface energy materials has not yet been fully realized. One of the most exciting of these trends is the emergence of novel, low-glass-transition materials from the combination of the flexible siloxane backbone with flexible perfluoroether side-chains. This new direction is already a commercial reality.

Downloaded by DUKE UNIV on June 25, 2012 | http://pubs.acs.org
Publication Date (Web): November 9, 2010 | doi: 10.1021/bk-2010-1051.ch009

## References

1. Dow Corning, Daikin Set R&D. *C&EN*, **2005**, *83*(17), April 25.
2. Baradie, B.; Lai, P. H. M.; Shoichet, M. S. *Can. J. Chem.* **2005**, *83*, 553.
3. Owen, M. J. *Comments Inorg. Chem.* **1988**, *7*, 195.
4. Tsibouklis, J.; Stone, M.; Thorpe, A. A.; Graham, P.; Nevell, T. G.; Ewen, P. J. *Langmuir* **1999**, *15*, 7076.
5. Graham, P.; Stone, M.; Thorpe, A.; Nevell, T. G.; Tsibloukis, J. *J. Fluorine Chem.* **2000**, *104*, 29.
6. Pittman, A. G.; Ludwig, B. A. *J.Polym. Sci., Polym. Chem. Ed.* **1969**, *7*, 3053.
7. Thanawala, S. K.; Chaudhury, M. K. *Langmuir* **2000**, *16*, 1256.
8. Itami, Y.; Hupfield, P.; Kleyer, D.; Nakai, Y.; Matsutani, T. *PRA Fluorine and Silicone in Coatings*; Paper No. 11; Paint Research Association (PRA): Manchester, U.K., December 2005.
9. Kostov, G.; Ameduri, B.; Sergeeva, T.; Dolbier, Jr., W. R.; Winter, R.; Gard, G. L. *Macromolecules* **2005**, *38*, 8316.
10. Hopken, J.; Molller, M. *Macromolecules* **1992**, *25*, 1461.
11. Kim, B. G.; Son, E.-H.; Kim, S.-E.; Lee, J.-C. *Polym. Mater. Sci. Eng.* **2005**, *93*, 610.
12. Crowe, J. A.; Efimenko, K.; Genzer, J. In *Science and Technology of Silicones and Silicone-Modified Materials*; Clarson, S. J., Fitzgerald, J. J., Owen, M. J., Smith, S. D., Van Dyke, M. E., Eds.; ACS Symposium Series 964; American Chemical Society: Washington, DC, 2007; Chapter 15.
13. Kobayashi, H. *Makromol. Chem.* **1993**, *194*, 2569.
14. (a) Mabry, J.; Vij, A.; Viers, B. D. Oral Presentation, Silicones and Silicone-Modified Materials IV Symposium, American Chemical Society 232nd Fall National Meeting, San Francisco, CA, September 2006. (b) Mabry, J. M.; Vij, A.; Viers, B. D. *Polym. Preprints* **2006**, *47*(2), 1216.
15. Nishino, T.; Meguro, M.; Nakamsae, K.; Matsushita, M.; Ueda, Y. *Langmuir* **1999**, *15*, 4321.
16. Thorpe, A. A.; Nevell, T. G.; Young, S. A.; Tsibouklis, J. *Appl. Surf. Sci.* **1998**, *136*, 99.

17. Kobayashi, H.; Owen, M. J. *Macromolecules* **1990**, *23*, 492.
18. Owen, M. J. *J. Appl. Polym. Sci.* **1988**, *35*, 895.
19. She, H.; Chaudhury, M. K.; Owen, M. J. In *Silicones and Silicone-Modified Materials*; Clarson, S. J., Fitzgerald, J. J., Owen, M. J., Smith, S. D., Eds.; ACS Symposium Series 729; American Chemical Society: Washington, DC, 2000; Chapter 21.
20. Neinhuis, C.; Barthlott, W. *Ann. Bot.* **1997**, *79*, 667.
21. Callies, M.; Quere, D. *Soft Matter* **2005**, April 22, advance article online.
22. Newby, B.-M.; Chaudhury, M. K. *Langmuir* **1997**, *13*, 1805. See also Chaudhury, M. K. *General Adhesion Methods of Contact Mechanics*; Center for Polymer Interfaces, Lehigh University: Bethlehem, PA, p 45. http://polymers.msel.nist.gov/combi/NCMC-2_Presentations/02-mChaudhury.PDF.
23. Chaudhury, M. K.; Owen, M. J. *Langmuir* **1993**, *9*, 29.
24. Chaudhury, M. K.; Whitesides, G. M. *Langmuir* **1991**, *7*, 1013.
25. Lee, C. L.; Johannson, O. K.; Flaningam, O. L.; Hahn, P. *Polym. Prepr.* **1969**, *10* (2), 3111.
26. Stern, S. A.; Shah, V. M.; Hardy, B. J. *J. Polym. Sci., Part B: Polym. Phys.* **1987**, *25*, 1263.
27. Avakian, P.; Starkweather, H. W., Jr. In *Modern Fluoropolymers*; Scheiers, J., Ed.; John Wiley and Sons: New York, 1997; Chapter 3.
28. Scheiers, J. In *Modern Fluoropolymers*; Scheiers, J., Ed.; John Wiley and Sons: New York, 1997; Chapter 24.
29. Kerbow, D. L. In *Polymer Data Handbook*; Mark, J. E., Ed.; Oxford University Press: New York, 1999; p 842.
30. Eckberg, R. P.; Griswold, R. M. In Proceedings of the 29th Annual Meeting of the Adhesion Society, February 19–22, 2006; p 299.
31. Ritter, S. *C&EN* **2006**, *84*(15), 71, April 10.
32. Ameduri, B.; Boutevin, B. *Well-Architectured Fluoropolymers: Synthesis, Properties and Applications*; Elsevier: Amsterdam, 2004; pp 315, 322.
33. Dvornic, P. R.; Tomalia, D. A. *Curr. Opin. Colloid Interface Sci.* **1996**, *1*, 221.
34. Krska, S. W.; Son, D. Y.; Seyferth, D. In *Silicon-Containing Polymers*; Jones, R. G., Ando, W., Chojnowski, J., Eds.; Kluwer Academic Publishers: Dordrecht, The Netherlands, 2000; Chapter 23.
35. (a) Muzafarov, A. M.; Shumilkina, N. A.; Tereshchenko, A. S. *Polym. Prepr.* **2006**, *47*(2), 1149. (b) Shumilkina, N. A.; Myakushev, V. D.; Tatarinova, E. A.; Gallyamov, M. O.; Khokhlov, A. R.; Buzin, M. I.; Muzafarov, A. M. *Dokl. Chem.* **2005**, *403*, 155, Part 2.

Downloaded by DUKE UNIV on June 25, 2012 | http://pubs.acs.org
Publication Date (Web): November 9, 2010 | doi: 10.1021/bk-2010-1051.ch009

Downloaded by OHIO STATE UNIV LIBRARIES on June 24, 2012 | http://pubs.acs.org
Publication Date (Web): November 9, 2010 | doi: 10.1021/bk-2010-1051.ch010

## Chapter 10

# Fluorine-Containing Organosilicon Polymers of Different Architectures. Synthesis and Properties Study

**N. A. Sheremetyeva,[1] N. V. Voronina,[1,2] A. V. Bystrova,[1]
V. D. Miakushev,[1] M. I. Buzin,[3] and A. M. Muzafarov*,[1]**

**[1]N.S. Enicolopov Institute of Synthetic Polymer Materials of Russian Academy of Sciences, Profsoyuznaya ul. 70, 117393 Moscow, Russia
[2]Physics Department of M.V. Lomonosov Moscow State University, 119991 Moscow, Russia
[3]A.N. Nesmeyanov Institute of Organoelement Compounds of Russian Academy of Sciences, Vavilova ul. 28, 119991 Moscow, Russia
*fax: +7 495 335 9000; e-mail: aziz@ispm.ru**

Three types of polymers: linear, hyperbranched polymers and dendrimers were modified via polymer-analogous reaction with the same fluorine-containing reagent to study the influence of the introduction of fluorinated units into the polymer structures on their properties. Quite an unusual feature of this approach is our focus on the investigation of polymer matrix properties rather than on surface activity, chemical inertness, solubility in supercritical $CO_2$, hydrophobicity or oleophobicity studies, which are typical for fluorine-containing polymers; and the use of these fragments to develop matrix properties.

## Introduction

The introduction of fluorine-containing substituents in polymers normally results in dramatic changes in their structure and properties due to the unique features of the fluorinated parts (*1*, *2*). First of all they introduce additional specific interactions in the system, their “oleophobicity” acting as a driving force for reorganization of the molecular structure. Second, such a modification leads to significant changes in interaction with solvents. Third, the considerable decrease of surface energy gives these systems surface active properties that are

In Advances in Silicones and Silicone-Modified Materials; Clarson, S., et al.;
ACS Symposium Series; American Chemical Society: Washington, DC, 2010.

Downloaded by OHIO STATE UNIV LIBRARIES on June 24, 2012 | http://pubs.acs.org
Publication Date (Web): November 9, 2010 | doi: 10.1021/bk-2010-1051.ch010

interesting not only from a practical point of view, but also because they make these polymers suitable for investigation with the Langmuir-Blodgett method (*3*).

The structure and properties of the initial polymer matrix make an important contribution to the properties of final system. The aim of this current work was to estimate the influence of polymer matrix architecture on the properties of fluorine-containing systems. Several polymer matrixes of linear and dendritic structure were chosen for investigation. In general we focused on a comparison of the fluoroderivatives of carbosilane dendrimers and hyperbranched polymers of the same chemical nature. The fluorine-containing outer shell simultaneously transforms dendrimer into the core-shell system, remarkable both in scientific and practical terms. Such systems could be used, for example, as efficient carriers of catalyst in supercritical $CO_2$ applications. However, we were interested mainly in the investigation of the stability of such molecular organization in solution upon change of the solvent quality. The preparation of this type of fluorine-containing derivative is not straightforward. The use of linear perfluoroalkyl substituents leads to so strong an intermolecular interaction, that the products obtained are non-soluble and accordingly lost for investigation in solutions or monolayers (*4*). Utilization of small dendrons improves solubility, but does not solve the problem of investigation of objects of this type with higher molecular mass (*5*). Taking into account the fact that amphiphilic dendrimers are ideal objects for the study of self-organization processes (*6*) the choice of the optimum size and structure of the fluorine-containing substituents is very important. In the present study tris(γ-trifluoropropyl) substituents bearing considerable number of fluorocarbon groups, but not able to form mesophase due to their branched structure were used for polymer-analogous transformations. Obviously, finding the balance between organizing properties of fluorine-containing substituents and the solubility of the system is a non-trivial task and should be realized systematically with the utilization of a large number of fluorine-containing substituents. At the same time it is rather difficult to evaluate the differences without developing sufficient background information. Accordingly, we consider this study to be only a starting point of this research.

To be systematic all polymers were modified using the same reaction and modifying agent. The hydrosilylation reaction, widely used for the introduction of perfluorinated segments in homo- and block-copolymers (*7–11*), allows one to modify polymers of different architectures as well as to obtain products with different fluorine content, that is why it was used as the main modification method in this study.

## Experimental

### Materials and Methods

All solvents were dried over calcium hydride and distilled. Organosilanes and chlorosilanes were distilled just before use. Platinum 1,3-divinyl-1,1,3,3-tetramethyl-1,3-disiloxane complex in xylene solution (catalyst) was obtained from Aldrich and used as received.

Downloaded by OHIO STATE UNIV LIBRARIES on June 24, 2012 | http://pubs.acs.org
Publication Date (Web): November 9, 2010 | doi: 10.1021/bk-2010-1051.ch010

$^1$H NMR spectra were recorded with a "Bruker WP-250SY" instrument (250.13 MHz) in $CDCl_3$ solution, tetramethylsilane was used as a standard. Gel permeation chromatography was performed in THF (detector – refractometer).

Intrinsic viscosities in different solvents were measured with an Ubbeholde viscometer (capillary size 0.3 mm) at 25 °C (accuracy 0.1 °C).

Dynamic light scattering (DLS) measurements were conducted in MTBE and $C_6F_6$ at 25 °C with a scattering angle of 90° on an ALV/DLS/SLS-5000 Compact Goniometer System and an ALV-5000/60X0 Multiple Tau Digital Real Correlator (ALV-GmbH). A He-Ne laser (JDS Uniphase Corporation) ($\lambda$=632.8 nm) was used as a light source.

The glass transitions were studied by means of differential scanning calorimetry (DSC) using a Mettler DSC-822e thermosystem at a heating rate of 10 °C/min. Sample weights were typically ~ 5 - 10 mg. The glass transition temperatures were estimated from the midpoint of a step corresponding to the heat capacity jump in the course of devitrification.

The DTA-TGA (differential thermal analysis-thermogravimetric analysis) analyses were carried out on a thermogravimetric analyzer (Derivatograf-K, MOM, Hungary); the temperature cycle was programmed from 20 to 900 °C at a rate of 5 °C/min.

The surface pressure ($\pi$) – surface area ($A$) isotherms were recorded on a Nima type 612D (Coventry, England) PTFE film balance equipped with a Wilhelmy-type pressure sensing system. The polymer layer was compressed by means of the movable barriers and $\pi$-$A$ isotherms were continuously recorded. The velocity of compression was 4 Å$^2$ / molecule min. Dendrimers were spread on the surface from hexafluorobenzene solution with a typical concentration of 1 mg/ml. Water used as a liquid subphase was purified with an Aquilon D-301 (Moscow, Russia) deionizer leading to a specific resistance of 18.2 MΩ cm.

## Sodiumoxy-tris(γ-trifluoropropyl)silane

A solution of NaOH (4.88 g, 0.12 mol) in methanol (34 mL) was added to the stirred solution of hexakis(γ-trifluoropropyl)disiloxane (40.0 g, $6.1\times10^{-2}$ mol) in acetone (100 mL) and toluene (300 mL). The reaction mixture was refluxed with successive removal of the acetone, methanol and water, generated in the reaction. After stopping of water generation the reaction mixture was kept at reflux for 8 hours, then cooled down and evacuated to remove the toluene. The obtained white powder was analyzed by titration with 0.1N HCl. Found (%): Na, 5.74. Calc. (%): Na, 6.42. $^1$H NMR ($CDCl_3$): $\delta$ 0.65 (s, 5H, $C\underline{H}_2CH_2CF_3$), $\delta$ 0.9 (m, 1H, $C\underline{H}_2CH_2CF_3$), $\delta$ 2.1 (m, 6H, $CH_2C\underline{H}_2CF_3$).

## 3,3-Dimethyl-1,1,1-tris(γ-trifluoropropyl)disiloxane

A mixture of sodiumoxytris(γ-trifluoropropyl)silane toluene solution (187 mL, sodium content 2.29 weight %) and pyridine (19.6 g, $2.5\times10^{-1}$ mol) was added dropwise to chlorodimethylsilane (15.4 g, $1.6\times10^{-1}$ mol) solution in 40 mL of toluene. The reaction mixture was refluxed for 4 hours, afterwards 500 mL of MTBE were added and the mixture was washed with several portions of deionized water. The organic layer was dried over sodium sulfate, filtered and evaporated. The crude product – a transparent colourless liquid – was purified by distillation at 73 °C/1.2 mmHg. Yield: 31.0 g (70%). $^1$H NMR ($CDCl_3$): δ 0.1 (s, 9H, $Si(CH_3)_2$); 0.81 (m, 6H, $C\underline{H}_2CH_2CF_3$); 2.05 (m, 6H, $CH_2C\underline{H}_2CF_3$), 4.7 (m, 1H, SiH).

## Linear Polymers

### *Polybutadiene (PB)*

Polybutadiene (PB) with 90% content of 1,2-units was synthesized by means of anionic polymerization in THF at -70 °C as described elsewhere (*12*). $M_w$ 11000 Da. $M_w/M_n$ 1.19. [η](THF) 0.15 dL/g.

### *Fluoroderivative of Polybutadiene with 50% Substitution of Double Bonds (F-PB-50)*

3,3-Dimethyl-1,1,1-tris-(γ-trifluoropropyl)disiloxane (2.33 g, $6\times10^{-3}$ mol) and platinum catalyst (7.5 μL) were added to 0.71 g (1.3×10-2 mol) of PB. The reaction mixture was kept in a closed argon-filled flask at 110 °C for 48 hours. The obtained product was purified by precipitation from THF solution with methanol (yield 80%). Found (%): Si, 10.69; C, 46.34; H, 6.34; F, 32.88; O, 3.75. Calc. (%): Si, 10.92; C, 46.44; H, 6.29; F, 33.24; O, 3.11. $^1$H NMR ($CDCl_3$): δ 0.05 (s, 2.7H, $Si(CH_3)_2$), 0.4 (m, 0,9H, $CH_2Si$), 0.8 (m, 2.7H, $C\underline{H}_2CH_2CF_3$), 1.2 (m, 4.45H, $-CH_2-$), 2.0 (m, 2.7H, $CH_2C\underline{H}_2CF_3$), 4.9 (m, 0.9H, $\overline{C}H_2=$), 5.3 (m, 0.65H, CH=).

### *Fluoroderivative of Polybutadiene with 100% Substitution of Double Bonds (F-PB-100)*

3,3-Dimethyl-1,1,1-tris-(γ-trifluoropropyl)disiloxane (2.85 g, $7.2\times10^{-3}$ mol) and platinum catalyst (5 μL) were added to 0.29 g ($5.4\times10^{-3}$ mol) of PB. The reaction mixture was kept in a closed argon-filled flask at 110 °C till full disappearance of vinyl functionalities (δ 4.9 ppm ($C\underline{H}_2=CH-Si$) and δ 5.3 ppm ($CH_2=C\underline{H}-Si$)) controlled by $^1$H NMR (48 hours). The obtained product was purified by precipitation from THF solution with methanol (1.42 g, yield 65%). Found (%): Si, 12.31; C, 40.98; H, 5.53; F, 37.34; O, 3.84. Calc. (%): Si, 12.35; C, 40.80; H, 5.65; F, 37.62; O, 3.58. $^1$H NMR ($CDCl_3+C_6F_6$): δ 0.05 (s, 6H, $Si(CH_3)_2$), 0.4 (m, 1.9H, $CH_2Si$), 0.8 (m, 6H, $C\underline{H}_2CH_2CF_3$), 1.2 (m, 5.1H, $-CH_2-$), 2.0 (m, 6H, $CH_2C\underline{H}_2CF_3$).

Downloaded by OHIO STATE UNIV LIBRARIES on June 24, 2012 | http://pubs.acs.org
Publication Date (Web): November 9, 2010 | doi: 10.1021/bk-2010-1051.ch010

Downloaded by OHIO STATE UNIV LIBRARIES on June 24, 2012 | http://pubs.acs.org
Publication Date (Web): November 9, 2010 | doi: 10.1021/bk-2010-1051.ch010

### *Polymethylvinylsiloxane (-[MeSiViO]$_n$-)*

Polymethylvinylsiloxane (-[MeSiViO]$_n$-) was synthesized from dimethoxymethylvinylsilane according to the method described in ref. (*13*) in active media (acetic acid) with addition of acetyl chloride. Conversion of methoxy groups was monitored by $^1$H NMR spectroscopy.

### *Fluorine-Containing Polymethylvinylsiloxane with 5% Substitution of Vinyl Groups with tris(γ-trifluoropropyl) Groups (F-[MeSiViO]$_n$-5)*

A total of 7μL of platinum catalyst and 0.37g (9×10$^{-4}$ mol) of 3,3-dimethyl-1,1,1-tris-(γ-trifluoropropyl)disiloxane were added to 0.68g (7.9×10$^{-3}$ mol) of [MeSiViO]$_n$ dissolved in 2 ml of dry MTBE. The reaction mixture was stirred at 50°C in an argon-filled closed flask equipped with a Teflon coated magnetic stirrer bar. Afterwards solvent was evaporated and the reaction mixture was kept at 80 °C for 24 hours. Conversion of Si-H groups was followed by $^1$H NMR. Purification by precipitation from MTBE solution with ethanol gave 0.66 g (yield 63%) of the product. Found (%): Si, 29.26; C, 40.18; H, 6.46; F, 7.97; O, 16.13. Calc. (%): Si, 29.19; C, 40.28; H, 6.57; F, 8.10; O, 15.86. $^1$H NMR ($CDCl_3$): δ 0.2 (m, 3.3 H, $SiCH_3$); 0.50 (m, 0.2 H, $SiCH_2$); 0.90 (m, 0.3 H, $C\underline{H}_2CH_2CF_3$); 2.10 (m, 0.3 H, $CH_2C\underline{H}_2CF_3$); 5.9 (m, 2.85 H, $CH_2$=, CH=).

### *Fluorine-Containing Polymethylvinylsiloxane with 50% Substitution of Vinyl Groups with Tris(γ-trifluoropropyl) Groups (F-[MeSiViO]$_n$-50)*

A total of 8 μL of platinum catalyst and 0.71 g (1.8×10$^{-3}$ mol) of 3,3-dimethyl-1,1,1-tris-(γ-trifluoropropyl)disiloxane were added to 0.29 g (3.4×10-3 mol) of [MeSiViO]n dissolved in 1 ml of dry MTBE. The reaction mixture was stirred at 40 °C in argon-filled closed flask equipped with a Teflon coated magnetic stirrer bar untill full conversion of Si-H groups judged by $^1$H NMR (72 hours). Purification by precipitation from MTBE solution with ethanol gave 0.89 g (yield 89%) of the product. $^1$H NMR ($CDCl_3$): δ 0.2 (m, 6 H, $SiCH_3$); δ = 0.50 (m, 2 H, $SiCH_2$); δ = 0.90 (m, 3 H, $C\underline{H}_2CH_2CF_3$); 2.10 (m, 3 H, $CH_2C\underline{H}_2CF_3$); 5.9 (m, 1.5 H, $CH_2$=, CH=).

### *Fluorine-Containing Polymethylvinylsiloxane with 100% Substitution of Vinyl Groups with Tris(γ-trifluoropropyl) Groups (F-[MeSiViO]$_n$-100)*

A total of 10 μL of platinum catalyst and excess of 3,3-dimethyl-1,1,1-tris-(γ-trifluoropropyl)disiloxane (3.63 g, 9.2×10$^{-3}$ mol) were added to 0.31 g (3.6×10$^{-3}$ mol) of [MeSiViO]$_n$ dissolved in 2 ml of dry MTBE. The reaction mixture was stirred at 40°C in an argon-filled closed flask equipped with a Teflon coated magnetic stirrer bar untill full disappearance of vinyl functionalities judged by $^1$H NMR (72 hours). Purification by precipitation from MTBE solution with ethanol gave 1.32 g (yield 83%) of the product. Found (%): Si, 17.50; C, 35.02; H, 5.25; F, 35.49; O, 6.74. Calc. (%): Si, 17.53; C, 34.99; H, 5.20; F, 35.58;O, 6.70. $^1$H NMR (CDCl$_3$): δ 0.2 (m, 9 H, SiCH$_3$); 0.50 (m, 2 H, SiCH$_2$); 0.90 (m, 6 H, $C\underline{H}_2CH_2CF_3$); 2.10 (m, 6 H, $CH_2C\underline{H}_2CF_3$).

## Hyperbranched Polymers

### *Hyperbranched Polymethyldiallylsilane (PMDAS) and Polymethyldiundecenylsilane (PMDUS)*

These were synthesized according to the known method (*14*, *15*). Platinum catalyst was added to the monomer solution (50 vol.%) in dry hexane (1 μL of catalyst to 1 ml of solution). The reaction mixture was stirred at room temperature in an argon-filled closed flask equipped with a Teflon coated magnetic stirrer bar for 24 hours. Elimination of Si-H bonds was monitored by $^1$H NMR. The obtained samples were purified by means of column chromatography and fractionated by means of preparative chromatography.

### *Fluorine-Containing Hyperbranched Polymethyldiallylsilane (F-PMDAS)*

3,3-Dimethyl-1,1,1-tris-(γ-trifluoropropyl)disiloxane (3.31 g, $8.4\times10^{-3}$ mol) and platinum catalyst (8 μL) were added to 0.53 g ($4.2\times10^{-3}$ mol) of PMDAS. The reaction mixture was kept in a closed argon-filled flask at 110 °C untill full conversion of allyl functionalities (δ 4.86 ppm ($C\underline{H}_2$=CH-CH$_2$-Si) and δ 5.74 ppm (CH$_2$=$C\underline{H}$-CH$_2$-Si)) monitored by $^1$H NMR (72 hours). Purification by precipitation from THF solution with ethanol gave 1.93 g (yield 89%) of the product. Found (%): Si, 15.58; C, 41.04; H, 6.21; F, 32.73; O, 4.44. Calc (%): Si,16.19; C, 41.54; H, 6.34; F, 32.85; O, 3.08. $^1$H NMR (CDCl$_3$): δ -0.9 (s, 3H, SiCH$_3$); 0.1 (m, 6H, Si(CH$_3$)$_2$); 0.58 (m, 6H, SiCH$_2$); 0.8 (m, 6H, $C\underline{H}_2CH_2CF_3$); 1.3 (m, 4H, -CH$_2$-); 2.05 (m, 6H, $CH_2C\underline{H}_2CF_3$).

### *Fluorine-Containing Hyperbranched Polymethyldiundecenylsilane (F-PMDUS)*

3,3-Dimethyl-1,1,1-tris-(γ-trifluoropropyl)disiloxane (3.64 g, $9.2\times10^{-3}$ mol) and platinum catalyst (15 μL) were added to the solution of 1.62 g ($4.6\times10^{-3}$ mol) PMDUS in 8 mL of dry MTBE. The reaction mixture was kept in a closed argon-filled flask at 40 °C till full conversion of undecenyl functionalities (δ 4.92 ppm ($C\underline{H}_2$=CH-(CH$_2$)$_9$-Si) and δ 5.80 ppm (CH$_2$=$C\underline{H}$-(CH$_2$)$_9$-Si)) monitored by $^1$H NMR (48 hours). Purification by precipitation from MTBE solution with ethanol gave 3.1 g (yield 90 %) of the product. $^1$H NMR (CDCl$_3$): δ -0.9 (s, 3H, SiCH$_3$); 0.1 (m, 6H, Si(CH$_3$)$_2$); 0.58 (m, 6H, SiCH$_2$); 0.8 (m, 6H, $C\underline{H}_2CH_2CF_3$); 1.3 (m, 29H, -CH$_2$-); 2.05 (m, 6H, $CH_2C\underline{H}_2CF_3$).

Downloaded by OHIO STATE UNIV LIBRARIES on June 24, 2012 | http://pubs.acs.org
Publication Date (Web): November 9, 2010 | doi: 10.1021/bk-2010-1051.ch010

### Dendrimers

#### *Poly{tris-(γ-trifluoropropyl)siloxy}carbosilane Dendrimer (G-7.5(F))*

This was synthesized via hydrosilylation of the polyallylcarbosilane dendrimer $Si_{253}{}^{256}$(All) with 3,3-dimethyl-1,1,1-tris(γ-trifluoropropyl)disiloxane as described in detail in ref. (*16*).

#### *Poly{tris-(γ-trifluoropropyl)siloxy}carbosilane Dendrimer with Cyclic Siloxane Fragments (G-7.5(F, Si-O-Si))*

This was obtained by heterofunctional condensation of the dendrimer $Si_{509}{}^{256}$(Cl) with tris(γ-trifluoropropyl)silanol as described in detail in ref. (*17*).

Downloaded by OHIO STATE UNIV LIBRARIES on June 24, 2012 | http://pubs.acs.org
Publication Date (Web): November 9, 2010 | doi: 10.1021/bk-2010-1051.ch010

## Results and Discussion

### Polymer Matrixes

Non-saturated polymers such as polybutadiene are ideal for polymer-analogous transformations due to the high reactivity of the double bonds. Its synthesis by anionic polymerization permits preparation of polymers with different content of 1,2- and 1,4- addition units, controlled molecular mass and narrow molecular weight distribution.

Hydrosilylation is widely used for the modification of linear polymers containing double bonds to obtain silane-modified rubbers (*18–20*). It was shown, that both 1,2- and 1,4- units of polybutadiene take part in the hydrosilylation reaction, but in the case of vinyl groups the reaction runs quantitatively and faster (*21*).

Polybutadiene with 90% of 1,2- units was synthesized by means of anionic polymerization in THF.

Linear polymers with siloxane backbones are known for their remarkable flexibility. Thus it was expected, that their fluoroderivatives would have the most conformational freedom for any structural rearrangements induced by fluorine-containing groups. To carry out polymer-analogous transformations via hydrosilylation polymethylvinylsiloxane was synthesized from dimethoxymethylvinylsilane via polycondensation in active media in the presence of acetyl chloride. Methoxy group conversion was proved by $^1$H NMR spectroscopy. The synthesis of a carbosilane dendrimer of sixth generation G-6(All), hyperbranched polymethyldiallylsilane (PMDAS) and polymethyldiundecenylsilane (PMDUS) is described elsewhere (*14*, *15*, *22*). It should be noted, that PMDAS and G-6(All) have identical structural units.

Some characteristics of the obtained polymers are shown in Tables 1, 2, 3, 4, and 5.

Downloaded by OHIO STATE UNIV LIBRARIES on June 24, 2012 | http://pubs.acs.org
Publication Date (Web): November 9, 2010 | doi: 10.1021/bk-2010-1051.ch010

## Synthesis of Fluoroderivatives

Polymer-analogous transformation of polybutadiene was carried out in two versions with 50 and 100 % conversion of double bonds (Scheme 1) via hydrosilylation with 3,3-dimethyl-1,1,1-tris(γ-trifluoropropyl)disiloxane in bulk. The modifying agent and platinum catalyst were successively added to the polymer, the reaction mixture was kept closed at 110 °C for 48 hours, and conversion was monitored by $^1$H NMR spectroscopy. The obtained fluoroderivatives were isolated by precipitation. Yield was about 60-70%.

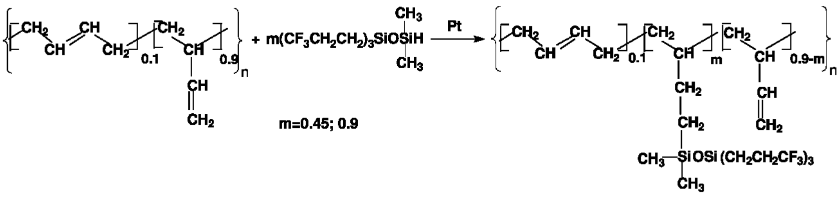

*Scheme 1. Synthesis of fluorine-containing derivatives of polybutadiene F-PB-50 and F-PB-100*

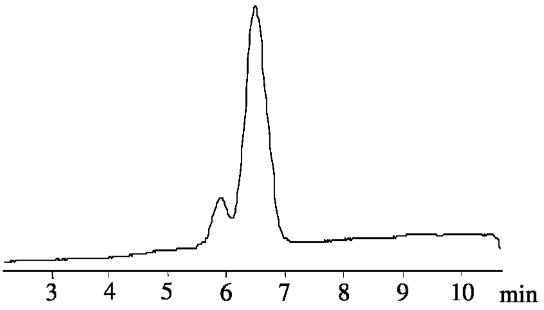

*Figure 1. GPC trace of F- PB-50*

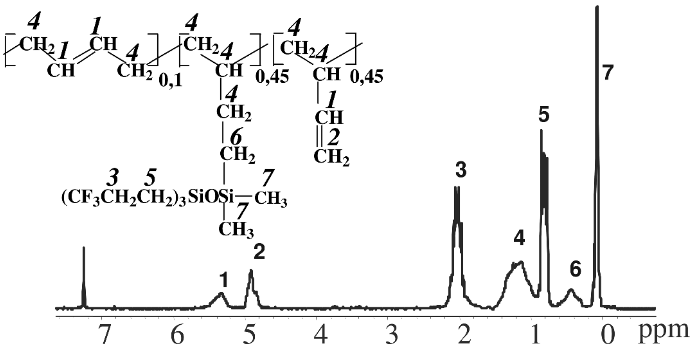

*Figure 2. $^1$H NMR spectrum of F-PB-50*

Downloaded by OHIO STATE UNIV LIBRARIES on June 24, 2012 | http://pubs.acs.org
Publication Date (Web): November 9, 2010 | doi: 10.1021/bk-2010-1051.ch010

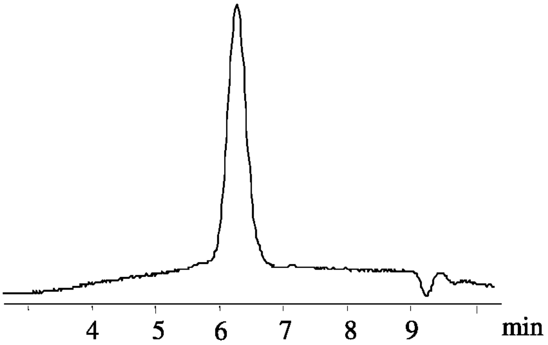

*Figure 3. GPC trace of F-PB-100*

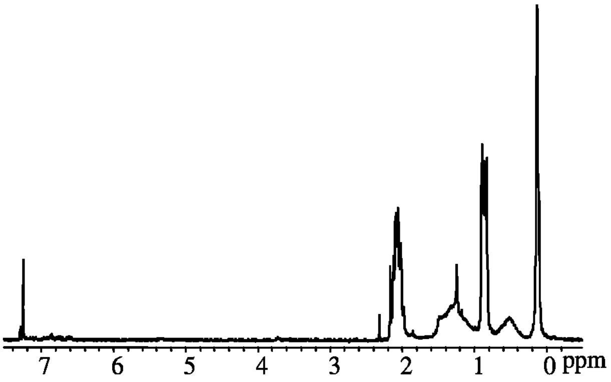

*Figure 4. $^1$H NMR spectrum of F-PB-100*

The polymers were characterized by GPC and $^1$H NMR. The GPC trace of F-PB-50 (Figure 1) shows, that modification went in the correct direction with a negligible amount of side-reactions, such as cross-linking through double bonds (less than 15%). The structure of the polymer was confirmed by $^1$H NMR spectroscopy (Figure 2).

As follows from the monomodal GPC curve of F-PB-100 (Figure 3) side-reactions were almost absent in this case in spite of bulk reaction, which ought to be favourable to side-reactions. Apparently hydrosilylation in these conditions goes very fast thus eliminating the capability of side-reactions. It is worth noting, that in this case even double bonds in the back-bone participate in the reaction, because there are no signals of CH= proton in the NMR spectrum (Figure 4).

The synthesis of fluoroderivatives of polymethylvinylsiloxane (Scheme 2) was carried out by hydrosilylation with 3,3-dimethyl-1,1,1-tris(γ-trifluoropropyl)disiloxane in MTBE solution. The modifying agent was added in quantities requisite for reaching 5, 50 and 100 % conversion. $^1$H NMR spectra of the obtained polymers are shown in Figure 5.

Downloaded by OHIO STATE UNIV LIBRARIES on June 24, 2012 | http://pubs.acs.org
Publication Date (Web): November 9, 2010 | doi: 10.1021/bk-2010-1051.ch010

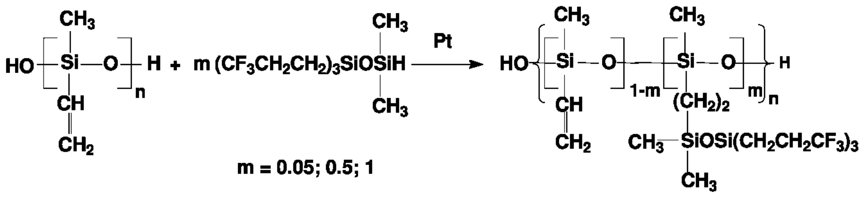
HO
CH3
Si
O
CH
CH2
H
n
+ m (CF3CH2CH2)3SiOSiH
CH3
CH3
Pt
m = 0.05; 0.5; 1
HO
1-m
(CH2)2
m
n
H
CH3 SiOSi(CH2CH2CF3)3

*Scheme 2. Synthesis of fluorine-containing derivatives of polymethylvinylsiloxane*

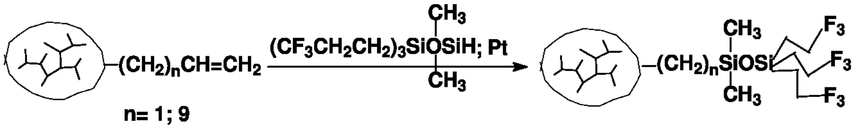
(CH2)nCH=CH2
n= 1; 9
CH3
(CF3CH2CH2)3SiOSiH; Pt
CH3
(CH2)nSiOSi
F3
F3
F3

*Scheme 3. Synthesis of fluorine-containing hyperbranched polycarbosilanes*

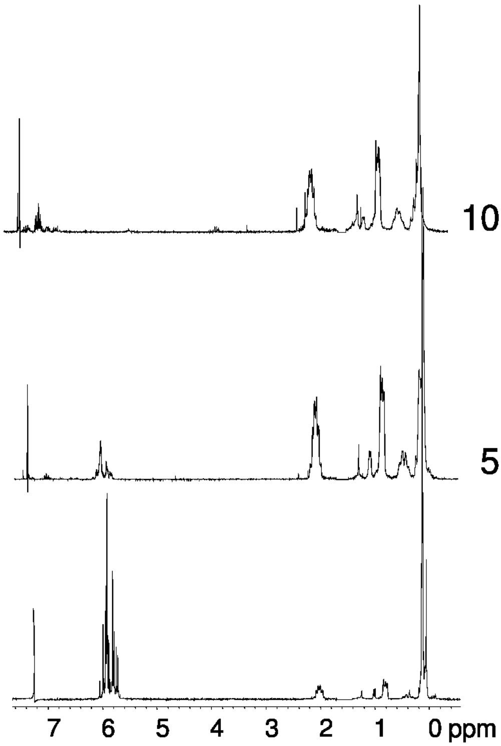

*Figure 5. $^1$H-NMR spectra of fluoroderivatives of polymethylvinylsiloxane*

Modification of the hyperbranched polymer with 3,3-dimethyl-1,1,1-tris(γ-trifluoropropyl)disiloxane was carried out in conditions similar to those for the polymethylvinylsiloxane modification. The hydrosilylation was carried out in MTBE at 40 °C (Scheme 3).

Downloaded by OHIO STATE UNIV LIBRARIES on June 24, 2012 | http://pubs.acs.org
Publication Date (Web): November 9, 2010 | doi: 10.1021/bk-2010-1051.ch010

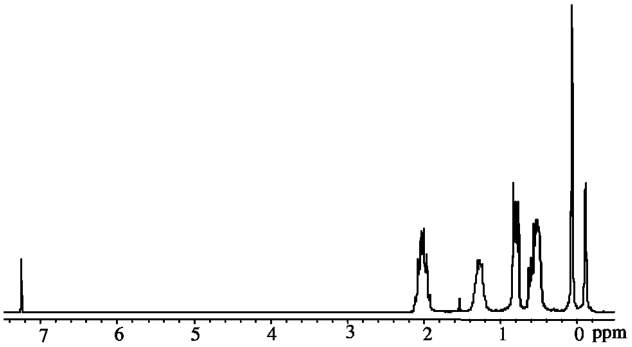

*Figure 6. $^1$H NMR spectrum of F-PMDAS*

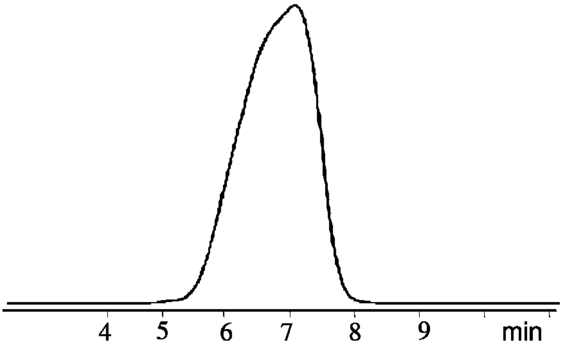

*Figure 7. GPC trace of F-PMDAS*

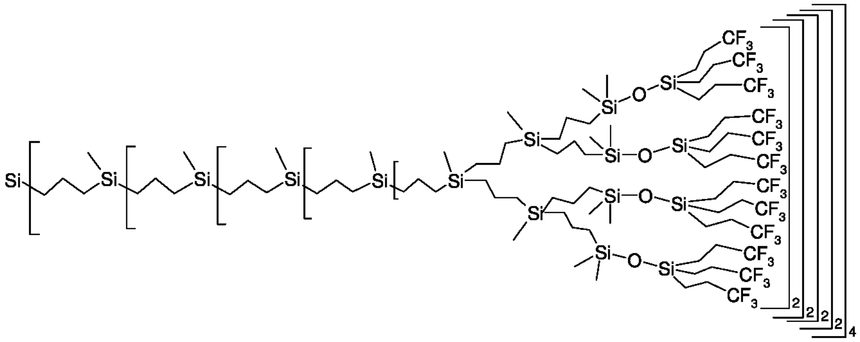

*Scheme 4. Structure of the dendrimer G-7.5(F)*

The reaction was monitored by means of $^1$H NMR. The absence of allyl group signals in the NMR spectrum (Figure 6) confirms full conversion. Moreover the protons of modifying fragments and methyl groups on silicon are close to the calculated ratio. The GPC trace of the obtained product (Figure 7) demonstrated monomodal molecular mass distribution.

Downloaded by OHIO STATE UNIV LIBRARIES on June 24, 2012 | http://pubs.acs.org
Publication Date (Web): November 9, 2010 | doi: 10.1021/bk-2010-1051.ch010

**Table 1. Glass transition temperatures of initial and fluorine-containing polymers**

| *Initial polymer* | *$T_g$, °C* | *F-polymer* | *$T_g$, °C* |
|---|---|---|---|
| PB | ~0 | F-PB -50 | -22 |
| | | F-PB-100 | -25 |
| -[MeSiViO]$_n$- | -130 | F-[MeSiViO]$_n$-5 | -128 |
| | | F-[MeSiViO]$_n$-50 | -53 |
| | | F-[MeSiViO]$_n$-100 | -40 |
| PMDAS | -85 | F-PMDAS | -51 |
| PMDUS | -73 | F-PMDUS | -63 |
| G-6(All) | -90 | G-7.5(F) | -45 |
| | | G-7.5(F, Si-O-Si) | -40 |

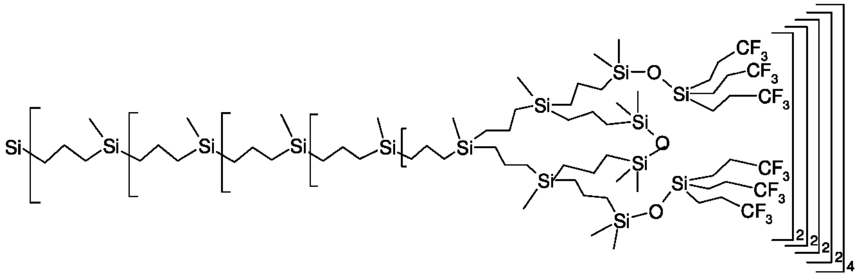

*Scheme 5. Structure of the dendrimer G-7.5(F, Si-O-Si)*

Dendrimer G-7.5(F) (Scheme 4) was synthesized by hydrosilylation reaction of dendrimer G-6(All) and 3,3-dimethyl-1,1,1-tris(γ-trifluoropropyl)disiloxane as described in detail in ref. (*16*).

Dendrimer (G-7.5(F, Si-O-Si)) (Scheme 5) was obtained by heterofunctional condensation of dendrimer $Si_{509}{}^{256}(Cl)$ with tris(γ-trifluoropropyl)silanol as described in detail in ref. (*17*).

The molecular weight of initial and fluorine-containing polymers and their viscosity in different solvents are presented in Tables 2, 3, 4, and 5.

## Properties

### *Thermal Properties*

As follows from Table 1 the introduction of fluorocarbon substituents into the polymers has a high impact on their glass transition temperatures. In the case of polybutadiene the glass transition temperature decreased as a result of the polymer-analogous reaction. On the contrary, for all other polymers both linear and dendritic with lower $T_g$s they increased.

Downloaded by OHIO STATE UNIV LIBRARIES on June 24, 2012 | http://pubs.acs.org
Publication Date (Web): November 9, 2010 | doi: 10.1021/bk-2010-1051.ch010

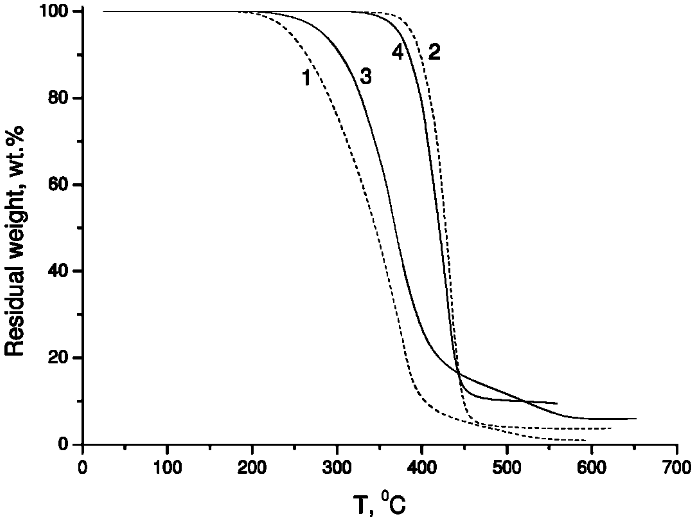

*Figure 8. TGA curves for F-PB-100 (1, 2) and F-PB-50 (3, 4) in air and argon, respectively*

The nature of the glass transition in all the discussed systems is apparently the same. Due to the high content of fluorine-containing groups their intermolecular interaction plays a determinative role in vitrification and devitrification processes. That is why the value of the glass transition temperature is defined by the mobility of the fluorocarbon substituent, which is realized in the range -50 °C – -20 °C.

Note the proximity of the glass transition temperatures of the dendrimers and PMDAS. On the one hand the set of structural units is practically the same for both systems; on the other hand the organization of the compared systems is significantly different: dendrimers are core-shell structures by definition with a carbosilane core and a fluorocarbon shell while in the case of the hyperbranched polymer different structural variations could be realized. However, coincidence of vitrification temperatures indicates that in bulk conditions the hyperbranched system also forms a core-shell structure. It will be shown later, that this system is very adaptable to the environment.

From the comparison of the fluorine-containing dendrimers with and without cyclic fragments one can see the influence of the organization of the outer layer on the properties. Assuming additivity of fluorocarbon contribution to glass transition temperature dendrimer G-7.5(F, Si-O-Si) containing half the modifying groups should have lower $T_g$ (intermediate between G-7.5(F) and initial dendrimer G6(All)), but in fact the difference is very small. There are two reasons for this: first, in both dendrimers the fluorine-containing groups are located in the surface layer, so the difference is only in density, which is in any case high, second, introduction of siloxane cross-links should also increase the $T_g$ relative to dendrimers without cyclic fragments.

Thermogravimetric analysis permits the determination of the upper limit of polymer thermal stability.

Downloaded by OHIO STATE UNIV LIBRARIES on June 24, 2012 | http://pubs.acs.org
Publication Date (Web): November 9, 2010 | doi: 10.1021/bk-2010-1051.ch010

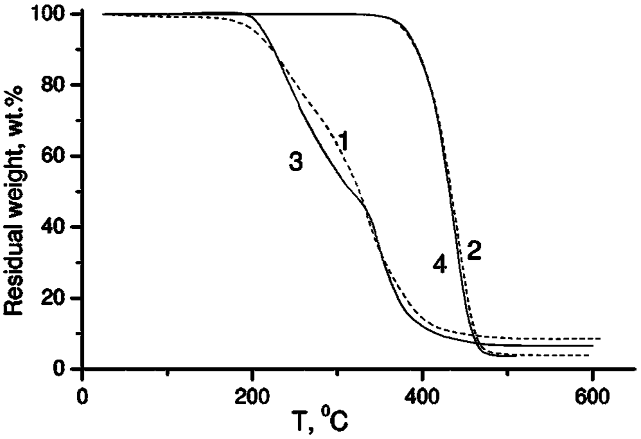

*Figure 9. TGA curves for F-PMDAS (1, 2) and G-7.5(F) (3, 4) in air and argon. respectively*

As follows from Figure 8 thermodestruction of fluorine-containing polybutadienes is a one stage process. Curves of mass loss are very similar for both samples. Onset of mass loss is observed at 370 °C (5% loss), mass reduction after this temperature is rather abrupt. Apparently thermodestruction does not lead to any cross-linking processes, because the mass of the solid residue does not exceed 5-10%.

Thermooxidative destruction starts for both samples at about 220 °C, but consists of two stages: first in the range 250-380 °C is smoother as compared to thermodestruction seemingly because of oxide formation temporarily increasing the mass and accordingly decreasing the mass loss rate. The second stage can be attributed to the destruction of the oxides formed in the first stage.

TGA curves of F-PMDAS and dendrimer G-7.5(F) are shown in Figure 9. Their thermal behavior both in air and in inert atmosphere is similar. Thermodestruction starts at about 400 °C and proceeds by almost 100 % in a narrow temperature range. As in the case of linear polymers thermooxidation goes in two stages and starts at 200 °C. The beginning of the process can be attributed to the oxidation of fluorocarbon fragments of the outer layer. In the second stage above 330 °C the process sharply accelerates being evidence of destruction of primary structure and separation of big fragments.

Thus as follows from the obtained data the upper limit of thermal stability for both linear and dendritic systems is 350 °C in inert surroundings and 180 °C in an oxidative atmosphere.

## *Solution Properties*

The structure reorganization produced by introduction of fluorine-containing fragments should be sensitive to the chain flexibility in each case. Changes in the interaction with solvents of different nature can be regarded as an indicator of the structural differences. Accordingly the comparison of the intrinsic viscosity of the fluorine containing derivatives of linear polymers, carbosilane dendrimers and hyperbranched polymers will give important information on their special properties introduced by modification with fluorine-containing groups.

F-PB-100 viscosity in THF is almost 2 times less relative to initial PB whereas its molecular mass increased by almost eight times (Table 2). This fact gives an indication of the conformation changes induced by fluorine-containing groups. The only explanation of the viscosity decrease is densification of the molecular coil due to interaction of fluorine-containing fragments. Use of a selective solvent (hexafluorobenzene, non-solvent for initial PB) leads to an even denser structure, but due to a different reason – compaction of the hydrocarbon part in bad solvent. Thus, the behaviour of the polybutadiene's fluoroderivatives is quite predictable – their molecular structure reorganizes to form more compact objects.

It was expected, that the viscosity change induced by modification will be most significant in the case of flexible linear polymers with a low modification degree, such as F-[MeSiViO]$_n$-5, because such polymers have enough freedom for conformational rearrangements. The fact that this assumption appeared faulty means that interaction between modifying groups, used in this work, is not strong enough to provoke such transformations. So it would be interesting to explore similar systems, providing stronger interaction among fluorocontaining fragments yet still without crystallization or mesophase formation.

Owing to their globular conformation dendritic macromolecules have low viscosity, which differs them significantly from linear polymers. As in the case of a linear polymer matrix, modification of hyperbranched polymers leads to an amphiphilic system, sensitive to the quality of solvent.

The most unexpected results were obtained in the case of F-PMDAS (Table 4).

As follows from the table THF is a good solvent for both PMDAS and its fluoroderivative as the maximum viscosities for both polymers are observed in THF (0.11 and 0.13 dL/g respectively). Higher solubility of hyperbranched polymer, which is soluble even in hexafluorobenzene, permits the comparison of intrinsic viscosities in the wide range of solvents. Viscosity values for unmodified PMDAS varying from 0.06 dL/g in $C_6F_6$ and 0.07 dL/g in toluene till 0.11 dL/g in THF demonstrate, that though being globular objects hyperbranched polymers still have enough conformational freedom for considerable size changes. Nevertheless after the fluorination the influence of the solvent becomes even more significant: 0.03 dL/g in toluene and 0.13 dL/g in THF.

High compaction of molecular globules especially in the case of bad solvent for fluorinated fragments is apparently a consequence of the ability to hide outer fluorine-containing fragments in the inner sphere of the globule thus densifying the globule and keeping solubility, thanks to minimization of the contacts between toluene and fluorinated parts (Scheme 6).

Downloaded by OHIO STATE UNIV LIBRARIES on June 24, 2012 | http://pubs.acs.org
Publication Date (Web): November 9, 2010 | doi: 10.1021/bk-2010-1051.ch010

**Table 2. $M_w$ and intrinsic viscosity of initial polybutadiene and its fluorine-containing derivatives**

| *Polymer* | *$M_w$ (GPC)* | *M (calc.)*[*] | *[η], dL/g* | |
|---|---|---|---|---|
| | | | *THF* | *$C_6F_6$* |
| PB | 11000 | - | 0.15 | n/s[**] |
| F-PB-50 | 23000 | 47000 | 0.10 | 0.08 |
| F-PB-100 | 28000 | 83000 | 0.08 | 0.07 |

[*] Here and further M(calc.) was calculated from GPC data of original polymer and substitution degree, determined from $^1H$ NMR spectra. [**] nonsoluble.

**Table 3. $M_w$ and intrinsic viscosity of initial polymethylvinylsiloxane and its fluorine-containing derivatives**

| *Polymer* | *$M_w$ (GPC)* | *M (calc.)* | *[η], dL/g* | | | |
|---|---|---|---|---|---|---|
| | | | *Hexane* | *MTBE* | *THF* | *$C_6F_6$* |
| -[MeSiViO]$_n$- | 19000 | - | 0.10 | 0.12 | - | n/s |
| F-[MeSiViO]$_n$-5 | 28000 | 23000 | 0.12 | 0.14 | 0.16 | 0.10 |
| F-[MeSiViO]$_n$-50 | 27500 | 62000 | n/s | 0.12 | 0.15 | 0.11 |
| F-[MeSiViO]$_n$-100 | - | 110000 | n/s | - | 0.15 | 0.14 |

**Table 4. $M_w$ and intrinsic viscosity of initial hyperbranched polycarbosilanes and their fluorine-containing derivatives**

| *Polymer* | *Mw (GPC)* | *M (calc.)* | *[η], dL/g* | | | | |
|---|---|---|---|---|---|---|---|
| | | | *MTBE* | *THF* | *Toluene* | *$CHCl_3$* | *$C_6F_6$* |
| PMDUS | 35000 | - | - | 0.27 | 0.35 | 0.19 | n/s |
| F-PMDUS | - | 74000 | - | 0.49 | 0.29 | 0.23 | 0.22 |
| PMDAS | 10000 | - | - | 0.11 | 0.07 | 0.08 | 0.06 |
| F-PMDAS | - | 41000 | 0.09 | 0.13 | 0.03 | 0.02 | 0.07 |

Downloaded by OHIO STATE UNIV LIBRARIES on June 24, 2012 | http://pubs.acs.org
Publication Date (Web): November 9, 2010 | doi: 10.1021/bk-2010-1051.ch010

Downloaded by OHIO STATE UNIV LIBRARIES on June 24, 2012 | http://pubs.acs.org
Publication Date (Web): November 9, 2010 | doi: 10.1021/bk-2010-1051.ch010

**Table 5. $M_w$ and intrinsic viscosity of initial and fluorine-containing dendrimers**

| *Polymer* | *M (calc.)* | *[η], dL/g* | | |
|---|---|---|---|---|
| | | *MTBE* | *THF* | *$C_6F_6$* |
| G-6(All) | 32014 | - | 0.04 | n/s |
| G-7.5(F) | 132990 | 0.03 | 0.02 | 0.03 |
| G-7.5(F, Si-O-Si) | 91040 | 0.03 | 0.03 | 0.03 |

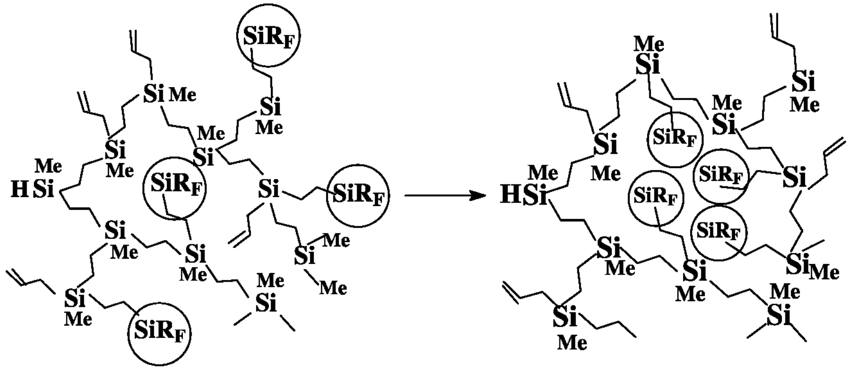

*Scheme 6. Reorganization of F-PMDAS in a poor solvent for fluorine-containing fragments.*

PMDUS in not soluble in $C_6F_6$ due to its much higher content of alkyl fragments. Its viscosity in other solvents is also considerably higher, than for PMDAS as a result of the much less density of its molecular structure. The consequences of the fluorination are also different. It should be noted that in this case the increase of molecular mass upon fluorination is 2 times less, than for PMDAS. Nevertheless the impact of the fluorine-containing fragments is still pronounced, the viscosity in THF undergoes noticeable changes increasing from 0.27 dL/g to 0.49 dL/g for the original and modified structure, respectively. The most dramatic changes in intrinsic viscosity values in regard to solvent quality were observed for F-PMDUS in THF and $C_6F_6$ indicating a sufficiently flexible structure to hide the carbosilane skeleton under the fluorine-containing shell.

Intrinsic viscosities of the dendrimers in different solvents are presented in Table 5. Note that the dendrimer G-7.5(F) and F-PMDAS as well as their precursors have the same composition, thus any differences in intrinsic viscosity can be attributed to differences in structural organization.

As follows from Table 5 the dendrimers' ability to reorganize due to solvent nature is much less compared to linear and hyperbranched polymers. Introduction of cyclic fragments into the dendrimer structure further increases its rigidity. Intrinsic viscosities of dendrimer G-7.5(F, Si-O-Si) in all the investigated solvents are fairly similar. Cyclic fragments confine the conformational mobility of the system and do not allow it to reorganize in response to solvent change.

Downloaded by OHIO STATE UNIV LIBRARIES on June 24, 2012 | http://pubs.acs.org
Publication Date (Web): November 9, 2010 | doi: 10.1021/bk-2010-1051.ch010

**Table 6. Hydrodynamic radii of dendrimers G-7.5(F) and G-7.5(F, Si-O-Si), calculated from viscosity and DSL data**

| *Dendrimer* | *MTBE* | | *$C_6F_6$* | |
|---|---|---|---|---|
| | *$R_{[\eta]}$, nm* | *$R_{DLS}$, nm* | *$R_{[\eta]}$, nm* | *$R_{DLS}$, nm* |
| $Si_{509}^{256}$(F) | 4.03 | 4.05 | 3.9 | 4.2 |
| $Si_{509}^{128}$ F(Si-O-Si) | 3.5 | 3.7 | 3.4 | 3.9 |

One more important demonstration of the specificity of dendrimer structure is the insolubility of its fluoroderivative in toluene, while its hyperbranched counterpart is fully soluble. This is evidence of differences of the mobility of structural fragments in these systems. Reorganization of the structure consisting of migration of fluorinated fragments into the inner part of the molecule is impossible for the core-shell structure of the dendrimer. I.e. the observed behavior can be attributed to the differences in the distribution of the fluorine containing groups in the molecular particles. A formation of a fluorine-containing surface layer, so-called "fluorinated skin", in dendrimers can be supposed (*4*, *23*). It would interact with solvents differently as compared with the hyperbranched molecular structure, where the same groups would be dispersed within the polymer particle. All other factors could be neglected due to the identical chemical composition in both cases.

Hydrodynamic radii of dendrimers were measured by means of DLS in MTBE and $C_6F_6$ (Table 6). Similarity of the radius values for different solvents also confirms the invariance of dendrimer structure with regard to solvent change. Values obtained by DLS are also in good agreement with those calculated from viscosity data according to the following formula $[\eta] = 2.5\frac{4}{3}\pi\frac{R^3N_A}{M}$ (where $[\eta]$ – intrinsic viscosity, R- hydrodynamic radius, M – molecular mass of the polymer, $N_A$ – Avogadro number), which is derived from the Einstein equation for the viscosity of hard spheres (*24*).

Hence predictably, the fluoro-dendrimer demonstrates the smallest abilitiy for molecular structure reorganization upon changes of solvent quality. Its counterpart containing internal cross-links is even more rigid. Surprisingly, the most flexible behavior in regard to solvent quality was demonstrated not by linear fluorocontaing polymers, but rather by fluoroderivatives of hyperbranched polycarbosilanes.

### *Behaviour on the Air-Water Interface*

Due to their low surface energy fluorine-containing polymers form monolayers on the air-water interface. Unlike amphiphilic molecules with hydrophilic structural parts (*25*) fluorine-containing fragments are not solvated by water which is why reorganizations taking place in their monolayers more adequately reflect those in bulk. In this regard the comparison of polymeric

Downloaded by OHIO STATE UNIV LIBRARIES on June 24, 2012 | http://pubs.acs.org
Publication Date (Web): November 9, 2010 | doi: 10.1021/bk-2010-1051.ch010

systems with the same fluorine-containing fragments, but different polymer matrixes, reveals the influence of the initial polymer matrix on the molecular organization of the samples. Let us consider the measured compression isotherms of all the fluorine-containing systems depicted in Figures 101112131415.

F-PB-50 (Figure 10) and F-PMDAS (Figure 11) behave ordinary upon compression. Their Langmuir isotherms are similar, having a plateau and very small hysteresis. Examining the surface pressure values, it seems that only fluorinated groups have contacts with the water surface and no other monolayer rearrangement could be detected during compression.

The compression isotherm of F-PMDUS (Figure 12) has two steps: because the quite long and flexible undecylenic spacers probably sense the differences between end-groups containing two fluorosiloxane substituents and only one for linear units.

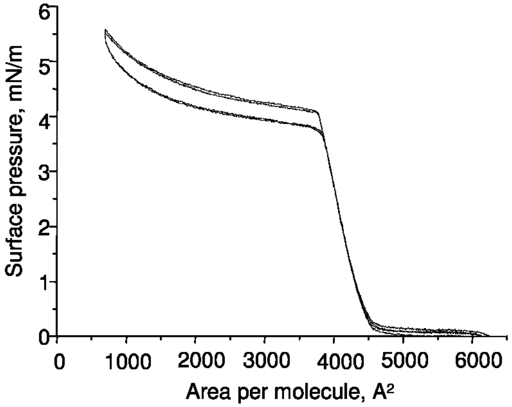

*Figure 10. Compression isotherm of F-PB-50 at air-water interface*

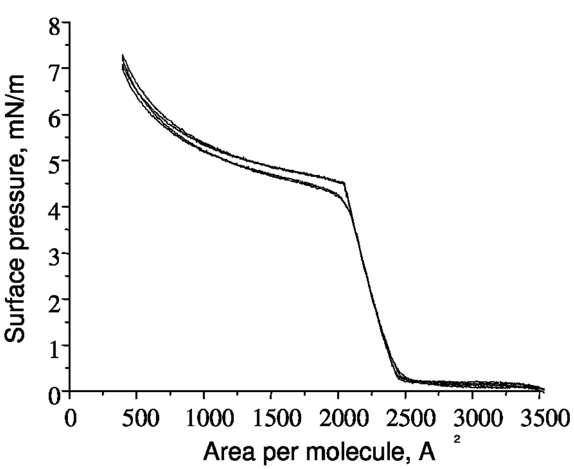

*Figure 11. Compression isotherm of F-PMDAS at air-water interface*

Downloaded by OHIO STATE UNIV LIBRARIES on June 24, 2012 | http://pubs.acs.org
Publication Date (Web): November 9, 2010 | doi: 10.1021/bk-2010-1051.ch010

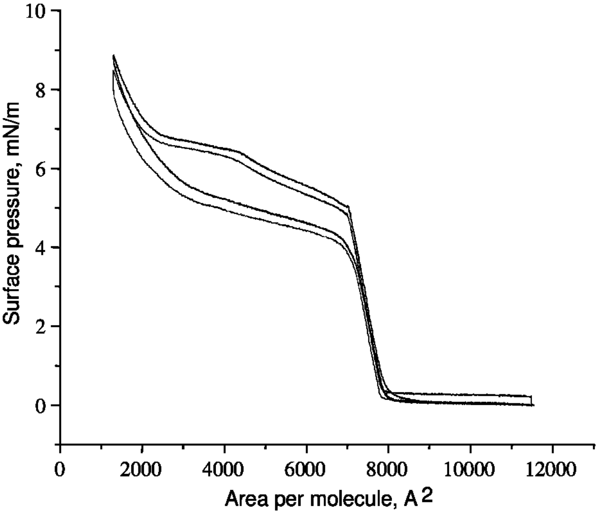

*Figure 12. Compression isotherm of F-PMDUS at air-water interface*

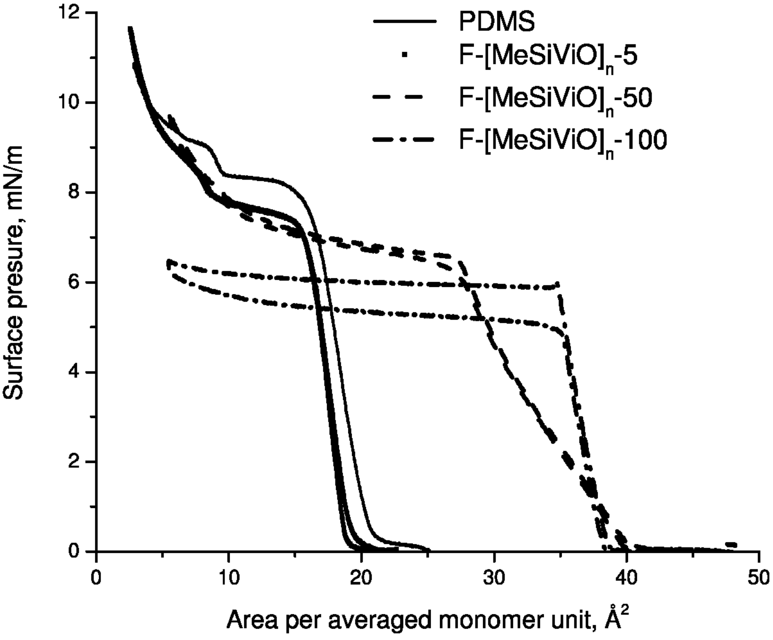

*Figure 13. Compression isotherms of fluorine-containing derivatives of -[MeSiViO]$_n$-, with PDMS as a reference at the air-water interface*

Downloaded by OHIO STATE UNIV LIBRARIES on June 24, 2012 | http://pubs.acs.org
Publication Date (Web): November 9, 2010 | doi: 10.1021/bk-2010-1051.ch010

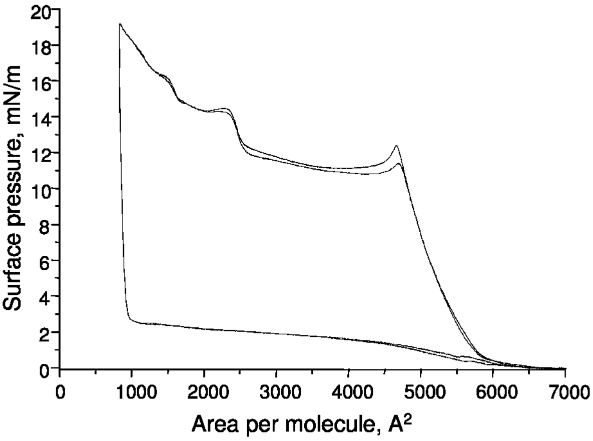

*Figure 14. Compression isotherm of G-7,5(F, Si-O-Si) at air-water interface*

Strange isotherms are observed upon compression of polymethylvinysiloxane fluoroderivatives. In this case both the siloxane main chain and fluorosubstituted side groups are surface active. The isotherms shown in Figure 13 reflect changes in behavior of fluorine-containing siloxanes that correlated with fluorocontaing groups concentration. Two main tendencies could be observed. With increasing content of fluorocontaing side-groups in polymer composition the area per unit ncreases corresponding to the larger size of the fluorocontaing groups. The second is conventional changes in surface pressure values along with increasing concentration of fluorocontaing groups. In the case of the fully substituted sample the value of surface pressure coincides with the results observed for other samples studied indicating that the siloxane chain is completely isolated from the water surface.

The behaviour of the fluorine-containing dendrimers is quite different because of their dense outer layer. Compression of G-7.5(F, Si-O-Si) monolayer is followed by a plateau formation and further compression leads to the formation of two and three layers (Figure 14). Significant hysteresis was observed upon decompression; the system took 30 min to recover to the initial state after removing the pressure. A second compression cycle is equal to the first, confirming that the system returns to the initial state after decompression.

Compression isotherm of G-7.5(F) (Figure 15) looks even more complicated. During first compression one can distinguish formation of mono-, bi- and threelayer and also significant hysteresis. Second compression however looks fundamentally different in respect to G-7.5(F, Si-O-Si). While in former case system recovered to the initial state in half an hour, in the latter case it did not recovered neither in 30 minutes nor in 3 hours. The shape of second and further compressions gives evidence, that it is not the initial dendrimers that are being compressed, but rather stable aggregates formed during first compression. This solid like matter formed could be then dissolved in THF indicating physical nature of the transformation observed under monolayer compression.

Downloaded by OHIO STATE UNIV LIBRARIES on June 24, 2012 | http://pubs.acs.org
Publication Date (Web): November 9, 2010 | doi: 10.1021/bk-2010-1051.ch010

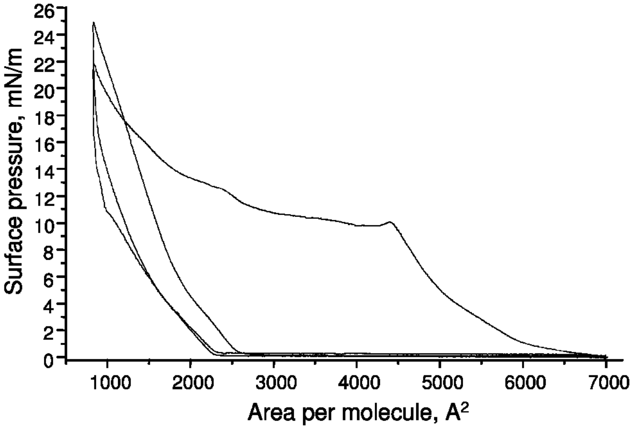

*Figure 15. Compression isotherm of G-7.5(F) at air-water interface*

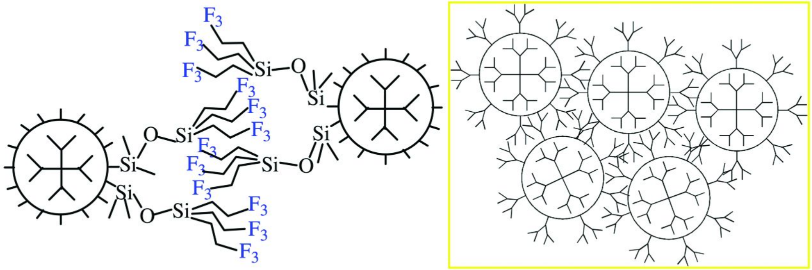

*a)* *b)*

*Figure 16. Hypthetical model of physical network formed by dendrimers of high generations*

Taking into account, that for all objects under consideration the specific interaction is defined by the same fluorine-containing fragments, it could be assumed, that the changes observed are the result of densification of the fluorine-containing shell in the case of dendrimers of high generations. The appearance of some new organization of dendrimer under compression resulting in a stable physical interaction suggests some mechanical contacts formation. Figure 16 demonstrates a model of this type of contacts which could lead to changes of dendrimer matter as the surface layer density increases. The model depicts the formation of mechanical knots which in their turn are the part of the macroscopic physical network. The specific point of this study is that we have an intermediate state of the same nature in the case of G-7.5(F, Si-O-Si) which suggests that the huge hysterisis observed in this case is just a step before further increase of surface layer density became enough to form physical knots. Clearly, at present we have only some suggestions regarding the nature of this physical network formation, which needs futher elaboration. Nevertheless we find it helpful to discuss such a model of organization of high generation dendrimers and to use this model as a motivation for further investigations.

## Conclusion

The rather unconventional approach of utilizing fluorine-containing modificating agents, used in this study has produced quite interesting results regarding the peculiar properties of the organization of fluorine-containing polymers in solution and at the air-water interface. Unexpected findings illustrating unique features of either one or another polymer matrix were made in both cases. Thus the highest sensitivity of hyperbranched polymers to the solvent quality was non-trivial, but at the same time explainable. Yet the clearest demonstration of the influence of molecular structure organization is the easily detectable difference between fluorine-containing derivatives of regular and non-regular hyperbranched polymers. Despite having the identical chemical composition, these systems behave quite different.

Finally, the result of the gradual increase of molecular structure complexity was the discovery of a qualitative transition, namely, upon reaching a certain density of the outer layer, dendrimers of high generation are able to form a physical network.

Obviously the approach used could be broadened both by increasing the number of polymer matrixes under consideration and the use of new fluorine-containing modifying reagents. In the latter case it is worth intensifying the organizing ability of the fluorine-containing fragments, but yet still avoiding the transition to their domination as happens in the case of the introduction of long linear fragments.

Downloaded by OHIO STATE UNIV LIBRARIES on June 24, 2012 | http://pubs.acs.org
Publication Date (Web): November 9, 2010 | doi: 10.1021/bk-2010-1051.ch010

## References

1. Owen, M. J.; Kobayashi, H. *Surf. Coat. Int.* **1995**, *78*, 52.
2. Kobayashi, H.; Owen, M. J. *Polym. Adv. Technol.* **1993**, *4*, 355.
3. Hendlinger, P.; Laschewsky, A.; Bertrand, P.; Delcorte, A.; Legras, R.; Nysten, B.; Moebius, D. *Langmuir* **1997**, *13*, 310.
4. Lorenz, K.; Frey, H.; Stuhn, B.; Mulhaupt, R. *Macromolecules* **1997**, *30*, 6860.
5. Lee, S. R.; Yoon, D. K.; Park, S.-H.; Lee, E. H.; Kim, Y. H.; Stenger, P.; Zasadzinski, J. A.; Jung, H.-T. *Langmuir* **2005**, *21*, 4989.
6. Schenning, A. P. H. J.; Elissen-Roman, C.; Weener, J.-W.; Baars, M. W. P. L.; van der Gaast, S. J.; Meijer, E. W. *J. Am. Chem. Soc.* **1998**, *120*, 8199.
7. Hopken, J.; Moeller, M.; Boileau, S. *Polym. Prepr.* **1990**, *31*, 324.
8. Wilczek, L. U.S. Patent 5,233,071, 1993.
9. Hwang, S. S.; Ober, C. K.; Perutz, S.; Iyengar, D. R.; Schneggenburger, L. A.; Kramer, E. J. *Polymer* **1995**, *36*, 1321.
10. Paulasaari, J. K.; Weber, W. P. *Macromolecules* **1999**, *32*, 6574.
11. Samuel, J. D. J. S.; Dhamodharan, R.; Ober, C. K. *J. Polym. Sci., Part A: Polym. Chem.* **2000**, *38*, 1179.

12. Halasa, A. F.; Lohr, D. F.; Hall, J. E. *J. Polym. Sci., Polym. Chem. Ed.* **1981**, *19*, 1357.
13. Vasilenko, N. G.; Demchenko, N. V.; Egorova, E. V.; Muzafarov, A. M. *Dokl. Chem.* **2009**, *424*, in press.
14. Muzafarov, A. M.; Gorbatsevich, O. B.; Rebrov, E. A.; Ignat′eva, G. M.; Chenskaya, T. B.; Myakushev, V. D.; Bulkin, A. F.; Papkov, V. S. *Polym. Sci., Ser. A* **1993**, *35*, 1575.
15. Drohmann, C.; Moeller, M.; Gorbatsevich, O. B.; Muzafarov, A. M. *J. Polym. Sci., Part A: Polym. Chem.* **2000**, *38*, 741.
16. Shumilkina, N. A.; Myakushev, V. D.; Tatarinova, E. A.; Gallyamov, M. O.; Khokhlov, A. R.; Buzin, M. I.; Muzafarov, A. M. *Dokl. Chem.* **2005**, *403*, 155.
17. Shumilkina, N. A.; Myakushev, V. D.; Tatarinova, E. A.; Buzin, M. I.; Voronina, N. V.; Laptinskaya, T. V.; Gallyamov, M. O.; Khokhlov, A. R.; Muzafarov, A. M. *Polym. Sci., Ser. A* **2006**, *48*, 1240.
18. Witte, J.; Guenter, L.; Pampus, G. DE Patent 2,344,734, 1975.
19. Kang, J. W.; Poulton, J. T.; Kitamura, T. U.S. Patent 6,017,985, 2000.
20. Baum, K.; Baum, J. C.; Ho, T. *J. Am. Chem. Soc.* **1998**, *120*, 2993.
21. Guo, X.; Farwaha, R.; Rempel, G. L. *Macromolecules* **1990**, *23*, 5047.
22. Tatarinova, E. A.; Rebrov, E. A.; Myakushev, V. D.; Meshkov, I. B.; Demchenko, N. V.; Bystrova, A. V.; Lebedeva, O. V.; Muzafarov, A. M. *Russ. Chem. Bull.* **2004**, *53*, 2591.
23. Stark, B.; Lach, C.; Farago, B.; Frey, H.; Schlenk, C.; Stuehn, B. *Colloid. Polym. Sci.* **2003**, *281*, 593.
24. Einstein, A. *Ann. Phys.* **1906**, *19*, 289.
25. Tereshchenko, A. S.; Getmanova, E. V.; Buzin, A. I.; Ignat′eva, G. M.; Tatarinova, E. A.; Bystrova, A. V.; Myakushev, V. D.; Muzafarov, A. M. *Russ. Chem. Bull.* **2007**, *56*, 2200.

Downloaded by OHIO STATE UNIV LIBRARIES on June 24, 2012 | http://pubs.acs.org
Publication Date (Web): November 9, 2010 | doi: 10.1021/bk-2010-1051.ch010

## Chapter 11

# Radially Layered Poly(amidoamine-organosilicon) Dendrimers

**Petar R. Dvornic*** **and Michael J. Owen**

**Michigan Molecular Institute, Midland, MI 48640**
***Dvornic@mmi.org**

Downloaded by STANFORD UNIV GREEN LIBR on June 25, 2012 | http://pubs.acs.org
Publication Date (Web): November 9, 2010 | doi: 10.1021/bk-2010-1051.ch011

Radially layered copolymeric poly(amidoamine-organosilicon) (PAMAMOS) dendrimers which consist of hydrophilic polyamidoamine (PAMAM) interiors and hydrophobic organosilicon (OS) exteriors are an unusual new class of dendritic copolymers. They may be viewed as globular, amphiphilic, "covalently-bonded inverted micelles". Their synthesis involves either Michael addition of organosilicon acrylates or methacrylates to amine-terminated PAMAM dendrimer precursors or their haloalkylation by chloroalkyl- or iodoalkylsilanes. Compositional variety of the resulting dendrimers is achieved by variation of the generation of PAMAM precursor and the type and functionality of the organosilicon reagent. A range of different PAMAMOS dendrimers can be obtained having (a) different number of PAMAM branch cell layers in their interiors, (b) one or more layers of OS branch cells in their exteriors, (c) a variety of inert (e.g. trimethylsilyl or trimethylsiloxy) or reactive (e.g. alkoxysilyl, vinylsilyl, or vinylsiloxy) end-groups, and (d) different relative amounts of these end-groups. While examples of these dendrimers with inert trimethylsilyl terminal groups show interesting surface properties, the methoxysilyl-substituted homologs are excellent precursors for the first tractable dendrimer-based networks that can be prepared as elastomers, plastomers or coatings of various substrates. Because of their unique composition comprising interconnected nanoscopic hydrophilic and hydrophobic domains, these dendrimer-based networks show highly unusual properties which include permselectivity and the ability to encapsulate

In Advances in Silicones and Silicone-Modified Materials; Clarson, S., et al.;
ACS Symposium Series; American Chemical Society: Washington, DC, 2010.

various inorganic or organic electrophiles. These properties lead to exciting application possibilities, such as "molecular sponges", nanoscopic "reactors" or inorganic-organic nano-composites.

Downloaded by STANFORD UNIV GREEN LIBR on June 25, 2012 | http://pubs.acs.org
Publication Date (Web): November 9, 2010 | doi: 10.1021/bk-2010-1051.ch011

One readily predictable direction that research and development in the macromolecular arena will take is an ever-widening exploration of copolymers of different composition and structure. Although the discovery of new homopolymers is still a significant feature of the current polymer scene, a more certain avenue for progress is to explore the results of copolymerizing already discovered homopolymers. In advocating this approach we take the positive view that copolymerization will yield a set of properties that combines some of the advantageous aspects of both components and not the worst of both worlds. Such optimism implies that interesting, novel materials might result from combinations of polymers whose individual properties are very different. In order to preserve distinct attributes from both partners, this implies a block rather than random copolymerization approach. Given the considerable scientific interest in macromolecular surfactants, one obvious example of this would be to combine a very hydrophobic polymer with a very hydrophilic one.

Another clearly evident future direction for macromolecular exploration is towards well-controlled polymer architectures. The four major classes of such architectures have been described as linear, cross-linked, randomly branched, and dendritic (*1*). Within these categories one of the most controlled structures is that of the dendrimer. They are among the most recent types of polymers to be recognized and consequently have not yet been extensively commercially exploited. However, in an exploration of novel copolymeric combinations this is more of an advantage than a drawback. Dendrimers are composed of three regions, a core, an interior branching region of various generations, and an exterior surface region. In order to preserve the block copolymer characteristic in a dendrimeric structure, radially-layered materials offer the most obvious approach. Since each generation of branches occupies a space shell of the order of 1 nm in thickness, dendrimers are clearly in the nanoscopic size range; another domain of current intense scientific interest.

The question next arises as to which copolymer system to select. At this point personal experience and situation determine which direction to follow. We are based in Midland, Michigan, the home of Dow Chemical, Dow Corning Corporation, and Michigan Molecular Institute (MMI). The hydrophilic polyamidoamine (PAMAM) dendrimers were first developed at the Dow Chemical Company by Tomalia and coworkers in the 1980's (*2*). Subsequently, MMI became the center of PAMAM research and its subsidiary, Dendritech Inc. (also in Midland, MI) was the first company to commercially produce dendrimers. Dow Corning Corporation is the leading producer of silicones. There is thus an inevitability that a cooperative program of research between MMI and Dow Corning would focus on radially-layered polyamidoamine-organosilicon copolymeric (PAMAMOS) dendrimers which can be considered as inverted

Downloaded by STANFORD UNIV GREEN LIBR on June 25, 2012 | http://pubs.acs.org
Publication Date (Web): November 9, 2010 | doi: 10.1021/bk-2010-1051.ch011

unimolecular nano-scaled micelles. Over twelve different types and generations of these dendrimers are now commercially available from Dendritech Inc. or from Aldrich.

The prime property we hoped to preserve from the PAMAM component was its ability to complex metal ions into its hydrophilic structure. The prime property anticipated from the organosilicon component was low surface energy. To no surprise, these surface activity expectations were realized but another aspect of organosilicon chemistry, facile cross-linking chemistry, has also emerged as at least as important a feature. Consequently, the uniqueness of the materials reported here derives from these three aspects. In particular, PAMAMOS dendrimers provide the only presently known, dendritic network system that can form technologically useful, cross-linked coatings and films. The current state of our knowledge regarding these three key aspects of PAMAMOS dendrimers is summarized in the following sections.

## Synthesis and Cross-Linking

PAMAMOS preparation starts from amine-terminated, ethylenediamine (EDA) core PAMAM dendrimers (also obtainable from Dendritech Inc.), which can be used without any further purification. They are prepared by a divergent growth method involving a reiterative sequence of a Michael addition reaction of methyl acrylate to primary amines followed by amidation of the resulting methyl ester intermediate with ethylene diamine. We have used generation 0 through 5 PAMAMs for PAMAMOS preparation.

A variety of synthetic routes have been explored for converting from PAMAM to PAMAMOS dendrimers employing different cross-over reactions to go from the wholly organic, divergent PAMAM synthesis to an organosilicon sequence. The two most useful approaches proved to be (a) a Michael addition reaction of silicon-containing acrylates, and (b) a haloalkylation with various silanes and siloxanes (*3*). Reaction schemes 1(a) and 1(b) below are examples of the Michael addition approach, while reaction scheme 1(c) exemplifies the haloalkylation route. Reaction schemes 1(a) and 1(c) are those employed to produce the PAMAMOS materials discussed in the following section on surface activity and shown in Table 1. In these reaction schemes the parent PAMAM is shown as $G_x$-$(NH_2)_y$. Subscript x is the generation number of the PAMAM and subscript y is the number of terminal amine groups. As x increases through 1, 2, 3 ,4 etc., y correspondingly increases through 8, 16, 32, 64 etc.

$$G_x\text{-}(NH_2)_y + CH_2{=}CHCO_2(CH_2)_3Si(CH_3)_3 \rightarrow$$
$$G_x\text{-}[N\{(CH_2)_2CO_2(CH_2)_3Si(CH_3)_3\}_2]_y \qquad 1(a)$$

$$G_x\text{-}(NH_2)_y + CH_2{=}CHCO_2(CH_2)_3Si(OCH_3)_2CH_3 \rightarrow$$
$$G_x\text{-}[N\{(CH_2)_2CO_2(CH_2)_3Si(OCH_3)_2CH_3\}_2]_y \qquad 1(b)$$

$$G_x\text{-}(NH_2)_y + XCH_2Si(CH_3)_2CH{=}CH_2 \rightarrow$$
$$G_x\text{-}[N\{CH_2Si(CH_3)_2CH{=}CH_2\}_2]_y \qquad 1(c)$$

In scheme 1(c) X can be Cl, Br or I. The trimethylsilyl entity of 1(a) is abbreviated TMS in PAMAMOS samples such as those shown in Table 1. Similarly, the dimethoxymethylsilyl entity of 1(b) is shortened to DMOMS, and 1(c)'s dimethylvinyl is given as DMV. These three schemes are specifically chosen to illustrate the dendrimers discussed in this chapter. A wider set of reactions can result in more varied PAMAMOS dendritic copolymers and these have been discussed in more detail elsewhere (*4*).

The alkoxysilylated PAMAMOS of reaction scheme 1(b), PAMAMOS-DMOMS, can be easily cross-linked by the methods of sol-gel chemistry (*4*). The process consists of water hydrolysis of the methoxy groups into the corresponding silanols, Si-OH, groups, followed by condensation of these silanol intermediates into siloxane, Si-O-Si, interdendrimer bridges. This process is self-catalyzed by the basic PAMAM domains and can be readily accomplished by simple exposure of the PAMAMOS-DMOMS dendrimers to water in either the liquid or vapor state. Since the process is a chain reaction in which a part of the water used in the alkoxysilyl hydrolysis is regenerated in the subsequent silanol condensation step, a less than stoichiometric amount of water is required. Furthermore, the reaction can be catalyzed with a variety of different catalysts, which coupled with variation in reaction conditions such as temperature, relative humidity and reaction time, leads to precise control of the rate and extent of cross-linking.

This route is our preferred approach to cross-linked PAMAMOS elastomers and plastomers (*4*). Reaction scheme 1(c) would seem to offer an alternative approach to cross-linking via hydrosilylation with a SiH functional monomer or polymer. However, should this be attempted by conventional platinum catalysis, a marked excess is necessary because of the propensity of the PAMAM core to sequester metal atoms and ions, thus effectively removing the catalytic species from the locus of the desired reaction.

## Surface Activity

Most PAMAMOS dendrimers are soluble in organic solvents such as THF, toluene, acetone, chloroform and the lower alcohols. Water solubility is dependent on composition, as would be expected with such a hydrophilic/hydrophobic hybrid polymer. For example, most of our materials have an OS outer layer that is over 50% complete and are insoluble in water. These dendrimers can be conveniently studied by the Langmuir trough technique. At lower degrees of surface derivitization they are too water soluble to spread as films, but their surface activity can be studied by direct solution surface tension measurement. Such studies have already been reported (*5*). Their degree of surface activity is considerable with values less than 30 mN/m being attained. Although some kinks are evident in the plots of surface tension of aqueous solution versus log concentration, no definite break to a plateau surface tension value, indicative of a critical micelle concentration, is seen up to the highest concentrations examined (0.5%). Micellization would not be anticipated with the PAMAMOS globular polymer architecture as it is already, effectively, a unimolecular micelle.

Downloaded by STANFORD UNIV GREEN LIBR on June 25, 2012 | http://pubs.acs.org
Publication Date (Web): November 9, 2010 | doi: 10.1021/bk-2010-1051.ch011

We have published some examples of surface pressure/area Langmuir trough isotherms in an earlier Silicones and Silicone-Modified Materials symposium (*6*). These films are generally liquid-like and can be compressed to surface pressure values much higher than the *circa* 10 mN/m value typical of polydimethylsiloxanes (PDMS). Values greater than 50 mN/m have been recorded. This indicates a much stronger interaction with water than the siloxane-water hydrogen bond interaction of PDMS, which can be associated with PAMAM interiors of the PAMAMOS dendrimers that have amide and amine groups capable of much stronger hydrogen bonding with the water surface. Thus higher surface pressures than those achieved with PDMS are to be expected, providing the OS component does not prevent these hydrophilic groups from interacting with the water surface.

All of the Langmuir plots obtained show some degree of hysteresis with the expansion portion of the plot not reversibly following the preceding compression cycle. Hysteresis is commonplace in polymer surface studies such as contact angle and contact mechanics studies and its occurrence here is not unexpected. The extent of hysteresis experienced is dependent on procedural conditions such as the rate of compression and expansion and the amount of material delivered to the surface. Because of this, we set standard conditions for all measurements, including a barrier sweep rate of 50 mm/min and an amount of 20 μl chloroform spreading solution. The hysteresis is more pronounced for dendrimers with lower generation PAMAM interiors and less OS surface modification. This fits with the expectation that the more open and less congested the dendrimer's outermost surface, the more extensive would be water penetration to the interior causing the observed hysteresis.

Because of this hysteresis, two values of the limiting area just prior to the film collapse are possible; one determined from the compression curve and one from the expansion curve. Accordingly both sets of values are listed in Table 1. Expectedly, these areas generally increase with the size of the parent PAMAM dendrimer and with the degree of substitution of the NH group. The calculated areas are approximations by Zhang et al. (*7*) from PAMAM data obtained from size exclusion chromatography and small angle neutron scattering assuming spherical geometry. Our added assumption is that the added OS generation can be approximated by comparing with the next higher PAMAM generation values. This is not meant to be an exact comparison, but the general concordance implies that much of the globular architecture of the PAMAMOS dendrimers is preserved on the water surface.

Downloaded by STANFORD UNIV GREEN LIBR on June 25, 2012 | http://pubs.acs.org
Publication Date (Web): November 9, 2010 | doi: 10.1021/bk-2010-1051.ch011

## Complexation of Metal Ions

The topological disposition of PAMAMOS networks is predetermined by the type of OS branch cells, the number of OS layers in the PAMAMOS dendrimer precursor used and the selection of any cross-linking co-reagent (*3*). Appropriate choices of these parameters enable the preparation of networks with a highly regular distribution of hydrophilic, nucleophilic PAMAM spheroids within a hydrophobic OS matrix. Such networks can serve as unique nano-scaled templates for precise placement of a variety of guest species in 2D (monolayer)

Downloaded by STANFORD UNIV GREEN LIBR on June 25, 2012 | http://pubs.acs.org
Publication Date (Web): November 9, 2010 | doi: 10.1021/bk-2010-1051.ch011

**Table 1. PAMAMOS Langmuir Trough Data[a]**

| *PAMAMOS sample* | *MW(Calc.)* | *Area per molecule ($A^2$/mol)* | | |
|---|---|---|---|---|
| | | *Π/A Isotherm* | | *Calc.* |
| | | *Compression* | *Expansion* | |
| 2-1-83DMV | 5,880 | 890 | 570 | 855 |
| 3-1-85DMV | 12,245 | 1,060 | 830 | 1,219 |
| 3-1-92TMS | 11,976 | 1,640 | 1,080 | 1,219 |
| 4-1-68TMS | 21,760 | 3,540 | 2,280 | 2,011 |
| 4-1-88TMS | 23,941 | 3,700 | 2,510 | 2,011 |
| 4-1-100TMS | 25,249 | 4,490 | 2,530 | 2,011 |
| 4-1-98DMV | 26,700 | 3,590 | 2,660 | 2,011 |

[a] The identification system (X-Y-Z-ABC) used for naming these samples indicates: generation of the PAMAM interior (X), number of external OS layers (Y), % of PAMAM NH groups substituted by OS units as determined by NMR (Z) and abbreviated name of the respective OS groups (see text before).

and 3D (thin coating) nanoscopic arrangements. The guests towards which PAMAMOS networks exhibit pronounced affinity include electrophiles such as inorganic cations $Ag^+$, $Cu^+$, $Cu^{2+}$, $Ni^{2+}$, $Cd^{2+}$, $Zn^{2+}$, $Fe^{2+}$, $Fe^{3+}$, $Au^{3+}$, $Co^{2+}$, $Pd^{2+}$, $Rh^{3+}$, $Pt^{2+}$, $Pt^{4+}$, $Eu^{3+}$, $Tb^{3+}$, $Sm^{3+}$, $Dy^{3+}$, etc., and electrophilic organic and organometallic compounds, with which interactions are through complexation mostly by tertiary amine nitrogens and neighboring carbonyl oxygens (*8*).

As a consequence of their nanoscale organization, these PAMAMOS networks are optically clear, perfectly transparent and colorless and can be readily cast into films, sheets and coatings that are insoluble in solvents such as methanol, water, methylene chloride, THF and acetone. Depending on the specific PAMAMOS dendrimer used, its density of functionality and composition of the curing reaction mixture, mechanical properties of these networks may be varied from elastomeric to plastomeric, with $T_g$s from well below -50°C to well above room temperature (*4*).

A variety of techniques were explored to shed light on the nature and disposition of these encapsulated ions in PAMAMOS matrices. Scanning electron microscopy (SEM), transmission electron microscopy (TEM) and atomic force microscopy (AFM) were all consistent with the hypothesis that the metal ions were preferentially encapsulated in the PAMAM cores but none of these approaches provided definitive proofs of this morphology (*6*). Small angle neutron scattering (SANS) and high-resolution x-ray photoelectron spectroscopy (XPS) proved to be very helpful in this regard. SANS studies were carried out at the National Institute of Standards and Technology Center for Cold Neutron Research at Gaithersburg, Md, in collaboration with Dr. Barry Bauer and co-workers (*9*). XPS analysis was provided by Dr. Chris McMillan at Dow Corning Corporation.

Downloaded by STANFORD UNIV GREEN LIBR on June 25, 2012 | http://pubs.acs.org
Publication Date (Web): November 9, 2010 | doi: 10.1021/bk-2010-1051.ch011

Table 2 summarizes some pertinent information garnered from these studies. Fuller details and more extensive analysis have been published elsewhere (*8*, *10*, *11*) but Table 2 is included here to underscore some very significant aspects concerning the complexation of metal ions in PAMAMOS networks using $Cu^{2+}$ ions as an important example. The data was gathered for a generation 4 PAMAM with one DMOMS outer layer.

For the un-doped sample with no incorporated metal salt, the core-to-core spacing for neighboring dendrimer units is 3.7 nm (*9*). This result was confirmed by small angle x-ray scattering which gave a value of 3.6 nm and is in reasonable agreement with dilute solution viscometry and size exclusion chromatography measurements (*12*) of generation 4 PAMAM dendrimers (5.0 and 4.5 nm diameter, respectively). Expectedly, this core-to-core spacing increases as the $Cu^{2+}$ increases. Note that the 16.7 wt. % level corresponds to a 1:1 ratio of copper ions to tertiary nitrogen atoms, a strong interaction between which had already been established by Ottaviani et al. (*13*).

The XPS Cu content data also increase with increased bulk concentration but the level of copper detected is an order of magnitude less than bulk, even in the normal angle mode which probes to greatest depth (8-10 nm). The copper levels are even less at low grazing angle (2-3 nm) suggesting that copper is preferentially binding below the immediate organosilicon surface of the dendritic network, i.e. within the PAMAM interior. The XPS High resolution N 1s spectra were also illuminative. This peak can be deconvoluted into three components, one at 399.8 eV corresponding to amide nitrogen, one at 400.4 eV corresponding to *tert*-N, and one at 402.0 eV that has been assigned to positively charged $N^+$ (*14*). The inrease in this last peak with increasing Cu content is good evidence of the anticipated copper/nitrogen interaction. Above a certain Cu concentration critical for each PAMAM generation, $Cu^{2+}$ cations "spill over" into the surrounding OS matrix and most likely bind with Si-O-Si oxygens.

## Applications

Applications for these covalently bonded, inverted nanoscopic micelles include: phase transfer agents; molecular adsorbants; additives to organic systems; solubilization of inorganic salts in organic media; and impregnation of mezoporous substrates, textiles and other fibrous materials. The cross-linked nano-scaled, honeycomb-like elastomeric or plastomeric films, sheets or coatings, a biocide-containing example of which is shown diagrammatically in Figure 1, offer a wide range of prospective uses. These include: nanolithography with conductive metal particles; ultra-low dielectric constant nano-porous insulators; nano-patterning; conductive or magnetic transparent coatings for glass, plastics, paper, textiles and other related surfaces; optoelectronic coatings; environmentally benign antifouling coatings; semi-permeable membranes with embedded catalytic species; molecular sponges for purification of liquids; and chemical warfare agent detection and decontamination coatings. A recent review of PAMAMOS applications emphasizes electronics, photonics and magnetics; sensors; protective and antifouling coatings; and the purification and decontamination areas (*15*).

Downloaded by STANFORD UNIV GREEN LIBR on June 25, 2012 | http://pubs.acs.org
Publication Date (Web): November 9, 2010 | doi: 10.1021/bk-2010-1051.ch011

**Table 2. PAMAMOS SANS and XPS Data**

| *Bulk $Cu^{2+}$content (wt. %)* | *Core-to-core spacing (nm)* | *XPS Cu content [ Normal/low angle] (atom %)* | *XPS $N^+$content [402.0 eV] (atom %)* |
|---|---|---|---|
| 0 | 3.7 | 0/0 | 0 |
| 0.5 | - | 0.1/0 | 6 |
| 2.4 | 4.1 | 0.2/0.1 | 12 |
| 4.1 | - | 0.4/0.1 | 11 |
| 5.0 | 4.5 | - | - |
| 8.0 | - | - | 18 |
| 11.5 | 5.2 | 1.5/0.8 | 30 |
| 16.7 | 5.5 | - | - |

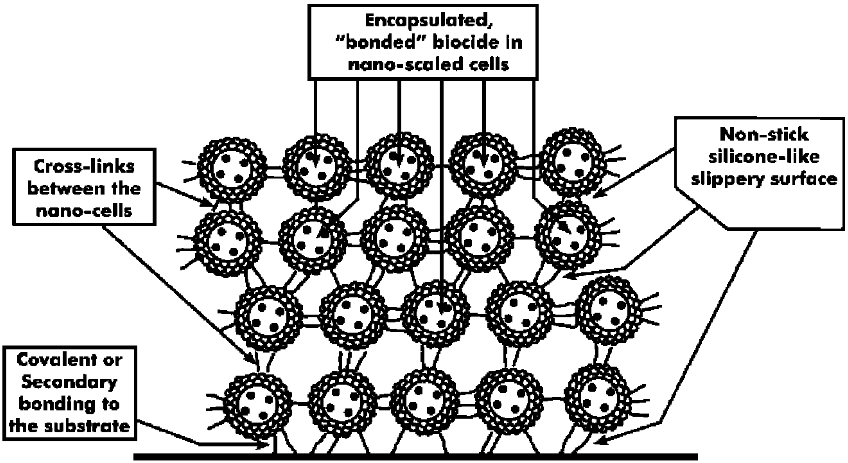
Encapsulated, "bonded" biocide in nano-scaled cells
Cross-links between the nano-cells
Non-stick silicone-like slippery surface
Covalent or Secondary bonding to the substrate
SUBSTRATE

*Figure 1. Schematic representation of a PAMAMOS honeycomb-like network coated on a substrate. Large circles represent PAMAM domains embedded in a silicone matrix and connected via Si-O-Si bonds (straight lines). Small dots represent electrophilic guests encapsulated within the PAMAM domains.*

## Electronics and Photonics

The precise organization of hydrophilic, nucleophilic PAMAM cells in the OS matrix produces a honeycomb-like nanostructure of the PAMAMOS networks which offer an unusual nano-scaled template for the controlled placement of selected guest species. Hence, glass, plastic, metal, silica, silicon, paper or wood can be coated with thin PAMAMOS coatings to become 2D writing boards that encapsulate guests in their PAMAM nano-domains which can be made of inorganic or organic species and organized into letters, numbers or more complex shapes.

For example, transparent, colorless PAMAMO-DMOMS solvent solutions can be used as an invisible ink which can be developed as blue print by immersion in aqueous $CuSO_4$ solution. Further treatment with $Na_2BH_4$ aqueous solution will change the color to copper. More importantly, the resulting PAMAMOS-Cu° nano-composites exhibit conductivity of the order of $10^2$ to $10^3$ S/cm, which ranks them in the class of good polymer semiconductors. These features offer a novel approach to computer chip nano-lithography. PAMAMOS solutions have also been shown to be excellent inks for micro-patterning using the well known Harvard micro-stamping technique (*16*). Considering the simplicity of this imaging technique and the possibilities of imparting conductivity or magnetism to the created patterns by encapsulating nano-scaled metallic or oxide particles into the deposited dendrimer molecules, this appears to be another attractive approach to microlithiography.

Another novel prospect for PAMAMOS in electronics is in the preparation of nano-porous interlayer dielectrics. Here we take advantage of the very different thermal and oxidative stabilities of the PAMAM interiors and OS exteriors. PAMAMs start degrading at *circa* 100-120°C and effectively decompose into volatile degradation products by 200-220°C, whereas OS counterparts can withstand temperatures as high as 300-350°C, yielding pure silica above about 600°C (*17*). We have shown in very limited preliminary experiments that it is possible to thermally treat such networks to obtain nano-porous structures by thermal treatment with pore sizes akin to the diameters of the PAMAM cores used. Dielectric constants as low as 1.6-1.7 were obtained.

Downloaded by STANFORD UNIV GREEN LIBR on June 25, 2012 | http://pubs.acs.org
Publication Date (Web): November 9, 2010 | doi: 10.1021/bk-2010-1051.ch011

## Sensors

Since PAMAMOS network technology offers an extremely effective way of producing a variety of differently colored nano-complexes, we challenged several different arrays of these complexes with a variety of liquid and gaseous analytes. Examples are arrays of $Cr^{3+}$, $Fe^{2+}$, $Ni^{2+}$, $Cu^{2+}$, $Co^{2+}$, $Mn^{2+}$, and $Rh^{3+}$ etc. that show measurable analyte-specific patterns when exposed to methanol, ethanol, isopropanol, $As^{3+}$, $As^{5+}$, etc. Many of these responses were readily apparent to the naked eye.

## Protective and Antifouling Coatings

Nano-structured PAMAMOS-$Cu^{2+}$ and –$Zn^{2+}$ nanocomplexes are under evaluation in a unique approach to environmentally benign anti-fouling coatings that may protect man-made water-submerged objects from aquatic nuisance organisms such as zebra and quagga mussels in fresh water or barnacles and the like in a marine environment. Conventional, commercial antifouling paints all tend to pollute the environment by leaching toxic biocides. This has become a serious enough problem that one of the most effective anti-foulants known, tri-*n*-butyl tin, has been banned for use in the USA.

The PAMAMOS approach combines useful properties of present day commercial paints in coatings in which a biocide such as a $Cu^{2+}$ or $Zn^{2+}$ salt or other electrophile is chemically bound and physically encapsulated inside the nanoscopic dendritic cells of the network, while at the same time a smooth and low energy surface is outwardly presented. Since the ions or molecules of the encapsulated biocides are positioned proximate to the dynamic coating surface at no more than 1-2 nm depth, they are able to exert their antifouling activity across the interface and effectively repel unwanted aquatic organisms. Moreover, as these biocide entities are firmly bound (i.e. strongly complexed) and physically entrapped inside the highly branched nucleophilic dendritic nano-cells, they are unable to migrate into the surrounding water. Consequently, these unique nano-structured coatings provide effective pollution protection and environmentally safe application of proven bio-repellants in combination with smooth, non-stick silicone-based surfaces.

Downloaded by STANFORD UNIV GREEN LIBR on June 25, 2012 | http://pubs.acs.org
Publication Date (Web): November 9, 2010 | doi: 10.1021/bk-2010-1051.ch011

### Purification and Decontamination

PAMAMOS networks can also be used for adsorption and elimination of chemical agents from aquatic or air streams (*18*). For example, they have been shown to be effective in a vapor-phase decontamination application where glass fibers coated with PAMAMOS $Cu^{2+}$ or $Zn^{2+}$ complexes demonstrated the ability to scrub HCN from air streams (*19*).

## Conclusions

In an earlier contribution to this series of symposia on Silicones and Silicone-Modified Materials (*6*) we concluded that the unprecedented properties of PAMAMOS dendrimers and their networks clearly result from the synergism of two distinctly different chemical compositions and unique molecular architecture. The passage of time has confirmed this conclusion. The most important characteristic of the PAMAM core has proved to be its ability to encapsulate metal ions, whereas the organosilicon portion provides low surface energy and the facile ability to be cross-linked into elastomeric and plastomeric films. PAMAMOS networks have proven useful for the preparation of a variety of nano-complexes and nano-compositions and opened up novel engineering nanotechnology applications.

## Acknowledgments

Numerous colleagues at MMI and Dow Corning Corporation have contributed extensively to PAMAMOS research and development. We would particularly like to express our gratitude to Bob Bubeck, Lee Hoffman, Steve Kaganove, Steve Keinath, Chris McMillan, Sue Perz, Joe Rousseau, Abhijit Sarkar and Tracy Zhang.

We gratefully acknowledge financial support of parts of this work by DARPA (contract number W911SR-05-C-0026) and NSF (contract number DMI-0522183).

## References

1. (a) Dvornic, P. R.; Tomalia, D. A. *Curr. Opin. Colloid Interface Sci.* **1996**, *1*, 221. (b) Dvornic, P. R.; Tomalia, D. A. *Sci. Spectra* **1996**, *5*, 36.
2. Tomalia, D. A.; Baker, H.; Dewald, J.; Hall, M.; Kallos, G.; Martin, S.; Roeck, J.; Ryder, J.; Smith, P. *Polym. J.* **1985**, *17*–117.
3. Dvornic, P. R.; de Leuze-Jallouli, A. M.; Owen, M. J.; Perz, S. V. *Macromolecules* **2000**, *33*, 5366.
4. Dvornic, P. R.; Li, J.; de Leuze-Jallouli, A. M.; Reeves, S. D.; Owen, M. J. *Macromolecules* **2002**, *35*, 9323.
5. Dvornic, P. R.; de Leuze-Jallouli, A. M.; Perz, S. V.; Owen, M. J. *Mol. Cryst. Liq. Cryst.* **2000**, *353*, 223.
6. Dvornic, P. R.; de Leuze-Jallouli, A. M.; Owen, M. J.; Perz, S. V. In *Silicones and Silicone-Modified Materials*; Clarson, S. J., Fitzgerald, J. J., Owen, M. J., Smith, S. D., Eds.; ACS Symposium Series 729, American Chemical Society: Washington, DC, 2000; p 241.
7. Zhang, T.; Dvornic, P. R.; Kaganove, S. N. *Langmuir* **2007**, *23*, 10589.
8. Bubeck, R. A.; Dvornic, P. R.; Hu, J.; Hexemer, A.; Li, X.; Keinath, S. E.; Fischer, D. A. *Macromol. Chem. Phys.* **2005**, *206*, 1146.
9. Bubeck, R. A.; Bauer, B. J.; Dvornic, P. R.; Owen, M. J.; Reeves, S. D.; Parham, P. L.; Hoffman, L. W. *Polym. Mater. Sci. Eng.* **2001**, *84*, 366.
10. Dvornic, P. R.; Bubeck, R. A.; Reeves, S. D.; Li, J.; Hoffman, L. W. *Silicon Chem.* **2003**, *2*, 207.
11. Dvornic, P. R.; Bubeck, R. A.; Owen, M. J. In *Silicones in Coatings IV*, Paint Research Association: London, 2002; Paper 3, 15.
12. Uppuluri, S.; Keinath, S. E.; Tomalia, D. A.; Dvornic, P. R. *Macromolecules* **1998**, *31*, 4498.
13. Ottaviani, M. F.; Montali, F.; Turro, N. J.; Tomalia, D. A. *J. Phys. Chem. Chem.B* **1997**, *101* (21), 158.
14. Jansen, J. J.; Van Bekkum, H. H. *Carbon* **1995**, *33* (8), 1021.
15. Dvornic, P. R. *J. Polym. Sci., Part A:Polym. Chem.* **2006**, *44*, 2755.
16. Kohli, N.; Dvornic, P. R.; Kaganove, S. N.; Worden, R. M.; Lee, I. *Macromol. Rapid Commun.* **2004**, *25*, 935.
17. Chujo, Y.; Matsuki, H.; Kure, S.; Saegusa, T.; Yazawa, T. *J. Chem. Soc. Chem. Commun.* **1994**, 635.
18. Arkas, M.; Tsiourvas, D.; Paleos, C. M. *Chem. Mater.* **2005**, *17*, 3439.
19. Kaganove, S. N.; Zhang, T.; Dvornic, P. R. In *Pacifichem 2005*, Honolulu, HI, December 2005.

Downloaded by STANFORD UNIV GREEN LIBR on June 25, 2012 | http://pubs.acs.org
Publication Date (Web): November 9, 2010 | doi: 10.1021/bk-2010-1051.ch011

## Chapter 12

# Etching of Silicone Elastomers: Controlled Manipulation of Surface Roughness

**Michael A. Brook,* Lihua Liu, Shigui Zhao, and Zaid N. Mammo**

**Department of Chemistry, McMaster University, 1280 Main St. W.,**
**Hamilton, Ontario, Canada L8S 4M1**
***mabrook@mcmaster.ca**

Downloaded by UNIV OF GUELPH LIBRARY on June 24, 2012 | http://pubs.acs.org
Publication Date (Web): November 9, 2010 | doi: 10.1021/bk-2010-1051.ch012

The compatibility of biomaterials is related, among many other factors, to surface roughness. We describe a simple method using aqueous solutions of KOH in methanol (optionally with THF) to etch silicone elastomers to give materials ranging from about 20 nm to nearly 1 μ rms roughness. Surface depolymerization occurred linearly with time: roughness also increased with time, but not linearly. The degree of roughness was dependent on base concentration, reaction time and the presence of THF. Once the catalyst migrates into the silicone phase, base-catalyzed silicone degradation is more rapid than transfer back to the alcoholic solution, which leads to asymmetric surface pitting, the depth and frequency of which are controlled by solvency.

## Introduction

Silicone polymers are widely used as biomaterials, particularly in the eye. Thus, silicone oils serve as retinal tamponades (*1*, *2*), most contact lenses are now based on silicone hydrogels (*3–6*), and intraocular lenses (IOLs) may be made of silicone elastomers (*7*). While many properties of silicones contribute to their utilization in these devices, optical transparency, oxygen permeability and biocompatibility are particularly important. However, the ability of cells to grow on silicone surfaces may also be important.

Depending on where the silicone biomaterial is located in the body, it may or may not be desirable to have cells adhere and proliferate on the surface. For instance, breast implants used post-mastectomy need to adhere to local tissue to

In Advances in Silicones and Silicone-Modified Materials; Clarson, S., et al.;
ACS Symposium Series; American Chemical Society: Washington, DC, 2010.

maintain the implant location and cell growth on the surface is beneficial in this application. This is not universally the case, however. In an intraocular lens, for example, growth of cells on the posterior surface of the lens (posterior capsule opacification) is particularly problematic because the cell layer can occlude vision (*8*). Thus, there is an interest in developing surfaces for various parts of the body on which cell growth can be controlled.

A variety of factors determine the affinity that specific cell lines have for a given biomaterials' surface. These can include hydrophobicity/hydrophilicity, the affinity of the surfaces for protein adsorption, the facility with which protein denaturation occurs on such surfaces, the availability of nutrients, etc. (*9*, *10*) In addition, the modulus (rigidity) (*11*) and surface roughness of surfaces are important factors in cellular adhesion and proliferation (*12–14*). While inevitably there is an interplay between these factors, we wished to understand the specific role played by silicone surface roughness on cellular adhesion and proliferation. Prior to doing so, it was necessary to develop a robust methodology that would permit the introduction of surface roughness in a predictable way at several length scales. We describe the utilization of base-induced surface depolymerization as a strategy to create surface roughness on silicone elastomers at the nm to micrometer scales.

Downloaded by UNIV OF GUELPH LIBRARY on June 24, 2012 | http://pubs.acs.org
Publication Date (Web): November 9, 2010 | doi: 10.1021/bk-2010-1051.ch012

## Experimental Section

### Reagents

KOH was obtained from Aldrich and organic solvents were purchased from Caledon Laboratories. Water used was purified by treating in a reverse osmosis unit followed by a Millipore unit (18 mΩ resistivity). SYLGARD 184 (silicone elastomer kit) and DC1107 (polyhydromethylsiloxane) were purchased from Dow Corning. The elastomer was formed by mixing the curing agent (1 part) with the silicone prepolymer (10 parts), and pouring into a Petri dish, where it were allowed to cure for 48 h at room temperature. Silicone slabs were cut into small circular disks of *ca.* 1.0 cm diameter x 0.3 cm thick and were used directly.

### Techniques

Swelling measurements were made by measuring increases in weight after swelling disks in solvent. For all graphs, the errors bars represent standard deviation of at least 3 measurements. Surface roughnesses were obtained using a Veeco WYKO NT1100 Optical Profiling System (Mode: VSI, Objective 50X, FOV 2.0X). SEM data was collected on a JEOL JSM 7000F using an accelerating voltage of 15kV).

### Etching Processes

KOH was dissolved in water and then mixed with MeOH and, optionally, THF. One silicone elastomer disk was placed in a vial that contained the basic

Downloaded by UNIV OF GUELPH LIBRARY on June 24, 2012 | http://pubs.acs.org
Publication Date (Web): November 9, 2010 | doi: 10.1021/bk-2010-1051.ch012

etchant solution and shaken for different time at room temperature (orbital shaker, 2 rps).

At the conclusion of the etching process, the elastomer disks were removed from the vials, and washed extensively to remove any physically adhering materials. In a typical washing cycle, the rubber slabs were washed with acetone, THF, acetone, hexanes, acetone, water, acetone, and finally flushed with nitrogen then placed in vacuum chamber at room temperature overnight to dry. Finally, surface characteristics were determined.

## Results

Unlike most polymers, silicones are both readily polymerized and depolymerized under equilibrating conditions. The equilibrium constant for the process of linear chain growth from (or ‘unzipping’ to) cyclics is near 1 (Figure 1) (*15*). Thus, exposing a preformed silicone elastomer to an appropriate catalyst, typically an acid or base, initiates the equilibration leading to the formation of cyclics (such as octamethylcyclotetrasiloxane ($D_4$) and decamethylcyclopentasiloxane ($D_5$)) (*16*) and lower molecular weight linear polymers that can diffuse away from the surface of the elastomer. When such a depolymerization process occurs homogeneously across the elastomer surface, the elastomer will lose mass, but the roughness of the surface would not be expected to change. By contrast, surface roughness will be induced when degradation is asymmetric across the surface.

KOH is a prototypical catalyst used to polymerize silicones and, additionally, to depolymerize silicones for recycling. We chose to examine the ability of this catalyst to introduce surface morphology of a platinum-cured silicone elastomer (SYLGARD 184). The elastomer was prepared by mixing the prepolymer and curing agent in a 10:1 ratio. The mixture was poured into a Petri dish and allowed to cure at room temperature for 48 hours and then coupons approximately 1 cm diameter, 0.3 mm thick were cut from the film. Disks were placed at room temperature in the basic solvent mixture normally for up to 48 hours, after which they were removed, rinsed with a variety of solvents, and then dried. In addition to differences in KOH concentration that should affect the rate of any degradation, the solvents were varied from those that were not very soluble/swellable in silicones (water, MeOH) to those that are (THF, isopropanol). The surfaces were analyzed by scanning electron microscopy and optical profilometry.

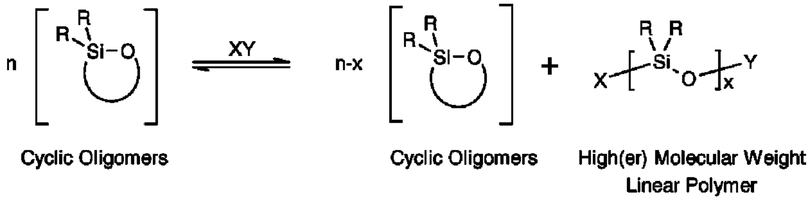

*Figure 1. Silicone equilibrium polymerization*

Downloaded by UNIV OF GUELPH LIBRARY on June 24, 2012 | http://pubs.acs.org
Publication Date (Web): November 9, 2010 | doi: 10.1021/bk-2010-1051.ch012

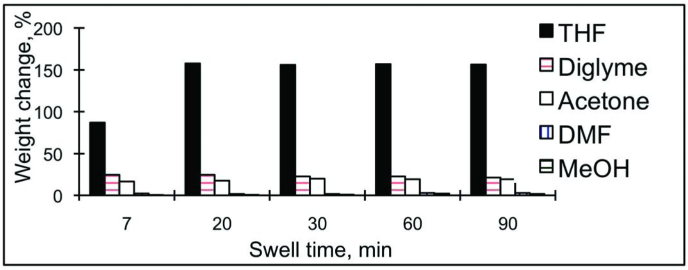

*Figure 2. Swelling extent of a (single batch of) PDMS elastomer in different solvents*

Initially, survey experiments demonstrated a strong dependence of reactivity on KOH solvency. Isopropanol, for example, a reasonable solvent for both silicones and KOH, led to rapid degradation of the elastomer. It proved difficult to reliably and reproducibly form well defined surfaces. More frequently, rapid and complete decomposition of the elastomer occurred. During that process, cracks formed (see also below), propagated, and elastomers were reduced to particles before undergoing complete depolymerization. Similarly, degradation was directly related to KOH concentration. Survey experiments demonstrated that a convenient degradation process (within 12-48 hours) occurred with 1-5 wt% KOH in the solvents described below: lower concentrations were often inconveniently slow, higher concentrations were on occasion too fast (data not shown). Therefore, the experiments described below generally utilized 1% or 5wt% KOH in a variety of less effective solvents than isopropanol.

Swelling studies showed that solubility/swellability of SYLGARD 184 elastomers increased in an approximate log scale on moving from MeOH Π acetone Π THF (Figure 2). Therefore, solutions of 5wt% KOH, 10wt% $H_2O$ were made up in mixtures based on these three solvents. Methanol, not a very effective solvent for silicones, was used as the base solvent, which was then optionally modified by the addition of THF: the effect of acetone is intermediate to the methanol only and methanol/THF data (data not shown).

The loss of material, during etching of a smooth silicone elastomer (no features could be seen on the profilometer micrograph) exposed to 1% KOH; 89%MeOH; 10%$H_2O$, leads to roughness that is relatively homogeneously spread across the surface (Figure 3A) at shorter reaction times. However, at extended periods of time, cracks appear as shown by profilometer images obtained at room pressure (Figure 3B), and SEM images measured at high vacuum (Figure 3C,D). Similar behavior was observed with 5% KOH; 85%MeOH; 10%$H_2O$ as etching solution (Figure 4). The loss of material from the surface increased approximately linearly with time (Figure 5A). There was also a time dependent increase in the roughness, as determined using a profilometer: Rq increased from about 20-30 nm (*17*) to nearly 600 nm (Figure 5B) [Rq: the root mean square (rms) average between the height deviations and the mean line/surface, taken over the evaluation length/area. The mathematical formula used to calculate Rq is available from www.veeco.com.].

Downloaded by UNIV OF GUELPH LIBRARY on June 24, 2012 | http://pubs.acs.org
Publication Date (Web): November 9, 2010 | doi: 10.1021/bk-2010-1051.ch012

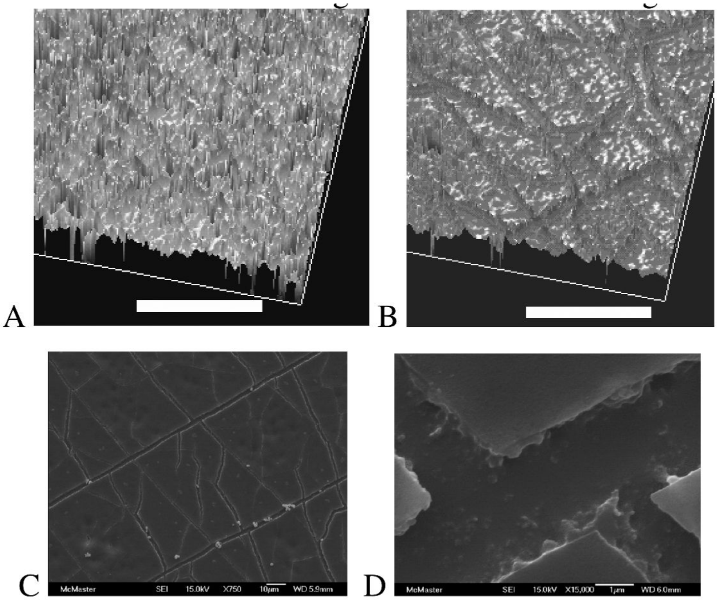
A
B
C
McMaster SEI 15.0kV X750 10μm WD 5.9mm
D
McMaster SEI 15.0kV X15,000 1μm WD 6.0mm

*Figure 3. Surface profiles (300 x 225 μ) after etching in 1.0% KOH/(MeOH+10%$H_2O$) for A: 5 h (Rq 370) , B: 18 h (Rq 340) scale bar = 50 μ.*

When THF, a good solvent for silicones, was included in the etching solution (5% KOH; 75% MeOH; 10% THF; 10% $H_2O$), degradation occurred far more rapidly and led to rougher surfaces, up to nearly 800 micron roughness; rougher surface could be obtained, but cracks started to appear concomitantly. However, the morphology of the resulting surface was quite different in the absence of THF. As shown more clearly in the surface after 5 hours, a uniform distribution was observed with 'pock marks' or pits on the surface: the surface after 5 hours was similar to that obtained after 18 hours in the absence of THF (Figure 6): the pits are broader and deeper in than in the absence of THF. This enhancement in rate of degradation is shown in Figure 7.

## Discussion

Silicone depolymerization reactions at ambient temperature require an active catalyst to initiate nucleophilic substitution. In the case of the reactions described above, KOH functions to initiate depolymerization which, through a series of bimolecular and unimolecular (backbiting) processes, ultimately leads to low molecular weight linear and cyclic silicones. In the case of an elastomer, these materials can diffuse away from the surface. If all exposed siloxane monomer units reacted with the same ease, homogenous depolymerization across the surface would be expected, leading to loss of elastomeric material, but with no induction of surface roughness. Thus, the observed rougher surfaces must result from differential reactivity of siloxanes presenting at the interface.

Downloaded by UNIV OF GUELPH LIBRARY on June 24, 2012 | http://pubs.acs.org
Publication Date (Web): November 9, 2010 | doi: 10.1021/bk-2010-1051.ch012

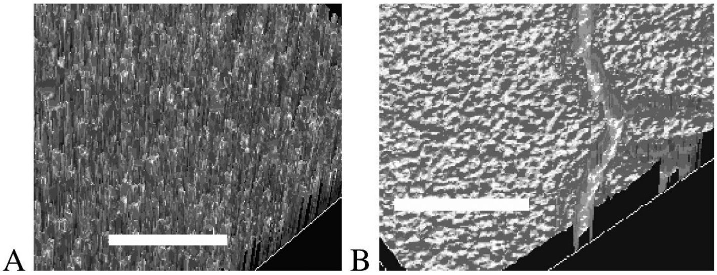

*Figure 4. Etching in 5.0% KOH/(MeOH+10%$H_2O$) for A: 5 hours (Rq 576), 24 hours (Rq 588), scale bar = 50 μ.).*

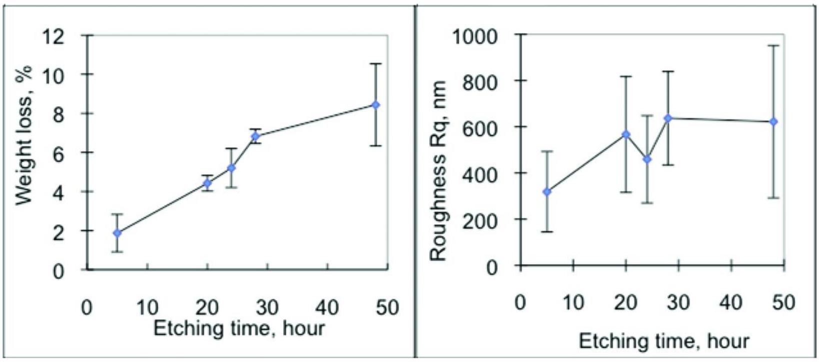

*Figure 5. A: Weight loss and B: increase in roughness over time after exposure to 5%KOH; 85%MeOH;10%$H_2O$.*

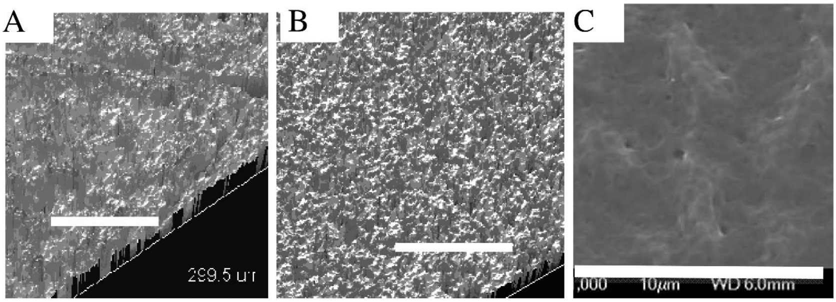

*Figure 6. Morphology of surfaces etched A: 1.0% KOH; 79% MeOH; 10%THF;10%$H_2O$ (Rq 815), 24 h. B: 5.0% KOH; 75%MeOH; 10%THF; 10%$H_2O$ (Rq 360) for 5 h. C: SEM of B, scale bar = 50 μ.*

Downloaded by UNIV OF GUELPH LIBRARY on June 24, 2012 | http://pubs.acs.org
Publication Date (Web): November 9, 2010 | doi: 10.1021/bk-2010-1051.ch012

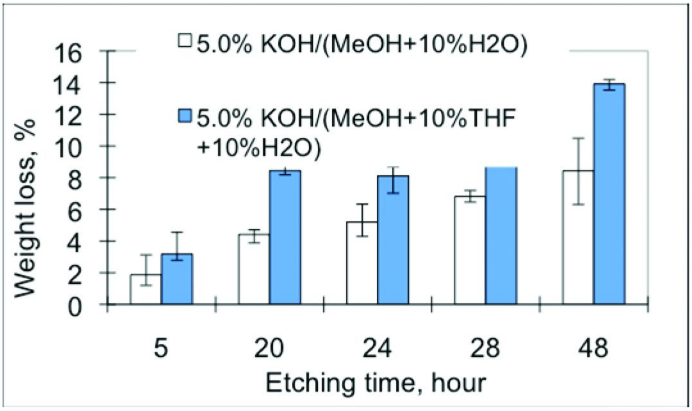

*Figure 7. Relative effectiveness of surface erosion in the absence (open bar) or presence (filled bar) of 10%THF.*

In addition to the depolymerization processes that occur in homogenous media, a separate process affects the outcome of the reaction: in this case, the catalyst can reside in two different phases; in the (swollen) silicone elastomer; or in the alcoholic KOH solution. If the rate of exchange of the catalyst between these two phases is slower than the rate of depolymerization, it would be expected that surface roughness would result. The KOH, once reacting at the surface, would 'eat into' the silicone, creating a pit, prior to reentering the alcoholic solution phase. The relative depth of the pit will increase with the difficulty of transfer of catalyst back to the alcoholic solution. The overall degradation process is accelerated with higher catalyst concentrations, although the ultimate roughness is similar in a given solvent system.

Such a model permits an understanding of the role played by THF. Mobility of the catalyst within the elastomer will be higher when it is more highly swollen with THF. In addition, swelling will induce strain within the network, increasing the rate of decomposition processes that lead to preferential cleavage of more highly strained linkages. Thus, larger and deeper pits would be expected in the more highly THF-swollen elastomer. As the crosslink density increases with loss of chain length between crosslinks, strain will be increased leading eventually to formation and propagation of cracks in the elastomer.

Different cells respond differently to a variety of features on synthetic polymer surfaces (*18*). Roughness is a relatively easily modified parameter to control cell growth (*17*). At the micron scale length, structural features may be encoded by a variety of strategies. The development of microcontact printing by Whitesides, is particularly applicable to the generation of surfaces with micron size features: the spacing of such features can control cell spreading (*19*). Brennan has demonstrated that cell adhesion to silicone surfaces with these feature sizes is extremely low (*20*). It is more challenging to generate rough surfaces at the nanometer scale in a controlled fashion.

The simple technology described above allows silicone surfaces from about 10-800 nm roughness to be generated with random features. With such materials in hand, it will be possible to establish optimum surfaces structures for proliferation of different cell types such that surfaces can be engineered for different biomaterials applications, which will be the subject of future reports.

# Conclusions

The controlled erosion of silicone elastomers, leading to roughened surfaces from 20 - ~800 nm, can be achieved using aqueous KOH in organic solvents. At extended periods of time, cracks form and propagate, ultimately increasing the fragility of the material, particularly at higher concentrations of KOH and THF. However, the controlled erosion to give desired roughness is achieved by manipulating the concentration of KOH and THF in methanol/water, both of which increase rate and degree of asymmetric etching. The asymmetry is proposed to arise from a partition of the active catalyst between silicone and alcohol phases.

# Acknowledgments

We gratefully acknowledge the financial support of the Natural Sciences and Engineering Research Council of Canada (NSERC).

# References

1. Scott, I. U.; Flynn, H. W., Jr.; Azen, S. P.; Lai, M.-Y.; Schwartz, S.; Trese, M. T. *Ophthalmology* **1999**, *106*, 1399–1408.
2. Orzalesi, N.; Migliavacca, L.; Bottoni, F.; Miglior, S. *Curr. Eye Res.* **1998**, *17*, 828.
3. Woods, C. A.; Jones, D. A.; Jones, L. W.; Morgan, P. B. *Optom. Vis. Sci.* **2007**, *84*, 505–10.
4. Woods, C. A.; Morgan, P. B. *Clin. Exp. Optom.* **2004**, *87*, 19–23.
5. Friends, G. D.; Kunzler, J. F.; Ozark, R. M. *Macromol. Symp.* **1995**, *98*, 619–31.
6. Kunzler, J. F. *Trends Polym. Sci.* **1996**, *4*, 52–9.
7. Werner, L. *Curr. Opin. Ophthal.* **2008**, *19*, 41–49.
8. Schaumberg, D. A.; Dana, M. R.; Christen, W. G.; Glynn, R. J. *Ophthalmology* **1998**, *105* (7), 1213–1221.
9. Brash, J. L. *J. Biomater. Sci., Polym. Ed.* **2000**, *11*, 1135–1146.
10. Liu, L.; Sheardown, H. *Biomaterials* **2005**, *26*, 233–244.
11. Harris, A. K.; Wild, P.; Stopak, D. *Science* **1980**, *208*, 177–179.
12. Dalton, B. A.; Evans, M . D. M.; McFarland, G. A.; Steele, J. G. *J. Biomed. Mater. Res.* **1999**, *45*, 384–394.
13. Evans, M. D. M.; Dalton, B. A.; Steele, J. G. *J. Biomed. Mater. Res.* **1999**, *46*, 485–493.
14. Fitton, J. H.; Dalton, B. A.; Beumer, G.; Johnson, G.; Griesser, H. J.; Steele, J. G. *J. Biomed. Mater. Res.* **1998**, *42*, 245–257.

Downloaded by UNIV OF GUELPH LIBRARY on June 24, 2012 | http://pubs.acs.org
Publication Date (Web): November 9, 2010 | doi: 10.1021/bk-2010-1051.ch012

15. Chojnowski, J. Polymerization. In *Siloxane Polymers*; Clarson, S. J., Semlyen, J. A.; Eds.; Prentice Hall: Englewood Cliffs, NJ, 1993; Chapter 1, p 5.
16. Brook, M. A. *Silicon in Organic, Organometallic, and Polymer Chemistry*; Wiley: New York, 2000.
17. Whitehead, K. A.; Verrana, J. *Food Bioprod. Process.* **2006**, *84*, 253–259.
18. Wong, J. Y.; Leach, J. B.; Brown, X. Q. *Surf. Sci.* **2004**, *570*, 119–133.
19. Xia, N.; Thodeti, C. K.; Hunt, T. P.; Xu, Q. B.; Ho, M.; Whitesides, G. M.; Westervelt, R.; Ingber, D. E. *FASEB J.* **2008**, *22*, 1649–1659.
20. Carman, M. L.; Estes, T. G.; Feinberg, A. W.; Schumacher, J. F.; Wilkerson, W.; Wilson, L. H.; Callow, M. E.; Callow, J. A.; Brennan, A. B. *Biofouling* **2006**, *22*, 11–21.

Downloaded by UNIV OF GUELPH LIBRARY on June 24, 2012 | http://pubs.acs.org
Publication Date (Web): November 9, 2010 | doi: 10.1021/bk-2010-1051.ch012

Downloaded by COLUMBIA UNIV on June 25, 2012 | http://pubs.acs.org
Publication Date (Web): November 9, 2010 | doi: 10.1021/bk-2010-1051.ch013

## Chapter 13

# Novel Organo-Siloxane Copolymers for Flame Retardant Applications

**Ravi Mosurkal,[1] Vincent Tucci,[5] Lynne A. Samuelson,[1] Kenneth D. Smith,[2] Phillip R. Westmoreland,[2] Virinder S. Parmar,[3] Jayant Kumar,[4] and Arthur C. Watterson*,[5]**

**[1]U.S. Army Natick Soldier RDEC, Natick, MA 01760**
**[2]Department of Chemical Engineering,**
**University of Massachusetts−Amherst, Amherst, MA 01003**
**[3]Bioorganic Laboratory, Department of Chemistry, University of Delhi,**
**Delhi 10 007, India**
**[4]Center for Advanced Materials, University of Massachusetts,**
**Lowell, MA 01854**
**[5]Institute for Nano-Science and Engineering Technology,**
**University of Massachusetts, Lowell, MA 01854**
***E-mail: Arthur_Watterson@uml.edu**

Environmentally safe polysiloxane copolymers, such as copolyamides, copolyesters and copolyimides with aromatic linkers were biocatalytically synthesized using lipase as a bio-catalyst. Their thermal and flame-retardant properties were investigated. Polysiloxane copolyamides show excellent flame-retardant properties in terms of heat release capacities and char yields. The crosslinked copolyamides further improved the heat release capacity to as low as 90 J/g-K. However, the degradation temperatures are relatively low compared to copolyimides synthesized enzymatically and non-enzymatically. The copolyimides synthesized using various dianhydride monomers without using any biocatalyst showed improved degradation temperatures of up to 440-470 °C compared to copolyamides/esters (390 - 410 °C).

In Advances in Silicones and Silicone-Modified Materials; Clarson, S., et al.;
ACS Symposium Series; American Chemical Society: Washington, DC, 2010.

Downloaded by COLUMBIA UNIV on June 25, 2012 | http://pubs.acs.org
Publication Date (Web): November 9, 2010 | doi: 10.1021/bk-2010-1051.ch013

# Introduction

Biocatalytic synthesis of polymers is of great importance in making functional materials using environmentally benign conditions (*1–3*). Enzyme-mediated synthesis has several advantages including environmentally responsible and economical synthesis, yielding processable and stable materials. We have recently shown that biocatalytically synthesized siloxane-based polyesters and polyamides have great potential as flame-retardant (FR) materials (*4*). The thermal and flame-retardant properties of these polymers were further improved by crosslinking techniques using hexamethylenetetramine (HMTA) as a crosslinker (*5*). In this paper, we review the biocatalytic synthesis of siloxane copolyamides/esters using lipase as a biocatalyst. We also present a simple synthesis of siloxane-aryl copolyimides using aromatic dianhydrides and aminopropyl terminated polydimethyl siloxane without using any biocatalyst or solvent. The thermal and flame-retardant properties such as degradation temperatures, heat release capacities, and char yields of these polymers are also presented.

# Experimental

## Materials

Novozyme-435, an immobilized enzyme, was received gratis from Novozymes, Denmark and used as received. All other chemicals and solvents were used without further purification. Aminopropyl terminated polydimethylsiloxane (PDMS) (Mw 900-1100) was purchased from Gelest Inc. and dimethyl 5-hydroxyisophthalate, dimethyl 5-aminoisophthalate, 4,4′-oxydiphthalic anhydride, 4,4′-(4,4′-isopropylidene diphenoxy)bis(phthalic anhydride), 1,4,5,8-naphthalene tetracarboxylic dianhydride, 1,2,4,5-benzenetetracarboxylic dianhydride, and 4,4′-biphthalic anhydride were purchased from Aldrich.

## Synthesis

### *Biocatalytic Synthesis of Siloxane Copolyesters and Copolyamides: Example* **3**

In a simple procedure (Scheme 1), equimolar amounts of previously dried dimethyl 5-hydroxy isophthalate and aminopropyl-terminated polydimethysiloxane (Mw 900-1100) were mixed in a three-neck round-bottom flask. Under nitrogen atmosphere, 10 % of the enzyme by weight, Novozyme-435 (immobilized *Candida antarctica* lipase B, protein content 1 % with respect to the weight of the monomers) was added. The resulting reaction mixture was stirred at 90°C under vacuum using a mechanical stirrer for homogeneous polymerization. After 48 hours, the reaction mixture was quite viscous. The reaction was quenched by adding chloroform solvent and then filtered to remove the enzyme. The solvent was removed under reduced pressure to isolate the polymer. The crude polymer was purified by washing with hexane and methanol to remove unreacted monomers and oligomers obtaining **4** in 80 % yield (confirmed by NMR spectroscopy).

The synthesis of copolyimides was carried out following a procedure which was similar to the one followed in making copolyamides/esters except that dianhydride monomers (Scheme 2) and aminopropyl-terminated polysiloxane were used. The reaction was stopped after 8 hours of heating at 90 °C under vacuum.

### Synthesis of Siloxane Copolyimides without Enzyme

To synthesize these copolyimides, the procedure for enzymatic synthesis was followed except that enzyme was not added. A typical reaction was carried out simply by mixing the amino-terminated PDMS and the corresponding anhydride and heating the reaction mixture at 90 °C under vacuum for 8 hours. The polymers obtained with this simple method without using enzyme were similar to those obtained biocatalytically except there was an intermediate step forming polyamic acids and the end products were mixtures of both imide and amic acid. All the polyimides except **6** (*6*) in Figure 1 were synthesized without using any biocatalyst. All the polymers synthesized were characterized by $^1$H NMR spectroscopy. **5**: $CDCl_3$, δ 9.31 (bs, 2H, Ar=Aromatic), 3.34 (t, 2H, e), 1.62 (m, 2H, d), 0.55 (t, 2H, c), 0.09 (m; a,b); **7**: insoluble; **8**: $CDCl_3$, δ 8.79 (s, 4H; Ar), 4.21 (t, 2H; e), 1.80 (m, 2H; d), 0.76 (t, 2H; c), 0.11 (m; a,b); **9**: $CDCl_3$, δ 7.83 (d, 2H, Ar), 7.36 (bd, 8H; Ar), 7.06 (d, 4H; Ar), 3.67 (t, 2H; e), 1.78 (6H; dimethyl protons in Ar linker), 1.63 (m, 2H; d), 0.64 (t, 2H; c), 0.11 (m; a,b).

Downloaded by COLUMBIA UNIV on June 25, 2012 | http://pubs.acs.org
Publication Date (Web): November 9, 2010 | doi: 10.1021/bk-2010-1051.ch013

### Crosslinking with HMTA

Crosslinking of siloxane-copolyamide samples was carried out using hexamethylenetetramine (HMTA). In a typical crosslinking procedure, the copolyamide and HMTA were dissolved in chloroform, and the resultant solution was heated slowly on a hot plate to remove the solvent for 10 minutes and then oven-dried under vacuum at 90-120 °C overnight to remove any residual water.

### Characterization

$^1$H NMR spectra were recorded on a Bruker Instrument 250 MHz ARX spectrometer equipped with a Silicon Graphics workstation. Thermal decomposition was studied under air using a TA Instruments 2050 thermogravimetric analyzer (TGA). Flammability was measured using a pyrolysis-combustion flow calorimeter (PCFC, FAA microcalorimeter) (*7*). In this apparatus, a sample of 2-5mg is pyrolyzed at 1°C/s from approximately 100 to a maximum of 900 °C. A metered flow of $N_2$ sweeps the pyrolysis gases into a mixing volume with $O_2$ such that the $N_2/O_2$ mixture would have approximately the composition of atmospheric air. The mixture is oxidized at 900 °C to completion in a flow-tube reactor, $H_2O$ and $CO_2$ products are removed, and the $O_2$ depletion is measured continuously as a function of time. The heat release rate is calculated from the consumption rate of $O_2$. The total heat release and the heat-release capacity reported is the average of three measurements of each sample. The heat release capacity (J/g-K) reported is the ratio of peak heat release rate (W/g) to the heating rate (°C/s).

## Results and Discussion

### Synthesis

We have synthesized three types of siloxane-based copolymers, namely, copolyamides, copolyesters and polyimides (*4*). Copolyamides were synthesized biocatalytically using lipase as a biocatalyst. Copolyimides with various monomers (Figure 1) and aminopropyl-terminated siloxanes were initially synthesized biocatalytically using lipase as biocatalyst. However, these copolyimides could be synthesized without the biocatalyst as well. Heating the monomer and siloxane at 90 °C under vacuum gave an insoluble to partially soluble product in all cases. However, the flammability properties were invariant to these changes, which make them more interesting relative to copolyamides.

Downloaded by COLUMBIA UNIV on June 25, 2012 | http://pubs.acs.org
Publication Date (Web): November 9, 2010 | doi: 10.1021/bk-2010-1051.ch013

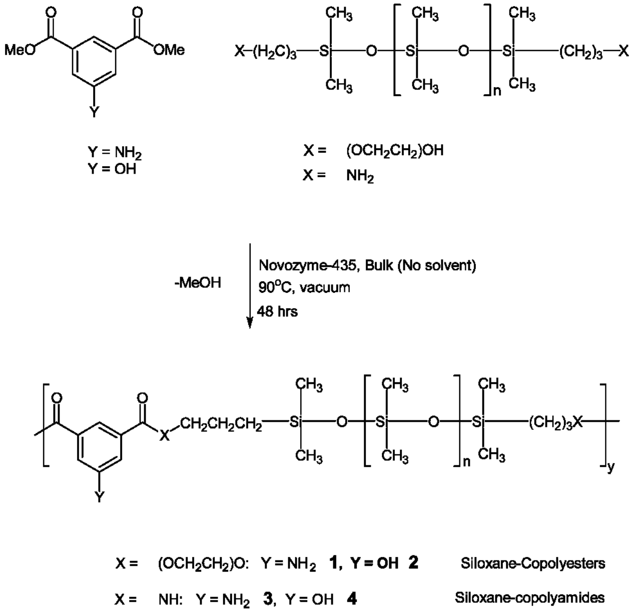
MeO
OMe
O
O
Y
Y = NH2
Y = OH
X-(H2C)3
CH3
Si
O
n
(CH2)3-X
X = (OCH2CH2)OH
X = NH2
-MeOH
Novozyme-435, Bulk (No solvent)
90°C, vacuum
48 hrs
X
CH2CH2CH2
(CH2)3X
y
X = (OCH2CH2)O: Y = NH2 1, Y = OH 2
Siloxane-Copolyesters
X = NH: Y = NH2 3, Y = OH 4
Siloxane-copolyamides

*Scheme 1. Enzymatic synthesis of siloxane copolyesters and copolyamides Biocatalytic synthesis of siloxane copolyimides*

Downloaded by COLUMBIA UNIV on June 25, 2012 | http://pubs.acs.org
Publication Date (Web): November 9, 2010 | doi: 10.1021/bk-2010-1051.ch013

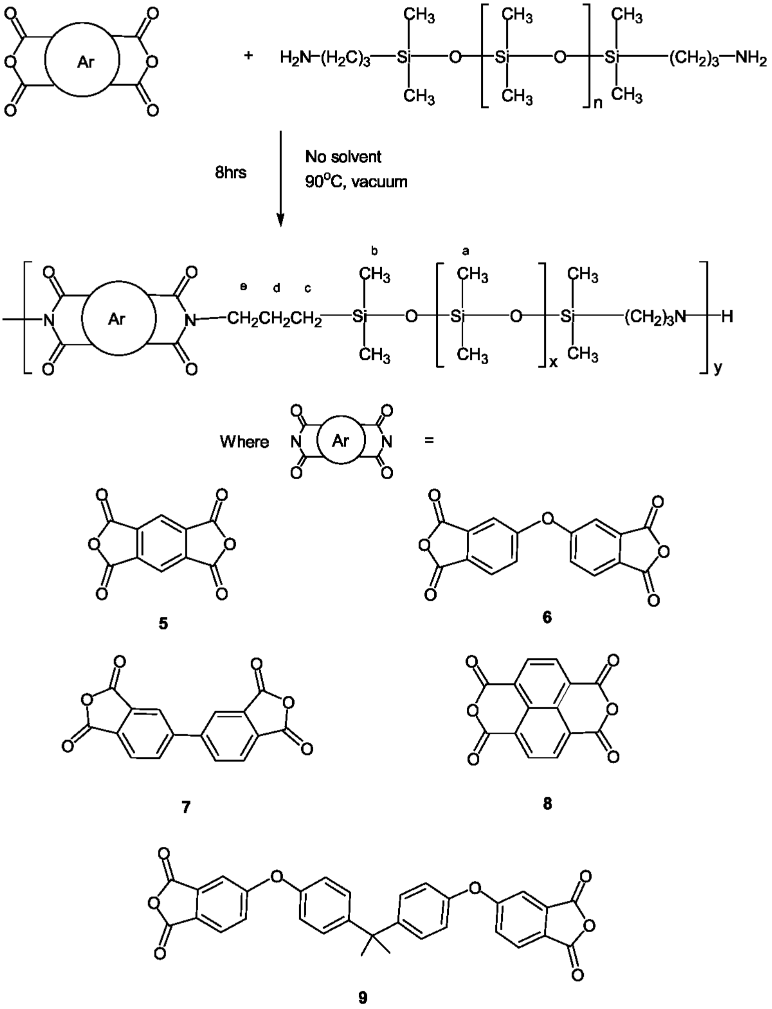

*Scheme 2. Synthesis of Siloxane copolyimides considered in this study.*

It is very well known in the literature that polyimide preparation traditionally involves initial formation of polyamic acid, followed by ring closure to form the polyimide (*8*). The formation of a stable five-member ring is the driving force for forming linear rather than crosslinked polymers. If the intermediate polyamide/polyamic acid is insoluble, the second step must be carried out by solid-state cyclization reaction at high temperatures. It is interesting to note that in our enzymatic synthesis, the cyclization takes place in-situ and gives rise to a clean linear polyimide product without the need of any further processing. This result shows that enzyme is playing a crucial role as a catalyst driving the reaction to imide formation, which otherwise is not possible under those conditions (*6*). However, the flammability properties are relatively constant, which indicates that the presence of amic acid structure is not detrimental to the flame-retardant properties of these polyimides. Moreover, it is expected that when the polyamic-acid-containing polyimide is subjected to high temperatures, the imide formation due to the endothermic reaction could indeed slightly reduce the heat release capacity. Thus the synthesis of most polyimides (except **6** in Figure 1) proceeds without using any biocatalyst, further simplifying the synthetic procedure and reducing the cost of these environmentally safe, flame-retardant polymers.

### *Crosslinking in Siloxane Copolyamides*

The copolyamides synthesized using environmentally benign synthetic routes have been shown to possess a high degree of flame retardancy (*4*). However, the products remained as viscous liquids with a heat release capacity around 240 J/g-K. Thus, there is a need to improve the flammability properties. Crosslinking these polysiloxane copolymers with hexamethylenetetramine (HMTA, a common crosslinking agent for phenolic resins (*9*)) improved both the mechanical properties and flame-retardant properties (*5*). Figure 1 shows the crosslinking product of copolyamide, **3** with 20 % HMTA and its NMR characterization, which reveals a few of the many possible crosslinking products.[10]

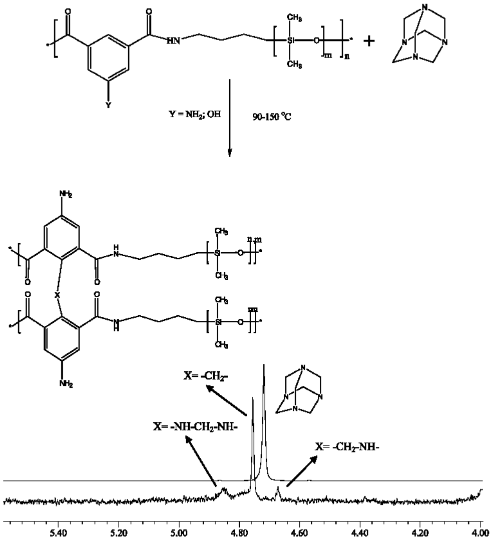

*Figure 1. Crosslinking of siloxane copolyamide with HMTA and the $^1$H NMR spectrum of possible crosslinked products.*

Downloaded by COLUMBIA UNIV on June 25, 2012 | http://pubs.acs.org
Publication Date (Web): November 9, 2010 | doi: 10.1021/bk-2010-1051.ch013

Downloaded by COLUMBIA UNIV on June 25, 2012 | http://pubs.acs.org
Publication Date (Web): November 9, 2010 | doi: 10.1021/bk-2010-1051.ch013

**Table 1. Heat release capacity of siloxane copolyamide (3, Scheme 1) as a function of HMTA weight percent**

| *% HMTA (by weight)* | *HR capacity ($Jg^{-1}K^{-1}$)* | *Total HR ($KJg^{-1}$)* | *Char yield (%)* |
|---|---|---|---|
| 0 | 194 | 15.8 | 11 |
| 1 | 173 | 13.1 | 12.3 |
| 5 | 156 | 12.6 | 14.4 |
| 10 | 108 | 11.4 | 14.9 |
| 15 | 125 | 13.6 | 12.5 |
| 20 | 90 | 12.8 | 13.2 |

The flammability results on the copolyamide, **3** (Scheme 1) from the Pyrolysis/Combustion Flow Calorimetry (PCFC) technique show that the heat release capacity of these crosslinked polymers drastically decreases with increasing HMTA weight percent (Table 1). In the copolymer crosslinked with 20 % of HMTA, the heat release capacity drops to 90 J/g-K, which is very promising and improved over the commercially available flame-retardant polymers such as Kevlar (292 J/g-K) (*7*) and PEEK (180 J/g-K) (*7*). However, the char yield and total heat release remained similar in all HMTA compositions.

$^1$H NMR spectral studies on all the copolyimides synthesized non-enzymatically revealed that they form polyimides with contamination of polyamic acid product (*6*). The degradation temperatures at 20 % weight loss from TGA and heat release capacity, total heat release and char yields from PCFC measurements of siloxane copolyimides, **5** – **9** are provided in Table 2.

As can be seen from the table, the degradation temperatures of copolyimides are found to be higher, ranging from 450 – 480 °C compared to polyamides (~400°C) (*4*). The copolyimides show the heat release capacities in the order of **5**<**8**<**7**<**6b**<**9**<**6a**. It is interesting to note that **5** has the lowest heat release capacity despite its lowest aromatic content among all the linkers, which suggests that, in these polymers, the degradation mechanism and siloxane content play crucial roles rather than the aromatic content. **8** was found to have the highest char yield, which could be attributed to its likely formation of graphite like char during degradation due to its fused aromatic structural feature. It is clearly seen that extended aromatic linker, **9** did not improve the heat release capacity. Total heat release is lower in case of **5**, **7** and **8** compared other polyimides which is consistent with their heat release capacities. Figure 2 shows the TGA curve of the copolyimide, **5**. It is apparent from the curve that the weight loss transition at approximately 200 °C could be due to the conversion of polyamic acid into the polyimide structure.

Downloaded by COLUMBIA UNIV on June 25, 2012 | http://pubs.acs.org
Publication Date (Web): November 9, 2010 | doi: 10.1021/bk-2010-1051.ch013

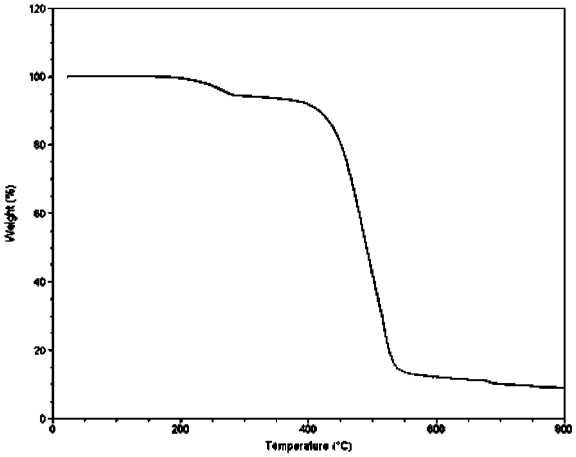

*Figure 2. Thermogravimetric analysis (TGA) curve of siloxane copolyimide,* ***5***

**Table 2. Degradation temperatures at 20 % weight loss ($T_{deg}$) from TGA measurements in air atmosphere and heat release capacity, total heat release and char yields from PCFC measurements of siloxane copolymers 5 – 9. 6a, 6b are enzymatic and non-enzymatic products, respectively**

| *Polymer* | *$T_{deg.}$ /Air (20% weight loss)* | *HR capacity ($Jg^{-1}K^{-1}$)* | *Total HR ($kJg^{-1}$)* | *Char yield (%)* |
|---|---|---|---|---|
| **5** | 450 | 310.3 | 13.3 | 4.0 |
| **6**a | 472 | 450.8 | 24.4 | 6.7 |
| **6**b | 480 | 418.4 | 22.4 | 7.9 |
| **7** | 414 | 363.4 | 11.4 | - |
| **8** | 432 | 324.1 | 13.6 | 12.4 |
| **9** | 430 | 425.5 | 21.4 | 10.9 |

Previously reported GCMS analysis (*4*) of pyrolyzed samples of siloxane copolyamides (*eg.* **3**) revealed the formation of cyclic siloxane compounds, such as $[SiO(CH_3)_2]_m$ (where $m = 5 – 12$). These results suggested that in our siloxane copolymers, dimethyl siloxane groups react with each other to form non-toxic cyclic compounds, which is an added advantage.

## Conclusions

Polysiloxane copolymers are found to be an interesting class of environmentally safe, non-halogenated, flame-retardant materials with high thermal stability and promising flame-retardant properties. The crosslinking of one of the copolyamides, **3,** improved the flammability properties tremendously by lowering the heat release capacity. The simple and economical synthesis without the use of enzymes makes polyimides economically more attractive FR materials over other copolymers. The study revealed that the aromatic content in the linker has a minimal role in improving the heat relase capacities in polyimides. The fused aromatic structures in linkers may be advantageous in lowering the heat release capacity in these polymers. The real advantage of any of the copolyamides/esters and some of the copolyimides compared to other FR polymers is that these materials can be solution-processed onto any substrate, which could make them not only environmentally safe but potentially cost-effective as well.

Downloaded by COLUMBIA UNIV on June 25, 2012 | http://pubs.acs.org
Publication Date (Web): November 9, 2010 | doi: 10.1021/bk-2010-1051.ch013

## Acknowledgments

We thank the Environmental Quality Basic Research (EQBR) program, US Army Natick Soldier RDEC for financial support, and Ravi Mosurkal thanks the National Research Council for a Senior Research Associateship award. Research at the University of Massachusetts Amherst was supported by Cluster F of CUMIRP, the Center for UMass/Industry Research on Polymers (Boeing; Federal Aviation Administration; General Electric Co.; Johns Manville; Multina, Inc.; National Institute of Standards and Technology, BFRL; Solvay; Advanced Polymers; and the US Army).

## References

1. Schmid, A.; Dordick, J. S.; Hauer, B.; Kieners, A.; Wubbolts, M.; Witholt, B. *Nature* **2001**, *409*, 258.
2. (a) Kobayashi, S.; Uyama, H.; Kimura, S. *Chem. Rev.* **2001**, *101*, 3793. (b) Gross, R. A.; Kumar, A.; Karla, B. *Chem. Rev.* **2001**, *101*, 2097.
3. Watterson, A. C.; Parmar, V. S.; Kumar, R.; Sharma, S. K.; Shakil, N. A.; Tyagi, R.; Sharma, A. K.; Samuelson, L. A.; Kumar, J.; Nicolosi, R.; Shea, T. *Pure Appl. Chem.* **2005**, *77*, 201.
4. Kumar, R.; Tyagi, R.; Parmar, V. S.; Samuelson, L. A.; Kumar, J.; Schoemann, A.; Westmoreland, P. R.; Watterson, A. C. *Adv. Mater.* **2004**, *16*, 1515.
5. Mosurkal, R.; Tucci, V.; Samuelson, L. A.; Bruno, F.; Westmoreland, P. R.; Kumar, J.; Watterson, A. C. *Polym. Prepr. (Am. Chem. Soc., Div. Polym. Chem.)* **2006**, *47*, 1110.
6. Mosurkal, R.; Samuelson, L. A.; Parmar, V. S.; Kumar, J.; Watterson, A. C. *Macromolecules*, submitted.
7. Richard, E. L.; Richard, N. W. *J. Anal. Appl. Pyrolysis* **2004**, *71*, 27.
8. (a) Stevens, M. P. *Polymer Chemistry: An Introduction*, 3rd ed.; Oxford University Press: Oxford, 1999; p 447. (b) Ogura, T.; Ueda, M. *Macromolecules* **2007**, *40*, 3527.
9. Zhang, X.; Looney, M. G.; Solomon, D. H.; Wittaker, A. K. *Polymer* **1997**, *38*, 5835.

Downloaded by PENNSYLVANIA STATE UNIV on June 24, 2012 | http://pubs.acs.org
Publication Date (Web): November 9, 2010 | doi: 10.1021/bk-2010-1051.ch014

## Chapter 14

# An Investigation into the Influence of Crosslinker Type and Solvent Composition on Physical Properties and Phase Transition Behavior of Poly(N-isopropylacrylamide) Hydrogels

**Candan Erbil,*[*] Ezgi Toz, Özgür Akdemir, and Nurseli Uyanık**

**Istanbul Technical University, Chemistry Department, 34469 Maslak, Istanbul, Turkey**
**[*]erbil@itu.edu.tr**

Poly(N-isopropylacrylamide) (PNIPAAm) hydrogels have been synthesized by free radical polymerization in 1,4-Dioxane using N,N′-methylenebisacrylamide (BIS) and α,ω-acryloxyorganofunctional poly(dimethylsiloxane) (VTPDMS) as crosslinkers. The disc samples equilibrated by swelling in water, water-methanol mixtures and methanol were examined by volumetric and stress-compression measurements to afford the values of swelling ratio ($V/V_o$), polymer-solvent interaction parameter ($\chi$), compression modulus (G) and effective crosslinking density ($\nu_e$).

It was observed that the incorporation of hydrophobic VTPDMS chains, instead of hydrophilic BIS molecules, as crosslinker into the structures of neutral NIPAAm hydrogels improved their mechanical strengths. The values of $\nu_e$, being greater than $\nu_t$ (theoretical crosslinking density) also indicated the presence of hydrophobic physical interactions, i.e., physical crosslinkings, between dimethyl siloxane groups in the PNIPAAm hydrogels crosslinked with VTPDMS. Further, the G-, $\chi$- and $\nu_e$-solvent composition curves of both NIPAAm/VTPDMS and NIPAAm/BIS hydrogels swollen to equilibrium in water/methanol mixtures (80/20, 50/50 and 20/80, in v/v %) at 23°C showed maxima corresponding to

In Advances in Silicones and Silicone-Modified Materials; Clarson, S., et al.;
ACS Symposium Series; American Chemical Society: Washington, DC, 2010.

0.20 and 0.50 of methanol volume fractions, respectively. It was assumed that the maxima on G, $\nu_e$ and $\chi$ versus solvent composition curves resulted from the competitions between interaction of methanol and water together versus their individual interactions with PNIPAAm/VTPDMS and PNIPAAm/BIS polymers.

## Introduction

Synthetic polymer hydrogels have been used extensively in the development of the smart drug delivery systems (*1*). The smart hydrogels show a phase transition accompanying drastic discontinuous or continuous volume change with variation of environment conditions such as temperature, pH, ions or aqueous - organic solvent compositions (*2–4*). Poly (N-isopropyl acrylamide) (PNIPAAm) hydrogel, which is one of the most widely studied examples of the hydrogel systems that undergo a temperature-controlled volume phase transition, is attracting interest in biomedical applications because it exhibits a well-defined lower critical solution temperature (LCST) in water around 32°C, which is close to the body temperature (*5*, *6*).

Pure NIPAAm hydrogels crosslinked by using hydrophilic tetrafunctional N,N′-methylene bisacrylamide (BIS) as crosslinker have low mechanical strength in the swollen state, i.e., below LCST (*7*, *8*). The combination of large swelling and high mechanical performance within the same gel structure is important for both industrial and biomechanical applications. The formation of nanocomposite gels, hydrophobically modified copolymers and double networks by incorporation of hydrophilic/hydrophobic inorganic filler or comonomer into the hydrogel structure can be given as the main examples of the methods which are used to improve the mechanical properties (*9–12*).

Using the hydrogel as drug delivery device and load it with hydrophilic or hydrophohic drug molecules, its volume change in low molecular weight solvent-water mixtures and the nature of the interactions between the network and solvent molecules should also be studied.

In this study, hydrogels composed of NIPAAm, BIS and vinyl terminated poly(dimethyl siloxane) (VTPDMS) (commercial product) as monomer, hydrophilic crosslinker and hydrophobic crosslinker, respectively, were prepared to investigate the effect of hydrophobic component, i.e., VTPDMS on the compression moduli of the samples attained equilibrium swollen state in water, methanol and water/methanol mixtures (80/20, 50/50 and 20/80 in v/v %) at 23°C and 37°C.

The most important parameters used to characterize the network structure of hydrogels are the polymer volume fraction in the swollen state ($\upsilon_{2s}$) and crosslinking density ($\nu_e$). These two parameters, which are related to one another, were determined through the use of equilibrium-swelling and uniaxial-compression experiments.

Downloaded by PENNSYLVANIA STATE UNIV on June 24, 2012 | http://pubs.acs.org
Publication Date (Web): November 9, 2010 | doi: 10.1021/bk-2010-1051.ch014

# Experimental

## Materials

N-isopropylacrylamide (NIPAAm); α,ω-acryloxyorganofunctional poly(dimethylsiloxane) (VTPDMS; Tegomer V-Si 2250 (n~20, 5<m<10), Goldschmidt AG) and N,N′-methylenebisacrylamide (BIS; Merck) were used as received. Azobis(isobutyronitrile) (AIBN; Merck) was recrystallized from chloroform. 1,4 Dioxane, methanol (Merck) and distilled-deionized water were used as solvents for polymerizations and swelling measurements.

Downloaded by PENNSYLVANIA STATE UNIV on June 24, 2012 | http://pubs.acs.org
Publication Date (Web): November 9, 2010 | doi: 10.1021/bk-2010-1051.ch014

## Synthesis and Characterization

The hydrogels made of neutral NIPAAm chains / hydrophilic tetrafunctional constituent, BIS and neutral NIPAAm chains / hydrophobic tetra functional macrocrosslinker, VTPDMS were synthesized by free radical solution polymerizations. Monomer (2.0 mol/L), BIS or VTPDMS ($1.25 \times 10^{-2}$ and $2.50 \times 10^{-2}$ mol / L) and AIBN ($5.8 \times 10^{-3}$ mol / L) were dissolved in 1,4-dioxane. The pregel solutions introduced into glass tubes of ~10 mm inner diameter were placed vertically in a large glass tube that was closed tightly with a rubber cap, and then filled oxygen-free nitrogen by using a syringe, and placed in a thermostat at 60°C for 72 hours. After the reaction periods needed to complete gelation processes, each test tube was broken. The cylindrical gels were cut in pieces of 10 mm height and immersed in methanol/water mixture (50/50, v/v %) and then distilled-deionized water for 1 week, to remove linear polymer chains and unreacted constituents.

Before the volume swelling ratio, $V/V_o$ and compression measurements, each of the purified gel samples were maintained in water, water/methanol mixtures and methanol at 23°C and 37°C to achieve swelling equilibria. Hounsfield H5K-S model tensile testing machine, settled a crosshead speed of 10 mm / min and a load capacity of 5N was used to perform uniaxial compression experiments on the each type of hydrogel samples. The effective crosslinking density, $\nu_e$ was calculated from the compression modulus (G), i.e., the slope of the linear portion of compression stress-strain curve, using the rubber elasticity theory (*13*, *14*). From the values of $\nu_e$ and $\upsilon_{2s}$ (polymer volume fraction of the hydrogels in the swollen-equilibrium state), the polymer-solvent interaction parameter, $\chi$ and average molecular weight between crosslinking points, $M_c$ were calculated using Flory-Rehner equilibrium swelling equation (*14–17*).

# Results and Discussion

An increase in the water absorption capacities of hydrogels is accompanied with a decrease in the mechanical properties. These properties can be modified by copolymerizing hydrophilic or hydrophobic monomers, varying the method of preparation or changing the concentration and type of crosslinking agent.

In the present study, it has been observed that the mechanical strength of neutral PNIPAAm hydrogels could be improved by the choice of hydrophobic crosslinker, instead of hydrophobic comonomer or inorganic filler. Scheme I shows the chemical structure of this commercial product, composed of soft and hydrophobic segments of dimethylsiloxane (n~20) and $–CH_2$ units (5<m<10).

PDMS-based elastomers have been widely used in variety dental and medical applications due to their good biocompability, high mechanical strength, transparency and excellent oxygen permeability (*18*, *19*). Further, PNIPAAm is a biocompatible and hydrophilic (but not biodegradable) polymer (*20*). It has been extensively studied on controlled drug release applications due to its LCST phenomenon. Because of these reasons, the hydrogels of acrylate-terminated PDMS and NIPAAm were formed to generate polymers improved both hydrophilicity of PDMS chains and mechanical strengths of conventional PNIPAAm networks.

Compression moduli of neutral NIPAAm hydrogels crosslinked with BIS and VTPDMS at 60°C and equilibrated in water, water/methanol mixtures and methanol at 23°C and 37°C were determined by means of Hounsfield H5K-S model tensile testing machine. The temperatures of the hydrogel disks of known dimensions were controlled by using an air-oven during the swelling equilibria and then, they were put into a double-walled glass cell at measuring temperature to maintain the equilibrium swelling (by circulating water through the double-walls of measuring cell by means of an external thermostated) just before the compression measurements. It was not observed any loss of water and changing in temperature just before and during the measurements because of the compression periods being nearly 1 min. Figures 1 and 2 show Load (N) vs. compression (mm) curves obtained from the uniaxial compression experiments for S1 equilibrated in water, water/methanol mixtures and methanol at 23°C and 37°C. Stress (Pa)-linear deformation factor, $-(\lambda - \lambda^{-2})$ plots in Figures 3 and 4 were drawn by using the data obtained from the linear portions of the curves in Figures 1 and 2.

Downloaded by PENNSYLVANIA STATE UNIV on June 24, 2012 | http://pubs.acs.org
Publication Date (Web): November 9, 2010 | doi: 10.1021/bk-2010-1051.ch014

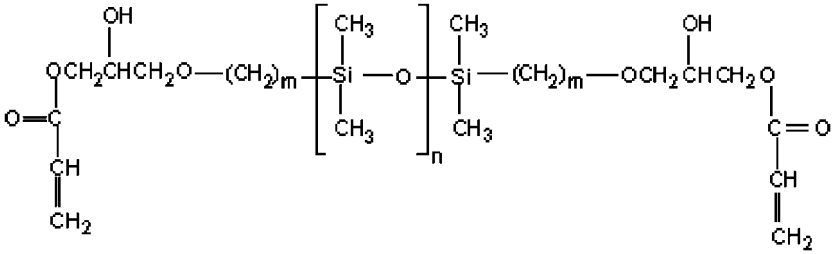

*Scheme I. Chemical structure of hydrophobic macrocrosslinker*

Downloaded by PENNSYLVANIA STATE UNIV on June 24, 2012 | http://pubs.acs.org
Publication Date (Web): November 9, 2010 | doi: 10.1021/bk-2010-1051.ch014

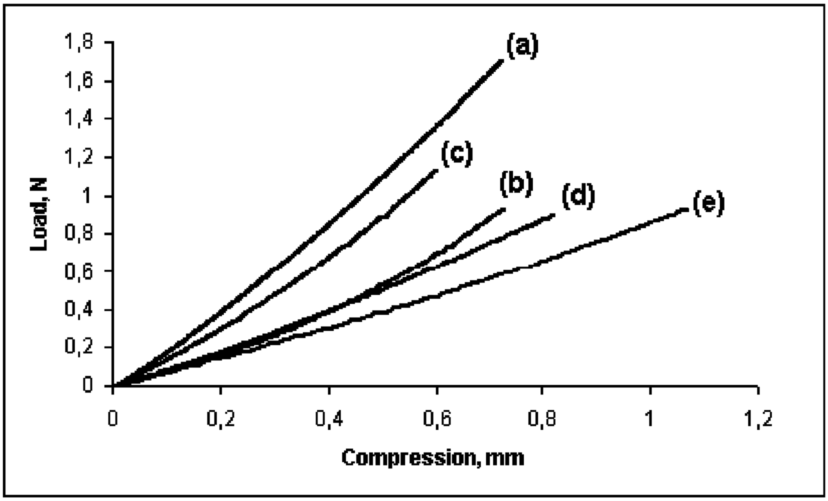

*Figure 1. Measured force, F (N) as a function of compression (mm) for S1 in water W (a), W/M-80/20 (b), W/M 50/50 (c), W/M 20/80 (d) and methanol M (e) at 23°C.*

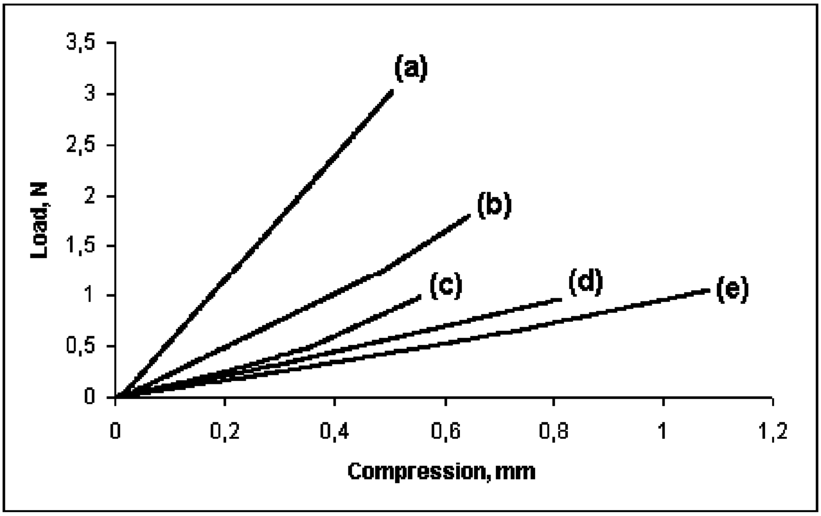

*Figure 2. Measured force, F (N) as a function of compression (mm) for S1 in water W (a), W/M-80/20 (b), W/M 50/50 (c), W/M 20/80 (d) and methanol M (e) at 37°C.*

Downloaded by PENNSYLVANIA STATE UNIV on June 24, 2012 | http://pubs.acs.org
Publication Date (Web): November 9, 2010 | doi: 10.1021/bk-2010-1051.ch014

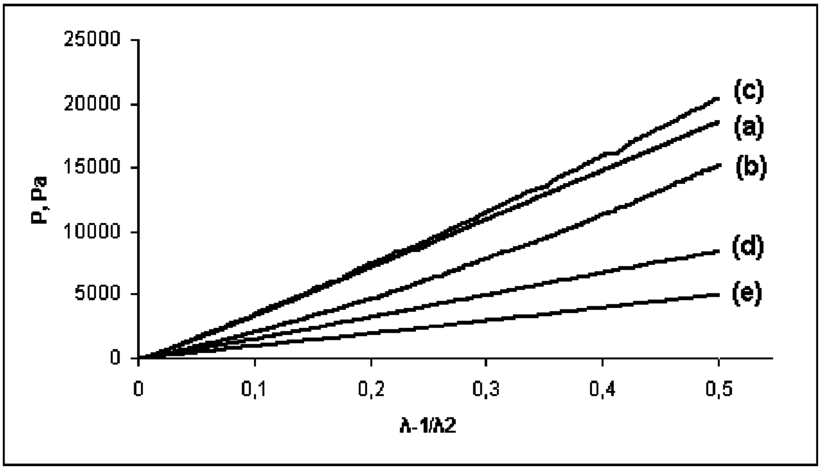

*Figure 3. Compression stress-strain curves (Pressure (Pa) vs. -(λ – $\lambda^{-2}$) ) for S1 in water W (a), W/M-80/20 (b), W/M 50/50 (c), W/M 20/80 (d) and methanol M (e) at 23°C.*

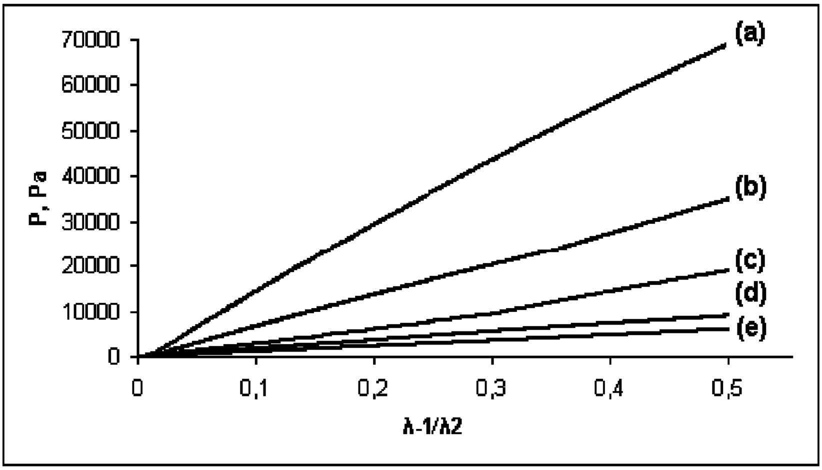

*Figure 4. Compression stress-strain curves (Pressure (Pa) vs. -(λ – $\lambda^{-2}$) ) for S1 in water W (a), W/M-80/20 (b), W/M 50/50 (c), W/M 20/80 (d) and methanol M (e) at 37°C.*

The slopes of these straight lines, i. e. compression moduli were used to compute the effective network concentration, $\nu_e$ from the equation 1

$$\nu_e = G / (RT\, \upsilon_{2s}^{1/3}\, \upsilon_{2r}^{2/3}) \qquad (1)$$

Here, $\upsilon_{2r}$ and $\upsilon_{2s}$ are the polymer volume fractions of the hydrogels in the tube and the swelling media, which are defined as the polymer in the relaxed state just after crosslinking and at swelling equilibrium state, respectively. Volumetric method was employed to study the swelling ratios of hydrogels.

Temperatures of the samples at 23°C and 37 °C were controlled by using an air-oven during the swelling equilibria. Diameter measurements of swollen and relaxed states (d and $d_o$, respectively) were used to calculate the volumetric compositions of the hydrogels. Assuming that the gels swell isotropically,

$$V / V_o = \upsilon_{2r} / \upsilon_{2s} = (d / d_o)^3 \qquad (2)$$

$\upsilon_{2r}$ was calculated as

$$\upsilon_{2r} = C_o (M_r / \rho_2) \qquad (3)$$

Here, $C_o$ is the initial monomer concentration, $\rho_2$ is the density of the dry polymer and $M_r$ is the molecular weight of repeat unit of the hydrogel. The densities of dried PNIPAAm hydrogels were taken as 1.10 x $10^3$ kg /$m^3$. Then, $\upsilon_{2s}$ were calculated from volumetric measurements using the following relation,

$$\upsilon_{2s} = \upsilon_{2r} (d_o / d)^3 \qquad (4)$$

In order to understand the effect of type and concentration of crosslinker, temperature and solvent composition on the mechanical performance and swelling properties of neutral NIPAAm hydrogels, the network parameters $\upsilon_{2r}$, $\upsilon_{2s}$, $\nu_e$, $\chi$ and $M_c$, which were used to describe the polymer-solvent systems were calculated from the following equations. Equation (5) is valid for neutral networks in the highly swollen state.

$$\chi = - [\ln (1 - \upsilon_{2s)} + \upsilon_{2s} + \nu_e V_1 \upsilon_{2r} \{(\upsilon_{2s} / \upsilon_{2r})^{1/3} - (\upsilon_{2s} / \upsilon_{2r}) (1/2)\}] / \upsilon_{2s}^2 \qquad (5)$$

$$M_c = \rho_2 / \nu_e \qquad (6)$$

Here, $V_1$ is the molar volume of solvent or solvent mixtures and, $M_c$ is the molecular weight between crosslinks, which is a parameter closely related to effective crosslinking density. The molar volumes of water, water/methanol (W/M) mixtures and methanol at 23°C and 37°C were calculated using density-temperature relations in the range of 20°C – 40°C (*21*, *22*).

Tables I and II and, Figures 12345678 summarize the synthesis conditions, swelling and mechanical properties of neutral NIPAAm hydrogels crosslinked with hydrophilic and hydrophobic tetrafunctional monomer (BIS) and macromer (VTPDMS), respectively.

Downloaded by PENNSYLVANIA STATE UNIV on June 24, 2012 | http://pubs.acs.org
Publication Date (Web): November 9, 2010 | doi: 10.1021/bk-2010-1051.ch014

**Table I. Polymerization conditions, compression moduli G, polymer-water interaction parameter $\chi$, average molecular weights between crosslinking points $M_c$ and effective crosslinking density $\nu_e$ at swelling equilibria in water at 23°C for neutral PNIPAAm hydrogels prepared in the presence of two different crosslinker[a]**

| *Sample no.* | *BIS (mol/l)* | *VTPDMS (mol/l)* | *G (Pa)* | *$\nu_e$ (mol/m$^3$)* | *$\chi$* | *$M_c$ (kg/mol)* |
|---|---|---|---|---|---|---|
| S1 | - | $1.25 \times 10^{-2}$ | 37780 | 71.2 | 0.58 | 15.4 |
| S2 | $2.50 \times 10^{-2}$ | - | 2560 | 9.9 | 0.50 | 111.0 |
| S3 | $2.50 \times 10^{-2}$ | $1.25 \times 10^{-2}$ | 20800 | 39.2 | 0.57 | 28.1 |
| S4 | $1.25 \times 10^{-2}$ | $2.50 \times 10^{-2}$ | 106670 | 477.4 | 0.60 | 2.3 |

[a] [NIPAAm]= 2.0 mol / l ; [AIBN] = $5.8 \times 10^{-3}$ mol/l ; t = 3 days ; T = 60°C $V_1 = 18.44 \times 10^{-6}$ m$^3$/mol.

The results presented are in accordance with our previous findings for similar kind of gels but have different crosslinker, comonomer and solvent compositions during the synthesis and swelling conditions, respectively (*23*). In the current study, it was observed that the mechanical strength of the Sample S1 (i.e., the NIPAAm hydrogel crosslinked with VTPDMS) in the equilibrium-swollen state was greater than those of the ones crosslinked with either BIS (i.e., the Sample S2) or VTPDMS/BIS mixture, containing the same amounts of VTPDMS and BIS with S1 and S2 (i.e., the Sample S3). Further, the increases in $\chi$ with increasing in VTPDMS content, together with G (Samples S1, S3 and S4 in Table I) indicated that there was a direct relation between the hydrophobic/hydrophilic crosslinker ratio (or hydrophobic crosslinker concentration) and thermodynamic interaction in neutral NIPAAm hydrogels.

In our previous study, we have reported that in the case of NIPAAm hydrogels containing VTPDMS, hydrophobic interactions between dimethylsiloxane molecules incorporated covalently into the network structures (Scheme I) were responsible for their high compression moduli, $\chi$ and $\nu_e$ values (*23*). In another word, they resulted from the contribution of physical crosslinks to chemical crosslinks. The results summarized in Table I also supported this interpretation, because the mechanical responses and polymer-water interaction parameters of the hydrogels composed of temperature-sensitive NIPAAm molecules and BIS (S1) or the lower ratio of VTPDMS/BIS mixture (S3) were lower than that of the one synthesized with the higher value of VTPDMS/BIS ratio (S4).

Table II summarizes the values of G and $M_c$, defining the mechanical and network properties of neutral NIPAAm hydrogels crosslinked with VTPDMS (S1), BIS (S2) and VTPDMS/BIS mixture (S3) in water, water/methanol mixtures and methanol at 23°C and 37°C.

Downloaded by PENNSYLVANIA STATE UNIV on June 24, 2012 | http://pubs.acs.org
Publication Date (Web): November 9, 2010 | doi: 10.1021/bk-2010-1051.ch014

Downloaded by PENNSYLVANIA STATE UNIV on June 24, 2012 | http://pubs.acs.org
Publication Date (Web): November 9, 2010 | doi: 10.1021/bk-2010-1051.ch014

**Table II. Physical parameters at swelling equilibria in water, water/methanol mixtures and methanol at 23°C and 37°C for neutral PNIPAAm hydrogels prepared in the presence of VTPDMS and BIS**

| *Sample/ Solvent Code* | $G^a$ *(Pa)* | $M_c{}^a$ *(kg/mol)* | $G^b$ *(Pa)* | $M_c{}^b$ *(kg/mol)* | $\nu_e$ $^b$ *(mol/m³)* | $\chi$ $^b$ |
|---|---|---|---|---|---|---|
| S1/W100 | 37780 | 15.4 | 141840 | 5.9 | 184.6 | 0.95 |
| S1/W80 | 46000 | 19.7 | 72750 | 14.5 | 75.7 | 1.07 |
| S1/W50 | 39640 | 19.5 | 37980 | 23.4 | 46.9 | 0.85 |
| S1/W20 | 16580 | 30.0 | 18020 | 31.7 | 34.7 | 0.56 |
| S1/W0 | 10300 | 42.6 | 10570 | 60.3 | 18.2 | 0.54 |
| S2/W100 | 2560 | 111.0 | 28890 | 17.7 | 62.3 | 0.57 |
| S2/W80 | 3760 | 78.1 | 20850 | 30.2 | 36.4 | 0.55 |
| S2/W50 | 7480 | 64.3 | 17660 | 44.2 | 24.9 | 0.58 |
| S2/W20 | 5090 | 84.4 | 2560 | 374.0 | 2.9 | 0.55 |
| S2/W0 | 2170 | 143.0 | 3290 | 271.0 | 4.1 | 0.54 |
| S3/W100 | 20800 | 28.1 | 160880 | 5.8 | 190.8 | 0.95 |
| S3/W80 | 57950 | 12.0 | 119320 | 7.9 | 139.2 | 0.94 |
| S3/W50 | 43590 | 15.5 | 52800 | 17.2 | 64.1 | 0.82 |
| S3/W20 | 17030 | 27.5 | 21460 | 23.7 | 47.3 | 0.55 |
| S3/W0 | 11700 | 36.6 | 13660 | 35.1 | 31.3 | 0.52 |

[a] G and $M_c$ values for 23°C. [b] G, $M_c$, $\chi$ and $\nu_e$ values for 37°C.

In order to maintain three-dimensional structures, the polymer chains of hydrogels are crosslinked either chemically or physically. In the present system, two types of chemical crosslinking agent were used: hydrophilic tetrafunctional monomer, BIS and hydrophobic tetrafunctional macromer, VTPDMS. Since these crosslinking molecules are difunctional, they create two chemical crosslinks per molecule. Thus, their theoretical crosslinking densities ($\nu_t$) are given by $\nu_t = 2c_o$, where $c_o$ is the initial concentration of the crosslinking agent. The initial concentrations of VTPDMS, BIS and VTPDMS/BIS mixtures in the Samples S1-S4 were taken as $1.25 \times 10^{-2}$ mol/L, $2.50 \times 10^{-2}$ mol/L and $3.75 \times 10^{-2}$ mol/L, and their $\nu_t$ values were calculated as 25 mol/m³, 50 mol/m³ and 75 mol/m³, respectively.

Downloaded by PENNSYLVANIA STATE UNIV on June 24, 2012 | http://pubs.acs.org
Publication Date (Web): November 9, 2010 | doi: 10.1021/bk-2010-1051.ch014

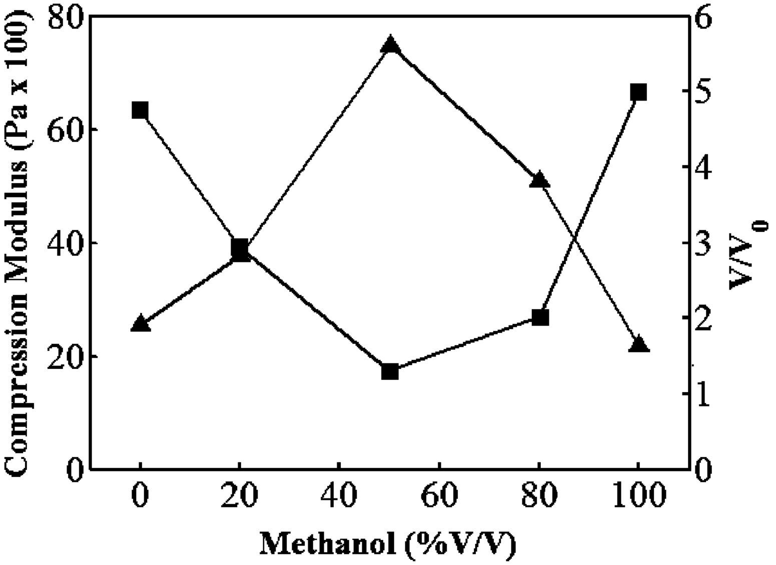

*Figure 5. Variation of volume swelling ratio (■) and compression modulus (▲) with solvent composition for NIPAAm/BIS hydrogel (S2) at 23°C.*

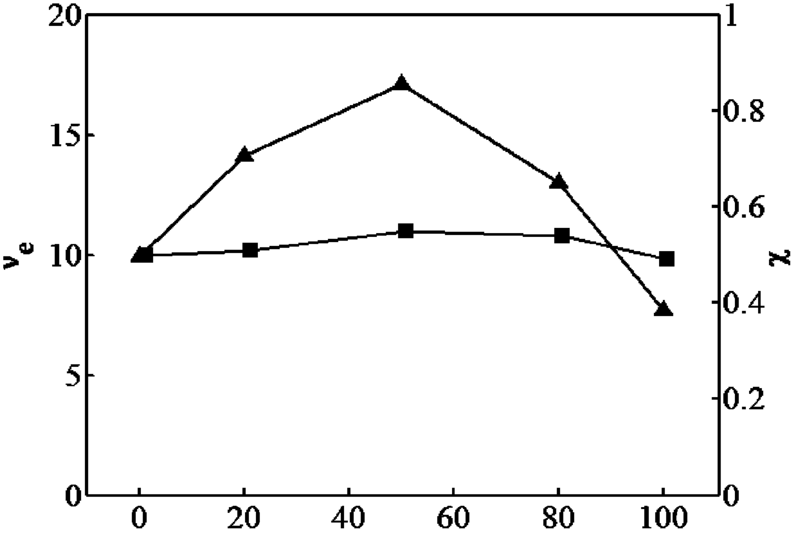

*Figure 6. Variation of χ (■) and $v_e$ (▲) with solvent composition for NIPAAm/BIS hydrogel (S2) at 23°C.*

Downloaded by PENNSYLVANIA STATE UNIV on June 24, 2012 | http://pubs.acs.org
Publication Date (Web): November 9, 2010 | doi: 10.1021/bk-2010-1051.ch014

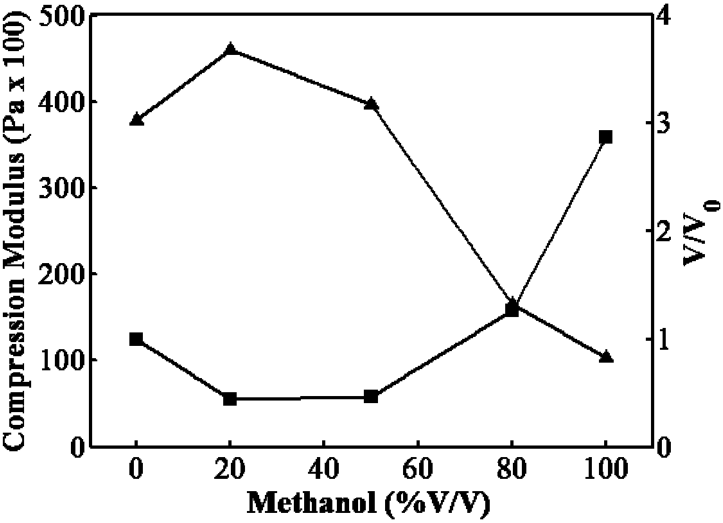

*Figure 7. Variation of volume volume swelling ratio (■) and compression modulus with solvent composition for NIPAAm/VTPDMS hydrogel (S1) at 23°C.*

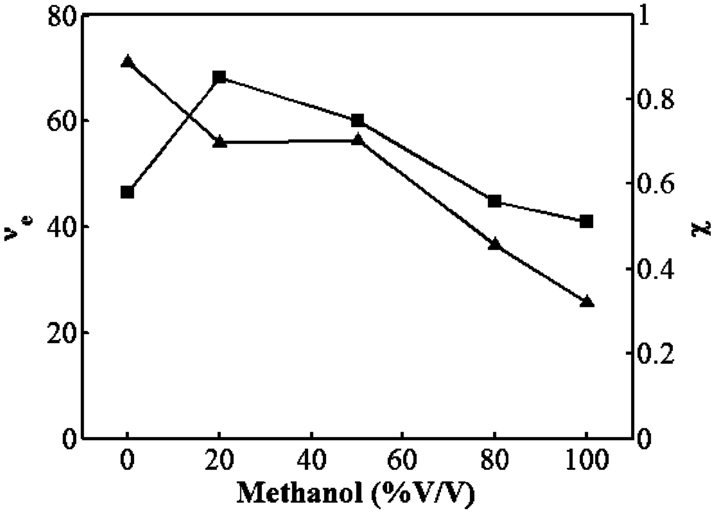

*Figure 8. Variation of χ (■) and $v_e$ (▲) with solvent composition for NIPAAm/ VTPDMS hydrogel (S1) at 23°C.*

In general, effective crosslinking density $\nu_e$, calculated from compression moduli of hydrogels varies with theoretical crosslinking density, $\nu_t$. But it was assumed that in the cases of S1, S3 and S4, the secondary forces also have an important effect on network parameters and, they are responsible from the high values of both $\nu_e$ and G. Their values in Tables I and II indicate the effect of hydrophobic physical interactions, i.e., physical crosslinkings, between dimethylsiloxane groups in the NIPAAm hydrogels crosslinked with VTPDMS.

Downloaded by PENNSYLVANIA STATE UNIV on June 24, 2012 | http://pubs.acs.org
Publication Date (Web): November 9, 2010 | doi: 10.1021/bk-2010-1051.ch014

In another words, the decreases in the values of $M_c$ in the presence of VTPDMS support the non-covalent inter-molecular interactions between the chains.

The neutral PNIPAAm hydrogels shrink and their water uptake decrease as the temperature increases above the LCST ($T_{swelling}$ > 32°C). This type of swelling is known as inverse temperature-dependence (*24*, *25*). At lower temperatures ($T_{swelling}$ < LCST ), water molecules forms hydrogen bonds with polar amide groups on the backbone and organize around hydrophobic isopropyl groups as iceberg water. As the temperature increases, hydrophobic interactions among hydrophobic segments become strengthened, while hydrogen bonding becomes weaker. The net result is shrinking of the hydrogels due to hydrophobic intermolecular interactions between polymer chains. In general, as the polymer chain contains more hydrophobic constitutent, LCSTs and swelling degrees of hydrogels decrease while their mechanical strengths increase. This means that the physical properties of inverse temperature-dependence hydrogels can be controlled by adjusting the ratio of hydrophilic and hydrophobic segments of polymer and solvent composition along with swelling temperature (*26–29*).

The influence of VTPDMS content reflects the contribution of secondary forces to covalent bonding between the PNIPAAm chains while the temperature effect results from a balance between hydrophobic interaction and breakage of hydrophilic hydrogen bonding. At 37°C, being a higher temperature than the LCSTs of neutral NIPAAm hydrogels, hydrogen bonds around hydrophilic groups are broken by thermal effect and thus, the volume swelling ratios and average molecular weight between crosslinking points of the NIPAAm chains containing both BIS and VTPDMS along with BIS and VTPDMS alone as crosslinker decrease, and consequently, their physical parameters such as G, $\nu_e$ and $\chi$ strongly increase (Table II).

For the samples S1-S3 swollen to equilibrium in water/methanol mixtures (80/20, 50/50 and 20/80, in v/v %) at 23°C**,** the effect of methanol on network parameters also was an increase in the values of G, $\nu_e$ and $\chi$ in comparison to the situations in pure methanol and water. Both NIPAAm/BIS (S2) and NIPAAm/VTPDMS (S1) hydrogels showed reentrant shrinking/swelling behavior in methanol-water mixtures when more of either solvent was added.

Methanol is a good solvent for PNIPAAm over all temperature range below its boiling point while in water, PNIPAAm solutions exhibit phase separation on heating at about 32°C. The effect of the composition of methanol-water mixtures on the swelling/shrinking behaviors and network parameters of PNIPAAm hydrogels may be visualized by analyzing the curves in Figures 5678. For the NIPAAm/VTPDMS and NIPAAm/BIS hydrogels in the solutions containing methanol of 20 % and 50 % v/v, respectively, the gels undergo a volume collapse and compression moduli increase. This means that, for the methanol volume fractions lower than 0.20 and 0.50, PNIPAAm-water interactions are disturbed by the presence of methanol molecules. After these compositions, the gels reswell continuously while the values of G and $\chi$ parameters decrease. In the solutions of higher methanol content than 20% and 50% (in v/v) containing the NIPAAm/VTPDMS and NIPAAm/BIS hydrogels, respectively, PNIPAAm-methanol interactions are stronger than PNIPAAm-water and water-methanol interactions. In another word, the maxima on G, $\nu_e$ and $\chi$

versus solvent composition curves at 23°C arise from the competitions between interaction of methanol and water together versus their individual interactions with NIPAAm/VTPDMS and NIPAAm/BIS polymers.

Hydrogels based on NIPAAm and its copolymers have been used in order to develop reversible temperature-controlled drug release systems. The main factors that determine the drug release from hydrogel systems are the network density, molecular structures and amounts of the loaded drugs. NIPAAm/VTPDMS hydrogels synthesized in the current study can be loaded with both hydrophilic and hydrophobic drug molecules because of hydrophobically modified temperature-sensitive structures, volume changes and reentrant phase transitions (and so the absorption capacities) in water, methanol and water-methanol mixtures at 23° C and 37°C.

Downloaded by PENNSYLVANIA STATE UNIV on June 24, 2012 | http://pubs.acs.org
Publication Date (Web): November 9, 2010 | doi: 10.1021/bk-2010-1051.ch014

## Conclusions

*Chemical crosslinking by both VTPDMS and VTPDMS/BIS mixtures in the synthesis of PNIPAAm hydrogels is mainly efficient.

*In the case of the hydrophobic crosslinker, unusual increases in the values of compression modulus and effective crosslinking density have been discussed on the basis of physical crosslinking resulting from the hydrophobic interactions between dimethyl siloxane groups.

*The effects of crosslinker-type and the composition of swelling medium on the swellability, phase transitions and mechanical strength, polymer-medium interaction parameter and effective crosslink density of the hydrogels at 23°C and 37°C have been discussed.

*As to the presented results above, these mechanically-strengthened PNIPAAm hydrogels that exhibit reentrant phase transition in aqueous-solvent mixtures can be suggested as drug delivery devices for both hydrophobic and hydrophilic molecules.

## Acknowledgments

The authors wish to thank Goldschmidt AG for supplying Tegomer VSi 2250 used.

## References

1. Qiu, Y.; Park, K. *Adv. Drug Delivery Rev.* **2001**, *53*, 321.
2. Park, K.; Park, H. Smart Hydrogels. In *Concise Polymeric Materials Encyclopedia*; Salamone, J. C., Ed.; CRC Press: Boca Raton, FL, 1999; pp 1476−1478.
3. Gupta, P.; Vermani, K.; Garg, S. *Drug Discovery Today* **2002**, *10*, 569.
4. Kopecek, J.; Yang, J. *Polym. Int.* **2007**, *56*, 1078.
5. Fujishige, S.; Kubato, K.; Ando, I. *J. Phys. Chem.* **1989**, *93*, 3311.
6. Tirrell, D. A.; Schild, H. G. *J. Phys. Chem.* **1990**, *94*, 4352.
7. Huglin, M. B.; Liu, Y.; Velada, J. L. *Polymer* **1997**, *38*, 5785.

8. Xue, W.; Champ, S.; Huglin, M. P. *Polymer* **2001**, *42*, 3665.
9. Lowe, T. L.; Benhaddou, M.; Tenhu, H. *Macromol. Chem. Phys.* **1999**, *200*, 51.
10. Zhang, J.; Peppas, N. A. *J. Appl. Polym. Sci.* **2001**, *82*, 1077.
11. Ma, J.; Xu, Y.; Zhang, Q.; Zha, L.; Liang, B. *Colloid Polym. Sci.* **2007**, *285*, 1581.
12. Nie, J.; Du, B.; Oppermann, W. *Macromolecules* **2005**, *38*, 5729.
13. Gutowska, A.; Bae, Y. H.; Jacobs, H.; Feijen, J.; Kim, S. W. *Macromolecules* **1994**, *27*, 4167.
14. Muniz, E. C.; Geuskens, G. *Macromolecules* **2001**, *34*, 4480.
15. Flory, J. *Principles of Polymer Chemistry*; Cornell University Press: New York, 1953.
16. Bahar, I.; Erbil, Y.; Baysal, B.; Erman, B. *Macromolecules* **1987**, *20*, 1353.
17. Sen, M.; Güven, O. *Polymer* **1998**, *39*, 1165.
18. Axisa, F.; Brosteaux, D.; De Leersnyder, E.; Bossuyt, F.; Gonzalez, M.; De Smet, N.; Schacht, E.; Rymarczyk-Machal, M.; Vanfleteren, J. *Proc. IEEE−EMBS* **2007**, 6592–6595.
19. Zhang, N.; Xie, J.; Guers, M.; Varadan, V. K. *Smart Mater. Struct.* **2004**, *13*, N1–N4.
20. Quan, C.; Wei, H.; Sun, Y.; Cheng, S.; Shen, K.; Gu, Z.; Zhang, X.; Zhuo, R. *J. Nanosci. Nanotechnol.* **2008**, *8*, 2377.
21. *International Critical Tables of Numerical Data, Physics, Chemistry and Technology*; Washburn, E. W., Ed.; McGraw Hill: New York, 1928; Vol. III.
22. Xue, W.; Huglin, M. B.; Jones, T. G. J. *Eur. Polym. J.* **2005**, *41*, 239.
23. Yıldız, Y.; Uyanik, N.; Erbil, C. *J. Macromol. Sci., Part A: Pure Appl. Chem.* **2006**, *43*, 1091.
24. Heskins, M.; Guillet, J. E. *J. Macromol. Sci., Chem.* **1968**, *2*, 1441.
25. Hirotsu, S. *J. Phys. Soc. Jpn.* **1987**, *56*, 233.
26. Dong, L. C.; Hoffman, A. S. *J. Controlled Release* **1990**, *13*, 21.
27. Winnik, F. M.; Ringsdorf, H.; Venzmer, J. *Macromolecules* **1990**, *23*, 2415.
28. Ishidao, T.; Akagi, M.; Sugimoto, H.; Iwai, Y.; Arai, Y. *Macromolecules* **1993**, *26*, 7361.
29. Katakai, R.; Yoshida, M.; Hasegawa, S.; Iijima, Y.; Yonezawa, N. *Macromolecules* **1996**, *29*, 1065.

Downloaded by PENNSYLVANIA STATE UNIV on June 24, 2012 | http://pubs.acs.org
Publication Date (Web): November 9, 2010 | doi: 10.1021/bk-2010-1051.ch014

Downloaded by PENNSYLVANIA STATE UNIV on June 25, 2012 | http://pubs.acs.org
Publication Date (Web): November 9, 2010 | doi: 10.1021/bk-2010-1051.ch015

## Chapter 15

# Ion Effects on Trisilanolphenyl-POSS as an Adhesion Promoter

**Sarah M. Huffer, Ufuk Karabiyik, Joshua R. Uzarski,
and Alan R. Esker***

**Department of Chemistry and the Macromolecules and Interfaces Institute,
Virginia Polytechnic Institute and State University, Blacksburg, VA 24061
*aesker@vt.edu**

Polyhedral oligomeric silsesquioxanes (POSS) have been an area of intense interest during the past two decades. Their unique properties may facilitate aerospace applications as space-survivable coatings and ablative insulation. Recent studies showed that trisilanol-POSS derivatives form self-assembled monolayers at the air/water (A/W) interface. One particular derivative, trisilanolphenyl-POSS (TPP), even forms Langmuir-Blodgett (LB) multilayer films by Y-type deposition on hydrophobic surfaces. In addition, TPP can complex metal ions, such as $Al^{3+}$. The purpose of this study was to improve adhesion between ceramics and metals and metals and polymers by preparing multilayer films with and without metal ions using TPP as an adhesion promoter. These multilayer systems were prepared by spincoating to make the layers of polystyrene, the LB-technique to create the TPP layers, and physical vapor deposition (PVD) to produce alumina layers. The resulting films were characterized for quality and stability using atomic force microscopy (AFM), optical microscopy (OM), X-ray photoelectron spectroscopy (XPS), and dewetting experiments. Results for alumina PVD show that films on TPP coated Si wafers are blistered and cracked in contrast to films on Si wafers coated with TPP plus aluminum ions. Similarly, polystyrene dewetting on TPP layers was suppressed when the TPP layers contained $Al^{3+}$.

In Advances in Silicones and Silicone-Modified Materials; Clarson, S., et al.;
ACS Symposium Series; American Chemical Society: Washington, DC, 2010.

Downloaded by PENNSYLVANIA STATE UNIV on June 25, 2012 | http://pubs.acs.org
Publication Date (Web): November 9, 2010 | doi: 10.1021/bk-2010-1051.ch015

# Introduction

Polyhedral oligomeric silsesquioxanes (POSS) have been studied with great interest for more than two decades (*1–3*). These organic/inorganic hybrid molecules have potential applications as low k dielectrics (*4*, *5*), high temperature nanocomposites (*6–8*), and space-survivable coatings (*9–12*). Additionally, trisilanol-POSS derivatives have been found to self-assemble as monolayers at the air/water (A/W) interface (*13–16*). Figure 1 shows a generic trisilanol-POSS. The OH groups attached to the cage are hydrophilic and can lie on the subphase while the R groups (phenyl for this study) are hydrophobic and take up a position away from the water surface. For the case of trisilanolphenyl-POSS (TPP), this amphiphilic character also allows the formation of Langmuir-Blodgett (LB) films. In general, amphiphilic materials can be studied at the A/W interface with techniques such as florescence microscopy (*17*, *18*) and Brewster angle microscopy (BAM) (*19*, *20*). Moreover, amphiphilic species that can be transferred to solid substrates avail themselves to high resolution techniques, such as atomic force microscopy (*21*, *22*) and X-ray diffraction (*23*, *24*). In this study, the ability to prepare and characterize thin POSS films will be used to study POSS-metal interactions.

Extensive research has focused on siloxane/metal complexes (*25–33*). Metallasilsesquioxanes have been used as representative surfaces for zeolites, clays, or silicates that are instrumental in catalysis. For example, titanasilsesquioxanes are active catalysts in the oxidation of olefins. The incompletely condensed silsesquioxanes, such as trisilanol-POSS, are the most useful in creating model surface silanol sites found in zeolites and amorphous silicas (*31*).

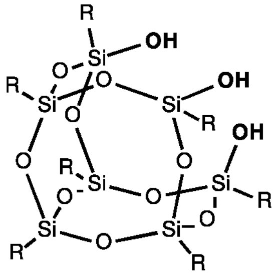

*Figure 1. Structure of a trisilanol-POSS derivative (R = phenyl for this study).*

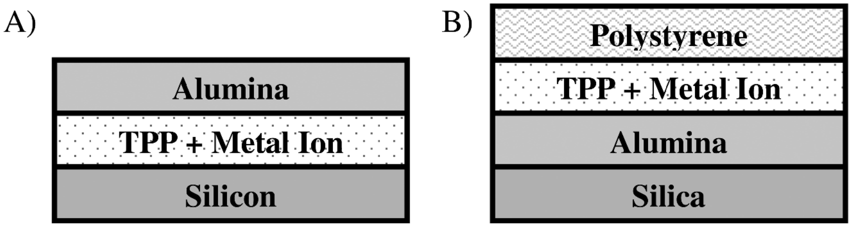

*Figure 2. Configurations for the multilayer films utilized in this study.*

The incorporation of metals in silsesquioxanes also improves the properties of the molecule by making them more rigid (*33*) as well as rendering them catalytically active for Diels-Alder reactions, polymerization, and epoxidation (*31*). Metallasilsesquioxanes also have electron withdrawing sites for bonding, and selective hydroxyl groups allow certain reagents to react at the surface, as occurs during alkene metathesis (*33*). In addition to catalytic activity, POSS-metal complexes in composites with polymers are also being studied for enhancing mechanical and thermomechanical properties. Chian, *et al.*, has shown that POSS fillers in an epoxy resin increase both the maximum shear strain and the maximal stress (*34*). Complexes of POSS with metals, such as aluminum, have been shown to increase the modulus of resins used in dental applications (*35*). Liu, *et al.*, also discovered that POSS enhanced thermomechanical properties, such as higher glass transition and initial thermal decomposition temperatures, in epoxy networks (*36*).

As already noted, POSS has long been studied for thermal protective systems (*9–12*). In this study, we will examine if the bonding properties of metallasilsesquioxanes are suitable for using these complexes as adhesion promotion layers in thermal protective systems. We recently discovered that metal ions, such as copper, silver, and iron, could be incorporated into LB-films of TPP. For the present study, the influence of $Al^{3+}$ ions incorporated into LB-films of TPP on the bonding of aluminum oxide layers prepared through physical vapor deposition (PVD) to a silicon wafer through a POSS film (schematically depicted in Figure 2A), and on the bonding of polystyrene to an alumina surface through a POSS layer (schematically depicted in Figure 2B) will be examined by x-ray photoelectron spectroscopy (XPS), atomic force microscopy (AFM), and optical microscopy.

Downloaded by PENNSYLVANIA STATE UNIV on June 25, 2012 | http://pubs.acs.org
Publication Date (Web): November 9, 2010 | doi: 10.1021/bk-2010-1051.ch015

## Experimental

### Materials

Trisilanolphenyl-POSS obtained from Hybrid Plastics, Inc., and used without further purification was dissolved in chloroform (0.05-0.5 $mg{\cdot}mL^{-1}$, HPLC grade) to prepare spreading solutions for LB-film deposition. Because of slow dissolution, the samples were prepared and stored for at least 24 h at room temperature in specially sealed vials to avoid the evaporation of chloroform. Aluminum nitrate was obtained from Sigma Aldrich, and 1 mM aluminum nitrate in Millipore water (18.2 MΩ, < 10 ppb organic) was used as a subphase for making the metal ion/TPP LB-films. Aluminum pellets (3-5 mesh) were also obtained from Sigma Aldrich with a purity of 99.999% for preparing alumina films through PVD. Polystyrene with a number average molar mass, $M_n = 1460$ g/mol, and a polydispersity index, $M_w/M_n = 1.06$, was used as received from Polymer Source, Inc. for dewetting studies. The polystyrene was dissolved in methyl ethyl ketone (MEK) as a 1% solution by weight. 4" (100) silicon wafers were obtained from Waferworld, Inc.

## Substrate Preparation

Silicon wafers were cut into roughly 25 x 40 mm$^2$ pieces. The wafer pieces were cleaned in a boiling mixture of 28% $NH_4OH$: 30% $H_2O_2$: Millipore water mixture in a 1:1:5 ratio by volume for 1.5 hours. Next, the wafers were placed in a concentrated $H_2SO_4$: 30% $H_2O_2$ mixture in a 7:3 ratio by volume. At this stage, the surface is a hydrophilic silica surface that can be used to create films depicted in Figure 2b after first rinsing the films with water and drying with nitrogen. In order to obtain the hydrophobic silicon surface depicted in Figure 2A, the hydrophilic silicon wafer was further treated with a buffered oxide etch (HF) solution (DOE and Ingalls, CMOS grade) for 5 minutes and exposed to 40% $NH_4F$ solution (DOE and Ingalls, CMOS grade). The wafers were subsequently rinsed with Millipore water and dried with nitrogen.

Downloaded by PENNSYLVANIA STATE UNIV on June 25, 2012 | http://pubs.acs.org
Publication Date (Web): November 9, 2010 | doi: 10.1021/bk-2010-1051.ch015

## Film Preparation

A standard KSV 2000 LB-trough (KSV Instruments, Inc.) was used to prepare LB-films of TPP and TPP with aluminum ions. The LB-trough is filled with Millipore water or a 1 mM aluminum nitrate solution at 22.5 °C. The barriers and suction are used to concentrate and remove surface active impurities from the trough until the surface tension of the subphase matches the literature value. Next, the TPP solution was spread between the barriers of the trough. After allowing ~20 min for the spreading solvent to evaporate, the TPP was compressed to a constant transfer surface pressure of 9.5 $mN{\cdot}m^{-1}$. The LB-films depicted in Figure 2a were created by dipping the hydrophobic silicon wafer through the TPP film at a rate of 10 $mm{\cdot}min^{-1}$, with waiting intervals of 15 s under the surface and 300 s above. Thirty layers of TPP were created by Y-type deposition with quantitative transfer ratios. For films depicted in Figure 2B, a single layer of TPP or TPP with aluminum ions was deposited on top of the hydrophilic alumina surface during the upstroke. Polystyrene was subsequently spincoated on top of the TPP monolayer using a solution of 1% PS by weight in MEK at a spinning rate of 4000 rpm. The PS film was annealed at 45 °C (glass transition temperature) for 2 hours to remove residual solvent. The PS films are ~ 28 nm (from ellipsometry).

## Physical Vapor Deposition (PVD)

Figure 3 shows a schematic of the apparatus that held the silicon wafers for PVD. The wafers were inverted to face the aluminum pellet, which sat in a boron nitride crucible (Kurt J. Lesker Co.) wrapped in a tungsten filament. A diffusion pump was used to reduce the pressure to 5x10$^{-6}$ mmHg. The filament connected to the power source heated the crucible and its contents. The temperature was increased slowly to around 1000 °C, and the aluminum was vaporized in this manner for 5 minutes to ensure that a layer of aluminum had been deposited. The aluminum rapidly oxidizes to form an aluminum oxide surface.

Downloaded by PENNSYLVANIA STATE UNIV on June 25, 2012 | http://pubs.acs.org
Publication Date (Web): November 9, 2010 | doi: 10.1021/bk-2010-1051.ch015

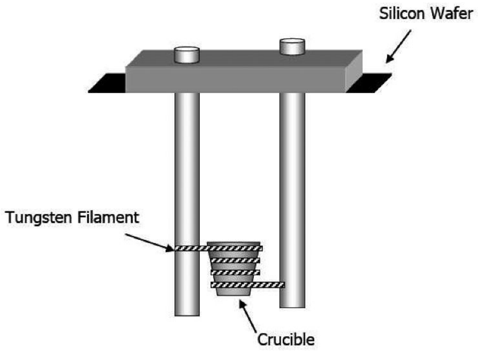

*Figure 3. Schematic depiction of the interior of the PVD apparatus*

### Dewetting Experiments

Dewetting was studied using an optical microscope operating in the reflection mode (Axiotech Vario 100 HD, Carl Zeiss Inc.). The films were annealed on a temperature-controlled heating stage (Linkam) from 25 to 200 °C at 1 $°C·min^{-1}$ and images of dewetting as a function of temperature were captured and viewed using Scion Image software.

### X-ray Photoelectorn Spectroscopy (XPS)

XPS measurements were made using a PHI 5400 (Perkin- Elmer) with Mg-Kα radiation at an angle of 45°.

### Atomic Force Microscopy (AFM)

AFM images were obtained in the Tapping Mode™ with a Digital Instruments Dimension 3000 Scope with a Nanoscope IIIa controller using etched single crystal silicon tips. 5 μm × 5 μm images were captured at a set-point ratio of ca. 0.6.

## Results

### Adhesion between Silica or Silicon and Alumina

Figure 4 shows a height and phase image for an aluminum layer placed onto a hydrophilic silica coated wafer by physical vapor deposition. X-ray photoelectron spectroscopy (XPS) confirmed that aluminum was present in high percentages on the silica surface with prominent aluminum 2s and 2p peaks. A tall oxygen peak was present at approximately 520 eV, indicating that the aluminum rapidly oxidizes to aluminum oxide. AFM images of the resulting film in Figure 4 reveal the root mean square (RMS) roughness is ~0.3 nm. Physical vapor deposition can also be used to place a uniform alumina layer onto a hydrophobic silicon wafer (HF etched) with properties comparable to the alumina layer on the silica surface.

Downloaded by PENNSYLVANIA STATE UNIV on June 25, 2012 | http://pubs.acs.org
Publication Date (Web): November 9, 2010 | doi: 10.1021/bk-2010-1051.ch015

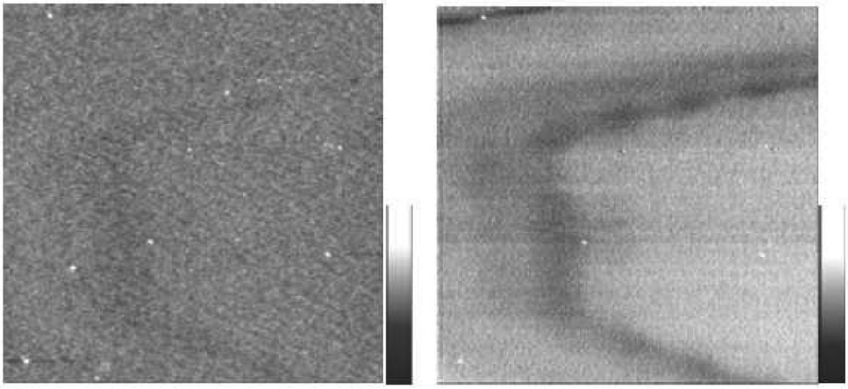

*Figure 4. Height (left) and phase (right) AFM images of the alumina coating obtained from PVD onto a hydrophilic silica surface. The 5 x 5 μm² images have z-scales of 5 nm and 5 degrees, respectively.*

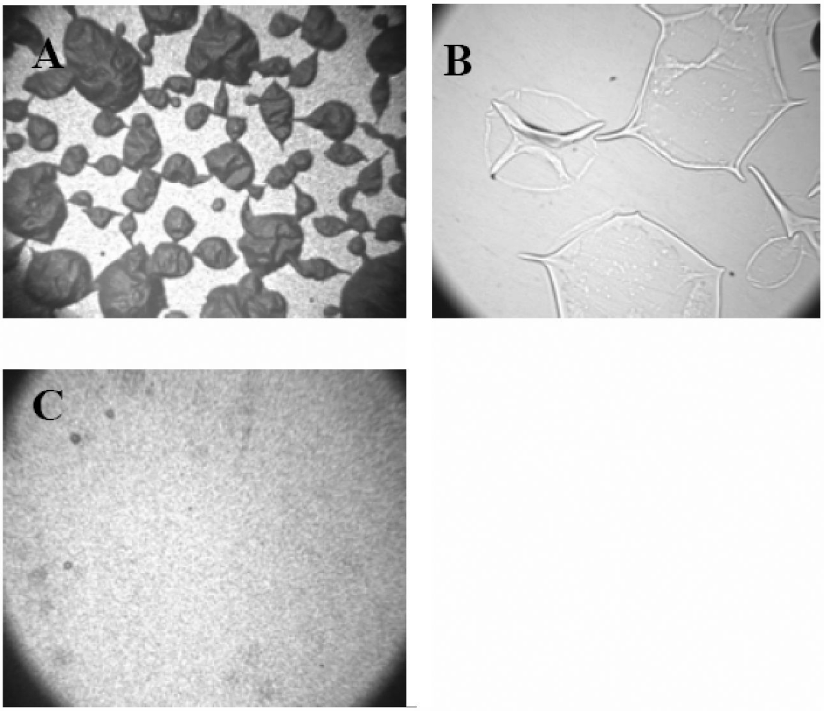

*Figure 5. Representative optical microscopy images of alumina coatings for films depicted in Figure 2A on A) 30 layers of TPP, B) 30 layers of TPP, and C) 30 layers of TPP with aluminum ions. All images are 2.28 x 3.04 mm².*

Downloaded by PENNSYLVANIA STATE UNIV on June 25, 2012 | http://pubs.acs.org
Publication Date (Web): November 9, 2010 | doi: 10.1021/bk-2010-1051.ch015

## Adhesion between TPP and Alumina

Having, established that a uniform alumina layer can be deposited onto silica and silicon surfaces, TPP was LB-deposited onto HF etched silicon with and without $Al^{3+}$. Subsequently, an alumina layer was added by physical vapor deposition to obtain the films depicted in Figure 2A. The TPP-coated silicon without aluminum ions developed surfaces with gross defects. Both blisters and cracks (Figure 5A and 5B) were observed. Independent of the type of defect observed, the portion of the hydrophobic Si wafer not coated with TPP exhibited a smooth alumina surface. This observation indicates that the blistered morphology was not an artifact of the deposition process, but rather a consequence of different interactions between TPP and alumina vs. alumina and the HF etched Si. In contrast, when $Al^{3+}$ was co-transferred with the TPP film, a homogeneous film with no visible blistering formed (Figure 5C) indicating that the presence of the aluminum ions inhibited dewetting of the aluminum/alumina surface during PVD and the subsequent oxidation of the film.

Figure 6 shows representative height and phase AFM images of the same alumina-coated sample in Figure 5B. The images were taken from smooth areas of the alumina film. The RMS roughness of the alumina film on 30 layers of TPP was 23 nm (vs. < 1 nm on silica). Figure 7 shows a representative height and phase image for the same film presented in Figure 5C (30 layers of TPP co-transferred with aluminum ions). The most striking difference is the three-fold increase in RMS roughness to ~69 nm when $Al^{3+}$ is present in the TPP layer. Hence, two factors could be contributing to the improvement of aluminum/alumina wetting on the TPP/aluminum ion layer. One possibility is a more favorable surface energy, while the other is enhanced wetting due to the increased roughness. Nonetheless, the rougher TPP/aluminum ion films clearly inhibit gross failures like blistering and cracking that occur without the aluminum ions.

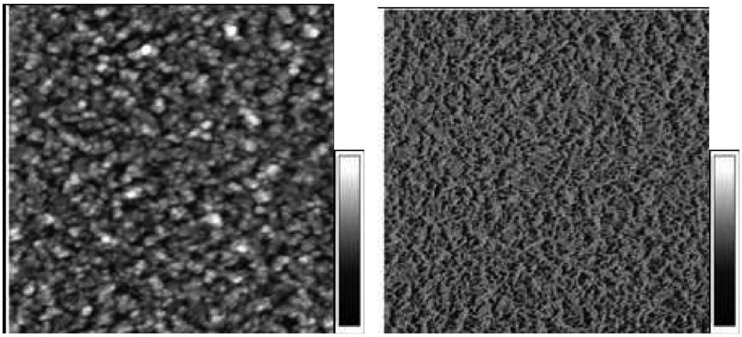

*Figure 6. 20 x 20 μm² height (left) and phase (right) AFM images of the alumina coating from PVD on 30 layers of TPP (film configuration depicted in Figure 2A). The images have z-scales of 200 nm and 50 degrees, respectively.*

In Advances in Silicones and Silicone-Modified Materials; Clarson, S., et al.;
ACS Symposium Series; American Chemical Society: Washington, DC, 2010.

Downloaded by PENNSYLVANIA STATE UNIV on June 25, 2012 | http://pubs.acs.org
Publication Date (Web): November 9, 2010 | doi: 10.1021/bk-2010-1051.ch015

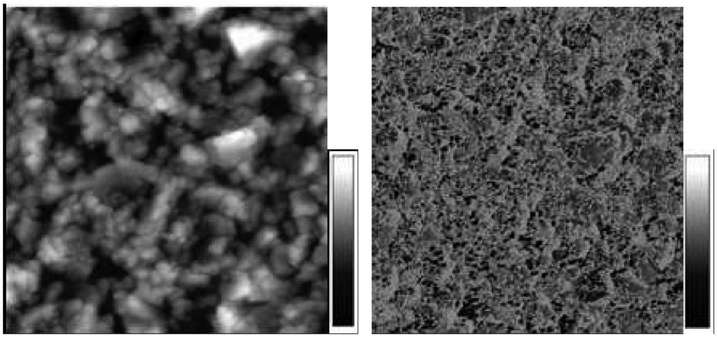

*Figure 7. 20 x 20 µm² height (left) and phase (right) AFM images of the alumina coating from PVD on 30 layers of TPP plus Al³⁺ (film configuration depicted in Figure 2A). The images have z-scales of 500 nm and 30 degrees, respectively.*

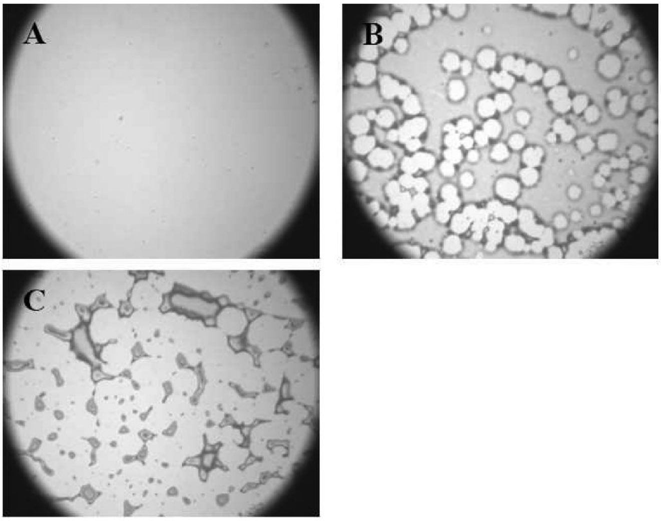

*Figure 8. 0.57 x 0.76 mm² optical microscopy images of polystyrene ($M_n$ = 1460 g/mol) on alumina coated with a single layer of TPP as a function of temperature: A) 110 °C, B) 140 °C, and C) 160 °C.*

## Adhesion between Polystyrene and Alumina with TPP Adhesion Promotion Layers

As discussed above, it was possible to coat silica with aluminum/alumina without an adhesion promotion layer. Since the resulting aluminum oxide layer is hydrophilic, only a net monolayer of TPP can be LB-deposited onto alumina as TPP only adds during an upstroke and is removed during a downstroke. This behavior is the same for TPP complexed with $Al^{3+}$. In a control experiment, XPS showed that TPP is not removed from the alumina surface by MEK during spincoating (solvent only). Hence, MEK provides an appropriate solvent for spincoating polystyrene directly onto the TPP treated surfaces to obtain the films schematically depicted in Figure 2B. Temperature ramp experiments from 25 °C to 200 °C at 1 $°C \cdot min^{-1}$ were conducted to study the dewetting properties and to test the adhesion of a polystyrene film to the modified alumina. Figure 8 shows the dewetting of the polystyrene layer on top of a single layer of TPP. At temperatures above 110 °C (Figure 8A), dewetting began around nucleation sites, such as impurities and defects. As the temperature increased from 110 °C (Figure 8A) to 140 °C (Figure 8B), the polystyrene film developed holes (white circles) around these nucleation sites. At 160 °C (Figure 8C), the polystyrene film was completely dewet, and droplets of polystyrene (irregular features on the lighter alumina background) remained on the surface. In contrast, Figure 9 shows how $Al^{3+}$ in the TPP monolayer suppresses dewetting of the polystyrene layer at the same temperatures shown in Figure 8. This suppression of dewetting relative to a TPP adhesion promotion layer may reflect subtle changes in surface energy attributed to the presence of $Al^{3+}$ ions. The exact role of the aluminum ions within the TPP film is not yet completely understood, and additional experiments are necessary to ultimately understand how the ions inhibit the dewetting process.

Downloaded by PENNSYLVANIA STATE UNIV on June 25, 2012 | http://pubs.acs.org
Publication Date (Web): November 9, 2010 | doi: 10.1021/bk-2010-1051.ch015

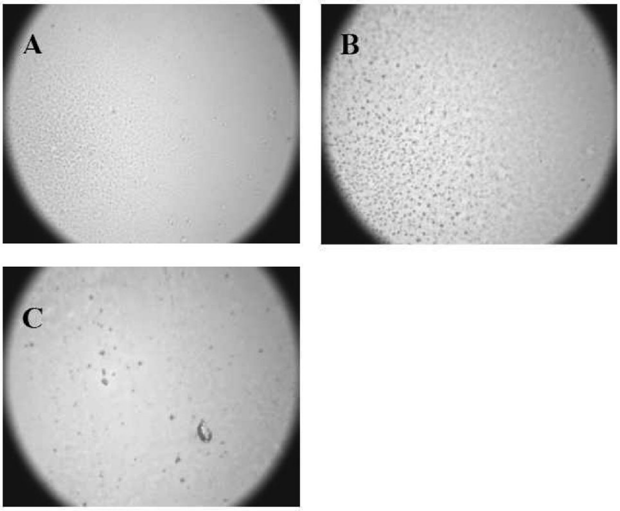

*Figure 9. 0.57 x 0.76 $mm^2$ optical microscopy images of polystyrene ($M_n$ = 1460 g/mol) on alumina coated with a single layer of TPP with $Al^{3+}$ as a function of temperature: A) 110 °C, B) 140 °C, and C) 160 °C.*

Downloaded by PENNSYLVANIA STATE UNIV on June 25, 2012 | http://pubs.acs.org
Publication Date (Web): November 9, 2010 | doi: 10.1021/bk-2010-1051.ch015

## Conclusions

Aluminum ions influenced the adhesion between TPP LB-films and alumina coatings prepared by PVD. AFM results for the configuration schematically depicted in Figure 2A revealed that the roughness of the alumina film increased with the addition of $Al^{3+}$ to the TPP layers. Nonetheless, OM images gave visual confirmation that the alumina layer on the TPP with $Al^{3+}$ film did not exhibit the cracking and blistering that occurred on TPP coatings without $Al^{3+}$. For the configuration schematically depicted in Figure 2B, the addition of $Al^{3+}$ suppressed dewetting of the polystyrene layer up to 200 °C. Without $Al^{3+}$, the polystyrene layer began to dewet at 110 °C and had completely dewet around 160 °C.

## Acknowledgments

The authors would like to thank the Virginia Space Grant Consortium (2005-06) and the National Science Foundation (CHE-0239633 and DMR-0244141) for funding, the POSS group at Edwards Air Force Base for materials, and Prof. John Morris at Virginia Tech for the use of his PVD apparatus.

## References

1. Baney, R. H.; Itoh, M.; Sakakibara, A.; Suzuki, T. *Chem. Rev.* **1995**, *95*, 1409–1430.
2. Haddad, T. S.; Lichtenhan, J. D. *J. Inorg. Organomet. Polym.* **1995**, *5*, 237–246.
3. Haddad, T. S.; Viers, B. D.; Phillips, S. H. *J. Inorg. Organomet. Polym.* **2001**, *11*, 155–164.
4. Su, R. Q.; Muller, T. E.; Prochazka, J.; Lercher, J. A. *Adv. Mater.* **2002**, *14*, 1369–1373.
5. Hogle, R. A.; Helly, P. J.; Ma, C.; Miller, L. J. U.S. Patent Application 20020192980, 2002.
6. Gonzalez, R. I.; Philips, S. H.; Hoflund, G. B. *J. Spacecr. Rockets* **2000**, *37*, 463–467.
7. Hoflund, G. B.; Gonzalez, R. I.; Philips, S. H. *J. Adhes. Sci. Technol.* **2001**, *15*, 1199–1211.
8. Tomczak, S. J.; Marchant, D.; Svejda, S.; Minton, T. K.; Brunsvold, A. L.; Gouzman, I.; Grossman, E.; Schatz, G. C.; Troya, D.; Sun, L. P.; Gonzalez, R. I. Materials for space applications. *MRS Symp. Proc.* **2004**, *851*, 395–406.
9. Hsiao, B. S.; White, H.; Rafailovich, M.; Mather, P. T.; Jeon, H. G.; Phillips, S. H.; Lichtenhan, J. D.; Schwab, J. J. *Polym. Int.* **2000**, *49*, 437–440.
10. Constable, G. S.; Lesser, A. J.; Coughlin, E. B *Macromolecules* **2004**, *37*, 1276–1282.
11. Zheng, L.; Kasi, R. M.; Farris, R. J.; Coughlin, E. B. *Polym. Mater. Sci. Eng.* **2001**, *84*, 114–115.
12. Li, G. Z.; Wang, L. C.; Ni, H. L.; Pittman, C. U. *J. Inorg. Organomet. Polym.* **2001**, *11*, 123–154.

13. Deng, J.; Hottle, J. R.; Polidan, J. T.; Kim, H. J.; Farmer-Creely, C. E.; Viers, B. D.; Esker, A. R. *Langmuir* **2004**, *20*, 109–115.
14. Deng, J.; Viers, B. D.; Esker, A. R.; Anseth, J. W.; Fuller, G. G. *Langmuir* **2005**, *21*, 2375–2385.
15. Hottle, J. R.; Deng, J.; Kim, H. J.; Farmer-Creely, C. E.; Viers, B. D.; Esker, A. R. *Langmuir* **2005**, *21*, 2250–2259.
16. Hottle, J. R.; Kim, H. J.; Deng, J.; Farmer-Creely, C. E.; Viers, B. D.; Esker, A. R. *Macromolecules* **2004**, *37*, 4900–4908.
17. Lösche, M.; Möhwald, H. *Rev. Sci. Instrum.* **1984**, *55*, 1968–1972.
18. Moy, V. T.; Keller, D. J.; Graub, H. E.; McConnell, H. M. *J. Phys. Chem.* **1986**, *90*, 3198–3202.
19. Hénon, S.; Meunier, J. *Rev. Sci. Instrum.* **1991**, *62*, 936–939.
20. Hönig, D.; Möbius, D. *J. Phys. Chem.* **1991**, *95*, 4590–4592.
21. Binnig, G.; Quate, C. F.; Gerber, C. *Phys. Rev .Lett.* **1986**, *56*, 930–933.
22. Chi, L. F.; Anders, M.; Fuchs, H.; Johnston, R. R.; Ringsdorf, H. *Science* **1993**, *259*, 213–216.
23. Dutta, P.; Peng, J. B.; Lin, B.; Ketterson, J. B.; Prakash, M.; Georgopoulos, P.; Ehrlich, S. *Phys. Rev. Lett.* **1987**, *58*, 2228–2231.
24. Kjaer, K.; Als-Nielsen, J.; Helm, C. A.; Laxhuber, L. A.; Möhwald, H. *Phys. Rev. Lett.* **1987**, *58*, 2224–2227.
25. Rentschler, E.; Gatteschi, D.; Cornia, A.; Fabretti, A. C.; Barra, A. L.; Shchegolikhina, O. I.; Zhdanov, A. A. *Inorg. Chem.* **1996**, *35*, 4427–4431.
26. Shchegolikhina, O. I.; Pozdniakova, Y. A.; Molodtsova, Y. A.; Korkin, S. D.; Bukalov, S. S.; Leites, L. A.; Lyssenko, K. A.; Peregudov, A. S.; Auner, N.; Katsoulis, D. E. *Inorg. Chem.* **2002**, *41*, 6892–6904.
27. Hanssen, R. W. J. M.; van Santen, R. A.; Abbenhuis, H. C. L. *Eur. J. Inorg. Chem.* **2004**, *4*, 675–683.
28. Dubois, G.; Reye, C.; Corriu, R. J. P.; Brandes, S.; Denat, F.; Guilard, R. *Angew. Chem., Int. Ed.* **2001**, *40*, 1087–1090.
29. Harkness, B. R.; Rudolph, M.; Takeuchi, K. *Chem. Mater.* **2002**, *14*, 1448–1451.
30. Duchateau, R.; van Santen, R. A.; Yap, G. P. A. *Organometallics* **2000**, *19*, 809–816.
31. Duchateau, R. *Chem. Rev.* **2002**, *102*, 3525–3542.
32. Dijkstra, T. W.; Duchateau, R.; van Santen, R. A.; Meetsma, A.; Yap, G. P. A. *J. Am. Chem. Soc.* **2002**, *124*, 9856–9864.
33. Abbenhuis, H. C. L. *Chem. Eur. J.* **2000**, *6*, 25–32.
34. Chian, W.; Mallampalli, C.; Winter, R. M. NSTI Nanotech 2005, NSTI Nanotechnology Conference and Trade Show, Anaheim, CA, May 8−12, 2005; Volume 2, pp 107−110.
35. Wheeler, P. A.; Fu, B. X.; Lichtenhan, J. D.; Weitao, J.; Mathias, L. *J. Appl. Poly. Sci.* **2006**, *102*, 2856–2862.
36. Liu, H.; Zheng, S.; Nie, K. *Macromolecules* **2005**, *38*, 5088–5097.

Downloaded by PENNSYLVANIA STATE UNIV on June 25, 2012 | http://pubs.acs.org
Publication Date (Web): November 9, 2010 | doi: 10.1021/bk-2010-1051.ch015

Downloaded by DUKE UNIV on June 24, 2012 | http://pubs.acs.org
Publication Date (Web): November 9, 2010 | doi: 10.1021/bk-2010-1051.ch016

## Chapter 16

# Polyhedral Oligomeric Silsesquioxane-Functionalized Perfluorocyclobutyl Aryl Ether Polymers

## An Overview of the Synthesis and Properties of Polyhedral Oligomeric Silsesquioxanes (POSS) Functionalized with Perfluorocyclobutyl (PFCB) Aryl Ether Polymer Blends and Copolymers

**Scott T. Iacono,[1] Stephen M. Budy,[1] Joseph M. Mabry,[*,2] and Dennis W. Smith, Jr.[*,1]**

**[1]Department of Chemistry and Center for Optical Materials Science and Engineering Technologies (COMSET), Advanced Materials Research Laboratory, Clemson University, Clemson, SC 29634**
**[2]Air Force Research Laboratory Materials Applications Branch, Edwards Air Force Base, CA 93524**
**[*]e-mails: dwsmith@clemson.edu, joseph.mabry@edwards.af.mil**

Perfluorocyclobutyl (PFCB) aryl ether polymers are semi-fluorinated polymers that produce processable, optically transparent materials for a multitude of materials applications. Incorporating low surface energy polyhedral oligomeric silsesquioxanes (POSS) into the PFCB polymer matrix produced enhanced hydro- and oleo-phobicity. PFCB polymers functionalized with POSS nanostructures include blends, copolymers, and block copolymers. For copolymers, trifluorovinyl aryl ether (TFVE) POSS monomers were prepared in good yields using an operationally simple corner capping methodology from commercial POSS trisilanols. The surface analysis of POSS functionalized PFCB polymer blends and copolymers using microscopy and optical profilometry showed the POSS structures produced sub-micron to nano-meter

In Advances in Silicones and Silicone-Modified Materials; Clarson, S., et al.;
ACS Symposium Series; American Chemical Society: Washington, DC, 2010.

roughness that contributes to enhanced water and hexadecane repellency.

## Introduction

Many plant species such as the lotus leaf exhibit a peculiar self-cleaning mechanism resulting from micron-sized nodes decorated on the surface. These nodes are covered with nano-sized wax particles on the surface. This structure induces the beading of water, which is naturally repelled from the surface, removing any entrained foreign debris (*1*, *2*). There are many noteworthy examples of coatings that successfully produce artificial ultrahydrophobic lotus leaf-like surfaces (*3*). However, many of these examples are prepared using aggressive post chemical and/or thermal surface treatments, expensive starting materials, or necessitate the need for lithography methods. As a consequence, there still exists a need to efficiently produce low surface energy materials, albeit not exclusively limited to hydrophobicity, amenable for large scale application.

Fluoropolymers continue to be of great interest for a wide range of material applications, particularly for low energy surfaces (*4*). Incorporating fluorine into a polymer backbone creates an interesting irony in terms of physical properties. On one hand, highly fluorinated polymers possess a high degree of chemical resistance, thermal stability, and excellent insulating ability. Conversely, perfluorinated polymers, like poly(tetrafluoroethylene) (PTFE), are intrinsically crystalline, leading to high processing costs. Therefore, interest continues in developing new fluoropolymers to overcome processing limitations while maintaining performance. Perfluorocyclobutyl (PFCB) aryl ether polymers are prepared by condensate-free, step-growth [2+2] thermal cyclodimerization of trifluorovinyl aryl ether (TFVE) monomers (Figure 1) (*5*, *6*). The cycloaddition event proceeds via a biradical intermediate in a predominately head-to-head fashion (*7*). The stereorandom nature of the PFCB aryl ether linkage affords an entirely amorphous, semi-fluorinated thermoplastic that is solution processable. TFVE monomers are easily functionalized for desired applications employing a halogen–metal exchange methodology developed by Smith *et al.* using the intermediate, 4-bromo(trifluorovinyl) aryl ether, as a commercial starting material (*8*, *9*). As a result of this tailorability, material applications of PFCB polymers include high performance optics (*10*), polymer light-emitting diodes (PLEDs) (*11*), atomic oxygen (AO) resistant coatings (*12*), polymeric proton exchange membranes (PEMs) for fuel cells (*13*), and liquid-crystalline polymers (*14*).

Polyhedral oligomeric silsesquioxane (POSS) compounds comprised of a functionalized nanometer-sized silicon-oxygen core framework have received much interest as robust building blocks for the development of high performance materials (*15*). POSS incorporation into polymers, either as blends or covalently bound copolymers, produces hybrid organic-inorganic composites. Modified properties of the virgin polymer include changes in glass transition temperature, crytallinity, mechanical toughness, chemical resistance, ease of processing, fire resistance, and atomic oxygen resistance (*15*).

Downloaded by DUKE UNIV on June 24, 2012 | http://pubs.acs.org
Publication Date (Web): November 9, 2010 | doi: 10.1021/bk-2010-1051.ch016

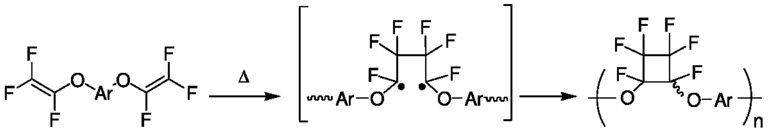

*Figure 1. Thermal [2+2] cyclopolymerization of trifluorovinyl aryl ethers.*

Herein, recent focus expands on the utility of PFCB polymers by introducing blended and covalently bound POSS cages for improving water and hexadecane repellency. These POSS-modified PFCB polymers produced hybrid composites with improved properties such as thermal stability, mechanical integrity, tunable refractive index, and gas permeability.

## Experimental

### Materials

Chemicals and solvents were purchased through Sigma Aldrich and purified according to reported procedures (*16*). POSS triols **1** and **2** were obtained from Hybrid Plastics. Fluorinated POSS (F-POSS) compounds were donated by the Air Force Research Laboratory, Propulsion Directorate or prepared according to previously published procedures (*17*). POSS trisodium silanolate salt **3** was prepared according to previously published procedures by Fukuda (*18*). Experimental procedures and spectroscopic data for POSS functionalized TFVE monomers **1c**–**3c** and **6**–**7** are reported elsewhere (*19*, *20*). 4,4'-Bis(4-trifluorovinyloxy)biphenyl (**4**) and 2,2-bis(4-trifluorovinyloxybiphenyl)-1,1,1,3,3,3-hexafluoropropane (**5**) were generously donated and are commercially available from Tetramer Technologies, L.L.C., Pendleton, SC and distributed through Oakwood Chemicals, Inc.

### General Procedures

All reactions were carried out under ultra high purity grade nitrogen. Flasks and syringes were flame-dried under vacuum and allowed to cool in a desiccator filled with $Ca_2CO_3$ prior to use. $^1H$, $^{13}C$ (proton decoupled), and $^{19}F$ (proton decoupled), and $^{29}Si$ NMR data were obtained on a JOEL Eclipse$^+$ 300. Gel permeation chromatography (GPC) data were collected in $CHCl_3$ using polystyrene as a standard (Polymer Labs Rascal PS-2) using a Waters 2690 Alliance System with UV-Vis detection. Differential scanning calorimetric (DSC) analysis and thermal gravimetric analysis (TGA) were performed on a TA Q1000 instrument and Mettle-Toledo 851 instrument, respectively. Transmission electron microscopy (TEM) micrographs were obtained from a Hitachi H9500 300 eV at the Clemson University Electron Microscope Facility. Surface analysis and roughness was performed on a Zygo New View 6300 3D white light optical profiler or a Digital Instruments Dimension 3100 atomic force microscopy (AFM) system.

Downloaded by DUKE UNIV on June 24, 2012 | http://pubs.acs.org
Publication Date (Web): November 9, 2010 | doi: 10.1021/bk-2010-1051.ch016

### Contact Angle Measurements

Contact angle analyses were performed on a FDS Data physics Contact Analyzer System or a Rime-Hart 100-00 115 Goniometry. Liquid drops were either automatically or manually dispensed with 8–10 µL drop sizes. The contact angles were determined via the software suite or via graphical fitting of the contact tangents in the captured image. Both approaches gave the same nominal value within ± 2 degrees. Static contact angle values report an average of the three values measured on various areas of the coated surface. Deionized water and hexadecane were used as test fluids to measure static contact angles.

## Results and Discussion

### POSS PFCB Polymer Blends

Fluorinated POSS (F-POSS) compounds were blended into PFCB polymer **poly5** ($M_{an}$ = 22000, PDI = 2.2; GPC in $CHCl_3$ using PS as standard) by dissolving a weight percentage of F-POSS relative to the polymer matrix in a minimal amount of hexafluorobenzene (Figure 2). Although the POSS and PFCB polymer dissolved in solvent produced a readily homogenous solution, the mixture was rigorously blended with a magnetic stirrer for five minutes. The solution was then spin cast onto borosilicate plates (ca. 0.5-0.75µm thick), producing optically transparent films for loadings less than 20 wt%.

Previous work by Mabry and Vij, showed the fluorodecyl$_8$T$_8$ POSS (**FP$_8$T$_8$**) compound possesses the highest degree of hydro- and oleo-phocity (*17*). The measured static contact angles of **FD$_8$T$_8$** was reported as 154° and 87° for water and hexadecane, respectively. Although other F-POSS compounds produce suitable free standing films from spin casting, the following blending work will focus on PFCB polymer blends with **FD$_8$T$_8$** since these produce the highest water and hexadecane contact angles.

Increasing **FD$_8$T$_8$** POSS wt% loadings shows a gradual increase in water and hexadecane contact angle (Figure 3). The 6F PFCB polymer (**poly5**) is considered hydrophobic with no F-POSS incorporation with water and hexadecane contact angles of 95° and 27°. **FD$_8$T$_8$** POSS loadings up to 15 wt% developed a water repellency plateau; the blend shows an overall 32% increase in water contact angle. At optimized **FD$_8$T$_8$** loadings of 10 wt%, a maximum hexadecane contact angle of 80° was observed increasing oleophocity by 158%. While films prepared from 15 wt% **FD$_8$T$_8$** POSS loading still appeared transparent and homogenous, at 20 wt% **FD$_8$T$_8$** POSS, significant incompatibility was observed producing opaque films. Work is currently in progress to determine liquid drop hysterisis by measuring advancing and receding contact angles.

Blending **FD$_8$T$_8$** into the PFCB polymer introduced additional fluorine content and increased surface roughness. These two characteristics produced a composite with lower surface energy. The relationship of contact angle and surface energy is governed by Young's equation which relates interfacial tensions among the surface to the liquid and gas phases of water (*21*). Furthermore, it is well known that surface roughness imparts increased hydrophobicity of a material

Downloaded by DUKE UNIV on June 24, 2012 | http://pubs.acs.org
Publication Date (Web): November 9, 2010 | doi: 10.1021/bk-2010-1051.ch016

as demonstrated by Cassie and Wenzel (*22*, *23*). Analysis of 15 wt% POSS PFCB polymer composite film surface by SEM analysis using energy dispersive X-ray (XDS) elemental mapping showed excellent dispersion of the POSS within the PFCB matrix.

AFM analysis of 15 wt% **$FD_8T_8$** blend compared with the virgin PFCB polymer showed a marked increase in surface roughness (Figure 4). From AFM analysis, virgin **poly5** and 15 wt% **$FD_8T_8$** composite blend gave a measured surface roughness (r.m.s.) of 0.527 nm and 1.478 nm, respectively. The incorporation of the nanosized F-POSS structures produces a three-fold increase in surface roughness possibly due to blooming and aggregation of these structures on the surface during the spin casting process. Additional surface characterization remains ongoing to determine the concentration gradient of the F-POSS structures on the surface compared to entrained F-POSS in the bulk material.

Solvent blending demonstrated good compatibility of F-POSS with PFCB polymers. Significant increases in the hydrophobicity and oleophobicity of PFCB polymers was observed with minimal F-POSS loadings by the increase in fluorine content and surface nanoroughness. The suppression of surface migration and increased POSS loading could be acheived by incorporating POSS structures covalently bound to a polymer backbone. This is the focus of the following sections where initial attempts to introduce non-fluorinated POSS would serve as model studies to understand effects on bulk copolymer properties. Consequently, the incorporation of fluorinated POSS as copolymers would serve to ultimately enhance hydro- and oleo-phobicity.

Downloaded by DUKE UNIV on June 24, 2012 | http://pubs.acs.org
Publication Date (Web): November 9, 2010 | doi: 10.1021/bk-2010-1051.ch016

## Chain Terminated POSS PFCB Copolymers

### *Monomer Synthesis*

The preparation of TFVE POSS monomers for chain terminated copolymers is shown in Figure 5 (*19*). POSS-functionalized TFVE monomers **1c** and **2c** were prepared from commercially available POSS triols **1** and **2**. Monomer **3c** was synthesized via the hydrolytic condensation of trifluoropropyltrimethoxysilane affording the trisodium silonate salt (**3**) (*18*). Initial corner-capping via the condensation of POSS triols **1**–**3** with acetooxyethyltrichlorosilane affords the POSS $T_8$ cages **1a**–**3a**. POSS alcohols **1b**–**3b** are produced in nearly quantitative yield by deprotection of the POSS esters **1a**–**3a** under mild acidic conditions. Dicyclohexyldicarbimide (DCC) coupling with 4-(trifluorovinyloxy)benzoic acid (available through Oakwood Chemicals) produces the desired monomers **1c**–**3c**. The overall, optimized four-step monomer synthesis produces modest to good yields of 40–76% for **1c**–**3c**.

### *Polymerization*

Copolymerization of POSS functionalized PFCB aryl ether monomers **1c**–**3c** with bisfunctionalized TFVE monomer 4,4'-bis(4-trifluorovinyloxy)biphenyl (**4**)

Downloaded by DUKE UNIV on June 24, 2012 | http://pubs.acs.org
Publication Date (Web): November 9, 2010 | doi: 10.1021/bk-2010-1051.ch016

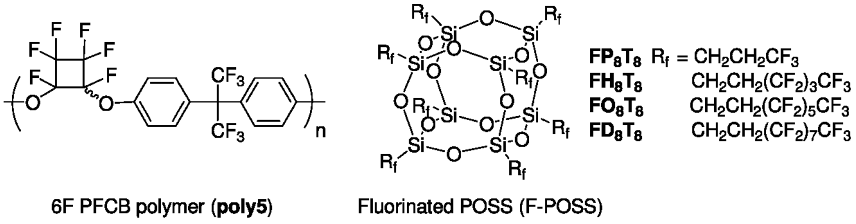
FP8T8 Rf = CH2CH2CF3
FH8T8 CH2CH2(CF2)3CF3
FO8T8 CH2CH2(CF2)5CF3
FD8T8 CH2CH2(CF2)7CF3
6F PFCB polymer (poly5)
Fluorinated POSS (F-POSS)

*Figure 2. Fluorinated POSS is solvent blended into 6F PFCB polymer matrix.*

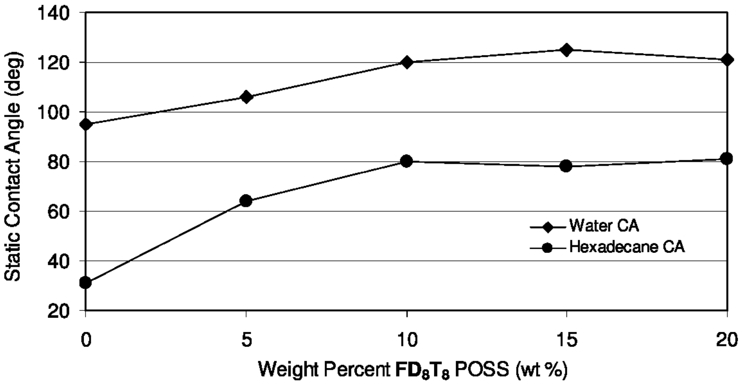

*Figure 3. Water and hexadecane static contact angle versus wt % of **FD$_8$T$_8$** blended into **poly5**.*

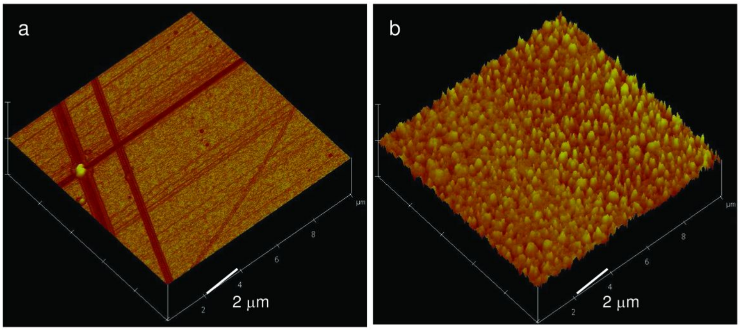

*Figure 4. AFM of (a) virgin PFCB polymer **poly5** and (b) 15 wt% **FD$_8$T$_8$** POSS **poly5** blend.*

was performed in bulk at 180 °C for 48–96 h in vacuum-sealed ampoules (Figure 6).

Selected properties of the chain terminated copolymers are shown in Table 1. POSS-functionalized copolymers produce optically transparent, free-standing films from either THF drop- or spin-casting. In all cases, the bulk polymerization produces nearly quantitative mass recovery after precipitation. Molecular weights of copolymers **2c-*co*-4** and **3c-*co*-4** are similar to the corresponding homopolymer **poly4**. The cyclopentyl-substituted POSS functionalized copolymers **1c-*co*-4**

Downloaded by DUKE UNIV on June 24, 2012 | http://pubs.acs.org
Publication Date (Web): November 9, 2010 | doi: 10.1021/bk-2010-1051.ch016

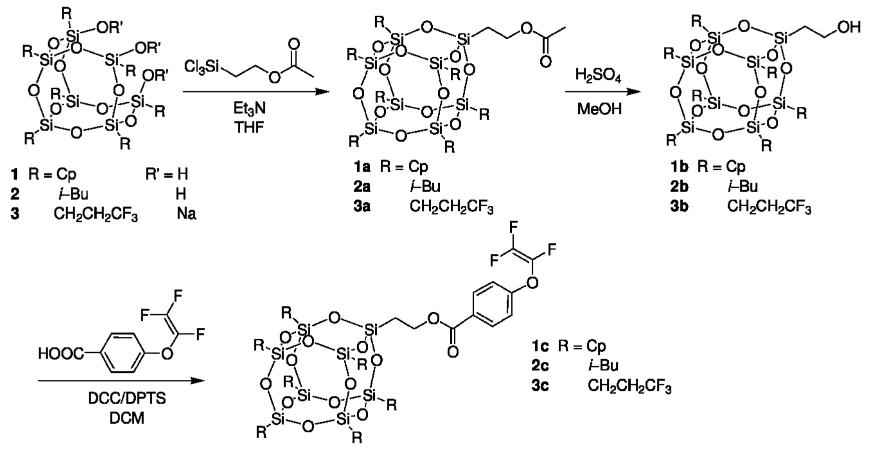
1 R = Cp R' = H
2 i-Bu H
3 CH2CH2CF3 Na
Cl3Si
Et3N
THF
1a R = Cp
2a i-Bu
3a CH2CH2CF3
H2SO4
MeOH
1b R = Cp
2b i-Bu
3b CH2CH2CF3
HOOC
DCC/DPTS
DCM
1c R = Cp
2c i-Bu
3c CH2CH2CF3

*Figure 5. Synthesis of POSS monomers functionalized with TFVE.*

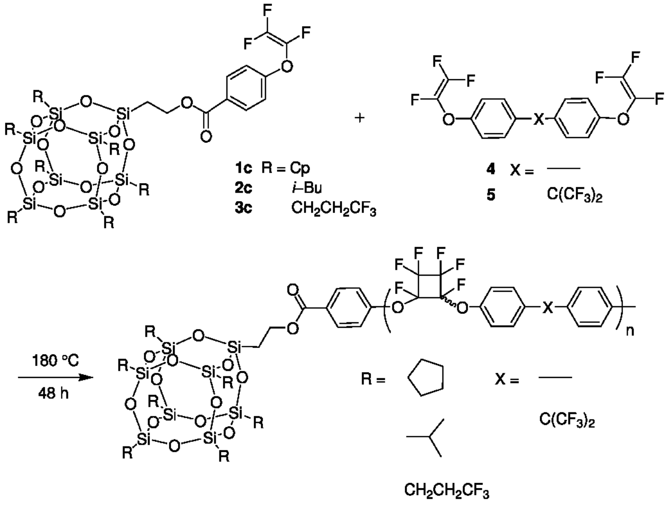
1c R = Cp
2c i-Bu
3c CH2CH2CF3
+
4 X = —
5 C(CF3)2
180 °C
48 h
R =
X = —
C(CF3)2
CH2CH2CF3
n

*Figure 6. Preparation of POSS chain terminated PFCB copolymers.*

showed significantly lower $M_n$ values compared to homopolymer **poly4**. This is due to the fact the monomer **1c** does not melt below 200 °C, nor is it soluble in the monomer melt at bulk polymerization temperature of 180 °C. Molecular weights were the highest for copolymers **3c-*co*-4** functionalized with the trifluoropropyl POSS. The compatibility of fluorinated POSS in the semi-fluorinated PFCB matrix is further evidenced by copolymer **3c-*co*-5**. In this case, the polymer backbone introduces the hexafluoroisopropylidene moiety increasing fluorine content by 33%.

### Thermal Properties

Table 1 shows the DSC analysis of homopolymers and copolymers functionalized with POSS. As previously reported, $T_g$ for amorphous, semi-fluorinated PFCB homopolymers **poly4** and **poly5** are 140 °C and 97° C, respectively. A plasticizing effect was observed with **2c-*co*-4**, particularly with increasing POSS content, lowering $T_g$ by 28% using 20 wt% monomer. On the other hand, compatibility was acheived using fluorinated POSS monomers in copolymer systems **3c-*co*-5** with no deviation in $T_g$.

### Degradation Analysis

Composite thermal stability was studied in nitrogen and air using thermogravimetric analysis (TGA) as shown in Table 1. Homopolymers **poly4** and **poly5** exhibit a high degree of thermal stability with recorded thermal decomposition temperatures ($T_d$) of 450 and 466 °C in nitrogen and 446 and 457 °C in air. For all copolymers studied, two onsets of degradation were observed in nitrogen and air. TGA indicated the onset of degradation in nitrogen and air results in a mass loss proportional to the weight percent of POSS content in the copolymers. Char yields randomly varied in the range of 11–54% in nitrogen for all copolymers studied using TGA analysis.

Downloaded by DUKE UNIV on June 24, 2012 | http://pubs.acs.org
Publication Date (Web): November 9, 2010 | doi: 10.1021/bk-2010-1051.ch016

## Pendant POSS PFCB Copolymers

New linear chain terminated PFCB polymers functionalized with POSS have been prepared through the facile corner capping of POSS triols. The composites produced moderate molecular weight, transparent polymers with excellent solvent processability and, in some cases, improvement in thermo-oxidative stability. Wettabilty analysis of the copolymer films did not show a significant improvement in water or hexadecane contact angle over the homopolymers. The preparation longer fluoroalkyl TFVE POSS monomers is the interest for future investigations in order to improve water and hexadecane repellency.

### Monomer Synthesis

The preparation of POSS monomers with bifunctional TFVE moieties **6** and **7** were prepared by an efficient condensation of commercial POSS silanols with 4,4'-bis(4-trifluorovinyloxy)biphenyl methylchlorosilane previously reported by Smith *et al.* using a metal–halogen exchange methodology (Figure 7) (*20*). The monomers were isolated in acceptable yields (29–30%) with a high degree of purity.

Monomer characterization was confirmed by multi-nuclei NMR ($^{1}$H, $^{19}$F, $^{13}$C, and $^{29}$Si) spectroscopy and elemental analysis. Figure 8 shows a representative $^{29}$Si NMR of POSS TFVE monomer **7** in $CDCl_3$. Symmetry arrangement of the silicon atoms exhibits four resonance peaks with ratios 1:3:4:1 for peak assignments *a, c,*

Downloaded by DUKE UNIV on June 24, 2012 | http://pubs.acs.org
Publication Date (Web): November 9, 2010 | doi: 10.1021/bk-2010-1051.ch016

**Table 1. Selected Properties of POSS Chain Terminated PFCB Copolymers**

| *polymer* | *wt% POSS* | *$M_n$ × $10^{-3}$ GPC*[a] | *$M_w/M_n$* | *$T_g$ (°C)*[b] | *$T_d$ (°C) $N_2$ (air)*[c] |
|---|---|---|---|---|---|
| **poly4** | 0 | 13.3 | 2.2 | 140 | 450 (446) |
| **1c-*co*-4** | 10 | 2.1 | 1.7 | 133 | 322, 464 (330, 489) |
| **1c-*co*-4** | 20 | 7.0 | 2.0 | 131 | 316, 518 (355, 479) |
| **2c-*co*-4** | 10 | 10.3 | 1.8 | 124 | 304, 461 (306, 563) |
| **2c-*co*-4** | 20 | 12.6 | 2.3 | 109 | 307, 521 (297, 558) |
| **3c-*co*-4** | 10 | 22.2 | 3.0 | 138 | 325, 450 (300, 450) |
| **3c-*co*-4** | 20 | 28.8 | 4.3 | 131 | 319, 467 (310, 460) |
| **poly5** | 0 | 4.0 | 1.9 | 97 | 466 (457) |
| **3c-*co*-5** | 20 | 8.8 | 1.6 | 100 | 318, 474 (310, 460) |

[a] GPC in $CHCl_3$ using polystyrene as standard. [b] DSC (10 °C/min) in nitrogen determined by second re-heating cycle. [c] TGA onset at 10 °C/min.

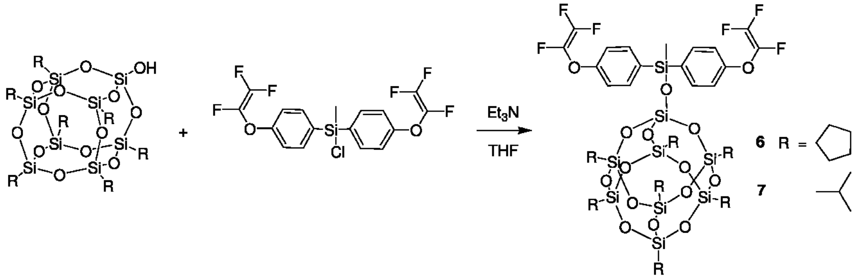

*Figure 7. Synthesis of bifunctionalized TFVE POSS monomers.*

*d, b*, respectively. The bridgehead *M* silicon atom (assigned as *a*) with adjoining diaryltrifluorovinylether moieties is shifted furthest downfield at –9.6 ppm. The *Q* silicon in the POSS cage assigned *b* is shifted at –109.9 ppm. The remaining regions pertain to the apex *T* silicon atoms of the POSS cage and shift –66.3 ppm and –67.2 ppm for *c* and *d*, respectively.

### *Polymerization*

Homopolymers (**poly4** and **poly5**) and copolymers (**4-*co*-6** and **4-*co*-8**) were prepared from the respective monomers by bulk polymerization at 190 °C producing POSS PFCB aryl ether copolymers (Figure 9). Selected polymer properties are shown in Table 2. All copolymers prepared showed similar molecular weight distribution compared to the PFCB aryl ether homopolymer *via* the thermal step-growth cyclopolymerization.

Downloaded by DUKE UNIV on June 24, 2012 | http://pubs.acs.org
Publication Date (Web): November 9, 2010 | doi: 10.1021/bk-2010-1051.ch016

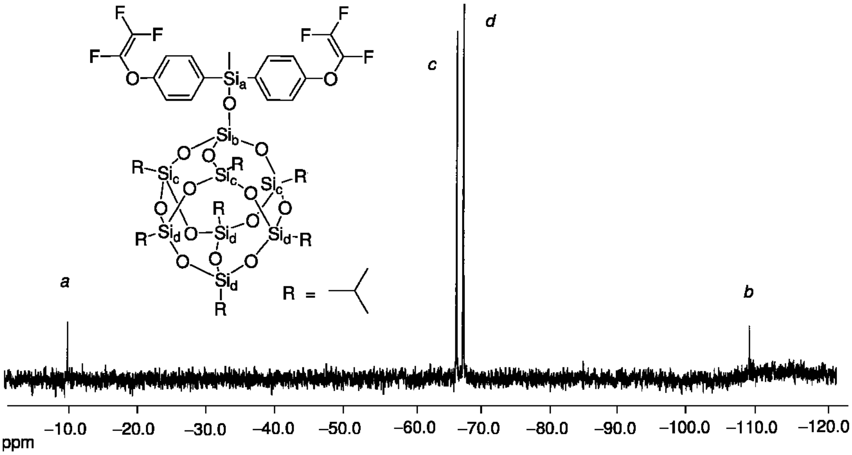

*Figure 8. $^{29}$Si NMR (60 MHz, inverse gate proton decoupled) of POSS TFVE monomer 7 in $CDCl_3$.*

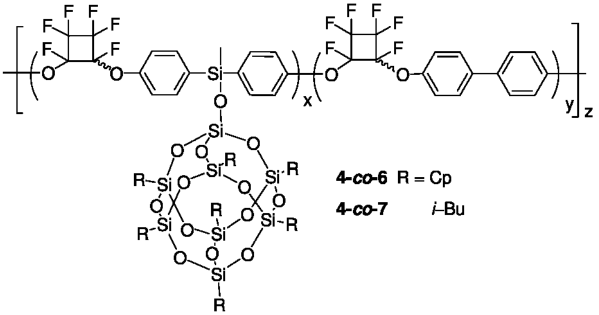

*Figure 9. Pendant POSS PFCB random copolymers.*

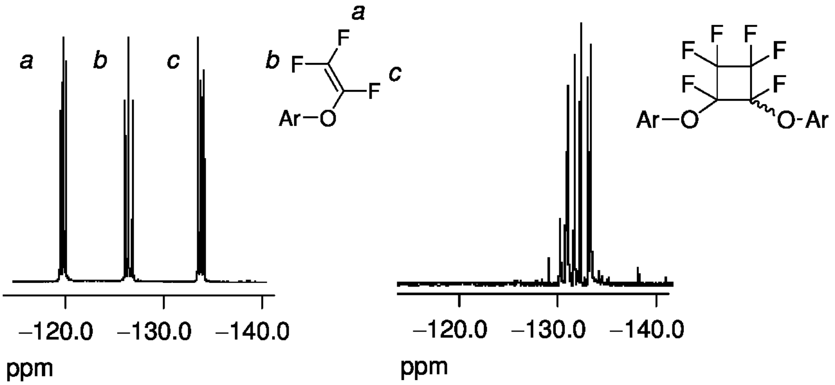

*Figure 10. $^{19}$F NMR (283 MHz) in $CDCl_3$ showing the conversion of POSS TFVE monomer 7 (left) incorporated into the random copolymer **4-co-7** (right).*

Table 2. Selected Properties of Pendant POSS PFCB Copolymers

| *polymer* | *wt% POSS* | *$M_n \times 10^{-3}$ GPC*[a] | *$M_w/M_n$* | *$T_g$ (°C)*[b] | *$T_d$ (°C) $N_2$ (air)*[c] |
|---|---|---|---|---|---|
| **poly4** | 0 | 13.3 | 2.2 | 140 | 450 (446) |
| **4-*co*-6** | 20 | 21.5 | 5.2 | 134 | 447 (439) |
| **poly6** | 100 | 6.6 | 3.5 | 131 | -- |
| **4-*co*-7** | 10 | 24.9 | 1.4 | 133 | 452 (442) |
| **4-*co*-7** | 20 | 20.5 | 3.2 | 128 | 440 (438) |
| **poly7** | 100 | 6.3 | 2.5 | 138 | -- |
| **4-*b*-7** | 10[d] | 21.9 | 3.4 | 149 | 452 (506) |
| **4-*b*-7** | 20[d] | 19.5 | 4.5 | 142 | 462 (501) |
| **poly5** | 0 | 8.0 | 2.0 | 100 | 466 (457) |
| **5-*co*-7** | 15 | 13.2 | 4.2 | 89 | -- |

[a] GPC in $CHCl_3$ using polystyrene as standard. [b] DSC (10 °C/min) in nitrogen determined by second re-heating cycle. [c] TGA onset at 10 °C/min. [d] Value indicates wt% of **poly4** or **poly5** used as a block unit.

Downloaded by DUKE UNIV on June 24, 2012 | http://pubs.acs.org
Publication Date (Web): November 9, 2010 | doi: 10.1021/bk-2010-1051.ch016

$^{19}F$ NMR analysis indicated complete conversion of the POSS monomers that were incorporated into the PFCB copolymer (Figure 10). The TVFE peaks are typically observed using $^{19}F$ NMR by three sets of doublet of doublets at –119.5 ppm (*cis*-Ar-O-CF=C*F*$_2$), –126.4 ppm (*trans*-Ar-O-CF=C*F*$_2$), and –133.8 ppm (Ar-O-C*F*=CF$_2$). $^{19}F$ NMR of copolymer **4-*co*-7** with 20 wt% POSS showed the resulting multiplet –130.0–(–135.5) ppm of the perfluorocyclobutyl aryl ether ring from the thermal cyclodimerization. Copolymer **4-*co*-6** functionalized with cyclopentyl groups showed the highest polydispersity, likely due to the insolubility of higher molecular weight polymers.

Differential scanning calorimetry (DSC) indicated a plasticizing effect shown by the decrease in the glass transition temperature ($T_g$) with POSS copolymers. The decrease was most noticeable for copolymers with *iso*-butyl groups (R = *i*-Bu) and further increased with higher POSS loadings up to 20 wt%, similar to the chain terminated PFCB polymers. The observed decrease may be the result of POSS incompatibility with the semi-fluorinated PFCB polymer matrix or may be due to the flexibility of the POSS isobutyl groups. POSS PFCB aryl ether homopolymers were also prepared by thermal polymerization with monomers **6** and **7**, producing **poly6** and **poly7**; the average chain segment length is five POSS molecules (n = 5) as determined by GPC analysis. These POSS prepolymers were used to produce block copolymers (**4-*b*-7**) *via* thermal polymerization with monomer **4**. Compared to the POSS PFCB copolymers, the block polymers showed an increase in $T_g$ demonstrating that the POSS block segments hinder chain mobility. Furthermore, the block copolymers **4-*b*-7** showed an increase in the thermal decomposition temperature observed from TGA compared with the two POSS PFCB copolymers **4-*co*-6** and **4-*co*-7**. Introducing block segments into the copolymer showed a 50

°C increase in thermal decomposition temperature in air compared with nitrogen in excess of 500 °C.

### *Film Preparation and Surface Analysis*

Copolymers with up to 20 wt% *iso*-butyl functionalized POSS produced solution processable, optically transparent, semi-flexible films. However, POSS loadings greater than 20 wt% produced polymers that were difficult to solution process producing gelled solids. Copolymers and block copolymers were solution processed (in THF) to prepare spin cast films (SCF) or drop cast films (DCF). TEM and EDX analysis revealed nanometer POSS clusters with varying sizes ranging from 5–20 nm.

The hydrophobicity of the copolymer films functionalized with *iso*-butyl POSS were tested using contact angle analysis (Table 3 and Figure 11). Compared with the homopolymer **poly4**, copolymer **4-*co*-7** showed an increase in water contact angle with increasing POSS content. The highest increase in water repellency was 16% for 20 wt% POSS copolymer **4-*co*-7** with an average contact angle of 104.7° compared with homopolymer **poly4** that averaged 91.3°. Furthermore, block copolymer **4-*b*-7** also showed a similar increase in water repellency compared with that of homopolymer **poly4**. The degree of surface roughness correlated with the increased water contact angles, as indicated by 3D white light optical profilometry. Profilometery analysis also reveals significant surface roughening of the POSS copolymer **4-*co*-7** compared with homopolymer **poly4** with an average surface roughness (r.m.s.) of 4.20 nm and 0.36 nm, respectively. In all cases, composites prepared by the drop cast film (DCF) method showed a 1.3 nm higher average surface roughness compared with the smoother spin cast films (SCF). More importantly, incorporation of the POSS nanofillers increases the surface roughness up to 12–19 times compared to that of the homopolymer films. Block copolymers **4-*b*-7** that were prepared by spin casting showed the highest surface roughness. As a further comparison, 20 wt% of fully-condensed *iso*-butyl$_8$T$_8$ POSS (Hybrid Plastics) was solvent blended into **poly4** and spin cast as a film. The resulting film's water contact angle was 15% lower than compared with PFCB homopolymer **poly4**. The surface roughness was not obtained because the blend produces a white opaque, heterogeneous film and cannot be measured by optical profilometry. However, upon visual inspection, a porous substrate with irreproducible film morphologies was observed suggesting incompatibility of *iso*-butyl POSS in the semi-fluorinated PFCB polymer matrix results in decreased water repellency.

Because the POSS PFCB polymers are highly solution processable in common organic solvents (e.g., THF), contact test fluids such as hexadecane and iodomethane failed to produce any measurable repellency and thus completely wetted the surface.

Downloaded by DUKE UNIV on June 24, 2012 | http://pubs.acs.org
Publication Date (Web): November 9, 2010 | doi: 10.1021/bk-2010-1051.ch016

Downloaded by DUKE UNIV on June 24, 2012 | http://pubs.acs.org
Publication Date (Web): November 9, 2010 | doi: 10.1021/bk-2010-1051.ch016

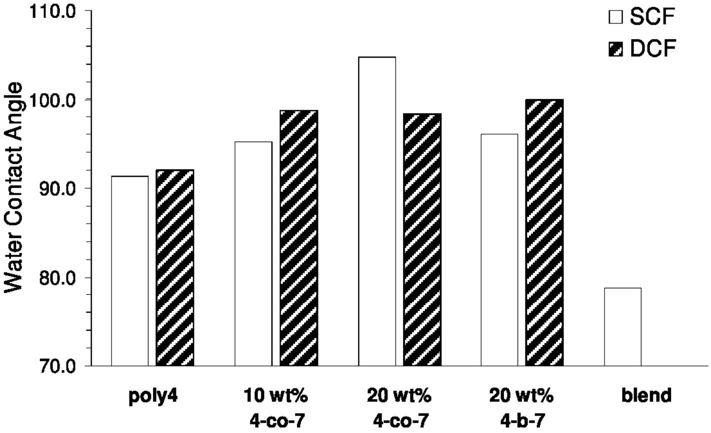

*Figure 11. Water contact angles of spin cast films (SCF) and drop cast films (DCF) of various film surfaces.*

**Table 3. Water Contact Angles of POSS PFCB Polymer Films**

| *polymer* | *SCF CA (θ)* | *SCF r.m.s. (nm)* | *DCF CA (θ)* | *DCF r.m.s. (nm)* |
|---|---|---|---|---|
| **poly4** | 91.3 | 0.36 | 92.0 | 0.38 |
| **4-*co*-7** | 95.3 | 0.44 | 98.7 | 0.46 |
| **4-*co*-7** | 104.7 | 4.20 | 98.3 | 5.62 |
| **4-*b*-7** | 96.0 | 5.67 | 100.0 | 6.88 |
| **blend** | 78.8 | -- | -- | -- |

The existence of nanoroughness has been shown to theoretically and experimentally contribute analogous hydrophobic behaviour similar to that caused by the texture of the lotus leaf (*24*, *25*). However, the 'lotus effect' is due to nano- and micro-structuring, which produces a large change in hydrophobicity due to macroscopic interaction between the water and surface. On the other hand, the observation of nanostructuring has a subtle increase in water repellency due to surface molecular perturbation of the water droplet. The subtle, yet enhanced hydrophobicity reported for pendant POSS PFCB copolymers is consistent with this observation by the presence of surface roughening due to nanometer-sized surface migration of hydrophobic alkyl functionalized POSS molecules. Continued work includes the preparation of fluorinated POSS functionalized TFVE monomers employing the aforementioned synthetic methodology. This would introduce the lower surface energy fluorinated POSS cages to enhance hydro- and oleo-phobicity.

Downloaded by DUKE UNIV on June 24, 2012 | http://pubs.acs.org
Publication Date (Web): November 9, 2010 | doi: 10.1021/bk-2010-1051.ch016

## Conclusions

POSS has been successfully used as a low surface energy nanofiller for the preparation of hydro- and oleo-phobic PFCB polymer blends, copolymers, and block copolymers. The fluorinated POSS PFCB polymer blends showed a significant improvement in both water and hexadecane repellency due to surface roughening as well as the increase in fluorine content. Within the family of copolymers, POSS chain terminated and pendant POSS copolymers produced solution processable films. These copolymer and block copolymer films exhibit modest increase in hydrophobicity due to POSS that produced nanoroughening. The ability to easily process these POSS functionalized fluoropolymers makes them particularly attractive for hydrophobic material applications including fibers, coatings, and bulk components. Utilizing the ability to artificially fabricate low surface energy, nanosized surface features combined with microstructuring could afford a potentially new class of materials possessing liquid or gas discrimination.

## Acknowledgments

We acknowledge the Air Force Office of Scientific Research (AFOSR) and the Air Force Research Laboratory (AFRL) Space and Missile Propulsion Directorate for their financial support. Funding is also supported by the Department of Energy (BES DE-FG02-05ER15718) and the National Science Foundation (DMR 0514622). We thank Dr. JoAn Hudson for TEM support through the Electron Microscope (EM) facility at Clemson University. We acknowledge Ms. Sherly Largo (EAFB) and Ms. Marietta Fernandez (EAFB) for AFM and SEM microscopy data. We also express thanks to Dr. Timothy Haddad (AFRL) for synthesis and characterization expertise. S.T.I. recognizes the Air Force Institute of Technology Civilian Institution Program (AFIT/CIGD) for sponsorship. D.W.S. is a *Cottrell Scholar of Research Corporation*.

## References

1. Neinhuis, C.; Barthlott, W. *Ann. Bot.* **1997**, *79*, 677.
2. Barthlott, W.; Nenhuis, C. *Planta* **1997**, *202*, 1.
3. Sun, T.; Feng, L.; Gao, X.; Jian, L. *Acc. Chem. Res.* **2005**, *38*, 644.
4. *Fluoropolymers*; Wall, L. A., Ed.; John Wiley & Sons: New York, 1972; Vol. XXV.
5. Babb, D. A. In *Fluoropolymers 1: Synthesis*; Hougham, G.; et al., Eds; Plenum Press: New York, 1999; pp 25–50.
6. Babb, D. A.; Ezzell, B. R.; Clement, K. S.; Richey, W. F.; Kennedy, A. P. *J. Poly. Sci., Part A: Polym. Chem.* **1993**, *31*, 3465.
7. Mifsud, N.; Mellon, V.; Jin, J.; Topping, C. M.; Echegoyen, L.; Smith, D. W., Jr. *Polym. Int.* **2007**, in press.
8. Spraul, B. K.; Suresh, S.; Jin, J.; Smith, D. W., Jr. *J. Am. Chem. Soc.* **2006**, *128*, 7055.
9. Ji, J.; Narayan-Sarathy, S.; Neilson, R. H.; Oxley, J. D.; Babb, D. A.; Tondan, N. G.; Smith, D. W., Jr. *Organometallics* **1998**, *17*, 783.

10. Smith, D. W., Jr.; Chen, S.; Kumar, S.; Ballato, J.; Shah, H.; Topping, C.; Foulger, S. *Adv. Mater.* **2002**, *14*, 1585.
11. Luo, J.; Liu, S.; Haller, M.; Liu, L.; Ma, H.; Jen, A. K.-Y. *Adv. Mater.* **2002**, *13*, 1763.
12. Jin, J.; Smith, D. W., Jr.; Topping, C.; Suresh, S.; Chen, S.; Foulger, S. H.; Rice, N.; Mojazza, B. *Macromolecules* **2003**, *36*, 9000.
13. Perpall, M. W.; Smith, D. W., Jr.; DesMarteau, D. D.; Creager, S. E. *J. Macromol. Sci., Part C: Polym. Rev.* **2006**, *46*, 297.
14. Spraul, B. K.; Suresh, S.; Glaser, S.; Perahia, D.; Ballato, J.; Smith, D. W., Jr. *J. Am. Chem. Soc.* **2004**, *126*, 12772.
15. Li, G.; Wang, L.; Hanli, Ni; Pittman, C. U., Jr. *J. Inorg. Organomet. Polym.* **2001**, *11*, 123, and references therein.
16. Armarego, W. L. F.; Perrin, D. D. *Purification of Laboratory Chemicals*; Butterworth Heinemann: Boston, 1996.
17. Mabry, J. M.; Vij, A.; Iacono, S. T.; Viers, B. M. *Angew. Chem.* **2007**, submitted for publication.
18. Koh, K.; Sugiyama, S.; Morinaga, T.; Ohno, K.; Tsujii, Y.; Fukada, T.; Yamahiro, M.; Iijima, T.; Oikawa, H.; Wantanbe, K.; Miyasitya, T. *Macromolecules* **2005**, *38*, 1264.
19. Iacono, S. T.; Budy, S. M.; Mabry, J. M.; Smith, D. W., Jr. *Macromolecules* **2007**, submitted for publication.
20. Iacono, S. T.; Budy, S. M.; Mabry, J. M.; Smith, D. W., Jr. *Adv. Mater.* **2007**, submitted for publication.
21. Young, T. *Philos. Trans. R. Soc.* **1805**, *95*, 65.
22. Cassie, A. B. D.; Baxter, S. *Trans. Faraday Soc.* **1944**, *40*, 546.
23. Wenzel, R. N. *Ind. Eng. Chem.* **1936**, *28*, 988.
24. Pal, S.; Weiss, H.; Keller, H.; Müller-Plather, F. *Langmuir* **2005**, *21*, 3699.
25. Rios, P. F.; Dodiuk, H.; Kenig, S.; McCarthy, S.; Dotan, A. *J. Adhes. Sci. Technol.* **2006**, *20*, 563.

Downloaded by DUKE UNIV on June 24, 2012 | http://pubs.acs.org
Publication Date (Web): November 9, 2010 | doi: 10.1021/bk-2010-1051.ch016

Downloaded by DUKE UNIV on June 25, 2012 | http://pubs.acs.org
Publication Date (Web): November 9, 2010 | doi: 10.1021/bk-2010-1051.ch017

## Chapter 17

# What Does It Take To Make a Stable POSS®/Polymer Composite?

**David A. Schiraldi*** **and Subramanian Iyer**

**Department of Macromolecular Science and Engineering,**
**Case Western Reserve University, Cleveland, OH 44106-7202**
***Correspondance: Das44@case.edu**

Polycarbonate (PC) and phenoxy resin have similar structures derived from bisphenol-A. Phenoxy resin possesses pendant hydroxyl groups along its backbone; instead of the carbonate carbonyls groups found in polycarbonate. This difference in structure significantly influences thermo-mechanical properties when these materials are blended with TPOSS, phenyl trisilanol polyhedral oligomeric silsesquioxanes. Composites of TPOSS with PC and with phenoxy resin were produced and characterized. The TPOSS was highly soluble in polycarbonate, interacted with phenyl groups in the polymer at a hierarchical level such that ring flipping motions were retarded, but individual bonds within the phenyl rings were not affected. The net result of this level of interaction was that TPOSS served as an antiplasticizer for polycarbonate. The TPOSS was also reasonably compatible with phenoxy resin, but exhibited considerable interactions with the polymer on a molecular level. The hydroxyl group on the phenoxy polymer was observed to hydrogen bond to the POSS silanol groups, and the phenyl groups in the polymer π-stacked with POSS-bound phenyls. With this two-fold binding between polymer and filler, a level of thermo/mechanical reinforcement was achieved; the suggested two-point binding can be thought of as a reversible, "supramolecular" grafting.

**Keywords:** composite; POSS; silsesquioxane; blending; structure; properties

In Advances in Silicones and Silicone-Modified Materials; Clarson, S., et al.;
ACS Symposium Series; American Chemical Society: Washington, DC, 2010.

Downloaded by DUKE UNIV on June 25, 2012 | http://pubs.acs.org
Publication Date (Web): November 9, 2010 | doi: 10.1021/bk-2010-1051.ch017

## Introduction

Polyhedral oligomeric silsesquioxanes, or POSS® are a family of nanoscale materials that have been well examined in the literature for over a decade, having been initially brought to market from an off-shoot of research and development carried out by the U.S. Air Force and their collaborators. These materials are now commercially available, and are finding uses in a diverse range of applications including dental composites (*1–3*), and photoresists (*4*). The majority of the published work in the field, however, has focused on enhancement of traditional polymeric materials. The rationale for such efforts is that the POSS grades, with their inherent hybrid inorganic-organic nature (Figure 1), would seem to be excellent candidates to provide molecular reinforcement. In such a scheme, the organic groups would act to increase compatibility with polymers, while the inorganic silicon oxide cage would serve as the stiff filler. POSS has been widely used to make copolymers with polyurethanes (*5*), polyethylenes (*6*), polystyrene (*7*), poly(methyl methacrylate) (*8*), polyimides (*9*, *10*) and thermosets (*11–17*). The mechanism of reinforcement in these copolymers is reasonably well understood, however the same cannot be said for composites produced by physical blending of polymers with POSS. Enhancement in polymer thermal and mechanical properties by selective addition of POSS has been reported (*18–21*). In our own hands, we have found such property enhancements to be possible and highly sensitive to the nature of the organic components on the POSS (Figure 2) (*22*). The ease with which POSS can be chemically modified to create a periphery which is compatible with, or even matches the structure of a matrix polymer is especially important for physical blends. An example of such an approach is from our work with polyesters and polyamides, in which polyether-containing POSS grades were produced and found to be compatible with the host polymers (Figure 3) (*23*). Modification of the central POSS cage to produce smectic liquid crystalline filler suitable for addition to smectic liquid crystalline polymers was also accomplished in a similar manner (*23*). In attempting to rationalize such reinforcement, the question of how/why such a system, with an aspect ration of 1 and a diameter of ca. 1-2 nm, could be expected to reinforce has been raised. One can ask whether POSS should be considered a nanoparticle or simply a large molecule. Some of the more successful POSS additives are liquids; how a liquid serves as a reinforcing filler is a fair question to ask, as is whether the fact that a POSS grade is a solid or liquid in the bulk has any real meaning for molecularly dispersed additives. Further complicating the issue are reports that POSS can form robust crystalline structure during processing (*22*, *24–26*), and that POSS can thermally degrade at a rate such that transformations of the filler must be considered a possibility when melt processing a polymer (Figure 4) (*27*). While the concepts of possible POSS degradation to produce silica-like particles, and/or aggregation of POSS into large domains remain possible components in reinforcing structures, it should be noted that transparent POSS nanocomposites which exhibit enhanced thermal/mechanical properties have been produced, and give no indication of detectable filler aggregates (Figure 5) (*28*). These questions serve as the backdrop for the present study, which intends to shed at least some light on the nature of interactions necessary to develop stable, useful polymer/POSS composites.

## Experimental

PKFE phenoxy resin was obtained from InChem Resins Inc. (Rock Hill SC), with reported number average and weight average molecular weights of 16,000 gm/mol and 60,000 gm/mol respectively. Polycarbonate (Makrolon® 2205) with a reported melt index of 35 was obtained from Bayer Material Sciences. Both polymers were used as received. Phenyl trisilanol POSS® (Hybrid Plastics) was used as received. The structures of the starting components are listed in Figure ().

The polymers were dried in a vacuum oven for 24 hours at 100°C prior to extrusion. Composites with different weight percentages of phenyl trisilanol POSS were prepared on a DACA microextruder (Model 2000) with co-rotating screws turning at 100 rpm and residence times of 5 minutes. Polycarbonate was processed at 260°C while phenoxy resin was processed at 230°C. Extruded samples were then compression molded on a Carver press (Model C) into films of approximately 0.3 mm thickness. These films were then used for characterization of materials.

### Characterization

Dynamic mechanical analyses (DMA) of the materials were carried out on a Thermal Analysis (TA) Q800 dynamic mechanical analyzer. Samples measuring 5mm in width and 15 mm in length were heated from 25°C to 180°C for polycarbonates (135°C for PKFE) at 3°C/minute in the tension mode at 1Hz, and amplitude of 20 microns. Differential scanning calorimetry (DSC) was carried out on a Mettler Toledo DSC model 822e/700. Samples were heated at 2 different ramp rates of 10°C/minute and 3°C/minute to separate the kinetic and thermodynamic effects and to relate to the results from the DMA. The data reported are the second heating cycles. Infrared Spectroscopy (IR) was carried out in the attenuated total reflection mode (ATR-IR) on a TravelIR (Sensir Technologies). ATR-IR samples were scanned from 650 $cm^{-1}$ to 4000 $cm^{-1}$ with a resolution of 2 $cm^{-1}$. All the data from the IR was normalized relative to the pure polymers. $^1H$ nuclear magnetic resonance (NMR) of PKFE/POSS and PC/POSS composites were carried out on a Varian 600 MHz machine to probe hydrogen bonding within the system and possible reactions occurring during melt blending. Samples for NMR titration experiments were prepared as follows; 2 solutions were prepared in deuterated chloroform, one containing 0.05M polymer and the other solution containing 0.05M polymer and 0.1M POSS. The molarities of the polymer solutions were calculated based on the molecular weight of the repeat unit and was kept constant to probe the effect of addition of POSS. Positron annihilation lifetime spectroscopy (PALS) was performed using the fast-fast coincident method with a time resolution of 230 ps, at a count rate of approximately $10^6$ counts/h (*29*, *30*). A 30 $\mu$Ci $^{22}NaCl$ positron source was sandwiched in between two compression molded films, each with thickness of 1 mm and 1 x 1 $cm^2$ area. All samples were run at room temperature. The positron

Downloaded by DUKE UNIV on June 25, 2012 | http://pubs.acs.org
Publication Date (Web): November 9, 2010 | doi: 10.1021/bk-2010-1051.ch017

Downloaded by DUKE UNIV on June 25, 2012 | http://pubs.acs.org
Publication Date (Web): November 9, 2010 | doi: 10.1021/bk-2010-1051.ch017

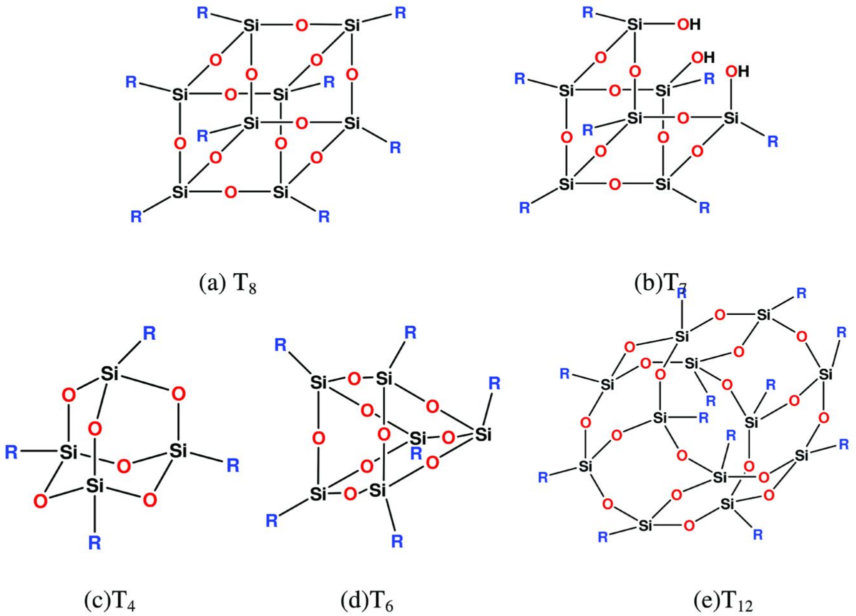

(a) $T_8$ (b)$T_7$

(c)$T_4$ (d)$T_6$ (e)$T_{12}$

*Figure 1. The range of POSS structures available*

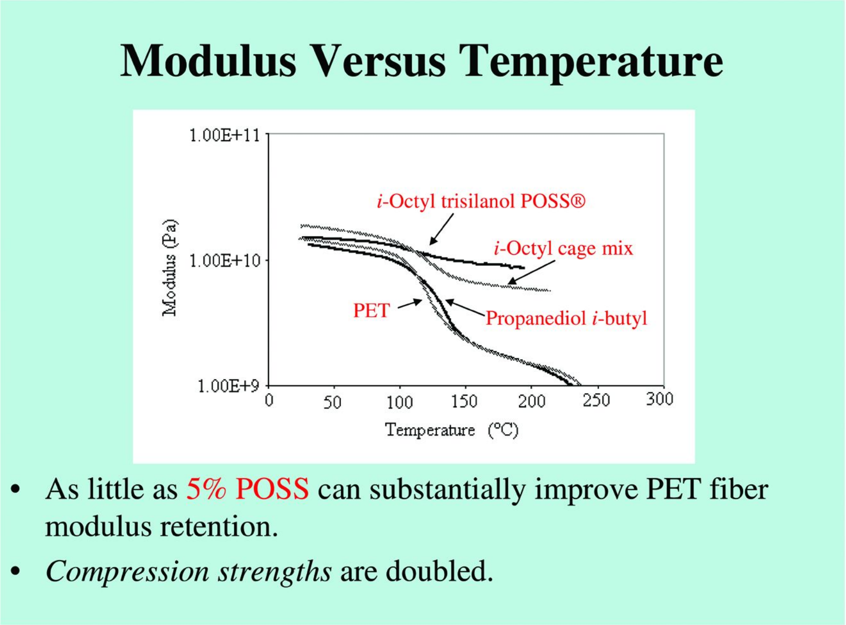

## Modulus Versus Temperature

- As little as 5% POSS can substantially improve PET fiber modulus retention.
- *Compression strengths* are doubled.

*Figure 2. Previous work with PET/POSS composite fibers showing reinforcement (22)*

Downloaded by DUKE UNIV on June 25, 2012 | http://pubs.acs.org
Publication Date (Web): November 9, 2010 | doi: 10.1021/bk-2010-1051.ch017

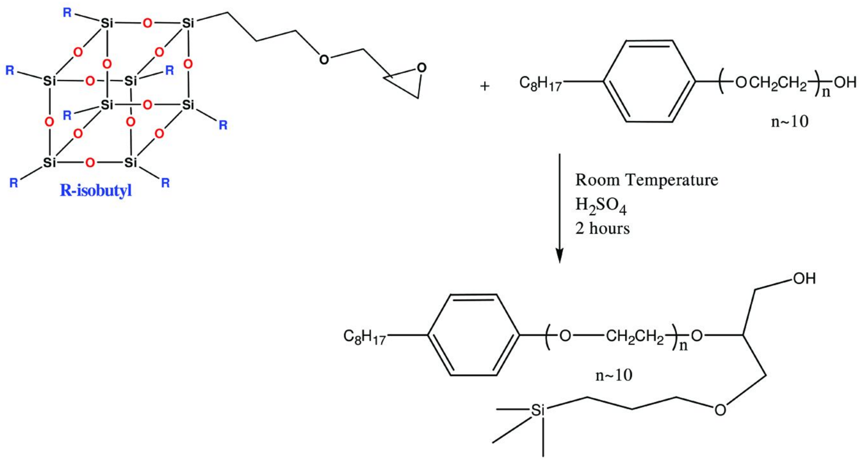

Figure 3. *Example of side-chain functionalization to derivatize POSS (23)*

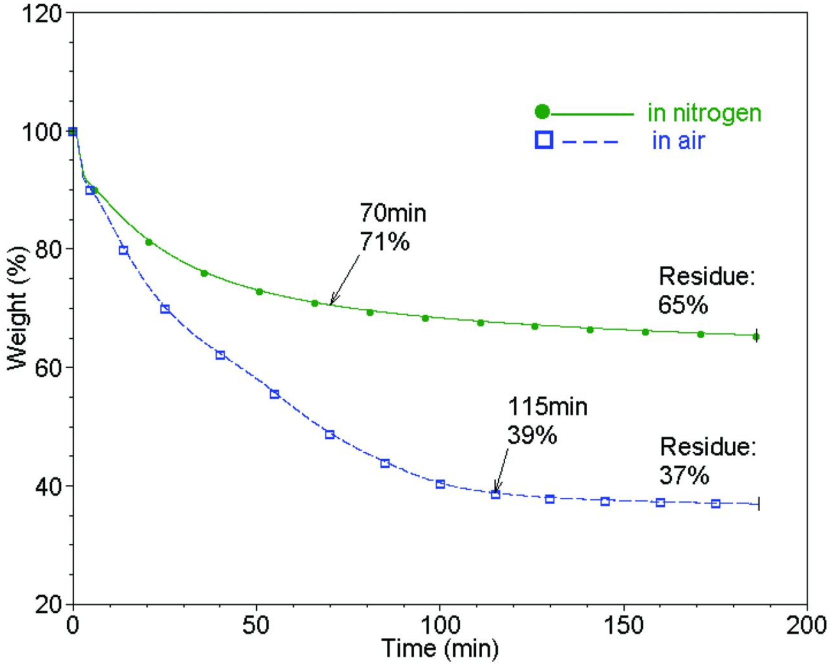

Figure 4. *Previous work showing thermal instability of POSS during processing (27)*

lifetime spectrum was determined by PATFIT software. The spectra were fitted to three exponentially decaying lifetime components. The average free volume hole radius ($r_h$) was calculated from the o-Ps lifetime ($\tau_3$) using the semi empirical equation (*31*, *32*),

Downloaded by DUKE UNIV on June 25, 2012 | http://pubs.acs.org
Publication Date (Web): November 9, 2010 | doi: 10.1021/bk-2010-1051.ch017

Hybrid Plastics™
714.962.0303
714.962.4924
Hybrid Plastics, Inc.
18237 Mt. Baldy Circle
Fountain Valley, CA 92708
www.hybridplastics.com

*Figure 5. Previous work with cellulose propionate to produce transparent materials (28)*

$$\tau_3\,(\mathrm{ns}) = 0.5\left[1 - \frac{r_h}{r_h + \delta r} + \frac{1}{2\pi}\sin\left(\frac{2\pi r_h}{r_h + \delta r}\right)\right]^{-1}$$

where $\delta r$ has been empirically determined to be $\delta r = 0.1656$ nm by fitting above equation to the o-Ps annihilation data for molecular solids of known pore size (*32*). The uncertainty in $r_h$ based on 10 spectra was (0.03 Å).

## Results

A comparison of polycarbonate (PC) and phenoxy resin was chosen for this work as these two polymers present similar structural backbones, the latter also possessing the possibility of hydrogen bonding absent in polycarbonate (*33*). Trisilanol phenyl POSS ("TPOSS") was chosen with design elements of possible hydrogen bonding and π-stacking in mind. A previous study in which a range of POSS grades were screened as additives to PC suggested TPOSS would have a greater compatibility and impact upon this polymer than other common grades available (*34*). Phenoxy resin composites with up to 15 wt% phenyl trisilanol POSS were optically transparent; these composites were then translucent up to 25 wt% POSS content. The analogous polycarbonate composites remained transparent up to 20 wt% POSS content. These results indicate that either the POSS is dispersed on the nanoscale in the composites or that POSS is soluble with both polymers up to at least 15-20 wt%.

DSC Traces for polycarbonate and phenoxy resin melt mixed with a range of TPOSS loadings are given in Figure 7 and Figure 8, respectively. The polycarbonate blends show a monotonic decrease in $T_g$ with increasing levels of TPOSS added. The phenoxy resin behaved quite differently, exhibiting increasing $T_g$ with added TPOSS up to 15 wt%, above which the glass transition temperature began to decrease. It is interesting to note that while TPOSS itself possesses a sharp crystalline melting point in the bulk, when combined with either of the polymers of this study, this melting point is not observed, consistent with molecular scale dispersion of the filler. The disappearance of dispersed POSS melting points was observed previously in polycarbonate composites (*34*). The polycarbonate DSC results are suggestive of simple plasticization, whereas the phenoxy resin/TPOSS thermal results are indicative of a more complex behavior.

Dynamic mechanical behavior of polycarbonate combined with TPOSS is given in Figure 9, suggestive of simple plasticization, consistent with the DSC results obtained with these materials. In Figure 10, the DMA spectra of phenoxy resin/TPOSS are given, again consistent with DSC results, showing increased $T_g$ up to 15 wt% TPOSS addition; an increase of up to 50% in the room temperature modulus, and as much as 200% in the rubbery modulus of phenoxy resin was observed with increasing levels of POSS filler. It should be noted that polycarbonate/POSS samples became noticeably brittle with increasing POSS levels, whereas no such effect was noted for the phenoxy resin blends. Neither FTIR nor fluorescence spectroscopy of polycarbonate/TPOSS composite materials yielded measurable differences that could be used to shed light on material structural behaviors. For the phenoxy resins, changes in the C-C stretch region (1502-1510 cm-1) in the FTIR (Figure 11) are indicative of binding to the 1,4-substituted phenyl rings (*35*, *36*). and fluorescence spectroscopy (Figure 12), shows a systematic shift in the bisphenol-A band consistent with π-π stacking. In contrast to these behaviors, the low temperature DSC of PC/TPOSS blends showed a significant retardation in the low temperature transition most likely associated with phenyl ring flips (Figure 13), whereas no such change was observed for phenoxy/TPOSS systems. This difference, wherein TPOSS significantly affects the phenyl rings in phenoxy resin, but affects chains containing phenyl rings in polycarbonate, points to scale effects in filler/matrix interactions. In the polycarbonate system, the highly soluble POSS material appears to be generally associated with the phenyl groups of the polymer (note that the polycarbonate FTIR carbonyl stretches are not noticeably affected by the presence of POSS). In the phenoxy resin system, TPOSS appears to sit atop the backbone phenyl rings, changing the nature of bonding in the polymer. To further probe bonding between TPOSS and phenoxy resin, the $^1$H NMR chemical shifts of polymer hydroxyl groups were measured as a function of added TPOSS (Figure 14). It has been well demonstrated that hydrogen bonding leads to a downfield shift and broadening of the free hydroxyl proton in polymers. The observed behavior in the NMR for phenoxy resin and TPOSS follows this behavior exactly as would be expected for a hydrogen bonding system. The PC/POSS composites do not show a significant chemical shift for any of the $^1$H NMR peaks.

Finally, free volumes in the subject composite materials were probed using positron annihilation lifetime spectroscopy (Figure 15). The results demonstrated an increase in the free volume radius as well as concentration of holes in phenoxy resin composites with increasing percentage of POSS. However, in the PC/POSS systems, the size of the holes remained constant while the concentration of holes increased with POSS loading.

Downloaded by DUKE UNIV on June 25, 2012 | http://pubs.acs.org
Publication Date (Web): November 9, 2010 | doi: 10.1021/bk-2010-1051.ch017

Downloaded by DUKE UNIV on June 25, 2012 | http://pubs.acs.org
Publication Date (Web): November 9, 2010 | doi: 10.1021/bk-2010-1051.ch017

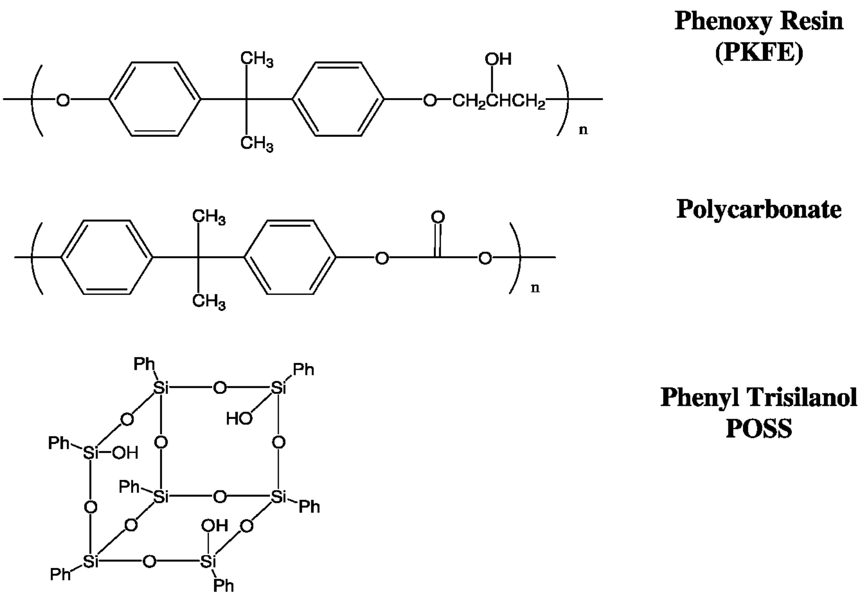
Phenoxy Resin (PKFE)
Polycarbonate
Phenyl Trisilanol POSS

*Figure 6. Materials use in the present work*

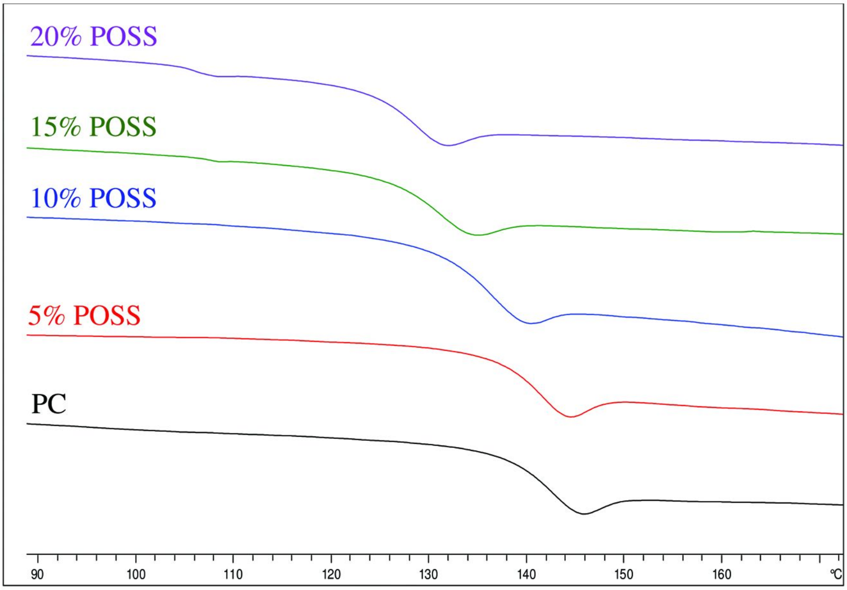

*Figure 7. DSC Traces for polycarbonate/POSS blends, 10°C/min scan rate (33)*

Downloaded by DUKE UNIV on June 25, 2012 | http://pubs.acs.org
Publication Date (Web): November 9, 2010 | doi: 10.1021/bk-2010-1051.ch017

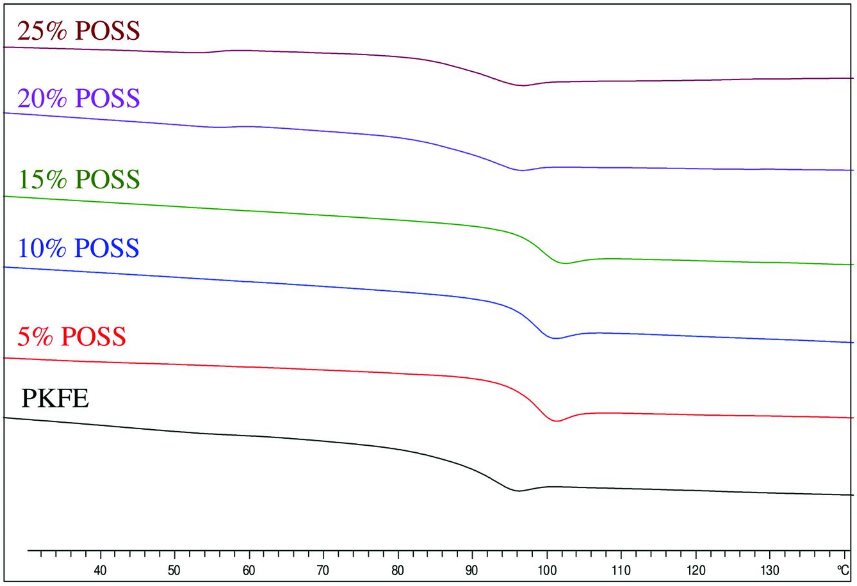

*Figure 8. DSC Traces for phenoxy resin/POSS blends, 10°C/min scan rate (33)*

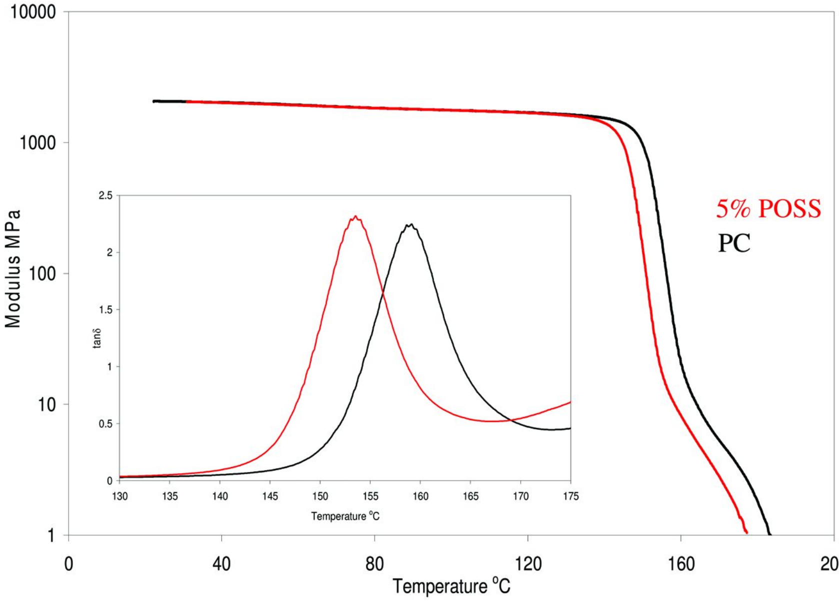

*Figure 9. DMA Traces for polycarbonate/POSS blends, 3°C/min scan rate (33)*

Downloaded by DUKE UNIV on June 25, 2012 | http://pubs.acs.org
Publication Date (Web): November 9, 2010 | doi: 10.1021/bk-2010-1051.ch017

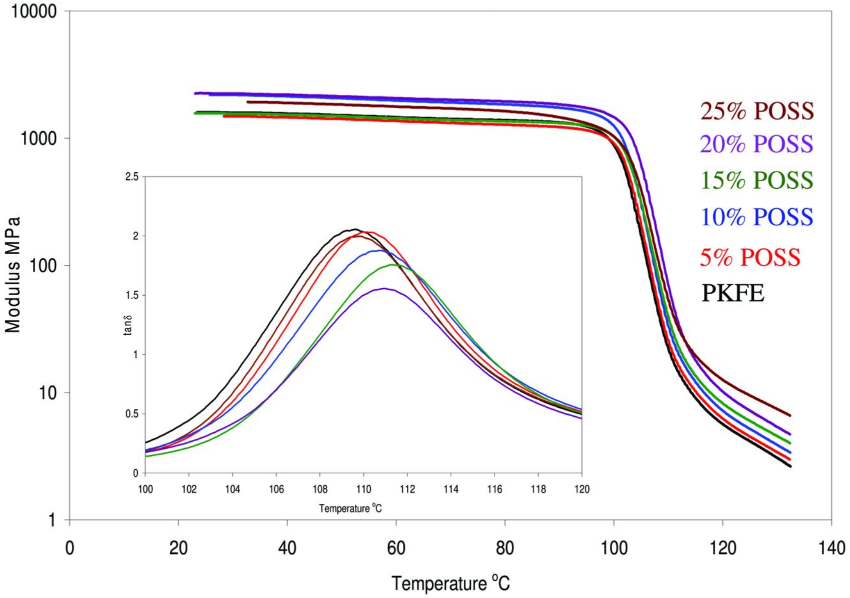

*Figure 10. DMA Traces for phenoxy resin/POSS blends, 3°C/min scan rate (33)*

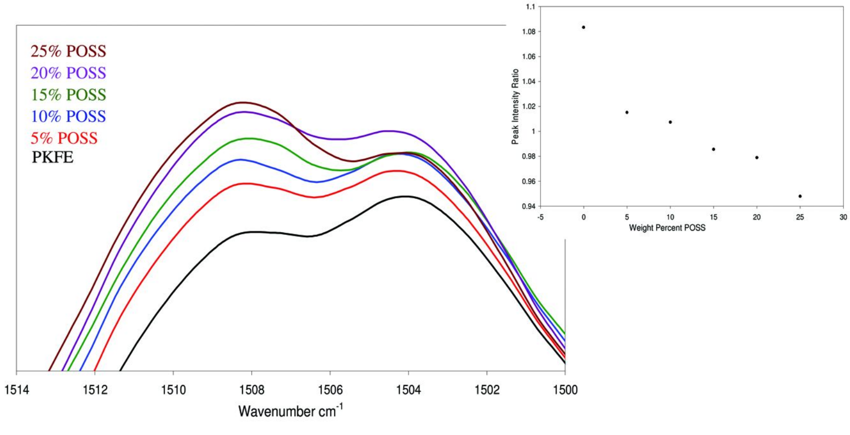

*Figure 11. Changes in the C-C FTIR stretches for phenoxy resin/POSS blends (33)*

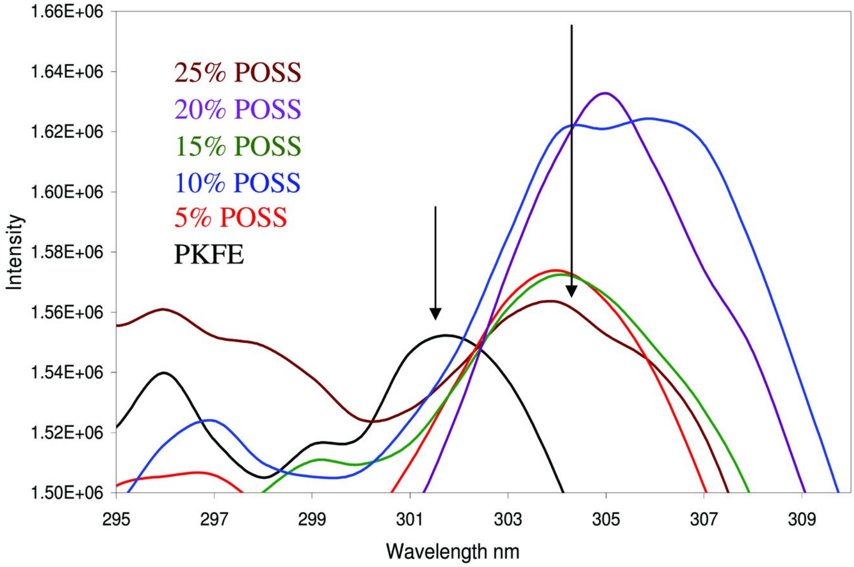

*Figure 12. Changes in the fluorescence spectra for phenoxy resin/POSS blends (33)*

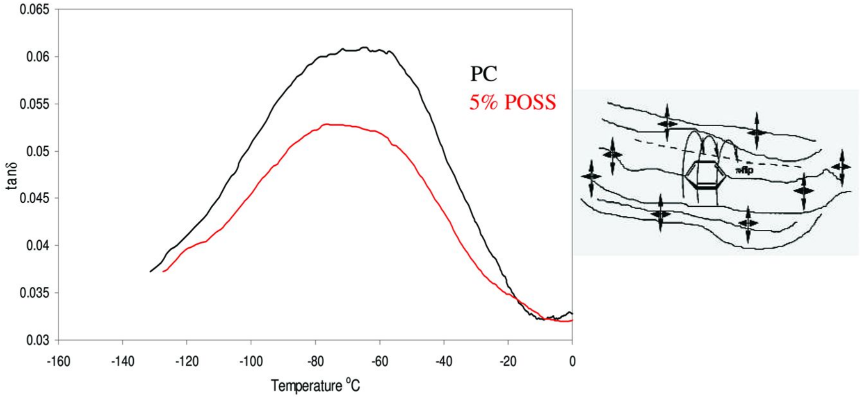

*Figure 13. Changes in the fluorescence spectra for polycarbonate/POSS blends*

Downloaded by DUKE UNIV on June 25, 2012 | http://pubs.acs.org
Publication Date (Web): November 9, 2010 | doi: 10.1021/bk-2010-1051.ch017

Downloaded by DUKE UNIV on June 25, 2012 | http://pubs.acs.org
Publication Date (Web): November 9, 2010 | doi: 10.1021/bk-2010-1051.ch017

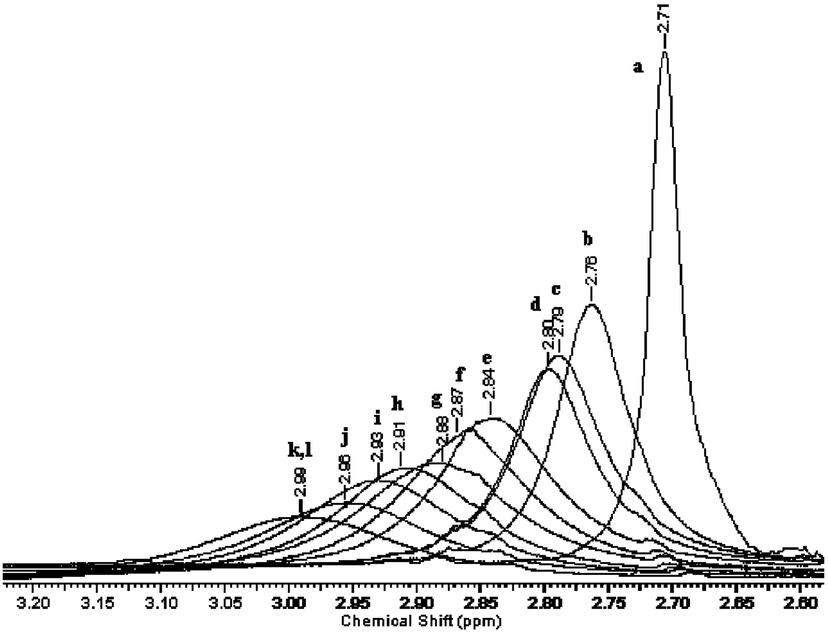

*Figure 14. Proton NMR of phenoxy resin/POSS showing hydroxyl group shift (33)*

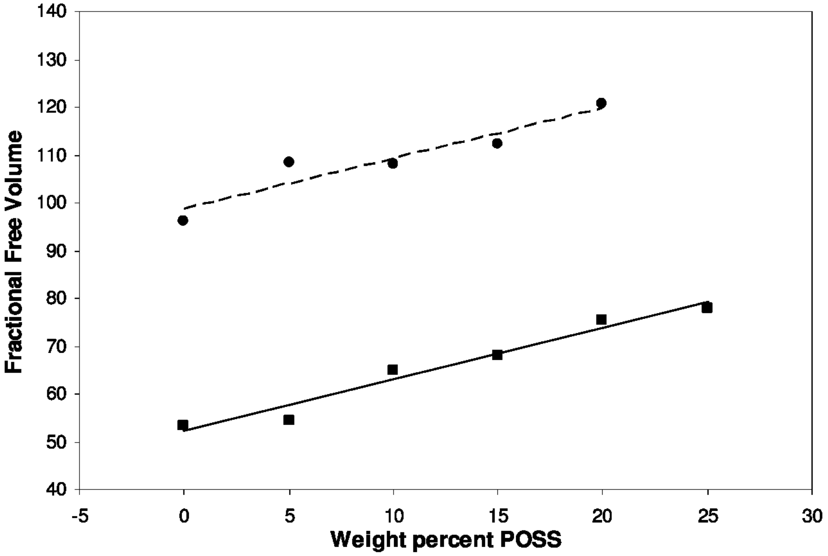

*Figure 15. PALS Free volume measurements; top PC, bottom phenoxy resin (33)*

Downloaded by DUKE UNIV on June 25, 2012 | http://pubs.acs.org
Publication Date (Web): November 9, 2010 | doi: 10.1021/bk-2010-1051.ch017

## Discussion

The data obtained from the DMA and DSC experiments in this study demonstrate that the hydroxyl groups in phenoxy resin strongly influence the properties of PKFE/POSS composites, whereas the carbonyl analog to this polymer, PC, lacks any such specific interactions with POSS. Decreases in composite $T_g$ values, accompanied with embrittlement of PC/POSS composites suggest antiplasticization behavior. Antiplasticization in glassy polymers, especially in polycarbonates has been studied in great detail and is believed to occur due to suppression of the low temperature beta transition of the material. The low temperature β transition in polycarbonate is caused by the flipping motion of the bisphenol-A segment, which is responsible for the high impact strength of the material (*37*, *38*). Our low temperature DMA scans on the polycarbonate composites with 5 wt% POSS indeed demonstrate significant lowering of the intensity of this low temperature tanδ peak. The addition of POSS inhibits the motion of the phenylene ring π-flip, thus limiting movement and reducing the toughness of the material. Similar effects of antiplasticization has been seen in compatible polycaprolactone/polycarbonate blends (*39*). While the results from DSC and DMA studies reveal significant loss in chain motion leading to a stiff material, the increase in the number of o-Ps annihilations with the addition of POSS indicates an increase in the free volume. The increase in free volume is known to be an indication of material plasticization. An increase in free volume with significant antiplasticization of the polymer is one of the new findings of this research (*33*). Thus POSS acts as an internal molecular lubricant in these systems. Depending on whether the polymers have significant low temperature transitions (ductile-brittle transition) soluble POSS can act either as a plasticizer or an antiplasticizer in the polymer.

In the case of phenoxy resin/POSS composites, the opposite effect to that of polycarbonate is observed. The addition of POSS enhances the mechanical performance of the material. Infrared spectroscopy demonstrates significant interactions between the phenoxy resin and the POSS particles, perhaps caused by preferential stacking of phenyl rings, possibly facilitated by hydrogen bonding between the hydroxyls groups between the polymer and POSS. The NMR titration data further supports this hypothesis.

Low temperature DMA scans of phenoxy resin and its composites with POSS also exhibits a low temperature phenylene π-flip motion, similar to that observed in PC. In phenoxy resin composites, however, unlike the case with PC composites, there is no suppression of this phenylene π-flip motion. We propose that the majority of POSS molecules that are soluble in the phenoxy resin matrix are tethered to the chain via hydrogen bonding and π-π stacking.

The addition of POSS does not affect the free volume hole size within polycarbonate composites, but does so for the phenoxy resin. The complicated variation of free-volume hole fractions in immiscible/partially miscible composites observed by the PALS technique is a result of the high sensitivity of the o-Ps particle not only to free-volume holes but also to any interfacial spaces, such as those created between boundaries of two phases (*40*). Since a higher percentage of free volume is created by the interphase region in phenoxy resin/POSS composites, as compared to PC/POSS composites, there is an increase in the overall free volume as well. The reasons for the constant free volume in PC/POSS composites could be due to significant solubility of POSS in polycarbonate and/or improved adhesion between phases. In the case of phenoxy resin/POSS composites, the possible increase in free volume could be caused by the higher excluded volume between the phases. Thus while the significant polymer/filler interactions (hydrogen bonding and phenyl stacking) in phenoxy resin/POSS composites act to improve the thermo-mechanical performance of the composite by increasing its glass transition, the increase in free volume of the composites due to incorporation of POSS tends to decrease the glass transition temperature of the composites. Up to 15 wt% loading of POSS in phenoxy resin, hydrogen bonding and π-π stacking interactions dominate the thermal behavior of the system, whereas above 15 wt% the thermal behavior is controlled by the free volume of the composite.

Downloaded by DUKE UNIV on June 25, 2012 | http://pubs.acs.org
Publication Date (Web): November 9, 2010 | doi: 10.1021/bk-2010-1051.ch017

## Conclusions

Composites of trisilanolphenyl POSS with polycarbonate and with phenoxy resin were produced and characterized. The TPOSS was highly soluble in polycarbonate, interacted with phenyl groups in the polymer at a hierarchical level such that ring flipping motions were retarded, but individual bonds within the phenyl rings were not effected. The net result of this level of interaction was that TPOSS served as an antiplasticizer for polycarbonate. The TPOSS was also reasonably compatible with phenoxy resin, but exhibited considerable interactions with the polymer on a molecular level. The hydroxyl group on the phenoxy polymer was observed to hydrogen bond to the POSS silanol groups, and the phenyl groups in the polymer π-stacked with POSS-bound phenyls. With this two-fold binding between polymer and filler, a level of thermo/mechanical reinforcement was achieved; the suggested two-point binding can be thought of as a reversible, "supramolecular" grafting of filler on polymer, resulting in property enhancements similar to those obtained with covalent POSS copolymers. These results are consistent with other POSS/polymer blends in the literature, and suggest that with means of producing strong non-covalent grafts of POSS to polymer, and probably not overemphasizing POSS solubility in polymer, property enhancement should be more generally available.

POSS® is a registered trademark of Hybrid Plastics Inc.

## References

1. Soh, M. S.; Yap, A. U. J.; Sellinger, A. *Eur. J. Oral Sci.* **2007**, *115*, 230–8.
2. Soh, M. S.; Yap, A. U. J.; Sellinger, A. *Eur. Polym. J.* **2007**, *43*, 315–27.
3. Fong, H.; Dickers, S. H.; Flaim, G. M. *Dent. Mater.* **2005**, *21*, 520–9.
4. Ali, M. A.; Gonsalves, K. E.; Agrawal, A.; Jeyakumar, A.; Henderson, C. L. *Microelectron. Eng.* **2003**, *70* (1), 19–29.
5. Fu, B. X.; Hsiao, B. S.; White, H.; Rafailovich, M.; Mather, P. T.; Jeon, H. G.; Phillips, S.; Licthenhan, J.; Schwab, J. *Polym. Int.* **2000**, *49* (5), 437.

6. Zheng, L.; Kasi, R. M.; Farris, R. J.; Coughlin, E. B. *Polym. Mater.: Sci. Eng.* **2001**, *84*, 114.
7. Zheng, L.; Kasi, R. M.; Farris, R. J.; Coughlin, E. B. *J. Polym. Sci., Part A: Polym. Chem.* **2002**, *40*, 885.
8. Patel, R. R.; Mohanraj, R.; Pittman, C. U., Jr. *J. Polym. Sci., Part B: Polym. Phys.* **2005**, *44* (1), 234.
9. Leu, C.-M.; Reddy, M.; Wei, K.-H.; Shu, C.-F. *Chem. Mater.* **2003**, *15*, 2261–5.
10. Lin, W.-J.; Chen, W.-C. *Polym. Int.* **2004**, *53*, 1245–52.
11. Ni, Y.; Zheng, S. *Macromol. Chem. Phys.* **2005**, *206* (20), 2075.
12. Constable, G. S.; Lesser, A. J.; Coughlin, E. B. *Macromolecules* **2004**, *37*, 1276–82.
13. Zeng, K.; Zheng, S. *J. Phys. Chem. B* **2007**, *111*, 13919–28.
14. Mather, P. T.; Jeon, H. G.; Romo-Uribe, A.; Haddad, T. S.; Lichtenhan, J. D. *Macromolecules* **1999**, *32*, 1194.
15. Romo-Uribe, A.; Mather, P. T.; Haddad, T. S.; Lichtenhan, J. D. *J. Polym. Sci., Part B: Polym. Phys.* **1998**, *36*, 1857.
16. Kim, G.-M.; Qin, H.; Fang, X.; Sun, F. C.; Mather, P. T. *J. Polym. Sci., Part B: Polym. Phys.* **2003**, *41*, 3299.
17. Lee, A.; Lichtenhan, J. D. *J. Appl. Polym. Sci.* **1999**, *73*, 1993.
18. Laine, R. C.; Brick, C.; Kim, S.-G.; Tamaki, R.; Chen, H.-J.; Choi, J. *Materials Chemistry*, 225th American Chemical Society National Meeting, New Orleans, LA, March 2003; Paper 11.
19. Schiraldi, D. A.; Zeng, J.; Kumar, S.; Iyer, S.; Dong, F. *Materials Chemistry*, 225th American Chemical Society National Meeting, New Orleans, LA, March 2003; Paper 9.
20. Esker, A. R.; Vastine, B. A.; Deng J.; Polidan, J. T.; Viers, B. D.; Satija. S. K. *Materials Chemistry*, 225th American Chemical Society National Meeting, New Orleans, LA, March 2003; Paper 2.
21. Coughlin, E. B. *Polymer Chemistry*, 228th American Chemical Society National Meeting, Philadelphia, PA, August 2004; Paper 275.
22. Zeng, J.; Iyer, S.; Gonzalez, R.; Kumar, S.; Schiraldi, D. A. *High Perform. Polym.* **2005**, *17*, 403–424.
23. Iyer, S.; Somlai, A.; Schiraldi, D. A. In *Polymers and Composites: Synthesis, Properties, and Applications (Polymer Yearbook)*; Pethrick, R. A., Zaikov, G. E., Thomas, D. H., Eds.; Nova Science Publishers: Hauppauge, NY, 2007; Vol. 21, pp 77−87.
24. Deng, J.; Farmer-Creely, C. E.; Viers, B. D.; Esker, A. R. *Langmuir* **2004**, *20*, 2527–30.
25. Deng, J.; Viers, B. D.; Esker, A. R. *Langmuir* **2005**, *21*, 2375–85.
26. Paul, R.; Esker, A. R. *Langmuir* **2006**, *22*, 6734–8.
27. Zeng, J.; Bennett, C.; Jarrett, W.; Iyer, S.; Kumar, S.; Mathias, L. J.; Schiraldi, D. A. *Compos. Interfaces* **2005**, *11*, 673–87.
28. Iyer, S.; Abu-Ali, A., Detwiler, A., Schiraldi, D. A. Transparent Polymer/Polyhedral Oligomeric Silsesquioxane (POSS®) Composites. In *Science and Technology of Silicones and Silicone-Modified Materials*; Clarson, S. J., Fitzgerald, J. J., Owen, M. J., Smith, S. S., Van Dyke,

Downloaded by DUKE UNIV on June 25, 2012 | http://pubs.acs.org
Publication Date (Web): November 9, 2010 | doi: 10.1021/bk-2010-1051.ch017

M. E., Eds.; ACS Symposium Series 964; American Chemical Society: Washington, DC, 2007; pp 313−325.

29. Srithawatpong, R.; Peng, Z. L.; Olson, B. G.; Jamieson, A. M.; Simha, R.; McGervey, J. D.; Maier, T. R.; Halasa, A. F.; Ishida, H. *J. Polym. Sci., Part B: Polym. Phys.* **1999**, *37*, 2754.
30. Kluin, J. E.; Yu, Z.; Vleeshouwers, S.; McGervey, J. D.; Jamieson, A. M.; Simha, R.; Sommer, K. *Macromolecules* **1993**, *26*, 1853–1861.
31. Tao, S. J. *J. Chem. Phys.* **1972**, *56*, 5499.
32. Nakanishi, N.; Jean, Y. C. In *Positron and Positronium Chemistry: Studies in Physical Theoretical Chemistry*; Schrader, D. M., Jean, Y. C., Eds.; Elsevier Science Publisher: Amsterdam, 1988; Vol. 57, pp 159−192.
33. Iyer, S.; Schiraldi, D. A. *Macromolecules* **2007**, *40*, 4942–52.
34. Zhou, Y.; Schiraldi, D. A. *Polymer* **2005**, *46*, 11640–7.
35. Garcia, E. I. *J. Polym. Sci., Polym. Phys. Ed.* **1984**, *22*, 107.
36. Yoong, S. Y.; Cohen, R. E.; Boyce, M. C.; Mulliken, A. D. *Macromolecules* **2006**, *39*, 2900.
37. Kim, G.-M.; Qin, H.; Fang, X.; Sun, F. C.; Mather, P. T. *J. Polym. Sci., Part B: Polym. Phys.* **2003**, *41*, 3299.
38. Lee, A.; Lichtenhan, J. D. *J. Appl. Polym. Sci.* **1999**, *73*, 1993.
39. Liu, J.; Jean, Y. C. *Macromolecules* **1995**, *28*, 5774.
40. Shuster, M.; Narkis, M.; Siegmann, A. *Polym. Eng. Sci.* **1994**, *34* (21), 1613.

Downloaded by DUKE UNIV on June 25, 2012 | http://pubs.acs.org
Publication Date (Web): November 9, 2010 | doi: 10.1021/bk-2010-1051.ch017

Downloaded by CORNELL UNIV on June 24, 2012 | http://pubs.acs.org
Publication Date (Web): November 9, 2010 | doi: 10.1021/bk-2010-1051.ch018

## Chapter 18

# The Role of Non-Bonded Interactions in Silica Formation in Vitro

**Siddharth V. Patwardhan,[1] David Belton, Graham Tilburey,[2] and Carole C. Perry***

**School of Biomedical and Natural Sciences, Nottingham Trent University, Clifton Lane, Nottingham NG11 8NS, U.K.**
**[1]Present address: Chemical and Process Engineering, University of Strathclyde, Glasgow G1 1XJ, U.K.**
**[2]Present address: Department of Mechanical and Industrial Engineering, Northeastern University, Boston, MA 02108, U.S.A.**
***Email: Carole.Perry@ntu.ac.uk**

In nature, several classes of biosilicifying organisms process soluble silicon to generate hierarchically organised ornate biogenic silica structures under mild conditions of pH and temperature. The organisms are also able to ‘shape’ the silica and generate composite materials that whilst living are able to stand the rigours of a ‘wet’ or ‘dry’ environment according to the organism itself. The silica structures are formed from an aqueous environment, probably rich in ions, small molecules and biopolymers such as proteins and carbohydrates. In order to understand the chemistry underpinning the formation of such composite materials, ‘simple’ bioinspired solution studies have been performed. Ions, small molecules and polymers affect silica condensation reactions *in vitro*. This contribution considers the role of non-bonded interactions such as electrostatic interactions, hydrogen bonding, van der Waals interactions and the hydrophobic effect in modifying both the rate of silica formation and the nature of the final product.

In Advances in Silicones and Silicone-Modified Materials; Clarson, S., et al.;
ACS Symposium Series; American Chemical Society: Washington, DC, 2010.

Downloaded by CORNELL UNIV on June 24, 2012 | http://pubs.acs.org
Publication Date (Web): November 9, 2010 | doi: 10.1021/bk-2010-1051.ch018

## Introduction

Silica and silicates are extensively used in industry and medicine. The materials find use in paints, foods, medicines, adhesives, detergents, chromatography materials, catalysts and photonic materials (*1–3*) and it has been estimated that the global market for silica is around two billion dollars per year (*4*). Millions of tons of silica-based materials are made using a wide range of synthetic procedures that often employ harsh conditions of temperature and/or pH (acidic (*5*) and basic). As well as high temperature routes to produce pyrolytic silicas, liquid phase processing (aqueous and non-aqueous) may be used to generate silicas that vary in particle size, degree of aggregation, porosity and surface functionality (*6*, *7*). Many of the industrial processes generate harmful by-products. Whatever the eventual use of the silica, it is its structure that determines its properties. By structure we mean order and organization on length scales from angstroms to the size of the final object, morphology, surface area, porosity and surface functionality.

In contrast, biological organisms from bacteria, single-celled protists, plants, invertebrates and vertebrates process orders of magnitude more silicon (~6.7x 10 (*9*) tpa) (*8*) than that produced industrially (~ 1x 10 (*6*) tpa) (*4*) and all of the biosilica is produced under benign or ‘green’ conditions using controlled aqueous chemistry. Minerals formed in the biological environment may have unusual physical properties (e.g., strength, degree of hydration) and the structures formed are genetically invariant and often exhibit order on many length scales. The biominerals are formed from an environment that is undersaturated with respect to silicon and under conditions of around neutral pH and low temperature *ca.* 4–40°C. Formation of biominerals may occur intra- or extra-cellularly and specific biochemical locations for mineral deposition that include lipids, proteins and carbohydrates are known (*9*). The formation of the biomineral phase is linked to cellular processes but at the molecular level it is clear that there will be intimate interactions between the biomineral (precursors and intermediates) as it develops and the chemical functionalities presented by the biomolecules in the biomineralising environment.

This chapter will describe non-bonded interactions and provide an overview of silicic acid condensation. Our experimental approach to the study of this process will be given and examples of the effect of non-bonded interactions (NBI) between additives and silica species on the material formed given. It should also be noted that intermolecular interactions between molecules themselves can lead to self-assembled structures and that these too can modify both the kinetics of silica formation and the form of the silica generated (*5*, *10–12*). Such behaviour will not be addressed further in this contribution.

## Non-Bonded Interactions

Non-bonded interactions operate between atoms that are not linked together by covalent bonds. Non-bonded interactions vary in strength from 0.1 kcal/mol to several hundreds of kcal/mole depending on the environment in which the interaction occurs (vacuum through to water) and the nature of the specific

Downloaded by CORNELL UNIV on June 24, 2012 | http://pubs.acs.org
Publication Date (Web): November 9, 2010 | doi: 10.1021/bk-2010-1051.ch018

interaction. In solution reactions, especially those taking place within a living organism, the medium for the reaction is water, except for reactions that occur in specific membrane-like compartments. However, reactions in life do not occur in 'deionised water' free from additives rather in a medium that contains ions and molecules and all of these are available for interaction, in principle, with other species that may be present. The same may be true for laboratory based reactions although here the number of components and the amounts of each component can be regulated. Non-bonded interactions include electrostatic interactions, hydrogen bonding, van der Waals interactions and the hydrophobic effect. As a comparison, covalent bond energies are of the order of 60-250 kcal/mol. Electrostatic interactions in water are of the order of 1-15 kcal/mole, hydrogen bonds are of the order of 2-5 kcal/mole, van der Waals interactions are of the order of 0.5-1 kcal/mole and the hydrophobic effect is of the order of 1 kcal/mole.

The effect of charge, distance and environment for reaction on the strength of non-bonded interactions can be understood by consideration of Coulomb's law where attraction between species of opposite charges (generally considered for positively charged nuclei and negatively charged electrons but can be more generally applied to any species for which there is a separation of charge) is represented as:

$$V = q_i q_j / 4\pi \varepsilon_0 \varepsilon_r r_{ij} \qquad (1)$$

where $q_i$, $q_j$ are charges, $r_{ij}$ is their separation, $\varepsilon_0$ is the permittivity of free space and $\varepsilon_r$ the relative dielectric constant of the medium (for water ca. 80, for methanol ca. 35 and for a lipid bilayer *ca.* 2). The charges may be taken as formal charges but partial charges may also need to be considered for some reacting species. The dielectric constant is dimensionless and accounts for solvation and charge shielding due to the presence of the solvent. Note that the effect of charge is felt much more strongly in a lipid bilayer than in a non aqueous solvent such as methanol than in water! Part of this effect has to do with the ability of particular solvents to hydrate ions (by attraction between the solvent molecule and the solute) such that they effectively enlarge the ions. This enlargement effectively shields the charges from each other thus diminishing the strength of interaction between such species.

Hydrogen bonds arise from electronegativity differences between an element and the hydrogen atom it is attached to that lead to a redistribution of charge within the covalent bond joining the two elements. For a hydrogen bond to form there needs to be one molecule with an electronegative element attached to hydrogen and another molecule containing an electronegative element. Clearly, for reactions in water, where there is an infinite network of hydrogen bonds, any additional hydrogen bonds that form between specific atoms must overcome the network present in water. This clearly happens when protein folding occurs to give the secondary building blocks, alpha helices and beta sheets that further fold to generate specific conformations of active proteins.

Van der Waals interactions are important for uncharged atoms as they come close together in space. The effect of one atom on another is to deform the electron cloud due to electronic repulsion. This sets up transient dipoles on both

Downloaded by CORNELL UNIV on June 24, 2012 | http://pubs.acs.org
Publication Date (Web): November 9, 2010 | doi: 10.1021/bk-2010-1051.ch018

atoms resulting in a weak attractive interaction between them, the so-called van der Waals interactions. Van der Waals interactions are weak but it is a result of these interactions that geometric specificity is achieved in biological systems.

The hydrophobic effect operates when there is a mixing of polar (e.g. water) and non-polar (e.g. oil) molecules. The effect is not due to the hydrophobic groups themselves rather due to a reorganisation of the solvent to minimise the amount of water, for example, that is not ordered in its normal fashion through hydrogen bonds etc.

Although non-bonded interactions are individually much weaker than covalent interactions, when they act in concert, as in a protein or a drug-receptor complex or indeed for a condensation reaction in the presence of additives as proposed here, their effect is cumulative and all non-bonding interactions will collectively operate to reduce the free energy of the reaction system, whatever it is. The non-bonded interactions pertinent for silica formation in the presence of additives are schematically represented in Figure 1.

## Silica Polymerisation

As has been described before (*1*, *3*, *13*), orthosilicic acid at 25°C is stable at levels below *ca.* 100 ppm (~ 1 mM). At higher concentrations, polymerisation occurs, which involves three distinct stages:

1. Polymerisation to form stable nuclei
2. Growth of nuclei leading to fundamental particles
3. Particle aggregation to form branched networks, larger particles or other structures.

The polymerisation of monosilicic acid in an aqueous phase generates one molecule of water for each condensation reaction that occurs. In the early stages of silica formation, rapid condensation reactions yield a range of oligomers that serve as nuclei. Typically these stable nuclei are of size 1-2 nm, possess an anhydrous $SiO_2$ core and surface silanol groups (Si-OH). Based on particle size, the composition of particles can be estimated as described by Iler (*1*).

The addition of small oligomers onto these nuclei and coalescence of these nuclei leads to particle growth. The particles can grow by aggregation, by Ostwald ripening and/or by ‘necking’ between coalesced particles. Assuming instantaneous coalescence, aggregation of particles is typically a consequence of collision between smaller particles. The rate of aggregation depends on the collision frequency, which is a function of the transport properties of the medium, pH, temperature and particle concentration. As polymerisation proceeds, the $pK_a$ of the particles/polysilicic acids decreases from *ca.* 9.8 for orthosilicic acid to *ca.* 6.8 for colloidal particles (*2*). It is important to note that even at circumneutral pH, the silica particles bear a negative charge in solution. The consequence of this is that as condensation progresses there are more charges/ charged species present in the condensing system. Surface charge plays an important role in particle aggregation. Charge may also have an effect on Ostwald ripening, the

Downloaded by CORNELL UNIV on June 24, 2012 | http://pubs.acs.org
Publication Date (Web): November 9, 2010 | doi: 10.1021/bk-2010-1051.ch018

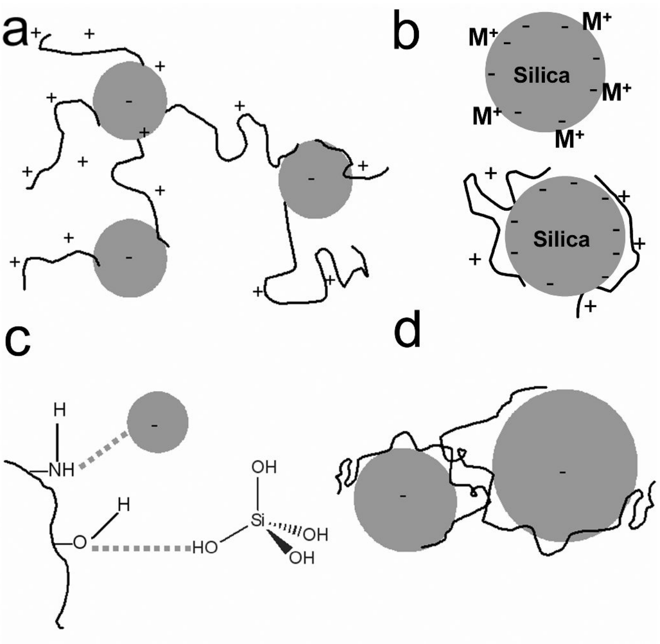

*Figure 1. Schematic presentation of electrostatic effect (a, b), hydrogen bonding (c) and the hydrophobic effect (d) for silica formation in the presence of additives.*

process by which soluble species such as monomers and dimers precipitate on relatively large and insoluble particles thus contributing to their growth. Charge will encourage interaction of the ‘larger’ particle and the small oligomers by promotion of nucleophilic condensation reactions between the species of disparate size. In the case of necking, due to a negative radius of curvature at the point of contact between two particles, silica from the surface of the bulk dissolves and re-precipitates at the point of contact between the particles.

## The Role of Additives in Structure Control

It is well known that the processes of silica formation and the resulting product yield, composition and morphology can be controlled by the presence of additives (*1*, *13*, *14*). It is clear that additives ranging from simple inorganic or organic molecules to complex organic polymers can be used as powerful tools for the controlled production of silica. The use of organic molecules as templates for the synthesis of inorganic minerals, silicates in particular, having a variety of shapes and morphologies has been demonstrated. Iler documented the role of organic additives presented in studies before 1979 (*1*). During the past several years however, bioinspired synthetic approaches, which enable silica synthesis under ambient conditions, have been developed as a consequence of isolating bioextracts from biosilica-forming organisms (*13*).

## Identification of Non-Bonded Interactions in Silica Formation Involving Additives

The aforesaid non-bonded interactions can affect the process of silica formation at a variety of different stages. Additives containing chemical functionalities that interact with ‘silicon’ species via non-bonded interactions have involvement with silicon species ranging from uncharged single silicon atom units through small oligomers to nanometre sized particles and larger structures carrying a significant amount of negative charge. In order to study silicic acid condensation and to identify the roles of non-bonded interactions, monitoring of the entire process of silica formation as well as characterisation of the bulk silicas generated is essential. In our studies we have chosen to work with a silicon catechol complex which liberates “pure” orthosilicic acid upon hydrolysis at ca. pH 7 (Figure 2a) unlike its alkoxysilane analogues which generate a mixture of polysilicic acids and partially unhydrolysed precursor (*15–17*). As described above, autopolymerisation of silicic acid takes place as the concentration of silicic acid used (30 mM) is higher than its equilibrium solubility (~ 1 mM) and the formation of dimers, trimers, oligomers, particles and final structures takes place as shown schematically in Figure 2a. The early stages of the reaction are monitored using a colorimetric method that allows changes in silicic acid concentration with time to be monitored. For the first reaction, dimerisation, the method shows no change in silicic acid concentration as both the reactants (monomers) and the product (dimer) produce an identical number of silicic acid molecules that can react with the reagent. The next stage is trimer formation that is observed as an irreversible third order reaction owing to the high concentrations involved (if reactions were performed at concentrations near the solubility limit then information on both the forward and the reverse reaction could theoretically be obtained). Further growth of oligomers follows reversible first order kinetics with respect to silicic acid concentration (*18*). The loss of silicic acid with time can be measured using a silicomolybdate assay and hence the rate constants for the reactions involved in the very early stages of silica oligomer formation can be calculated (Figure 2b-d). Additional information on the levels of soluble silicon (monomers and dimers) present in solution at any time, even if the net change in silicon concentration with time is too low to obtain kinetic information, can also be obtained.

The evolution of particle formation in solution can be studied using Dynamic Light Scattering (DLS); Figure 2e. The information obtained is the hydrodynamic radius of the species present which may be individual particles and/or aggregates. Some information on particle size distribution and rates of growth can be obtained but meticulous care must be taken to prevent contamination from dust which can lead to erroneous results. The study of solution chemistry leads to the understanding of molecular interactions between additives and silica species (monomers to particles). The non-bonded interactions between additives and silica can also have dramatic effects on the bulk properties of the silicas generated. We investigate these effects using gas adsorption (to collect information on surface area, porosity and distribution of porosity), thermal analysis (to understand the

Downloaded by CORNELL UNIV on June 24, 2012 | http://pubs.acs.org
Publication Date (Web): November 9, 2010 | doi: 10.1021/bk-2010-1051.ch018

entrapment of additives in final structures) and electron microscopy (to observe morphology and structure); Figure 2 f-h.

## Examples of Non-Bonded Interactions in Bioinspired Silicification

The structures of the molecules that have been used experimentally in our laboratory to explore the role of non-bonded interactions in the control of silica structure are presented in Figure 3. Additional information from other sources is referenced as appropriate through the body of the text.

Downloaded by CORNELL UNIV on June 24, 2012 | http://pubs.acs.org
Publication Date (Web): November 9, 2010 | doi: 10.1021/bk-2010-1051.ch018

### Electrostatic Interactions

Oligomers that are formed during silica polymerisation are negatively charged at neutral pH and also possess free hydroxyl groups. It is thus likely that the presence of an additive may alter the stability of such intermediates and/or the silicic acid polymerisation process due to electrostatic interactions.

The presence of cationic species in solution, either as metal ions present as part of the catecholate salt used in our experiments or as functionalities in molecules added to the reaction system, affect silica formation. Effects on the kinetics of the early stages of oligomer formation, particle growth, aggregation and the nature of the materials formed are observed. Previous work on silicic acid condensation in the presence of group 1 cations has shown a rate dependency related to the size of the hydration sphere of the cations with the largest hydrated ions (the smallest atoms) reacting the fastest (*18*). This behaviour is also manifest in the silica phase generated with the largest hydrated cations (most shielded charge, least electrostatic interaction) producing silicas with the highest surface areas. In addition, the ions ($NH_4^+$, $Et_3NH^+$, etc.) that are less hydrated get associated with the surfaces of silica oligomers/particles by electrostatic attractions reducing the rate of removal of silicic acid and producing silicas with vastly reduced surface area.

Nitrogen containing amino acids, particularly L-arginine and L-lysine were also found to promote silicic acid condensation. When a whole range of amino acids was considered, their effect on the early stages of condensation (e.g. the formation of trimers and other small oligomers) could be related to the pI of the amino acid (*15*). Aggregation of the condensing silica as observed by photon correlation spectroscopy (DLS) also showed pI dependent behaviour with the most significant increases being observed for L-arginine and L-lysine. This behaviour can be explained by consideration of the increasing negative charge on silica particles as they grow and the neutralisation of these charges in the presence of the positively charged amino acids thereby allowing the silica species to interact with one another to produce larger aggregates. Experiments with homopeptides of glycine (H as the side chain) and lysine (positively charged side chain) showed similar behaviour. In addition the presence of several charges within one molecule (increase in number of lysines per molecule) magnified the observed behaviour with increased rate of condensation and aggregation

Downloaded by CORNELL UNIV on June 24, 2012 | http://pubs.acs.org
Publication Date (Web): November 9, 2010 | doi: 10.1021/bk-2010-1051.ch018

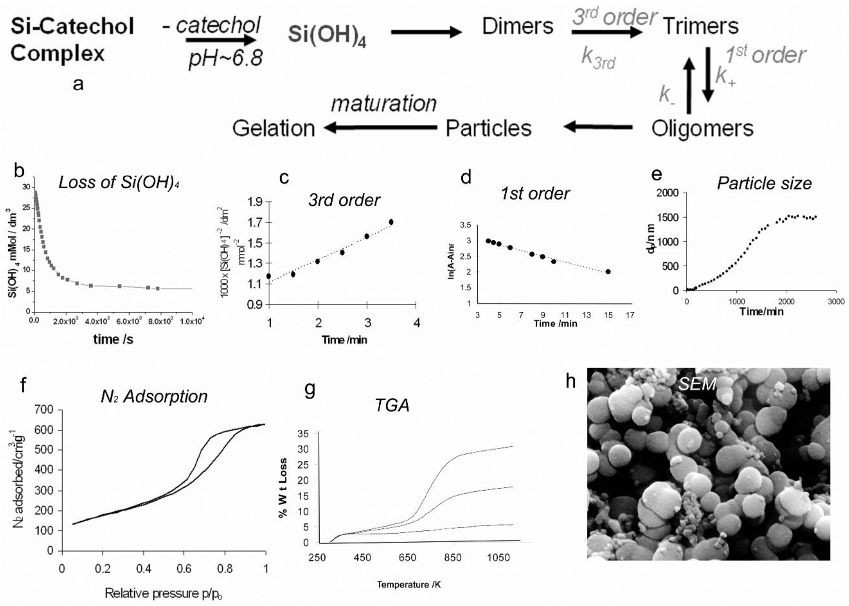

*Figure 2. Experimental protocol employed for the identification of and distinguishing of different effects (see text for details). (a) Stages involved in silica polymerisation. (b-e) Study of solution chemistry and (f-h) bulk materials properties.*

being observed. It is suggested that the peptides also bridge between the silica particles. Specifically, the attraction between positively charged additives (e.g. metal ions, small organic molecules and macromolecules) and negatively charged silica species alters the stabilities of silica oligomers and particles, the activities of silica species and solvent, thereby influencing the solution chemistry and structure formation of silica. The behaviour of diamines containing the same number of positively charged nitrogen groups but with different chain length has also been probed. Although the rates of condensation, aggregation and materials characteristics were modified as expected, the behaviour could not simply be explained by consideration of electrostatic interactions alone. Other non-bonded interactions were found to be important, see below.

## Hydrogen Bonding Interactions

The use of organic molecules to control the structure and morphology of silicas has long been known (*1*, *6*, *11*). Hecky *et al.* (*19*) postulated that hydroxyl-rich proteins (sugars and glycoproteins) associated with diatom cell walls might condense with silicic acid monomers (leading to the formation of Si-O-C bonds), thus serving as templates for orientation and growth of the silica. Support of this hypothesis was provided by thermodynamic calculations of Lobel *et al.* (*20*) However, more recent molecular orbital calculations studies suggest that the formation of Si-O-C bonds (for silica in the presence of serine for example) is unlikely (*21*, *22*). Similarly, Morse and coworkers have proposed

Downloaded by CORNELL UNIV on June 24, 2012 | http://pubs.acs.org
Publication Date (Web): November 9, 2010 | doi: 10.1021/bk-2010-1051.ch018

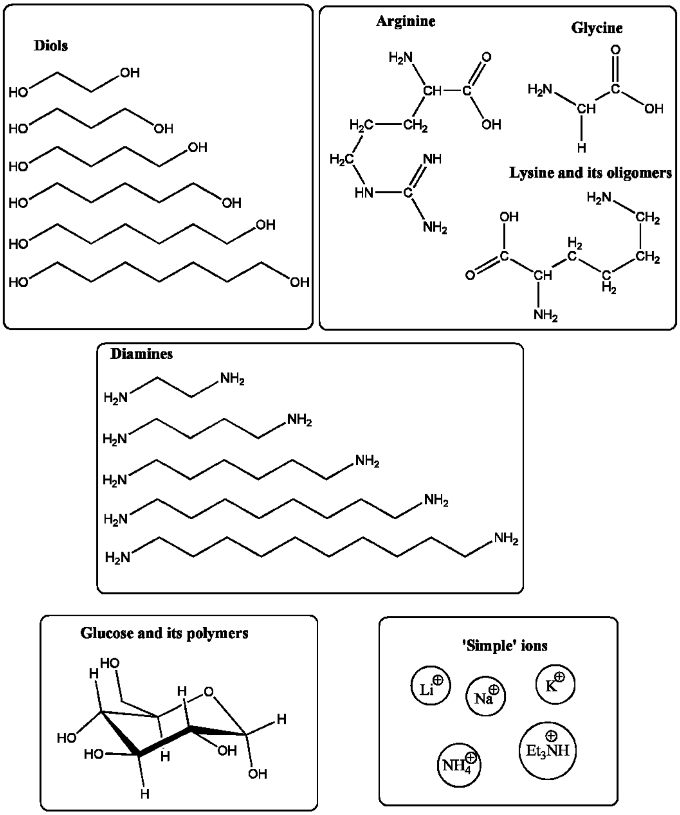

*Figure 3. Additives used in model silicification studies in order to understand non-bonded interactions in structure control.*

that the presence of blocks of hydroxyl rich amino acids in silicatein α from silicified sponge spicules may be key in silicatein catalyzed silica formation (*23*). In addition, *in vitro* experiments, utilising hydroxyl-containing molecules such as polyethylene glycol (PEG) (*24*) and polyserine (*25*) have been found to influence the structure of silica.

Hydrogen bond formation between silanol groups of silicic acid, oligomers and/or negatively charged silica particles and proton donors such as free amines or hydroxyl groups present in the additives occurs as presented in Figure 1c and is here illustrated by two examples – silica formation in the presence of saccharides and alkanediols. Reference to other work is also made. Early experiments using cellulose as a reaction additive found that the solution chemistry, i.e. kinetics of silica polymerisation was little affected. However, the presence of cellulose was found to exert a dramatic effect on the range of primary particle sizes generated and their aggregation patterns. In particular, cellulose was able to "stabilise" primary particles and at the same time generated a degree of ordering in the silicas. A similar effect was observed for small oligosaccharides of glucose (*26*).

We investigated the effect of additions of alkanediols to the model silicifying system as depicted in Figure 2. The results obtained from the kinetic experiments performed in the presence of the diols indicated no significant effect on any of the early stages of silica oligomer formation when compared with the blank sample (data not shown). However, effects were observed on the materials formed as the presence of the diols led to higher levels of silicic acid being present in solution and silicas with lower surface areas and increased porosity being produced. The observations can be explained by considering all of the species capable of forming hydrogen bonds in the experimental system in question. There are three species cable of constructing a hydrogen bond: silicic acid, water and the alkanediol species. Hydrogen bonding occurs in alcohols due to the polarisation that exists in the O-H bond. Silicic acid is expected to hydrogen bond with the diol as well as with water. However, for all the experiments conducted, water was in excess and hence the effect of the diols would be insignificant compared with the effect of the solvent, as is indeed observed. As particle growth continues the presence of the additive promotes reorganisation of the siliceous phase but the diol is not incorporated into the structures that form.

Downloaded by CORNELL UNIV on June 24, 2012 | http://pubs.acs.org
Publication Date (Web): November 9, 2010 | doi: 10.1021/bk-2010-1051.ch018

## The Hydrophobic Effect

The hydrophobic effect is a fundamental factor regulating *in vivo* processes, such as protein folding and protein-substrate interactions (*27*, *28*). The stability and hence the function of proteins, for example, is altered by the presence of solute due to the rearrangement of water molecules. This effect is particularly enhanced when the solutes added are hydrophobic in nature. Similarly, the hydrophobic effect is expected to play important role in silicic acid polymerisation and silica – additive interactions. A series of organic additives possessing increasingly larger hydrophobic domains (from $C_2$ to $C_{10}$) have been used to investigate their interactions with silicas (*29*). Effects on silicic acid condensation, aggregation and materials properties were observed that could not be explained by consideration of the electrostatic effects alone. Increased rates of condensation and aggregation were observed and materials with lower surface areas were produced in the presence of molecules having progressively larger hydrophobic structural components. The increase in silicification rates can be explained by the formation of a clathrate cage-like water structure around the nonpolar surfaces of the alkyldiamines. The cage-like structure may tie up some of the free water molecules (i.e. those not associated with ion hydration shells) (*30*) resulting in higher reactant (silicic acid) concentrations in the bulk aqueous environment and also a possible reduction in the hydration shells around the anionic silica species. Under these conditions, reactions involving anions, such as the condensation of a silicate anion with a neutral silicate species, would be expected to show an increase in rate as is observed (*31*). For shorter chain diamines the initial increase in observed aggregation rates could be attributed to surface charge neutralisation of the negatively charged primary silica particles by the cationic diamines – the electrostatic effect. However, as the diamine chain length increased, the diamines were found to additionally bridge the particle double layer, resulting in accelerated growth. The coacervation of diamine coated silica particles (the hydrophobic effect), which increased with increasing chain length, manifested itself as the continued rate and size increase that was observed. In other words, the addition of nonpolar organic species was found to alter the chemical potential and structure of water (solvent) due to the hydrophobic effect and electrostatic interactions (*29*). Similar interactions have been predicted in the studies of adsorption of surfactants on silica surface (*32*) and also in silica formation using poly(ethylene glycol) and gemini surfactants (*24*, *33*).

## Conclusions

Additives, through non-covalent interactions, can affect all aspects of silica deposition from the rates of formation of small oligomers and stable nuclei through to macroscopic properties including surface area, pore structure, particle size and aggregation patterns. It is in understanding molecular reactions involving non-bonded interactions between the species present that we will eventually be able to prepare ornate silicas such as biological organisms produce on a daily basis.

## Acknowledgments

The authors would like to thank Ineos Chemicals, the American Air Force and the European Union for funding of this project.

## References

1. Iler, R. K. *The Chemistry of Silica*; John Wiley & Sons: New York, 1979.
2. Perry, C. C.; Belton, D.; Shafran, K. *Prog. Mol. Subcell. Biol.* **2003**, *33*, 269–299.
3. Perry, C. C.; Keeling-Tucker, T. *J. Biol. Inorg. Chem.* **2000**, *5*, 537–550.
4. Kendall, T. *Ind. Miner.* **2000**, March, 49−59.
5. Yang, H.; Coombs, N.; Ozin, G. A. *Nature* **1997**, *386*, 692–695.
6. Brinker, C. J.; Scherer, G. W. *Sol-Gel Science: The Physics and Chemistry of Sol-Gel Processing*; Academic Press: Boston, 1990.
7. Hench, L. L.; West, J. K. *Chem. Rev.* **1990**, *90*, 33–72.
8. Tacke, R. *Angew. Chem., Int. Ed.* **1999**, *38*, 3015–3018.
9. Mann, S., Webb, J., Williams, R. J. P., Eds.; *Biomineralization*; VCH: Weinheim, Germany, 1989.
10. Beck, J. S.; Vartuli, J. C.; Roth, W. J.; Leonowicz, M. E.; Kresge, C. T.; Schmitt, K. D.; Chu, C. T. W.; Olson, D. H.; Sheppard, E. W.; McCullen, S. B.; Higgins, J. B.; Schlenker, J. L. *J. Am. Chem. Soc.* **1992**, *114*, 10834–10843.
11. Kresge, C. T.; Leonowicz, M. E.; Roth, W. J.; Vartuli, J. C.; Beck, J. S. *Nature* **1992**, *359*, 710–712.
12. Meegan, J. E.; Aggeli, A.; Boden, N.; Brydson, R.; Brown, A. P.; Carrick, L.; Brough, A. R.; Hussain, A.; Ansell, R. J. *Adv. Funct. Mater.* **2004**, *14*, 31–37.
13. Patwardhan, S. V.; Clarson, S. J.; Perry, C. C. *Chem. Commun.* **2005**, *9*, 1113–1121.
14. Perry, C. C. *Rev. Mineral. Geochem.* **2003**, *54*, 291–327.

Downloaded by CORNELL UNIV on June 24, 2012 | http://pubs.acs.org
Publication Date (Web): November 9, 2010 | doi: 10.1021/bk-2010-1051.ch018

15. Belton, D.; Paine, G.; Patwardhan, S. V.; Perry, C. C. *J. Mater. Chem.* **2004**, *14*, 2231–2241.
16. Kroger, N.; Lorenz, S.; Brunner, E.; Sumper, M. *Science* **2002**, *298*, 584–586.
17. Cha, J. N.; Shimizu, K.; Zhou, Y.; Christiansen, S. C.; Chmelka, B. F.; Stucky, G. D.; Morse, D. E. *Proc. Natl. Acad. Sci. U.S.A.* **1999**, *96*, 361–365.
18. (a) Harrison, C. C.; Loton, N. *J. Chem Soc., Faraday Trans.* **1995**, *91*, 4287−4297. (b) Belton, D.; Deschaume, O.; Patwardhan, S. V.; Perry, C. C. *J. Phys. Chem. B* **2010**, *114*, 9947−9955.
19. Hecky, R. E.; Mopper, K.; Kilham, P.; Degens, E. T. *Mar. Biol.* **1973**, *19*, 323–331.
20. Lobel, K. D.; West, J. K.; Hench, L. L. *Mar. Biol.* **1996**, *126*, 353–360.
21. Sahai, N.; Tossell, J. A. *Geochim. Cosmochim. Acta* **2001**, *65*, 2043–2053.
22. Sahai, N. *Geochim. Cosmochim. Acta* **2004**, *68*, 227–237.
23. Shimizu, K.; Cha, J.; Stucky, G. D.; Morse, D. E. *Proc. Natl. Acad. Sci. U.S.A.* **1998**, *95*, 6234–6238.
24. Sun, Q. Y.; Beelen, T. P. M.; van Santen, R. A.; Hazelaar, S.; Vrieling, E. G.; Gieskes, W. W. C. *J. Phys. Chem. B.* **2002**, *106*, 11539–11548.
25. Patwardhan, S. V. Silicification and Biosilicification: Role of Macromolecules in Bioinspired Silica Synthesis. Ph.D. Dissertation, University of Cincinnati, 2003.
26. (a) Harrison, C. C.; Lu, Y. In *Biomineralization 93*; Allemand, D., Cuif, J.-P., Eds.; Musee Oceanographique: Monaco, 1994. (b) Tilburey, G. T.; Patwardhan, S. V.; Huang, J.; Kaplan, D.; Perry, C. C. *J. Phys. Chem.* **2007**, *111*, 4630−4638.
27. Eggers, D. K.; Valentine, J. S. *J. Mol. Biol.* **2001**, *314*, 911–922.
28. Fisicaro, E.; Compari, C.; Braibanti, A. *Phys. Chem. Chem. Phys.* **2004**, *6*, 4156–4166.
29. Belton, D.; Patwardhan, S. V.; Perry, C. C. *Chem. Commun.* **2005**, *27*, 3465–3477.
30. Franks, F. *Water*; Royal Society of Chemistry: London, 1983.
31. Kinrade, S. D.; Pole, D. L. *Inorg. Chem.* **1992**, *31*, 4558–4563.
32. Zajac, J.; Chorro, C.; Lindheimer, M.; Partyka, S. *Langmuir* **1997**, *13*, 1486.
33. Karkamkar, A. J.; Kim, S.-S.; Mahanti, S. D.; Pinnavaia, T. J. *Adv. Funct. Mater.* **2004**, *14*, 507.

Downloaded by CORNELL UNIV on June 24, 2012 | http://pubs.acs.org
Publication Date (Web): November 9, 2010 | doi: 10.1021/bk-2010-1051.ch018

Downloaded by UNIV OF GUELPH LIBRARY on June 25, 2012 | http://pubs.acs.org
Publication Date (Web): November 9, 2010 | doi: 10.1021/bk-2010-1051.ch019

## Chapter 19

# Function of Silicon-Oxygen Bonds in Fabrication of Holographic Gratings

**Yusuke Kawakami* and Yeong Hee Cho**

**School of Materials Science, Japan Advanced Institute of Science and Technology, Nomi Ishikawa 9231292, Japan**
***kawakami@jaist.ac.jp**

High performance transmission holographic polymer dispersed liquid crystals were fabricated using a mixture of radically photo-polymerizable multi-functional acrylates and ring-opening photo-polymerizable epoxides as monomers by Nd-YAG laser ($\lambda$=532nm) in the presence of diphenyliodonium hexafluorophosphate and 3,3′-carbonylbis(7-diethylaminocoumarin). High diffraction efficiency over 97% was obtained for grating formed from dipentaerythritol penta/hexaacrylate, 1,5-bis(3-glycidoxypropyl)-1,1,3,3,5,5-hexamethyltrisiloxane, 1-vinyl-2-pyrrollidone (reactive diluent), and commercial liquid crystal, E7 (45:36:9:10 in weight percent). 1,5-Bis[2-(1,2-epoxycyclohex-4-yl)ethyl]-1,1,3,3,5,5-hexamethyl-trisiloxane gave a little lower diffraction efficiency (75%), but it gave gratings with reduced angular deviation (0.6 degree for signal beam at 32 degree incident angle) from Bragg profile. Spiroorthoester function was found to be polymerized with the laser. The volume shrinkage was much lower than that prepared with bis(epoxide)s. Gratings were also formed for matrix of trimethylolpropane triacrylate:methacryloxymethyltrimethoxysilane:1-vinyl-2-pyrrolidone in the range from 80:10:10 to 10:80:10 wt% and E7. Gratings with apparently high diffraction efficiency could be fabricated both for methacryloxymethyltrimethoxysilane (cross-linkable by hydrolysis) and methacryloxymethyltrimethylsilane (non cross-linkable by hydrolysis) with high concentration of trimethylolpropane triacrylate. Distinct difference was seen at higher concentration (> 40 wt%) of the methacrylates. Contrary to that gratings with reasonably high and stable diffraction efficiency were successfully fabricated with methacryloxymethyltrimethoxysilane, only low diffraction efficiency was obtained for non cross-linkable methacryloxymethyltrimethylsilane. Importance of hydrophilicity of the spacer group was examined using TL203 as a liquid crystal. Introduction of urethane group or hydroxy group in the spacer dramatically improved the performance of the gratings.

Downloaded by UNIV OF GUELPH LIBRARY on June 25, 2012 | http://pubs.acs.org
Publication Date (Web): November 9, 2010 | doi: 10.1021/bk-2010-1051.ch019

## Introduction

Much attention has been devoted to the polymer dispersed liquid crystal (PDLC) systems due to their potential applications in electro-optic technology, such as optical switches, reflective displays without polarizer, switchable windows, and many other display devices (*1–5*). One of the useful methods for formation of these systems is photo-polymerization-induced phase separation of liquid crystal (LC) from polymer matrix, using mixtures of photo-reactive multi-functional monomer and LC (*6*). Recently, holographic techniques have been applied to the systems known as holographic polymer dispersed liquid crystal (HPDLC), in which gratings are formed as the periodic polymer rich layers and LC rich layers created by interference of two incident laser beams (*7–11*).

Generally, in HPDLC systems, LC is phase-separated into sub micrometer size, in contrast to PDLC systems having micrometer size LC droplets. The performance of holographic gratings strongly depends on the final morphologies, sizes, distribution, and shapes of phase-separated LC domains. The size can be controlled by adjusting the kinetics of polymerization and phase separation of LC during the polymerization, which depends on 1) experimental conditions such as exposure beam intensity, inter beam angle, and exposure time, and 2) concentration, and physical properties such as viscosity of LC, and the chemical structure and functionality of polymer matrix components.

Until now, many research groups have studied on the use of acrylates and epoxides as monomers for polymer matrix in HPDLC systems (*12–14*). It will be interesting to use these monomers together with an anticipation of the formation of interpenetrating polymer networks (IPN) system to prevent volume shrinkage in grating formation.

In our previous study, we showed that performance of gratings could be very much enhanced by the introduction of siloxane components in LC or bis(epoxide)s in HPDLC or photo-polymer systems (*15–19*). It was expected that introduction of siloxane component into bis(epoxide) as a matrix component might give gratings with high diffraction efficiency with low volume shrinkage by the effects of siloxane component to enhance the phase separation of alkyl-substituted LC, E7, from the matrix and by the formation of IPN structure in the matrix by the simultaneous polymerization of multi-functional acrylate and bis(epoxide) in the grating formation process. There are a large number of articles on the very low, even no polymerization shrinkage of spiroorthoesters (*20*). If spiroorthoester can be polymerized under the irradiation of laser, they might be excellent materials for the fabrication of holographic gratings.

Since the performance of HPDLC is governed by the stability of precisely formed periodic polymer rich layer and LC rich layer created by interference of two incident laser beams, control of the formation of polymer matrix and phase separation of LC is very important (*21–24*). The principal role of multi-functional acrylate in grating formation is to make the LC phase-separate by the formation of cross-linked polymer matrix. Control of the rate and density of cross-linking in polymer matrix is one of the most important factors, which determines the size, distribution, and shape of phase-separated LC domains, accordingly the final morphology and performance. In order to obtain clear phase separation of LC from polymer matrix to homogeneous droplets, high cross linking density, but not rapid cross-linking, is very important. Too rapid initial cross-linking by multi-functional acrylate makes it difficult to control the diffusion and phase separation of LC. At the same time, high ultimate conversion of polymerizable double bond leading to high cross-linking is important for long-term stability. These are not easy to achieve at the same time.

Until now optimization of cross-linking process has been mainly pursued by controlling the average functionality of multi-functional acrylate by mixing dipentaerythritol penta-/hexaacrylate (**DPHA**), trimethylolpropane triacrylate (**TMPTA**) and tri(propyleneglycol) diacrylate (**TPDA**), or by diluting the system with mono-functional vinyl compounds like 1-vinyl-2-pyrrolidone (**NVP**) (*25–28*). Simultaneous siloxane network formation, by hydrolyzable acrylate like trialkoxysilyl (meth)acrylate, with matrix formation by radically polymerizable multi-functional acrylate is a new and attractive way to obtain gratings with high diffraction efficiency and low volume shrinkage. Our idea is to improve the property of gratings through importing the siloxane network formation in polymer matrix, by not only lowering the contribution of initial rapid radical cross-linking of **TMPTA** and realizing complete conversion of double bonds, but also maintaining the desirable total cross-linking density assisted by hydrolysis-condensation cross-linking of trialkoxysilyl group in the methacrylate component to control the phase separation of LC from polymer matrix (*29*). Such cross-linking can be promoted by the proton species produced from the initiating system together with radical species by photo-reaction (*30–32*). In our system, phase separation of LC is not so fast compared with a simple multi-functional acrylate system, and secondary cross-linking by the formation of siloxane network enforces the LC to completely phase-separate to homogeneous droplets, and high diffraction efficiency could be expected. We named this process as proton "assisted grating formation." The well-constructed morphology of the gratings was evidenced by scanning electron microscope (SEM).

Downloaded by UNIV OF GUELPH LIBRARY on June 25, 2012 | http://pubs.acs.org
Publication Date (Web): November 9, 2010 | doi: 10.1021/bk-2010-1051.ch019

Downloaded by UNIV OF GUELPH LIBRARY on June 25, 2012 | http://pubs.acs.org
Publication Date (Web): November 9, 2010 | doi: 10.1021/bk-2010-1051.ch019

# Experimental

## Materials for Holographic Recording

Multi-functional acrylates, tri(propylene glycol) diacrylate (**TPDA**), trimethylolpropane triacrylate (**TMPTA**) and dipentaerythritol penta-/ hexaacrylate (**DPHA**), purchased from Aldrich Chemical Co., were used as radically polymerizable cross-linking monomers. 1-Vinyl-2-pyrrolidone (**NVP**) was used as a radically polymerizable reactive diluent. Their chemical structures are illustrated in Figure 1.

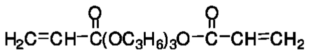

$H_2C{=}CH{-}\overset{O}{\overset{\|}{C}}(OC_3H_6)_3O{-}\overset{O}{\overset{\|}{C}}{-}CH{=}CH_2$

Tri(propylene glycol) diacrylate (**TPDA**), $n_D^{20}$=1.450

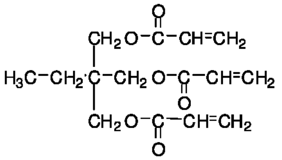

Trimethylolpropane triacrylate (**TMPTA**), $n_D^{20}$=1.474

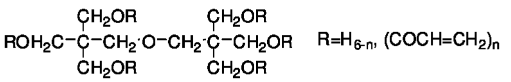

Dipentaerythritol penta-/hexa- acrylate (**DPHA**), $n_D^{20}$=1.49

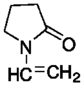

1-Vinyl-2-pyrrolidone (**NVP**), $n_D^{20}$=1.512

*Figure 1. Chemical structures of radically polymerizable multi-functional acrylates and reactive diluent.*

Structures of ring-opening cross-linkable monomers are shown in Figure 2.

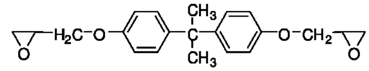

Bisphenol A diglycidylether (**A**)

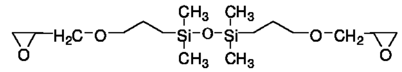

1,3-Bis(3-glycidoxypropyl)-1,1,3,3-tetramethyldisiloxane (**B**)

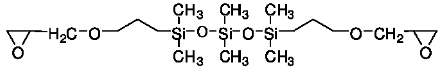

1,3-Bis(3-glycidoxypropyl)-1,1,3,3,5,5-hexamethyltrisiloxane (**C**)

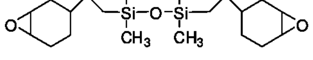

1,3-Bis[2-(1,2-epoxycyclohex-4-yl)ethyl]-1,1,3,3-tetramethyldisiloxane (**D**)

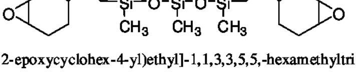

1,3-Bis[2-(1,2-epoxycyclohex-4-yl)ethyl]-1,1,3,3,5,5,-hexamethyltrisiloxane (**E**)

*Figure 2. Chemical structures of bi-functional ring-opening polymerizable monomers.*

Downloaded by UNIV OF GUELPH LIBRARY on June 25, 2012 | http://pubs.acs.org
Publication Date (Web): November 9, 2010 | doi: 10.1021/bk-2010-1051.ch019

Bisphenol-A diglycidyl ether (**A**) from Aldrich Chemical Co. and 1,3-bis(3-glycidoxypropyl)-1,1,3,3-tetramethyldisiloxane (**B**) from Shin-Etsu Co. were used without further purification. 1,3-Bis(glycidoxypropyl)-1,1,3,3,5,5-hexamethyltrisiloxane (**C**), 1,3-bis[2-(1,2-epoxycyclohex-4-yl)ethyl]-1,1,3,3-tetramethyldisiloxane (**D**), and 1,3-bis[2-(1,2-epoxycyclohex-4-yl)ethyl]-1,1,3,3,5,5-hexamethyltrisiloxane (**E**) were synthesized by hydrosilylation of allyl glycidyl ether or 4-vinyl-1-cyclohexene-1,2-epoxide (Aldrich Chemical Co.) with 1,1,3,3-tetramethyldisiloxane or 1,1,3,3,5,5-hexamethyltrisiloxane (Silar Laboratories) in toluene at 60~70°C for 24h in the presence of chlorotris(triphenylphosphine)rhodium(I) [$RhCl(PPh_3)_3$] (KANTO Chemical Co. Inc.), and the products were obtained as colorless liquids with low viscosity (*20*).

2-Allyloxymethyl-1,4,6-trioxaspiro[4.6]undecane **(SU)**: A solution of allyl glycidyl ether (14.55g, 0.127 mol) in $CH_2Cl_2$ (90mL) was added dropwise into the 300mL three-necked flask containing ε-caprolactone (29.16g, 0.255mol) and boron trifluoride diether complex (0.3mL) in $CH_2Cl_2$ (90mL) below 10°C. The reaction solution was stirred for 1 hour at the same temperature, and then for 18 hours at room temperature. A colorless liquid was obtained after distillation under reduced pressure (bp. 115-116°C/390 Pa; $M^+ = 228$; yield: 23.16g, 80%).

1,4-Bis[(1,4,6-trioxaspiro[4.6]undec-2-yl)methoxy]butane **(BSU)**: The procedure was as same as literature (*33*, *34*) and a sticky colorless liquid was obtained in 26% yield.

1,1,1,3,5,7,7,7-Octamethyl-3,5-bis[3-{(1,4,6-trioxaspiro[4.6]undec-2-yl)-methoxy}propyl]tetrasiloxane **(S4SU)**: Under the nitrogen atmosphere, 1,1,1,3,5,7,7,7-octamethyltetrasiloxane (2.00g, 7.1mmol) was added into the 30mL two-necked flask containing SU (3.23g, 14.1mmol) and 2mg $PtCp_2Cl_2$ in toluene (10mL). Vacuum distillation with glass tube oven gave a colorless liquid (yield: 3.04g, 58%).

1,1,3,3,5,5-Hexamethyl-1,5-bis[3-{(1,4,6-trioxaspiro[4.6]undec-2-yl)-methoxy}propyl]trisiloxane **(S3SU)**: 1,1,3,3,5,5-Hexamethyltrisiloxane (1.37g, 6.6mmol) and SU (3.00g, 13.1mmol) gave a colorless liquid (yield: 2.47g, 56%). Synthetic route is shown in Figure 3.

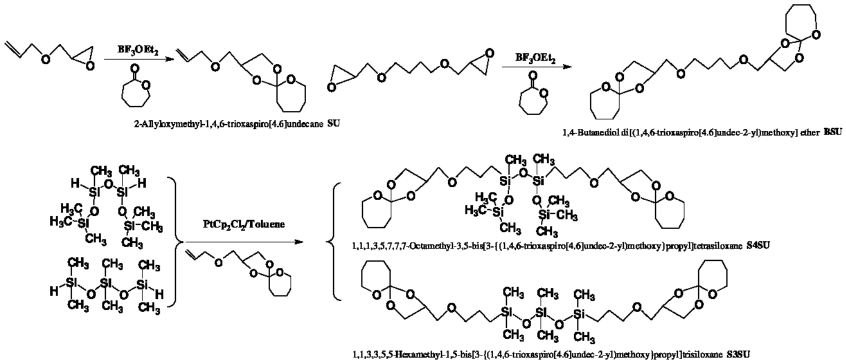
BF₃OEt₂
2-Allyloxymethyl-1,4,6-trioxaspiro[4.6]undecane SU
BF₃OEt₂
1,4-Butanediol di[(1,4,6-trioxaspiro[4.6]undec-2-yl)methoxy] ether BSU
PtCp₂Cl₂/Toluene
1,1,1,3,5,7,7,7-Octamethyl-3,5-bis[3-{(1,4,6-trioxaspiro[4.6]undec-2-yl)methoxy}propyl]tetrasiloxane S4SU
1,1,3,3,5,5-Hexamethyl-1,5-bis[3-{(1,4,6-trioxaspiro[4.6]undec-2-yl)methoxy}propyl]trisiloxane S3SU

*Figure 3. Chemical structures of spiroorthoesters.*

Downloaded by UNIV OF GUELPH LIBRARY on June 25, 2012 | http://pubs.acs.org
Publication Date (Web): November 9, 2010 | doi: 10.1021/bk-2010-1051.ch019

Structures of cross-linkable monomers by sol-gel process are shown in Figure 4.

Methacryloxymethyltrimethxysilane (**MM-TMS**), methacryloxymethyltrimethoxysilane (**MM-TMOS**), 3-methacryloxypropyltrimethoxysilane (**MP-TMOS**), 3-methacryloxypropyltriethoxysilane (**MP-TEOS**), 3-*N*-(2-methacryloxyethoxycarbonyl)aminopropyltriethoxysilane (**MU-TEOS**), and 3-*N*-(3-methacryloxy-2-hydroxypropyl)aminopropyltriethoxysilane (**MH-TEOS**), purchased from Gelest, Inc., and were used as reactive diluents. Methacrylate with trialkoxysilane are capable of not only radical polymerization but also hydrolysis-condensation.

Commercial LC, E7 (mixture of cyano bi-/terphenyls with high birefringence and adequate $T_{NI}$ (nematic-isotropic transition temperature) and TL203 ($T_{NI}$=74.6 °C, $n_e$=1.7299, $n_o$=1.5286, Δn=0.2013, Δε=11.0), purchased from Merck & Co. Inc., were used.

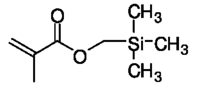

Methacryloxymethyltrimethylsilane (**MM-TMS**)

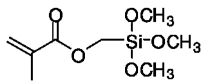

Methacryloxymethyltrimethoxysilane (**MM-TMOS**)

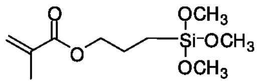

3-Methacryloxypropyltrimethoxysilane (**MP-TMOS**)

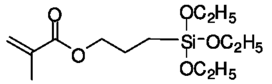

3-Methacryloxypropyltriethoxysilane (**MP-TEOS**)

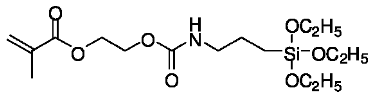

3-*N*-(2-methacryloxyethoxycarbonyl)aminopropyltriethoxysilane (**MU-TEOS**)

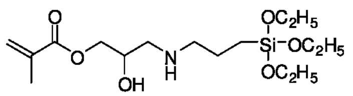

3-*N*-(3-methacryloxy-2-hydroxypropyl)aminopropyltriethoxysilane (**MH-TEOS**)

*Figure 4. Structures of tri(methoxysilyl)- and tri(methylsilyl) (meth)acrylates.*

The Rose Bengal (**RB**) and 3, 3′-Carbonylbis(7-diethylaminocoumarin) (**KC**, Kodak) as photo-sensitizer (**PS**), and *N*-phenylglycine (**NPG**) (Kanto Chemical) and diphenyliodonium hexafluorophosphate (**DPI**, AVOCADO research chemicals Ltd.) as photo-initiator (**PI**) were used as received to produce both cationic and radical species (*23*, *24*). Visible photo-initiator, **Irgacure 784** [bis($\eta^5$-cyclopentadienyl)bis[2,6-difluoro-3-(1*H*-pyrrol-1-y)]-titanium, Ciba-Geigy] to produce only radical species was also used. These **PS** and **PI** systems have sensitivity to visible wavelength of Nd-YAG laser ($\lambda$= 532 nm). The concentrations of the **PS** and **PI** in recording solution were varied in the range of 0.05 - 0.2 and 0.1 - 2.0 wt %, respectively.

Downloaded by UNIV OF GUELPH LIBRARY on June 25, 2012 | http://pubs.acs.org
Publication Date (Web): November 9, 2010 | doi: 10.1021/bk-2010-1051.ch019

### Optical Setup for Transmission Holographic Gratings

Nd-YAG solid-state continuous wave laser with 532nm wavelength (Coherent lnc., Verdi-V2) was used as the irradiation source as shown in Figure 5.

The beam was expanded and filtered by spatial filters, and collimated by collimator lens. *s*-Polarized beams were generated and split by controlling the two $\lambda/2$ plates and polarizing beam splitter. Thus separated two *s*-polarized beams with equal intensities were reflected by two mirrors and irradiated to recording solution at a pre-determined external beam angle (2θ) which was controlled by rotating the motor-driven two mirrors and moving the rotation stage along the linear stage. In this research, the external incident beam angle was fixed to 16° (θ) against the line perpendicular to the plane of the recording cell. Real-time diffraction efficiency was measured by monitoring the intensity of diffracted beam when the shutter was closed at a constant time interval during the hologram recording. After the hologram was recorded, diffraction efficiency was measured by rotating the hologram precisely by constant angle by using motor-driven controller, with the shutter closed to cut-off the reference light, to determine the angular selectivity.

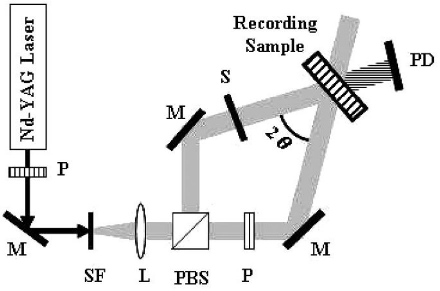

*Figure 5. Experimental setup for the holographic recording and real-time reading; P: 1/2λ plate, M: mirror, SF: spatial filter, L: collimating lens, PBS: polarizing beam splitter, S: shutter, 2θ: external inter-beam angle, PD: power detector.*

Holographic gratings were fabricated under at 40 mW/cm$^2$ intensity, and the optimum condition was established to obtain the high diffraction efficiency, high resolution, and excellent long-term stability after recording.

### Photo-DSC

The rate of polymerization was estimated from the heat flux monitored by photo-differential scanning calorimeter (photo-DSC) equipped with a dual beam laser light of 532nm wavelength. Matrix compounds were placed in uncovered aluminum DSC pans and cured with laser light by keeping the isothermal state of 30 °C at various light intensities.

### FTIR

Infrared absorption spectra in the range 4000-400 cm$^{-1}$ were recorded on polymer matrix compounds by Fourier Transform Infrared Spectroscopy (FTIR) (Perkin-Elmer, Spectrum One).

### Morphology of Holographic Gratings

Surface morphology of gratings was examined with scanning electron microscope (SEM, HITACHI, S-4100). The samples for measurement were prepared by freeze-fracturing in liquid nitrogen, and washed with methanol for 24h to extract the **LC**, in case necessary. Exposed surface of the samples for SEM was coated with a very thin layer of Pt-Pd to minimize artifacts associated with sample charging (HITACHI, E-1030 ion sputter).

### Diffraction Efficiency

Diffraction efficiency is defined as the ratio of diffraction intensity ($I_d$) to sum of transmitted beam intensities ($I_d + I_t$) after recording, as illustrated in Figure 6.

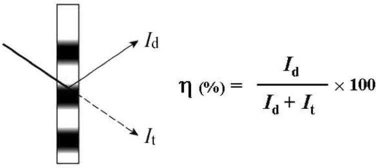

*Figure 6. Definition of diffraction efficiency.*

Downloaded by UNIV OF GUELPH LIBRARY on June 25, 2012 | http://pubs.acs.org
Publication Date (Web): November 9, 2010 | doi: 10.1021/bk-2010-1051.ch019

Downloaded by UNIV OF GUELPH LIBRARY on June 25, 2012 | http://pubs.acs.org
Publication Date (Web): November 9, 2010 | doi: 10.1021/bk-2010-1051.ch019

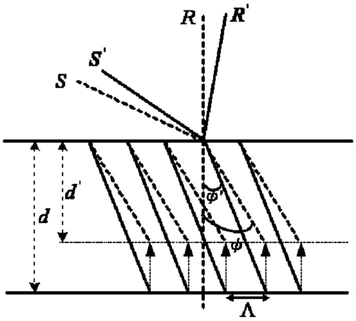

*Figure 7. Fringe-plane rotation model for slanted transmission holographic recording to measure the volume shrinkage.*

### Volume Shrinkage

For the measurement of volume shrinkage, slanted holographic gratings were fabricated by simply changing the angles of reference (R) and signal (S) beams, as shown in Figure 7 (*34*).

R and S are recording reference (0°) and signal (32°) beams. $\varphi$ is the slanted angle against the line perpendicular to the plane of the recording cell of gratings formed with S and R. Solid line in the grating indicates the expected grating. *d* is the sample thickness. Actual grating formed by S and R was deviated to actual grating shown by dashed line by volume shrinkage of the grating. Presumed signal beam (S‘), which should have given actual grating was detected by rotating the recorded sample with reference light R off. This rotation of angle was taken as deviation of slanted angle. R‘ and S‘ are presumed compensation recording reference and signal beams. $\varphi$‘ is the slanted angle in presumed recording with S‘ and R‘, and *d*‘ is the decreased sample thickness caused by volume shrinkage. Degree of volume shrinkage can be calculated by following equation (1);

$$\textbf{Degree of shrinkage} = 1 - d`/d = 1 - \tan\varphi` / \tan\varphi \quad (\tan\varphi` = \Lambda/d,\ \tan\varphi = \Lambda/d`) \quad (1)$$

## Results and Discussion

### Real-Time Diffraction Efficiency of Siloxane-Containing Bis(glycidyl Ether)s and Bis(cyclohexene Oxide)s

Real-time diffraction efficiency, saturation time, and stability of holographic gratings according to exposure time were evaluated. Figure 8 shows the effects of chemical structures of bis(glycidyl ether)s (**A-C**) and bis(cyclohexene oxide)s (**D**, **E**) on real-time diffraction efficiency at constant concentration of **E7** (10 wt%) in recording solution [**DPHA**:**NVP**:(**A-E**) = 50:10:40 relative wt%].

Downloaded by UNIV OF GUELPH LIBRARY on June 25, 2012 | http://pubs.acs.org
Publication Date (Web): November 9, 2010 | doi: 10.1021/bk-2010-1051.ch019

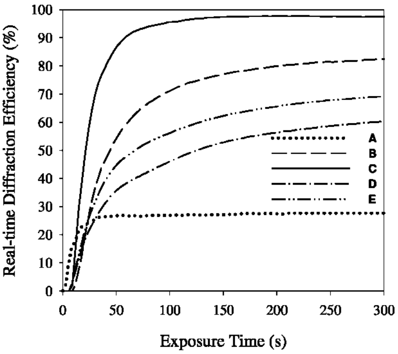

*Figure 8. Real-time diffraction efficiency of the gratings formed with (**A** - **E**) with 10 wt% **E7** [**DPHA**:**NVP**:(**A** - **E**) = 50:10:40 relative wt%].*

In general, high diffraction efficiency can be obtained by the formulation of recording solution with large differences in refractive indexes between polymer matrix and LC, and by inducing the good phase separation between polymer rich layer and LC rich layer. As expected, gratings formed with **B** having siloxane component had remarkably higher diffraction efficiency than gratings formed with **A** without siloxane component. Longer induction period for grating formation of **B** was attributed to lower viscosity of recording solution, and the diffraction efficiency gradually increased and reached to higher value, which resulted from the further phase separation of **E7** due to the flexible siloxane chain that helped migration of **E7** toward low intensity fringes. The highest diffraction efficiency 97% was observed for **C** with trisiloxane chain, probably due to its incompatible property with **E7**. However, compared with **B** and **C**, **D** and **E** did not give higher diffraction efficiency, even with same siloxane chain. This may be understood because of the difference in the chemical structure of ring-opening cross-linkable group. **D** and **E** have more sterically hindered cyclohexene oxide as functional group, and its diffusion toward high intensity fringes seems difficult compared with that of **B** or **C.**

## Volume Shrinkage of the Gratings Depending on the Structure of Bis(epoxide)

Photo-polymerizable system as holographic recording material usually causes significant volume shrinkage during the formation of gratings, which can distort the recorded fringe pattern and cause angular deviations in the Bragg profile. Therefore, it is very important to solve the problem of volume shrinkage in photo-polymerization systems.

Figure 9 shows the angular deviations from the Bragg profile of the slanted gratings formed with **C** and **E** having bis(glycidyl ether) and bis(cyclohexene oxide), respectively, at constant concentration of **E7** (10 wt%) [**DPHA**:**NVP**:(**C** or **E**) = 50:10:40 relative wt%].

Downloaded by UNIV OF GUELPH LIBRARY on June 25, 2012 | http://pubs.acs.org
Publication Date (Web): November 9, 2010 | doi: 10.1021/bk-2010-1051.ch019

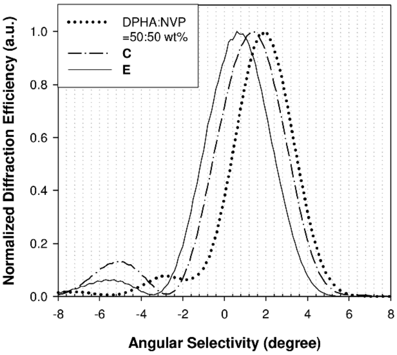

*Figure 9. Angular deviation from the Bragg profile of the gratings formed with **C** and **E** [**DPHA**:**NVP**:(**C** or **E**) = 50:10:40 relative wt%].*

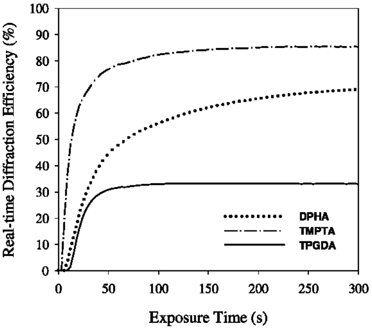

*Figure 10. Real-time diffraction efficiency of the gratings formed with **E** and various **MFA** with 10 wt% **E7** [**MFA**:**NVP**:**E** = 50:10:40 relative wt%].*

The angular shifts from the Bragg condition (0 degree) indicates the extent of volume shrinkage of the grating. As shown in Figure 9, grating formed with **E** having bis(cyclohexene oxide) showed smaller deviation from Bragg condition than grating formed with **C** having bis(glycidyl ether). Gratings formed with only multi-functional acrylate (**DPHA**:**NVP** = 50:50 relative wt%) showed the largest deviation angle. Large volume shrinkage in radical polymerization of the acrylate system is well known. Such volume shrinkage could be reduced by combining the ring-opening cross-linkable monomers. Especially, bis(cyclohexene oxide)s was effective to reduce the volume shrinkage.

## Optimization of Conditions To Form Gratings with High Diffraction Efficiency and Low Volume Shrinkage

Since the gratings formed with bis(cyclohexene oxide) showed only small volume shrinkage, optimization was carried out to create the gratings with low volume shrinkage and high diffraction efficiency. Changes in diffraction efficiency of the gratings formed with recording solutions consisting of **NVP** and **DPHA**,

**TMPTA**, and **TPDA** as **MFA** were observed at constant concentration of **E7** (10 wt%) [**MFA**:**NVP**:**E** = 50:10:40 relative wt%].

As shown in Figure 10, by changing the cross-linking agent, much higher diffraction efficiency over 85% was observed for **TMPTA** and **E**. In case of **DPHA,** the curing process seems to be too fast, leading to a polymer network containing a substantial amount of residual unsaturated functional groups. The high cross-linking density also makes the cured polymer harder, and less flexible, thus phase separation of **E7** should be suppressed to result in lower diffraction efficiency. In contrary, in case of **TPDA**, cross-linking density seems to be too low to push **E7** out toward the low intensity fringes.

To study the degree of phase separation of **E7** from polymer matrix, SEM measurement was carried out. Figure 11 shows the morphologies of gratings formed with **E** and various multi-functional acrylates by SEM at constant concentration of **E7** (10 wt%) [**multi-functional acrylate**:**NVP**:**E** = 50:10:40 relative wt%]. Bright and dark regions are polymer rich layers and **E7** rich layers, respectively.

Although layers were observed for gratings formed with any **MFA**, good phase separation was observed for grating formed with **TMPTA**. Gratings formed with **TPGDA** gave poorer-controlled phase separated structure, presumably because of low cross-linking density resulting in the decrease in elastic force to push out **E7**.

## Angular Selectivity

When the multiplex hologram recording is to be recorded, it is necessary to know the angular selectivity. The smaller the value, the more multiplex data or gratings can be recorded (*35*, *36*).

Angular selectivities ($\Delta\theta_{ang}$) were similar for all samples, irrespective of the structures of epoxides (about 4°) as typically shown in Figure 12. This value is in good agreement with theoretical value according to the Kogelnik's coupled wave theory (*37*) as follows in equation (1):

$$\Delta\theta_{ang} = \frac{1}{2n\sin\theta}\sqrt{\left[\left(\frac{\lambda}{T}\right)^2 - \left(\frac{\Delta n}{\cos\theta}\right)^2\right]} \qquad (1)$$

where n is the average refractive index of recording solution, θ is the internal incident beam angle, *T* is the thickness of the hologram, λ is the recording wavelength, and Δn is the modulation of refractive index of the recording solution after recording.

Downloaded by UNIV OF GUELPH LIBRARY on June 25, 2012 | http://pubs.acs.org
Publication Date (Web): November 9, 2010 | doi: 10.1021/bk-2010-1051.ch019

Downloaded by UNIV OF GUELPH LIBRARY on June 25, 2012 | http://pubs.acs.org
Publication Date (Web): November 9, 2010 | doi: 10.1021/bk-2010-1051.ch019

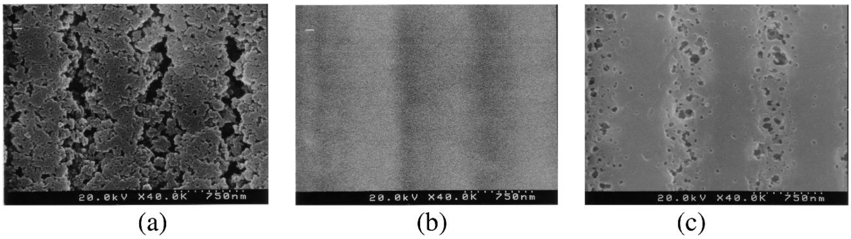

*Figure 11. SEM morphologies ×40K of the gratings formed with **E** and various MFA with 10 wt% **E7** [**MFA**:**NVP**:**E** = 50:10: 40 relative wt%] (a) **DPHA**, (b) **TMPTA**, (c) **TPGDA**.*

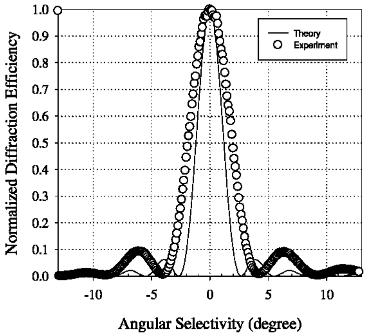

*Figure 12. Angular selectivity of gratings formed with **E** , **TMPTA**, and 5 wt% **E7** [**TMPTA**:**NVP**:**E** = 50:10:40 relative wt%].*

## Photo-Polymerization of SOE and Its Application for Holographic Gratings

Photo-polymerization of **SOE** was studied with FT-IR for the solution composed of **S4SU**:1-methyl-2-pyrrolidone (non-polymerizable) = 45:55 (in weight), **DPI** = 4wt%; **KC**= 0.1wt%, and with 40mW/cm$^2$ incident laser intensity at different irradiation time. A new peak of ester carbonyl group gradually appeared at 1732 cm$^{-1}$ with the increase of irradiation time, and this peak became obvious after 30-35 seconds. This phenomenon demonstrated that **S4SU** could be polymerized under the irradiation of 40mW/cm$^2$ 532 nm laser. The photo-sensitizer cation-radical, or proton generated there from, induced the cationic polymerization of **SOE** (*20*, *38*). In this process, multi-functional acrylate with faster rate could polymerize first at the maxima region of the interference fringe of the incident beams. The polymer formed from multi-functional acrylate was thermodynamically incompatible with **SOE**, and forced **SOE** out from polymerizing regions to low light intensity regions of the interference fringe. In low light intensity regions, after long-term illumination, **SOE** turned into polymer, and refractive index modulation would be generated.

Gratings could be actually fabricated with **SOE**'s together with **TMPTA** and **NVP**. Real-time diffraction efficiency curves were shown in Figure 13.

Downloaded by UNIV OF GUELPH LIBRARY on June 25, 2012 | http://pubs.acs.org
Publication Date (Web): November 9, 2010 | doi: 10.1021/bk-2010-1051.ch019

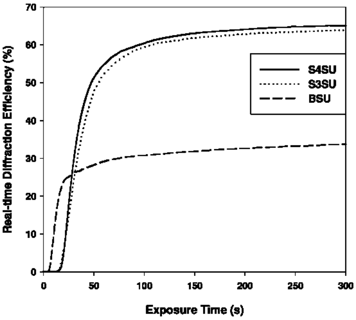

*Figure 13. Real-time diffraction efficiency of the gratings formed with **SOE** at a constant concentration of 1 wt % **DPI** and 0.1 wt % **KC**, and at 40 mW/cm$^2$ intensity with **SOE**:**TMPTA**:**NVP** = 40:40:20 (wt %).*

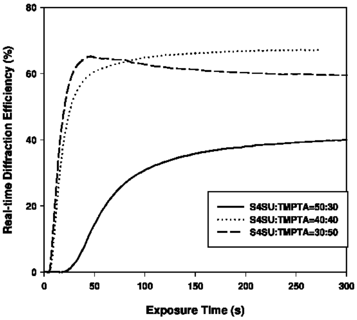

*Figure 14. Effects of ratio of **S4SU** and **TMPTA** on real-time diffraction efficiency at 40 mW/cm$^2$ intensity with 20 wt% **NVP**, 1 wt % **DPI** and 0.1 wt % **KC**.*

Some fabrication conditions were modified using **S4SU** as a representative. The ratio of **SOE** and **TMPTA** plays an important role in forming the gratings with high diffraction efficiency, since the polymerization rate and cross-linking density of **TMPTA** depend on the concentration of **TMPTA**, so, three ratios of **S4SU** and **TMPTA** were used. The results were shown in Figure 14.

It was found that when the ratio of **S4SU** and **TMPTA** was 50:30, introduction period was much longer than other two cases, and resulted diffraction efficiency was the lowest. The reason for this phenomenon is that the concentration of **TMPTA** is too low to cross-link high enough, and that it needs a longer time to form the cross-linked polymer. When the ratio was 30:50, the polymerization rate was high enough to form the holographic gratings in a short time, but the real-time diffraction efficiency slightly decreased after it reached a maximum. This might come from the initial fast non-equilibrium cross-linking followed by the relaxation of the structure because of the too high initial polymerization rate. There should be a balancing point, at which stable holographic gratings can be formed in a short time. The ratio seems to be at around S4SU and **TMPTA** in 40:40.

Downloaded by UNIV OF GUELPH LIBRARY on June 25, 2012 | http://pubs.acs.org
Publication Date (Web): November 9, 2010 | doi: 10.1021/bk-2010-1051.ch019

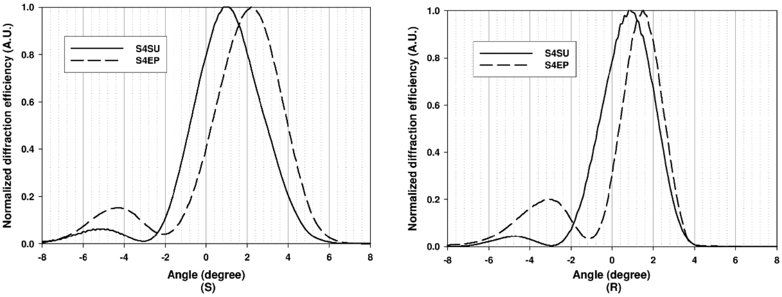

*Figure 15. Angular selectivity for the slanted holographic gratings formed with **S4SU** or **S4EP** and **TMPTA** (**S**: Angular selectivity measured with signal beam; **R**: Angular selectivity measured with reference beam).*

When the **DPI** concentration was lower than 5wt%, the diffraction efficiency of the final holographic gratings increased with the increase of the **DPI** concentration, but this value decreased, when the **DPI** concentration increased to 6wt%. Over this point, the polymerization rate of **TMPTA** is too fast that **S4SU** molecules cannot diffuse easily and resulted in the decrease of the final diffraction efficiency. The intensity of irradiation beams plays an important role when fabricating the holographic gratings with photopolymers, because the photo-polymerization rate is related to the intensity of irradiation as shown below (*39*):

$$R_\mathrm{p} = (\Phi I_0\,[\mathrm{A}]\,d)^{\delta}\,(k_\mathrm{p}/2k_\mathrm{t}^{1/2})\,[\mathrm{M}]$$

where $\Phi$ is the overall initiation efficiency of the process, $I_0$ is the illumination intensity, [A] is the concentration of the species that undergo photo-excitation, $d$ is the thickness of the system being irradiated, and $\delta$ is the value determined by reaction environments. The coefficients $k_\mathrm{p}$ and $k_\mathrm{t}$ are the rate constants of chain propagation and termination, respectively, and [M] is the concentration of monomer.

Degree of volume shrinkage was calculated with the deviations according to equation (1). **S4SU** and **S3SU** showed smaller deviation from Bragg condition, compared with the grating fabricated with **C** and **TMPTA** as shown in Figure 15. Ring-opening of two spiro rings of **SOE** would result in small volume shrinkage. Even volume expansion could be expected (*20*, *40*).

## Effectiveness of Siloxane Network Formation on HPDLC Grating Fabrication

Preliminary experiments confirmed that gratings could be formed using the system **TMPTA**:**MM-TMOS**:**NVP** (10:80:10 wt%) with a 35 wt% **E7** loading. Figure 16 shows the real-time diffraction efficiency of holographic gratings formed with **MM-TMOS** having trimethoxysilyl group capable of siloxane network formation and **MM-TMS** at the ratio of **TMPTA**:**MM-TMOS**, or **MM-TMS**:**NVP** from 10:80:10 wt% to 80:10:10 wt% at constant concentration of **E7** (35 wt%), which was also reported as optimum concentration in grating

Downloaded by UNIV OF GUELPH LIBRARY on June 25, 2012 | http://pubs.acs.org
Publication Date (Web): November 9, 2010 | doi: 10.1021/bk-2010-1051.ch019

formation via different polymerization rate in a former report (*18*). Very low concentration of radical photo-initiator system with **RB**-**NPG** = 0.05 wt% - 0.1 wt% was used to extract the effects of siloxane network formation on diffraction efficiency by suppressing the effects of radical cross-linking by **TMPTA**.

As shown in Figure 16, with low concentration of **MM-TMOS** or **MM-TMS** (**MM-TMOS, MM-TMS** = 10 - 30 wt%), namely with high concentration of **TMPTA**, similarly high initial transient diffraction efficiency over 70% were observed due to the non-equilibrium initial cross-liking of **TMPTA**. However, the diffraction efficiency dropped sharply after the maximum. When the concentration of **MM-TMOS** or **MM-TMS** was higher than 40 wt%, the diffraction efficiency of the gratings formed with **MM-TMOS** was remarkably higher than that formed with **MM-TMS**. Siloxane network formation of **MM-TMOS** by hydrolysis of trimethoxysilyl groups by atmospheric moisture followed by cross-linking via condensation of silanol seems to play an essential role to reinforce the networks produced by radical polymerization in grating formation. In case of **MM-TMS**, adequate cross-linking density could not be obtained. In the following experiments, the recording solution composed of **TMPTA**:**MM-TMOS**:**NVP** =10:80:10 wt% [totally 65 wt%] and **E7** (35 wt%) was used to show the importance of siloxane network formation.

Figure 17 shows the dependence of real-time diffraction efficiency of the gratings formed with **TMPTA**:**MM-TMOS**:**NVP** = 10:80:10 wt% [65 wt%] and **E7** [35 wt%] on the type and concentration of **PS** and **PI**.

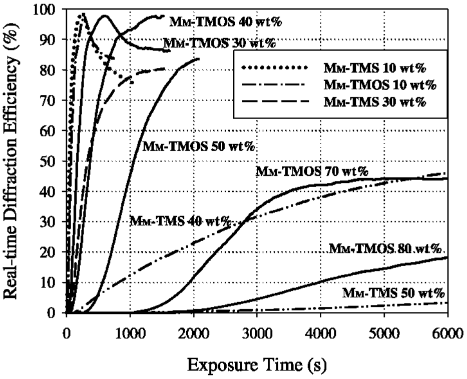

*Figure 16. Real-time diffraction efficiency of the gratings formed with **MM-TMOS** and **MM-TMS** in the ratio of **TMPTA**:**MM-TMOS**, **MM-TMS**:**NVP** from 10:80:10 wt% to 10:80:10 wt%, **E7** (35 wt%), and **RB**-**NPG** (0.05 wt% - 0.1 wt%).*

Downloaded by UNIV OF GUELPH LIBRARY on June 25, 2012 | http://pubs.acs.org
Publication Date (Web): November 9, 2010 | doi: 10.1021/bk-2010-1051.ch019

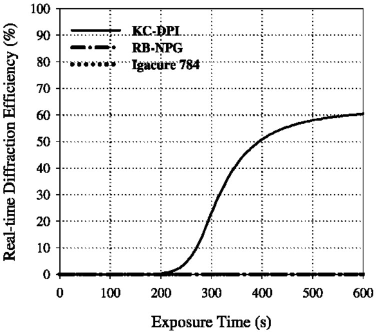

*Figure 17. Real-time diffraction efficiency of the gratings formed with* ***TMPTA****:****MM-TMOS****:****NVP*** *=10:80:10 wt%,* ***E7*** *(35 wt%), and* ***KC-DPI*** *(0.2 wt% - 1 wt%),* ***RB-NPG*** *(0.2 wt% - 1 wt%), or* ***Irgacure 784*** *(1.2 wt%)*

It should be pointed out that at higher concentration of **KC**-**DPI** (0.2 wt%-1 wt%), **RB**-**NPG** (0.2 wt%-1 wt%), and **Irgacure 784** (1.2 wt%), only **KC**-**DPI** initiator system was effective to form gratings with high diffraction efficiency in shorter induction period, strongly indicative that cationic species produced from **KC-DPI** by irradiation is responsible for the hydrolysis and following condensation to give siloxane networks.

## Effects of Alkyl and Spacer Groups in ω-Methacryloxyalkyltrialkoxysilanes on the Formation and Performance of Gratings

In the following study, liquid crystalline compound **TL203** was used. In order to systematically study the influence of alkyl group and spacer group of ω-methacryloxyalkyltrialkoxysilanes on the formation and performance of the formed gratings, their chemical structures were modified as shown in Figure2. The relative concentration was set as **TMPTA**:ω-methacryloxyalkyltrialkoxysilane:**NVP** = 10:80:10 wt% to clearly extract the effects of hydrolysis-condensation of trialkoxysilyl group on the formation of the gratings and the performance of the formed gratings.

Figure 18 shows the real-time diffraction efficiency of holographic gratings formed with various ω-methacryloxyalkyltrialkoxysilanes capable of radical photo-polymerization and hydrolysis- condensation.

When spacer was changed from methylene to propylene (**MP-TMOS**), the diffraction efficiency was dropped to 72% with longer induction period (576 sec). This seems to be because of the higher hydrophobicity of the spacer group compared with **MM-TMOS**. The rate of the hydrolysis-condensation of trialkoxysilyl functions seems very important.

By changing the trialkoxysilyl functional group from trimethoxy to triethoxy (**MP-TMOS** to **MP-TEOS**) with the same propylene spacer, not only the diffraction efficiency was decreased to 13%, but the induction period was also elongated to 693 sec, which again strongly suggested that the hydrolysis-condensation process of trialkoxysilane function is playing an essential role in grating formation.

Downloaded by UNIV OF GUELPH LIBRARY on June 25, 2012 | http://pubs.acs.org
Publication Date (Web): November 9, 2010 | doi: 10.1021/bk-2010-1051.ch019

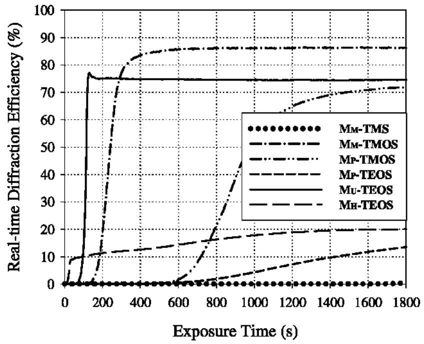

*Figure 18. Real-time diffraction efficiency of the gratings formed with various ω-methacryloxyalkyltrialkoxysilanes in the recording solution with 65 wt% matrix compounds of* ***TMPTA****:ω-methacryloxyalkyltrialkoxysilane:****NVP*** *= 10:80:10 wt% and 35 wt%* ***TL203****, and* ***KC-DPI*** *(0.2 wt% - 2 wt% to matrix compounds) with one beam intensity of 20 $mW/cm^2$.*

In grating formation, induction period basically depends on the time of the formation of cross-linked polymer matrix. In classical grating formation by radical polymerization of multi-functional acrylates, induction period is observed because polymerization does not start until the complete consumption of oxygen present in the system as an inhibitor. In the present system, the induction period depends on the actual gelation time of recording solution assisted by hydrolysis-condensation of trialkoxysilyl functions. The induction period varies by the physical property of ω-methacryloxyalkyltrialkoxysilane derivatives. The rate of the hydrolysis-condensation of trialkoxysilyl functions by moisture strongly depends on the hydrophobicity of the methacrylate monomer. Polymerization of recording solution leads to changes in the chemical potential of the system, and increases the miscibility gap between LC and polymerized matrix

To investigate the effects of chemical structures of spacer between trialkoxysilylalkyl group and methacrylate group, hydrophilic urethane and hydroxylpropylene groups were introduced in the spacer of the monomer structure. The highest diffraction efficiency of 75% and remarkably shorter induction period of 75 sec were obtained for grating formed with **MU-TEOS** having urethane linkage in spacer group. In addition, gratings formed with **MH-TEOS** having hydroxylpropylene group in the spacer showed the shortest induction period of 18 sec, although the diffraction efficiency was considerably low (20%) as shown in Figure 18.

## Analysis of Grating Formation Process by Photo-DSC and FTIR Spectra

Photo-polymerization rate profiles and conversions of reactive monomers were estimated from the heat flux measured by the photo-DSC. When the lowest laser intensity of 2 $mW/cm^2$ was used, the photo-DSC apparently showed three major peaks as shown in Figure 19.

Downloaded by UNIV OF GUELPH LIBRARY on June 25, 2012 | http://pubs.acs.org
Publication Date (Web): November 9, 2010 | doi: 10.1021/bk-2010-1051.ch019

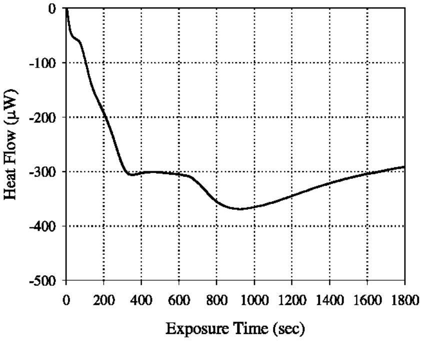

*Figure 19. Heat flow of photo-DSC of matrix compounds with **MU-TEOS** at the ratio of **TMPTA**:**MU-TEOS**:**NVP** = 10:80:10 wt%, and **KC-DPI** (0.2 wt% - 2 wt% to matrix compounds), with laser intensity of 2 mW/cm$^2$.*

The enthalpy of polymerization could be roughly estimated as 50,000 and 20, 000 *J*/mol, respectively, for double bond opening and silanol condensation (*41*). Although it is not easy to assign which process is contributing the most to each peak, it will be reasonable to assign the first peak to the initial radical polymerization and cross-linking of **TMPTA** with four functional group, and second and third for hydrolysis-condensation and polymerization of methacrylate, or vice versa. It might be possible to estimate the reaction rate by monitoring the rate of heat evolution from the polymerization sample.

In IR, a sharp absorption peak at 1634 cm$^{-1}$ corresponds to carbon-carbon double bond gradually decreased with increasing the irradiation time even with the irradiation intensity of 2 mW/cm$^2$, and disappeared completely by irradiation of 113 mW/cm$^2$ laser intensity for 300 sec. The absorption peak at 879 cm$^{-1}$ corresponds to Si-O-Si bending bands was observed from 480 sec irradiation time. The peak became stronger by increasing the irradiation time or by irradiation with higher laser intensity of 113 mW/cm$^2$. These results are very well in accordance with our suggestion of reaction profile.

Since the polymerization of **TMPTA** proceeds very rapidly with heat evolution, care must be taken to ensure that the reaction rate does not exceed the time resolution of the instrument, as the DSC response time is of the order of 0.5s. Relatively low light intensity of 8 mW/cm$^2$ was used to increase the induction time for the grating formation as shown in Figure 20. Actual heat evolution in the actual grating formation with 40 mW/cm$^2$ of two beam intensity should be much faster than the present result.

By comparing Figures 18 and 20, we can notice that the grating formation (total beam intensity= 40 mW/cm$^2$) of the system is slower than the appearance of the peak of heat evolution. This indicates that the gratings are formed after some cross-linking was formed. In case of propylene spacer, grating formation seems much slower than heat evolution maximum. This strongly suggests that the hydrolysis-condensation cross-linking after the initial radical polymerization is mainly contributing to the grating formation for these monomers.

Downloaded by UNIV OF GUELPH LIBRARY on June 25, 2012 | http://pubs.acs.org
Publication Date (Web): November 9, 2010 | doi: 10.1021/bk-2010-1051.ch019

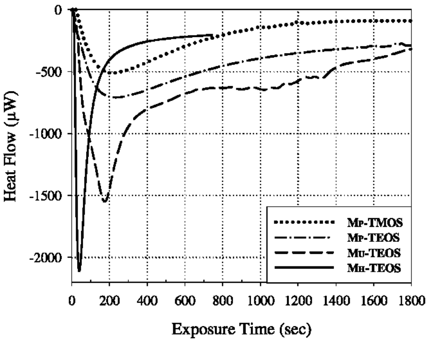

*Figure 20. Photo-DSC analysis of matrix compounds with various ω-methacryloxyalkyltrialkoxysilanes at the ratio of* ***TMPTA****:ω-methacryloxyalkyltrialkoxysilane:***NVP*** *= 10:80:10 wt% and* ***KC-DPI*** *(0.2 wt% - 2 wt% to matrix compounds), with laser intensity of 8 mW/$cm^2$.*

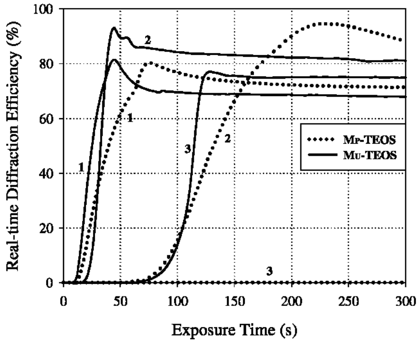

*Figure 21. Real-time diffraction efficiency of the gratings formed with* ***MP-TEOS*** *and* ***MU-TEOS*** *in recording solution of 65 wt% matrix compounds of* ***TMPTA****:ω-methacryloxyalkyltriethoxysilane:***NVP*** *= 90-X:X:10 wt%), 35 wt%* ***TL203****, and* ***KC-DPI*** *(0.2 wt% - 2 wt% to matrix compounds), with one beam intensity of 20 mW/$cm^2$: 1, 2, and 3 represent the X is 10 wt%, 50 wt%, and 80 wt%, respectively.*

Contrary to this, in the case of the methacrylate with urethane or hydroxypropylene spacer, the time difference between the heat evolution and grating formation became much shorter, and the profile of the heat evolution became sharp. **MU-TEOS** had the highest reaction rate and the sharpest heat evolution profile. This may indicate that cross-linking by both radical polymerization and hydrolysis condensation is occurring almost simultaneously, in this case. These behaviors directly influenced the diffraction efficiency as described in Figure 18. If the cross-linking formation by the polymerization of multi-functional acrylate, or by hydrolysis condensation is too fast, polymer matrix will form highly cross-linked networks in the initial stage, which restricts the diffusion of **TL203** to low intensity regions of interference fringes, and results in low diffraction efficiency. Monomer with urethane spacer seems to

Downloaded by UNIV OF GUELPH LIBRARY on June 25, 2012 | http://pubs.acs.org
Publication Date (Web): November 9, 2010 | doi: 10.1021/bk-2010-1051.ch019

have optimum balance of the initial cross-linking and diffusion of LC in grating formation among the samples studied, and resulted in the highest diffraction efficiency with moderate induction time.

From these results, we can point out the important role of the function of cross linking by hydrolysis condensation of trialkoxysilyl group on the performance of gratings, especially hydrophilic moiety of urethane or hydroxy group affected strongly on the rates of formation of cross-linking with siloxane network, even though the reaction rate was slower than the initial cross-linking by multi-functional acrylate. Modification of the formulation of recording solution with **MH-TEOS** might give gratings with higher diffraction efficiency, which is under study now.

To further confirm the effectiveness of urethane moiety in spacer, the concentration of **MP-TEOS** and **MU-TEOS** were varied as shown in Figure 21.

At low concentration of **MP-TEOS** and **MU-TEOS** (10 wt%), namely with high concentration of **TMPTA** (80 wt%), where **TMPTA** is playing an essential role in cross-linking, similarly high initial transient diffraction efficiency of about 70% and short induction periods about 12 sec were observed for both systems due to the non-equilibrium initial cross-liking of **TMPTA**. When the concentration of the monomers was 50 wt%, the grating with remarkably higher diffraction efficiency was formed much faster with **MU-TEOS** than with **MP-TEOS**. By increasing the concentration of **MP-TEOS** and **MU-TEOS** to 80 wt%, their differences in diffraction efficiency and induction periods became more remarkable. The **MP-TEOS** system could not form any grating in 300 sec, although it could start to form grating after 700 sec.

From these results, the chemical structure of spacer of ω-methacryloxyalkyltriethoxysilane seems to play an essential role to assist the formation of cross-linking networks in polymer matrix. The siloxane network formation and radical polymerization of **MU-TEOS** might be simultaneously promoted by hydrolysis of triethoxysilyl group and condensation of silanol assisted by the hydrophilic urethane group.

To study the morphology of gratings formed with **MU-TEOS**, **SEM** measurement was carried out. Figure 22 shows the surface morphologies of gratings formed with **MU-TEOS** at the ratio of **TMPTA**:**MU-TEOS**:**NVP**= 10, or 30:80, or 60:10 wt% and **TL203** (35 wt %) after washing with methanol for over night.

Periodic gratings were clearly formed and grating spacing were about 0.9 and 0.7 μm for gratings with 80 wt% and 60 wt%, respectively [Figure 22 (a) and (b)]. This value was in good agreement with the calculated spacing (0.96 μm) by Bragg's equation. Longer grating spacing was observed in case of 80 wt% [Figure 22 (a)] than the cases of lower concentration of 60 wt% **MU-TEOS** [Figure 22 (b)]. It maybe considered that in high concentration of **MU-TEOS**, volume shrinkage caused during formation of polymer matrix was restrained due to higher concentration of siloxane network in polymer matrix. However, some cracks were observed in gratings formed with 80 wt% **MU-TEOS** as shown in Figure 22 (a), which attributed to high vitrification of the polymer matrix, whereas, in case of 60 wt%, there was no crack in inside of gratings.

Downloaded by UNIV OF GUELPH LIBRARY on June 25, 2012 | http://pubs.acs.org
Publication Date (Web): November 9, 2010 | doi: 10.1021/bk-2010-1051.ch019

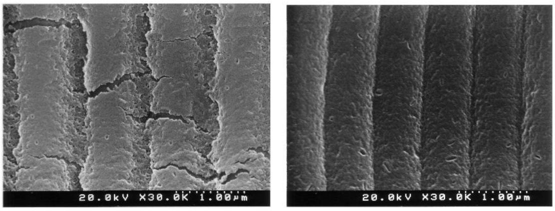
20.0kV X30.0K 1.00µm
20.0kV X30.0K 1.00µm

(a) (b)

*Figure 22. SEM morphologies of the gratings formed with* ***MU-TEOS*** *in recording solution with 65 wt% matrix compounds of* ***TMPTA****:****MU-TEOS****:****NVP****= 90-X:X:10 wt%, 35 wt%* ***TL203****, and* ***KC-DPI*** *(0.2 wt% - 2 wt% to matrix compounds): X is (a)* ***80 wt%,*** *×30K and (b)* ***60 wt%****, ×30K.*

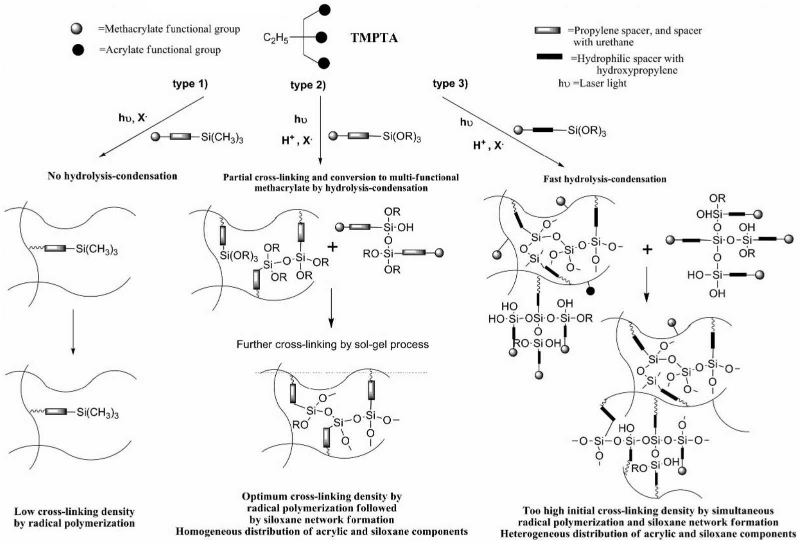
=Methacrylate functional group
=Acrylate functional group
$C_2H_5$
TMPTA
=Propylene spacer, and spacer with urethane
=Hydrophilic spacer with hydroxypropylene
hυ =Laser light
type 1)
type 2)
type 3)
hυ, X·
$Si(CH_3)_3$
hυ
H⁺, X·
$Si(OR)_3$
No hydrolysis-condensation
Partial cross-linking and conversion to multi-functional methacrylate by hydrolysis-condensation
Fast hydrolysis-condensation
Further cross-linking by sol-gel process
Low cross-linking density by radical polymerization
Optimum cross-linking density by radical polymerization followed by siloxane network formation
Homogeneous distribution of acrylic and siloxane components
Too high initial cross-linking density by simultaneous radical polymerization and siloxane network formation
Heterogeneous distribution of acrylic and siloxane components

*Scheme 1. Proposed matrix formation processes: 1) radical cross-linking by* ***TMPTA****, 2) simultaneous radical cross-linking of* ***TMPTA*** *and small amounts of multi-functional methacrylate formed via hydrolysis-condensation of trialkoxysilyl group, followed by further cross-linking by hydrolysis, 3) competing rapid cross-linking of (meth)acrylate functions and sol-gel process of trialkoxysilane function, followed by further cross-linking by radical polymerization and sol-gel process.*

To summarize the results, we may consider that the radically mono-functionally polymerizable 3-methacryloxypropyltrialkoxysilane became apparently multi-functional cross-linkable monomer by hydrolysis and condensation of trialkoxysilyl group as shown in Scheme 1, which induced the high concentration of cross-linking with moderate rate by the hydrolysis.

In case of methacryloxymethyltrimethylsilane, cross-linking density is not high enough to form grating. This process corresponds to type 1) in Scheme 1. In **TMOS** or **TEOS** system, the hydrolysis of trialkoxysilyl group is relatively slow compared with the fast radical polymerization of **TMPTA**. Thus, grating formation is not rapid, but following cross-linking by hydrolysis assisted the formation of polymer matrix and further diffusion of LC to form gratings with high diffraction efficiency. By the introduction of urethane function in the spacer, the hydrophilic nature of the spacer increases the hydrolysis of triethoxysilyl group by moisture, and converts mono-functional methacrylate to apparently multi-functional methacrylate, and assisted the formation of polymer matrix by radical polymerization together with cross-linking by hydrolysis condensation. This process corresponds to type 2) in Scheme 1. In case of the introduction of hydroxypropylene spacer, too much hydrophilic nature of the spacer strongly enhanced the hydrolysis of the trialkoxysilyl group, and created the situation where apparently high concentration of multi-functional (meth)acrylates in the initial polymerization solution, and resulted in rapid formation of grating by radical cross-linking, but low diffraction efficiency. This process corresponds to type 3) in Scheme 1.

Gradual formation of cross-linking, which facilitates the almost complete phase separation of LC, is very important to obtain high diffraction efficiency, and the decreased existence of few double bond is also very important for the long term stability. Well-balanced cross-linking by radical polymerization and sol-gel process in type 2) process for **MU-TEOS** seems to have given stable grating with high diffraction efficiency.

Downloaded by UNIV OF GUELPH LIBRARY on June 25, 2012 | http://pubs.acs.org
Publication Date (Web): November 9, 2010 | doi: 10.1021/bk-2010-1051.ch019

## Conclusions

High performance transmission holographic polymer dispersed liquid crystals were fabricated using a mixture of dipentaerythritol penta/hexaacrylate, 1,5-bis(3-glycidoxypropyl)-1,1,3,3,5,5-hexamethyltrisiloxane, 1-vinyl-2-pyrrollidone (reactive diluent), and commercial liquid crystal, E7 (45:36:9:10 in weight percent) by Nd-YAG laser (λ=532nm) in the presence of diphenyliodonium hexafluorophosphate and 3,3′-carbonylbis(7-diethylaminocoumarin). 1,5-Bis[2-(1,2-epoxycyclohex-4-yl)ethyl]-1,1,3,3,5,5-hexamethyl-trisiloxane gave a little lower diffraction efficiency (75%), but it gave gratings with reduced angular deviation (0.6 degree for signal beam at 32 degree incident angle) from Bragg profile. The volume shrinkage of the gratings formed with spiroorthoesters was much lower than that prepared with bis(epoxide)s. Gratings were also formed for matrix of trimethylolpropane triacrylate:methacryloxymethyltrimethoxysilane:1-vinyl-2-pyrrolidone in the range from 80:10:10 to 10:80:10 wt% and E7. Importance of hydrophilicity of the spacer group was examined using TL203 as a liquid crystal. Introduction of urethane group or hydroxy group in the spacer dramatically improved the performance of the gratings.

Downloaded by UNIV OF GUELPH LIBRARY on June 25, 2012 | http://pubs.acs.org
Publication Date (Web): November 9, 2010 | doi: 10.1021/bk-2010-1051.ch019

## Acknowledgments

The authors would like to thank the former students for their participation in the research works, and financial support by a Grant-in-Aid for Scientific Research (16205016) from the Ministry of Education, Science, Sports, Culture and Technology, Japan. This work was also partly supported by a City Area Program from the Ministry of Education, Science, Sports, Culture and Technology, Japan.

## References

1. Luther, B. J.; Springer, G. H.; Higgins, D. A. *Chem. Mater.* **2001**, *13* (7), 2281–2287.
2. Cho, Y. H.; Kim, B. K.; Lee, J. S. *Polymer* **2000**, *41*, 1325–1335.
3. Kyu, T.; Nwabunma, D. *Macromolecules* **2001**, *34* (26), 9168–9172.
4. Kubo, S.; Gu, Z. Z.; Takahashi, K.; Ohko, Y.; Sato, O.; Fujishima, A. *J. Am. Chem. Soc.* **2002**, *124* (37), 10950–10951.
5. Drzaic, P. S. *Liquid Crystal Dispersions*; World Scientific Publishing Company: River Edge, NJ, 1995.
6. Park, M. S.; Cho, Y. H.; Kim, B. K.; Jang, J. S. *Curr. Appl. Phys.* **2002**, *2* (3), 249–252.
7. Pikas, D. J.; Kirkpatrick, S. M.; Tomlin, D. W.; Natarajan, L.; Tondiglia, V.; Bunning, T. J. *Appl. Phys. A: Mater. Sci. Process.* **2002**, *74*, 767–772.
8. Jung, J. A.; Kim, B. K. *Opt. Commun.* **2005**, *247* (1-3), 125–132.
9. Bunning, T. J.; Natarajan, L. V.; Tondiglia, V. P.; Sutherland, R. L. *Annu. Rev. Mater. Sci.* **2000**, *30*, 83–115.
10. Lucchetta, D. E.; Criante, L.; Simoni, F. *J. Appl. Phys.* **2003**, *93* (12), 9669–9674.
11. Sutherland, R. L.; Natarajan, L. V.; Tondiglia, V. P.; Bunning, T. J. *Chem. Mater.* **1993**, *5*, 1533–1538.
12. Jazbinsek, M.; Olenik, I. D.; Zgonik, M.; Fontecchio, A. K.; Crawford, G. P. *J. Appl. Phys.* **2001**, *90* (8), 3831–3837.
13. Zhang, J.; Carlen, C. R.; Palmer, S.; Sponsler, M. B. *J. Am. Chem. Soc.* **1994**, *116*, 7055–7063.
14. Lucchetta, D. E.; Karapinar, R.; Manni, A.; Simoni, F. *J. Appl. Phys.* **2002**, *91* (9), 6060–6065.
15. Cho, Y. H.; Shin, C. W.; Kim, N.; Kim, B. K.; Kawakami, Y. *Chem. Mater.* **2005**, *17*, 6263–6271.
16. Cho, Y. H.; He, M.; Kim, B. K.; Kawakami, Y. *Sci. Technol. Adv. Mater.* **2004**, *5*, 319–323.
17. Cho, Y. H.; Kawade, R.; Kubota, T.; Kawakami, Y. *Sci. Technol. Adv. Mater.* **2005**, *6*, 435–442.
18. He, M.; Cho, Y. H.; Kim, N.; Kawakami, Y. *Des. Monomers Polym.* **2005**, *8*, 473–486.
19. He, M.; Cho, Y. H.; Kawakami, Y. *Polym. J.* **2006**, *38*, 678–685.
20. Chikaoka, S.; Takata, T.; Endo, T. *Macromolecules* **1992**, *25*, 625–628.
21. Date, M.; Takeuchi, Y.; Kato, K. *Jpn. J. Appl. Phys.* **1999**, *32*, 3164–3168.

22. Bunning, T. J.; Natarajan, L. V.; Tondiglia, V. P.; Sutherland, R. L.; Vezie, D. L.; Adams, W. W. *Polymer* **1995**, *36*, 2699–2708.
23. Natarajan, L. V.; Shepherd, C. K.; Brandelik, D. M.; Sutherland, R. L.; Chandra, S.; Tondiglia, V. P.; Tomlin, D.; Bunning, T. J. *Chem. Mater.* **2003**, *15*, 2477–2484.
24. Park, M. S.; Kim, B. K.; Kim, J. C. *Polymer* **2003**, *44* (5), 1595–1602.
25. Liu, Y. J.; Zhang, B.; Jia, Y.; Xu, K. S. *Opt. Commun.* **2003**, *218*, 27–32.
26. Sarkar, M. D.; Qi, J.; Crawford, G. P. *Polymer* **2002**, *43*, 7335–7344.
27. Escuti, M. J.; Kossyrev, P.; Crawford, G. P. *Appl. Phys. Lett.* **2000**, *77*, 4262–4264.
28. Cairns, D. R.; Bowley, C. C.; Danworaphong, S.; Fontecchio, A. K.; Crawford, G. P.; Li, L.; Faris, S. M. *Appl. Phys. Lett.* **2000**, *77*, 2677–2679.
29. Cho, Y. H.; Kawakami, Y. *Silicon Chem.* **2005**, *3*, 219–227.
30. Gomurashvili, Z.; Crivello, J. V. *Macromolecules* **2002**, *35*, 2962–2969.
31. Gomurashvili, Z.; Crivello, J. V. *J. Polym. Sci., Part A-1: Polym. Chem.* **2001**, *39*, 1187–1197.
32. Crivello, J. V.; Jiang, F. *Chem. Mater.* **2002**, *14*, 4858–4866.
33. Nishida, H.; Sanda, F.; Endo, T.; Nakahara, T.; Ogata, T.; Kusumoto, K. *J. Polym. Sci., Part A-1: Polym. Chem.* **2000**, *38*, 68–73.
34. Waldman, D. A.; Ingwall, R. T.; Dhal, P. K.; Horner, M. G.; Kolb, E. S.; Li, H.-Y. S.; Minns, R. A.; Schild, H. G. *SPIE* **1995**, *2689*, 127–141.
35. Rhee, U. S.; Caulfield, H. J.; Shamir, J.; Vikram, C. S.; Mirsalehi, M. M. *Opt. Eng.* **1993**, *32* (8), 1839–1847.
36. Mok, F. H. *Opt. Lett.* **1993**, *18* (11), 915–917.
37. Kogelnik, H. *Bell Syst. Tech. J.* **1969**, *48*, 2909–2947.
38. Tanigaki, K.; Saigo, K.; Ohnishi, Y.; Kato, H.; Mizutani, K.; Ogasawara, T.; et al. *J. Appl. Polym. Sci.* **1985**, *30*, 1419–1428.
39. Mishra, M. K.; Yagci, Y. *Handbook of Radical Vinyl Polymerization*; Marcel Dekker: New York, 1998.
40. Baily, W. J. *Macromol. Sci. Chem.* **1975**, *A9*, 849.
41. Patai, S., Rappoport, Z., Eds.; *The Chemistry of Organic Silicon Compounds*; John Wiley & Sons: New York, 1989.

Downloaded by UNIV OF GUELPH LIBRARY on June 25, 2012 | http://pubs.acs.org
Publication Date (Web): November 9, 2010 | doi: 10.1021/bk-2010-1051.ch019

Downloaded by PENNSYLVANIA STATE UNIV on June 23, 2012 | http://pubs.acs.org
Publication Date (Web): November 9, 2010 | doi: 10.1021/bk-2010-1051.ch020

## Chapter 20

# Foam Control

**Michael J. Owen**[*]

**Michigan Molecular Institute, Midland, MI 48640**
**[*]michaelowen01@chartermi.net**

Polydimethylsiloxane (PDMS) is the dominant product of the large, growing, over 60-year-old silicone market, now of the order of $10 billion in world-wide sales. Although not presented at the *"Silicones and Silicone-Modified Materials IV"* symposium in San Francisco, we felt it worthwhile to take a deeper look at an application that has been a major component of the industry throughout its history and which is expected to maintain its importance in the future. The chosen application is foam control and the approach is akin to that adopted in the earlier review chapter on properties and applications of silicones, namely an exploration, but at rather greater depth, of the relationship between the properties of PDMS and this application.

## Introduction

The defoaming capabilities of silicone fluid were apparent to the earliest investigators from the moment they cleaned their dirty glassware. However, it was not until the early 60's that truly efficient silicone antifoams for aqueous foams were developed. The breakthrough was the introduction of finely-divided hydrophobic solids into the silicone fluid, or, in the language of the silicone technologist, the compounding of such solids into fluids to produce silicone compounds. Hydrophobic solids were first introduced into hydrocarbon-based antifoams in 1963 (*1*), an invention that is recognized as a major milestone in the evolution of modern antifoams. Note, however, that silicone antifoam compositions containing silica aerogels or fumed silicas had been described earlier (*2*).

That finely-divided hydrophobic solids are detrimental to aqueous foam stability is apparent to anyone who has cleaned an electric shaving razor over

In Advances in Silicones and Silicone-Modified Materials; Clarson, S., et al.;
ACS Symposium Series; American Chemical Society: Washington, DC, 2010.

the bathroom sink. The audible and visual breaking of any foam in the sink is striking. This has led some investigators to suggest that it is the particulate not the fluid component of an antifoam that is the active species and even that there is no need for the latter component. This might be so if one could always rely on gravity to bring the hydrophobic particles into contact with the foam films or lamellae. However, sprinkling such powders over the foam is not universally convenient and perhaps the main role of the fluid is to deliver the hydrophobic solid to the surface of a foam film where it can be effective.

Two important keys to effective antifoam action seem to be that the antifoam material must be surface active, i.e. of lower surface energy, with respect to the foaming medium, and insoluble in it (*3*). The former criterion is essential for the antifoam to displace the foam stabilizers already present in the film lamellae surfaces of any troublesome persistent foam. The latter criterion has several aspects. It will enhance efficiency by ensuring no material is wasted by dissolution in the bulk of the foaming medium. More importantly, soluble surface-active materials often promote foaming and it would be counterproductive to have this characteristic to any great extent in an antifoam product. This characteristic can be readily demonstrated by incorporating silicone fluids in organic materials such as engine lubricating oils. Up to the point where the silicone is soluble in the oil it promotes foaming of the oil, but once the saturation point is reached the insoluble silicone will efficiently defoam that oil. These various properties of silicones were appreciated from the beginning of the silicone industry in the Second World War. For example, the first use of silicone to insulate the electrical systems of aircraft had much to do with its low surface energy and hydrophobicity. Quantitative public disclosure of these properties came after hostilities had ceased (*4*).

Thus it would seem that what might be most desirable is a hydrophobic fluid/solid combination for aqueous foams and an oleophobic fluid/solid combination for organic foams. It turns out that this is the case for aqueous defoaming but there is little need for oleophobic solids in antifoams used to control foaming organic or hydrocarbon liquids as in most instances, an insoluble, surface-active oleophobic fluid will suffice. This state of affairs can be attributed to the extra foam stabilizing mechanisms available in aqueous media. Oil foam films are usually relatively thick and stabilized by surface elasticity and surface viscosity effects, whereas aqueous films can become very thin due to electrical double-layer and entropic repulsion effects resulting from the close-packed surfactant assemblies at the two surfaces of each aqueous foam film. Put another way, oil foams tend to remain as round bubble foams, *kugelschaum* in the classic foam literature, while aqueous foams can often drain to polyhedral foams, or *polyhederschaum*, on account of the foam stabilizing mechanisms that only operate to marked effect in aqueous media. The essential point to appreciate is that aqueous foams can be, and often are, significantly more stable than their non-aqueous cousins. Of course, water is the most important terrestrial solvent and should be the first choice in any process development, so clearly antifoams for aqueous systems are the more important, challenging and interesting category.

The concept of foam control should cover the gamut from partial reductions in foam volume or persistence, through complete eradication of all traces of foam, to the inhibition of any tendency to produce foam. The reduction or destruction

Downloaded by PENNSYLVANIA STATE UNIV on June 23, 2012 | http://pubs.acs.org
Publication Date (Web): November 9, 2010 | doi: 10.1021/bk-2010-1051.ch020

Downloaded by PENNSYLVANIA STATE UNIV on June 23, 2012 | http://pubs.acs.org
Publication Date (Web): November 9, 2010 | doi: 10.1021/bk-2010-1051.ch020

of pre-existing foam is best described as *defoaming* or foam breaking, whereas the prevention of foam production is most appropriately described as *antifoaming* or foam inhibition. There is no ordered surfactant monolayer to be dealt with in the latter case and one might expect that different mechanisms could be operating, for example, a possible suppression of foam film nucleation effects. However, in practice, the same materials are effective defoamers and antifoams, suggesting that this is not the case. It implies that at least some initial development of foam films may be occurring even in the antifoaming case. Here, as is the usual custom in the industry, the two product terms defoamer and antifoam will generally be used interchangeably.

One situation that is different, and requires different compositions to control it, is the suppression of *microfoam*. This is characterized by very stable, small bubbles a few micrometers in size. These microbubbles can be troublesome in coatings and as they never develop significant film structure, conventional antifoam materials are not very effective in their control. Certain silicone-glycol copolymer materials are useful in this application (*5*). They appear to function by promoting coalescence of several microbubbles into a larger macrobubble whose larger size and surface area enables it to migrate to the surface of a coating faster than individual microbubbles. Varying the type and composition of the silicone-glycol copolymer to provide correct balance of defoaming action and compatibility but performance can be further improved by blending with suitable non-silicone cosurfactants.

## Antifoam Components

### Silicone Fluids

Polydimethylsiloxane [PDMS] comes close to the universal antifoam fluid. This application accounts for about 7% of the total usage of PDMS fluids (*6*). With its low surface tension in the 20 – 21 mN/m range depending on molecular weight, it is surface active with respect to the overwhelming majority of organic surfactants used in aqueous media. Only silicone surfactants and fluorosurfactants will have lower surface energies. Moreover, PDMS is certainly adequately insoluble in water. The water solubility of even oligomeric PDMS is only in the parts per billion range; with increasing molecular weight it decreases to parts per trillion (*7*). Being the mainstay of the silicone industry, PDMS is available at reasonable cost in a wide variety of molecular weights. These considerations may be why, as yet, there is no widespread use of fluoropolymers such as polyethers. However, fluorosilicone fluid antifoams based on polymethyltrifluoropropylsiloxane [PMTFPS] do enjoy some specialized uses such as in dry cleaning solvent recovery. PDMS fluids are soluble foam promoters in such solvents but PMTFPS is sufficiently insoluble to be effective as an antifoam. Its surface tension is somewhat higher than PDMS but still sufficiently lower than typical dry-cleaning solvents. Other areas where fluorosilicone antifoams are effective include diesel oil, crude oil-gas separation, and distillation of middle cut fuels (*8*). Occasionally one encounters other silicone antifoam fluids such as cyanoalkyl-substituted materials which are reported to be effective foam inhibitors for power fuels for internal-combustion engines and jet engines (*9*).

Moreover, silicone fluids such as PDMS contribute no foam-stabilizing tendencies of their own to aqueous foaming. For instance, there are no charged entities to contribute to charged double-layer repulsion effects. Furthermore, the surface shear viscosity of PDMS is the lowest known for any polymer (*10*), so no potential impact on foam stabilization can arise from this aspect. Naturally, despite these advantages, PDMS is not the only fluid used in antifoam compositions. The three other common classes of liquid phase components found in defoamers are: hydrocarbons, polyethers, and fluorocarbons.

Downloaded by PENNSYLVANIA STATE UNIV on June 23, 2012 | http://pubs.acs.org
Publication Date (Web): November 9, 2010 | doi: 10.1021/bk-2010-1051.ch020

## Hydrophobic Solids

The most widely used hydrophobic solid in antifoam product formulations is hydrophobic silica. As with PDMS, silica is widely available in different particle sizes at reasonable cost. Hydrophobization is possible with a variety of organic treatments but the use of hydrophobic silanes or siloxanes, particularly PDMS, are the preferred treatments. The three most common ways of preparing such a silica are to spray the silica with silicone oil and heat at 250-350°C, to treat with organochlorosilane vapors in an autoclave, and to disperse the silica in a silicone oil at elevated temperatures (*3*). In this context, it is possible to consider the hydrophobic silica as a solid silicone since its surface is silicone. Note, however, that certain antifoam formulations contain silicone resins as the hydrophobic particle component that are more deserving of the description solid silicones. Fluorochemical treatments of silica or dispersed fluoropolymer solids such as PTFE are possible, but not widely used. Hydrophobic organic waxes such as naturally occurring montan wax and fatty acid amides such as ethylenediamine distearamide are another important class of hydrophobic antifoam solid.

## Emulsions

The silicone fluid component of an antifoam compound can be considered as a very effective “delivery system” of the active dispersed hydrophobic solid to the foam films. However, in almost all cases there is a need to further enhance this “ease of delivery” of the antifoam fluid or compound to the foaming system. This is a third important key to efficient antifoaming, in addition to insolubility and surface activity. The incorporation of dispersants and emulsifiers in silicone antifoam formulations is another major milestone in effective antifoam development (*11*). Many commercial and industrial processes are water based and the insoluble antifoam compound will not always readily disperse when added to aqueous solutions. The emulsifying tendencies of the profoaming surfactant may help bring about its own downfall by aiding in antifoam compound dispersal but the simple, certain solution most frequently adopted is to pre-emulsify the compounds. Thus most commercial silicone antifoams are oil-in-water emulsions of silicone oil/solid compounds. Even the earliest silicone antifoams, developed before the benefits of hydrophobic silica incorporation became apparent, contain additives to facilitate the dispersion of the silicone thereby enhancing the foam-suppressing effect (*11*).

These emulsions are stabilized by emulsifiers which require somewhat contradictory characteristics. They need to be sufficiently stabilizing that the antifoam emulsion does not break in storage but not so stable that they resist entering and spreading of the compound droplet at the foam lamellae. Antifoams are added at low levels to the foaming medium so there is extensive dilution which aids in this desired emulsion breakage at the point of the action. Interestingly, these silicone antifoam emulsions are stabilized by conventional organic emulsifiers and not by silicone surfactants. The usual rules of preferred HLB (hydrophile/lipophile balance) and use of cosurfactants apply in much the same way as they do for the emulsification of organic fluids.

Downloaded by PENNSYLVANIA STATE UNIV on June 23, 2012 | http://pubs.acs.org
Publication Date (Web): November 9, 2010 | doi: 10.1021/bk-2010-1051.ch020

Because of the dangers of bacterial spoilage of these organic emulsifiers, such antifoam emulsions usually contain biocides to prevent this difficulty. Neither is this the end of potential complexity of a commercial antifoam product. We know that silicones are not the only possible fluid component. For certain applications combinations of silicones with other fluids, particularly glycols such as poly(propylene oxide) [PPO], have been found to offer advantages. Such products may contain specialized polymer-in-polymer emulsifiers to combine the dissimilar phases. This is an aspect of antifoam formulation where the incorporation of silicone surfactants, copolymers of PDMS and PPO, is necessary and beneficial.

## Formulation Variables

Even without such refinements, there are many variables for the formulation chemist to adjust in the preparation of antifoam products. Fluid variables include polymer type, molecular weight [MW] and polydispersity, degree of branching or cross-linking, and copolymerization possibilities. Hydrophobic solid variables include treatment type and extent, particle size and distribution, and aspect ratio. Obviously, the relative ratios of fluid, solid, emulsifiers, water content etc. can also be varied. This is the realm of the experienced formulator aided by the tools of designed experimentation. Certain variables are more important than others and more is known about their impact on product performance.

Thus fluid molecular weight can be an important variable. Should very rapid knockdown of an existing foam be desired then a relatively low MW fluid would be indicated. This would enter foam films and spread on them more rapidly than a higher MW material thereby delivering the hydrophobic solid sooner to where it can be most effective. If longer term retention of antifoam action is required then higher MW, aided perhaps by more stabilizing emulsifiers, might be in order. The particle size of the antifoam compounds, the antifoam emulsion droplets, and the hydrophobic solids all have important effects. More particles mean more points of attack on the foam but each individual assault will be smaller and perhaps, ultimately, too small to be effective. Clearly, optimum size effects are to be anticipated. One aspect of these size considerations is to supply hydrophobic solids whose size is related to the thickness of the foam films being encountered or at least are no smaller. In this way particles can bridge the foam film and beneficial defoaming mechanisms such as dewetting of the film from the hydrophobic solid surface can occur at both surfaces of the film leading to rapid film collapse. In practice, antifoam droplets are significantly larger than typical foam thicknesses.

There are various other aspects of antifoam action and application that are still imperfectly understood. Not enough is yet known about all the interactive effects of these many variables to design an optimum antifoam for a given foam control problem without some preliminary testing. Present knowledge and prior experience are usually sufficient for a small number of possibilities to be selected for field trails. Standardized test methods and model foaming solutions are available but are not always used. Commonly, little more than shake-tests are carried out on the actual foaming liquor in question before moving to *in situ* trials.

Downloaded by PENNSYLVANIA STATE UNIV on June 23, 2012 | http://pubs.acs.org
Publication Date (Web): November 9, 2010 | doi: 10.1021/bk-2010-1051.ch020

## Foam Control Mechanisms

It is a fundamental principle of thermodynamics that a system will tend to change spontaneously in the direction which will lower its free energy. The surface component of this free energy is the product of the surface energy per unit area and the total surface area. Note that for liquid systems surface energy per unit area (mJ/m$^2$) and surface tension per unit length (mN/m) are equivalent. Thus reductions in either surface tension or total area will be thermodynamically favored. In order for a profoaming surfactant to be adsorbed at the surface of a liquid it must produce a lower surface energy state, i.e. have a lower surface tension than the liquid. Likewise, if a defoamer is to be active at a surfactant-stabilized surface it must be more surface active than the surfactant. In the same way, reductions in total surface area are favored. It follows that foams are inherently unstable in a thermodynamic sense and anything more than a transient foam will generally require a stabilizer or profoamer to be present in the surface layers of foam films.

The stabilization results from four main effects: surface elasticity, viscous drainage retardation effects, reduced gas diffusion between bubbles, and other thin-film stabilization effects from the interaction of the opposite surfaces of the film (*3*). This last set of effects includes electric double-layer repulsions from ionic surfactants and entropic repulsion of polymer chains.

The stability of a single foam film is governed by the Gibbs elasticity which arises from the reduction in equilibrium surface concentration of adsorbed surfactant molecules when the film is extended. In a dynamic foam system the related time-dependent Marangoni effect is more relevant (*3*). Transient decreases in surface concentration caused by expansive fluctuations in the film surface result in increases in surface tension because of the finite rate of surfactant adsorption. This increase in surface tension provides the restoring force opposing expansion that is the source of the foam-stabilizing Marangoni effect. Such non-equilibrium surface properties are usually studied in dilatational experiments where the surface is periodically expanded and contracted. The complex dilatational modulus of a surface is a function of the dilatational elasticity and the dilatational surface viscosity. Stable foams possess high values of both these quantities: accordingly, antifoams should reduce them. Very little experimental data are available to test

Downloaded by PENNSYLVANIA STATE UNIV on June 23, 2012 | http://pubs.acs.org
Publication Date (Web): November 9, 2010 | doi: 10.1021/bk-2010-1051.ch020

these concepts but the effect has been verified for silicone antifoams in crude oils. Callaghan (*12*) has shown reductions in both the surface dilatational elasticity and viscosity in this system. These reductions presumably come about either by complete replacement of the profoamer species by an antifoam surface layer, or by dilution or mixing of the antifoam with the surfactant. These two possible mechanisms were originally advanced by Ross (*13*).

Viscous drainage retardation effects can arise from both increased bulk and surface shear viscosity. The stabilizing effect of bulk viscosity increase can be seen by adding glycerol to aqueous surfactant solutions; it is the only exception to our earlier generalization that foam stabilization mechanisms are surface processes requiring concentration of the stabilizer into the surface layers of a foam film. The very low surface shear viscosity of PDMS, the lowest known for any liquid polymer, has already been mentioned (*10*). It is recognized as a significant contributory factor to its effectiveness as an antifoam.

One of the fundamental equations of capillarity, the Laplace equation (*14*), shows that there is a pressure difference across a curved interface that increases as the curvature increases. As a consequence, gas diffusion occurs between adjacent bubbles causing the larger one to grow and the small one to diminish. These bubble size changes introduce mechanical stresses which ultimately break the foam films. This is the reason single films persist longer than the corresponding foam, but the effect seems to be a relatively minor factor in practical defoaming situations.

We have already seen that there are three fundamental requirements of a potential antifoam or defoamer material (*8*):

- It must be insoluble in the foaming medium
- It must be readily dispersible in the foaming medium
- It must have a lower surface energy than the foaming medium

Most antifoam oils have surface tensions in the 20 to 40 mN/m range whereas most organic surfactant solutions and other aqueous media have surface tensions between 30 and 50 mN/m. As shown in Table 1, PDMS has a surface tension *ca* 21 mN/m at high molecular weight. Being near the lower end of the antifoam oil surface tension range has much to do with its broad range of applicability. Table 1 also includes other surface properties of PDMS that are relevant to this discussion of foam control mechanisms.

The basic processes involved in the replacent of surfactant-stabilized surface layers and the subsequent collapse of foam films by defoamers are (*8*);

- Entering
- Bridging
- Dewtting
- Rupture

Figure 1 illustrates these processes from the work of Hill and Fey (*8*).
Entering is governed by the entering coefficient, E, given in equation 1:

$$E = \sigma_f + \sigma_{af} - \sigma_a \qquad \text{(i)}$$

Downloaded by PENNSYLVANIA STATE UNIV on June 23, 2012 | http://pubs.acs.org
Publication Date (Web): November 9, 2010 | doi: 10.1021/bk-2010-1051.ch020

**Table 1. PDMS Surface Property Data**

| *Property* | *Value* | *Comments* |
|---|---|---|
| Liquid surface tension | 21.3 mN/m | Extrapolated to “infinite” MW (*15*) |
| Interfacial tension with $H_2O$ | 42.7 mN/m | 1000 $M_n$ fluid (*16*) |
| Critical surface tension | 22.7 mN/m | Grafted thin film (*17*) |
| Solid surface energy | 22.6 mJ/m$^2$ | JKR contact mechanics (*18*) |
| Water contact angle | 108 deg | Grafted thin film (*17*) |
| Surface shear viscosity | < 10 μg/s | High MW (*10*)$^7$ fluid (*10*) |

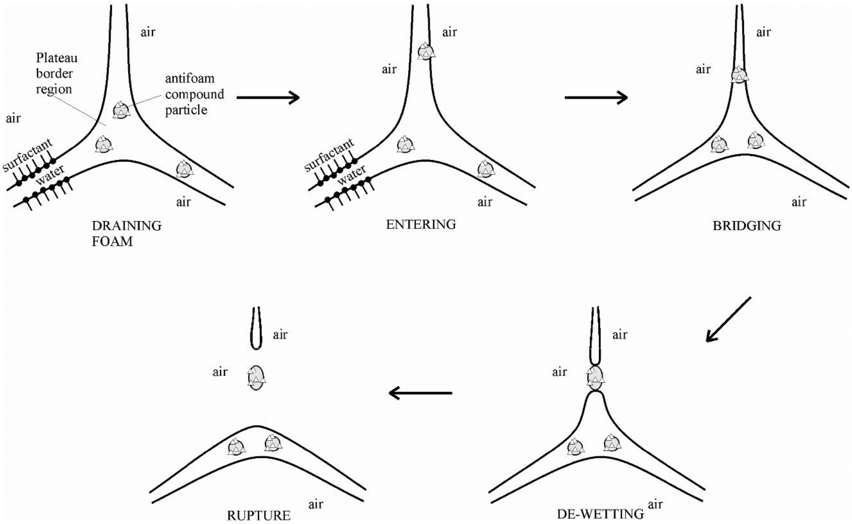
air
Plateau border region
antifoam compound particle
air
surfactant
water
air
DRAINING FOAM
air
air
surfactant
water
air
ENTERING
air
air
air
BRIDGING
air
air
air
RUPTURE
air
air
air
DE-WETTING

*Figure 1. Schematic of the processes by which an antifoam particle ruptures aqueous foam: a portion of a foam Plateau Border region, with an antifoam particle entering, bridging, dewetting and rupturing (from Ref. (8)).*

Where $\sigma_f$ is the surface tension of the foaming medium, $\sigma_a$ is that of the antifoam, and $\sigma_{af}$ is the interfacial tension between them. Entering is thermodynamically favorable when E is positive, thus the smaller the value of $\sigma_a$ the more likely it is that entering will occur of droplets of that antifoam into the foam films that they are there to destroy.

For complete replacement of a stabilizing layer to occur, spreading as well as entering should ensue. The spreading coefficient, S, is given by:

$$\mathbf{S = \sigma_f - \sigma_{af} - \sigma_a} \tag{ii}$$

These seem to be simple, useful equations. Nevertheless, they must be applied cautiously as they are based on the assumption of thermodynamic equilibrium. Hill and Fey (*8*) remind us that real systems are almost always so far from equilibrium that E and S are not very predictive of actual performance. They conclude that it is a necessary but not sufficient condition that E be positive for defoaming to occur. However, in all cases where spreading coefficients have been measured, no correlation has been found between the magnitude of the spreading coefficient and the ability to rupture foam

The displacement of the foam stabilizer and the mechanical disruption caused by these processes adequately explain the mode of action of defoamers consisting only of insoluble oils such as silicones used in crude oil foam control. Callaghan (*12*) has shown that the ability of PDMS to spread at oil foam film-air interfaces is crucial in this application. On the other hand, other studies indicate that spreading may occur in aqueous systems but it is not essential to film rupture (*19*, *20*). We have noted earlier in this chapter that blends of dispersed, hydrophobic solids are usually needed to control the more aggressive foaming encountered in aqueous systems. It is in such cases that the other components of the foam collapse process, bridging and dewetting, become important.

As an antifoam particle in a foam film approaches the air interface, an unsymmetrical three-phase thin film forms consisting of an aqueous layer bounded on one side by the antifoam particle and on the other by the air phase. This film is known as a psuedoemulsion film (*21*). It is shown schematically in Figure 2, taken from the work of Hill and Fey (*8*). This pseudoemulsion film has a high stability in strongly foaming aqueous systems and it is the presence of the hydrophobic particles in the oil drops that effectively destabilizes the pseudoemulsion film.

Once an antifoam compound droplet or hydrophobic silica particle has entered into a foam lamella, it can then bridge the film and occupy both of its surfaces if it is large enough. Subsequent dewetting of the particle by both sides of the film can then cause rapid collapse of the film. In this bridged situation, if the contact angle is large enough, a capillary pressure drop that pushes liquid away from the particle is developed (*22*). This flow results in migration of the air-liquid-solid interfaces towards each other until they meet and the film ruptures as it pinches off the particle. It may also be that the mechanical shock of this event can further help reduce foam stability. For complete dewetting to occur, the contact angle θ should expectedly be greater than 90°. This has been shown to be so for silicone-treated silica in hydrocarbon oil (*23*). However, for non-spherical particles dewetting may occur at contact angles less than 90° (*19*).

If particles must bridge foam films to rupture then we should anticipate a correlation between film thickness and antifoam particle size. In actuality, typical silicone antifoam particles are in the 5 to 40 μm range, significantly larger than foam film thicknesses which are usually in the 0.01 to 1 μm range (*8*). It may be that it is the dispersed particle size and not the antifoam compound droplet size that needs to correlate. It has also been suggested that the antifoam compound droplets reside mainly in the thicker Plateau borders between the foam lamellae. Koczo et al. (*24*) have shown that the tendency for particles to become trapped in the Plateau border regions strongly increases with increasing particle size. It has also been suggested that the emulsifier surfactants needed to prepare defoamer emulsions are active in the transport process of the hydrophobic silica to the oil/water interface

Downloaded by PENNSYLVANIA STATE UNIV on June 23, 2012 | http://pubs.acs.org
Publication Date (Web): November 9, 2010 | doi: 10.1021/bk-2010-1051.ch020

(*25*). This study also notes that removal of excess silicone oil from the emulsion lowers defoaming performance.

Clearly, the last word on antifoaming mechanisms has yet to be written. Debate continues about the detailed mechanism of antifoaming by these synergistic combinations of insoluble oil and hydrophobic solids. In Hill and Fey's words (*8*), "it is a complex problem that often seems needlessly obscure to technologists unfamiliar with the field". It is hoped that this preceding discussion has outlined the main aspects of current antifoam mechanism theory and clarified the differences between controlling foam in aqueous and non-aqueous systems.

Downloaded by PENNSYLVANIA STATE UNIV on June 23, 2012 | http://pubs.acs.org
Publication Date (Web): November 9, 2010 | doi: 10.1021/bk-2010-1051.ch020

## Applications

A wide range of industries utilize antifoam products either as process aids to improve the efficiency of a given process or to increase the quality or performance of products when they are subsequently used. Such additives are the largest single category of process aids used in the chemical industry (*26*). Operations such as distillation, pumping and agitation are commonplace in many chemical processes. Even though chemical engineers ingeniously contrive to minimize these difficulties by optimal design it is still often necessary to use antifoam products. Familiar examples of the enhanced product category include antacid tablets that destroy uncomfortable foam production while neutralizing the stomach acid causing the discomfort, detergents that do not foam excessively in washing machines, and paints that coat without problematic foaming during enthusiastic application. These are familiar examples in the sense that the final consumer of the product experiences their benefit but not so familiar in the sense that most consumers of at least the last two aforementioned instances are probably unaware of the inclusion of defoamers in the product formulation. The antacid application exploits another asset of PDMS, its essentially non-toxic nature. Under the name *Simethicone* its use as a drug ingredient is regulated by the FDA. Simethicone's inertness also permits it to be used in processing of foodstuffs and beverages, including sugar beet, potato products, wine and beer. Polydimethylsiloxane fluids used in aqueous processes pose no threat to wastewater treatment nor to the environment. Indeed, silicone antifoams are used to control foam during sewage treatment. The ultimate fate of such silicones, be it incineration or incorporation of sludge-associated PDMS into soils and landfills, will be conversion to silica, water and carbon dioxide (*27*).

With the multitude of antifoam types and products available, very few industries are solely reliant on only silicone defoamers. Oil and petrochemical processing is one such example because polyether-based products are insufficiently surface active, hydrocarbon-based antifoams are too soluble, and fluoropolymer-based antifoams other than fluorosilicones are rare and relatively expensive. Naturally, technological logic is not the sole driver in determining if an antifoam is to be employed, nor what specific type should be selected.; factors such as traditional practice and cost considerations also play a part. For example, the metal working industry tolerated the foaming difficulties inherent in the use of oil emulsions as cutting oils and coolants for many years. However, more recently

Downloaded by PENNSYLVANIA STATE UNIV on June 23, 2012 | http://pubs.acs.org
Publication Date (Web): November 9, 2010 | doi: 10.1021/bk-2010-1051.ch020

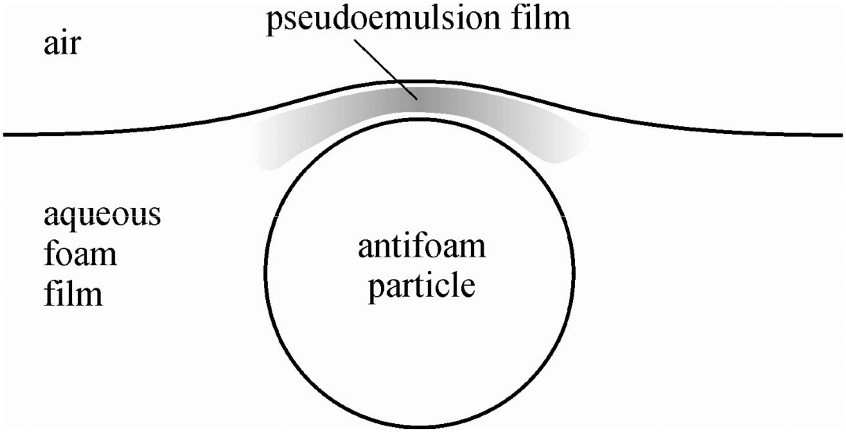

*Figure 2. An asymmetric thin film of water between oil and air called a psuedoemulsion film (From Ref. (8)).*

defoamers such as formulated silicones, dispersions of fatty amides in mineral oils, and calcium soaps have been introduced. With regard to cost it is important to bear in mind that it is not the unit cost of an antifoam that matters but the cost per application or unit of production. A relatively expensive formulated silicone antifoam can often be effectively used at such lower application levels than an inexpensive hydrocarbon oil based material that the former product becomes the cost effective choice.

**List 1.** Examples of Industries that use antifoams include:

- Agricultural chemicals
- Adhesives and sealants
- Chemical processing
- Coatings, paints and inks
- Construction
- Detergents and other cleaning compounds
- Fermentation processes
- Food and beverages
- Leather
- Medical products
- Metal working
- Oil and petrochemicals
- Pulp and paper production
- Textiles
- Wastewater treatment

PDMS-based antifoams are likely to be most useful in aqueous systems where concentrated solutions of efficient organic surfactants are used and also in hydrocarbon and other non-aqueous systems. Less efficient aqueous surfactants may be readily defoamed by less surface-active antifoams based on polyethers and hydrocarbons. An example of an aqueous system that utilizes high concentrations of powerful organic surfactants is in controlled foam detergents; non-aqueous systems where silicones are useful include chemical and petrochemical processing. Another advantage, the high thermal stability of PDMS, also comes into play in elevated temperature processes, such as distillation.

Soluble Antifoams are not strictly an application but this apparently contradictory class of materials is conveniently discussed at this point. The requirement that the active antifoam component be insoluble in the foaming medium has been adequately stressed in this chapter so it might seem surprising that there is a class of so-called *soluble antifoams*. This is somewhat of a misnomer as what is usually implied is a material that is soluble and readily dispersible under one set of conditions but becomes insoluble when these conditions change. Typically, use is made of the cloud-point phenomenon displayed by nonionic surfactants such as those based on poly(ethylene oxide) [PEO]. As the temperature is raised hydrogen bonding interactions that solubilize the hydrophilic PEO segment are weakened and the surfactant becomes insoluble at what is known as the cloud point. For applications as diverse as jet dying of textiles, automatic dish washing, and processing of sugar beet where the foaming problems are troublesome only at elevated temperatures, this phenomenon offers a ready convenience of introducing the defoamer. Silicone-glycol copolymers are often used in this way. They are also useful in lower temperature applications where the pure PDMS material might be too soluble. The use of silicone-glycol defoamers in diesel fuel is a case in point. Such silicone-glycols are an interesting class of surfactants that can strongly affect both the surface and interfacial tensions in the systems in which they are incorporated. Important secondary benefits such as improved wetting of substrates can result, hence their significant use in paints and coatings.

For systems that rely solely on an optimum Marangoni elasticity for their foam stability, it would be possible in principle to destabilize the foam by adding a soluble surfactant that migrated too rapidly to the surface. If it were intrinsically more surface-active than the pro-foaming surfactant this would prevent the latter from adsorbing at the surface and stabilizing the foam. Such small, highly mobile, surface-active species will be uncommon but could explain some otherwise puzzling instances where soluble agents appear effective. There has been a little interest in the patent literature but no evidence of significant commercialization of this concept. Note also that Ross's second mechanism of mixed surface layer formation (*13*) can also account for such soluble antifoaming instances.

## Future Trends

Any trend that promotes convenience to the user is likely to persist. In this context, the move to incorporation of the antifoam in the product package rather than as a later, separate processing step will doubtless continue. Such is already the case in the leather processing, detergent, and coatings areas.

Although the mode of action of antifoams seems to require separation of the synergistic combination of low surface energy fluid and dispersed, hydrophobic

Downloaded by PENNSYLVANIA STATE UNIV on June 23, 2012 | http://pubs.acs.org
Publication Date (Web): November 9, 2010 | doi: 10.1021/bk-2010-1051.ch020

solid, better control of this process will lead to improved products. One can readily envisage blends where a rapidly separating oil/solid combination would provide instant effectiveness while a much more cohesive partnership would confer longevity of action. Increasing the oil viscosity, incorporating fumed silica to build the viscosity of the mixture, and using branched or cross-linked silicone fluids are all documented ways of achieving this latter objective (*8*). Other novel branched polymer architectures such as star polymers, dendrimers and other hyperbranched materials may play a part in future antifoam development.

No major dislocations in usage of antifoams are foreseen. This is a mature application area with growth in one sector likely to be offset by improvements in efficiency in another. For instance, there may be a societal trend away from the use of animal products that could lead to a decline in leather production but it is very probable that the vegetable or synthetic alternatives will create new foaming challenges for the antifoam technologist. Similarly, even if we choose to stop burning dwindling oil stocks as fuels it will only be to increase their use as petrochemical feed-stocks. The processing of these will still require use of antifoams. The more likely trend is an expansion of tertiary oil recovery technologies, most of which involve surfactant usages that are likely to increase the need for foam control during extraction and subsequent refining.

Considering the major silicone antifoam use categories, their need in pulp and paper production, oil and chemical processing, and detergent foam control may fluctuate but is unlikely to disappear. Electronic databases, personal computers and e-mail seem not to have produced the paperless office forecast so confidently just a few years ago. A future with no cleaning of garments might be superficially appealing but such an extreme dislocation is not probable. However, continuing developments in fabric treatments that make for easier cleaning are quite conceivable and this may prove to be one of the applications where antifoam usage does eventually decline should population growth fail to compensate.

One trend, which is exemplified by the controlled foam detergents, is to incorporate the defoamer in other processing aids prior to use rather than adding it separately during processing. The leather processing industry is another example of this trend. Almost every stage from initial rawhide preparation through tanning and dyeing has the potential for foaming difficulties as many of these preparative steps incorporate surfactant emulsifiers and dispersants. Rather than deal with numerous optimized defoamers at each step the trend is to formulate the defoamer into each of the treatment products.

What might replace silicones as a major antifoam component? It is unlikely to be a material of higher surface energy as these would have more limited applicability. Even if some new fluid of similar surface energy were to become available it would likely have difficulties displacing silicones now that PDMS is a relatively inexpensive commodity material. Materials that are fluid and of lower surface energy are not common. The only entities known that produce lower surface energy polymers than PDMS are those based on aliphatic fluorocarbon groups such as $CF_3(CF_2)_n$-. Fluorine is bulkier than hydrogen and fluoropolymers tend to have higher glass transition temperatures and to form solids.

Only fluoropolymers with flexible backbones such as siloxane and polyether are realistic potential candidates for PDMS replacement. Most polymers become

Downloaded by PENNSYLVANIA STATE UNIV on June 23, 2012 | http://pubs.acs.org
Publication Date (Web): November 9, 2010 | doi: 10.1021/bk-2010-1051.ch020

solid at relatively low MW ; consider that *n*-hexadecane is the longest alkane that is liquid at room temperature. PDMS is unique in its ability to retain its liquid nature to very high MW. This is because of the combination of low intermolecular forces between the methyl groups and the highly flexible nature of the backbone. Fluorocarbon materials have the former characteristic but rarely the latter. Part of the explanation for PDMS flexibility lies in the unsubstituted oxygen in the backbone providing a sort of “flexibilizing” linkage. This is also evident in the polyether structure, explaining why methyl-substituted polyethers such as poly(propylene oxide) also are liquids, although poly(ethylene oxides) are solids.

The extension of these ideas to fluoropolymers suggests that potential antifoam candidates additional to fluorosilicones will be fluoroethers such as poly(perfluoropropylene oxide). Fluorosilicones are already used in niche applications where their relatively high cost is justified by the necessity of their action and the absence of any effective alternatives. It remains to be seen if fluoroethers will compete significantly with fluorosilicones. Certainly, as the field of application of silicone surfactants expands one can anticipate a growing need for foam controllers of this type. A future where fluoropolymer antifoams do for silicone surfactants what silicone defoamers have done for organic surfactants has already begun.

Downloaded by PENNSYLVANIA STATE UNIV on June 23, 2012 | http://pubs.acs.org
Publication Date (Web): November 9, 2010 | doi: 10.1021/bk-2010-1051.ch020

## References

1. Boylan, F. J. Defoamer Composition for Aqueous Systems. Hercules Powder Co. U.S. Patent 3,076,768, February 5, 1963.
2. Currie, C. C.; Hommel, M. C. Antifoam Emulsion. Dow Corning Corporation. U.S. Patent 2,595,928, May 6, 1952.
3. Owen, M. J. Defoamers. In *Kirk-Othmer Encyclopedia of Chemical Technology*, 5th ed.; John Wiley & Sons, Inc.: Hoboken, NJ, 2004; Vol. 8, p 236.
4. Hunter, M. J.; Warrick, E. L.; Hyde, J. F.; Currie, C. C. Organosilicon polymers. II. The open chain dimethylsiloxanes with trimethylsiloxy end groups. *J. Am. Chem. Soc.* **1946**, *68*, 2284–90.
5. Stones, M.; Easton, T. Microfoam elimination from waterborne inks. *Pitture Vernici, Eur. Coat.* **2000**, *76* (3), 69–76.
6. Fendinger, N. J.; Lehmann, R. G.; Mihaich, E. M. Polydimethylsiloxane. In *The Handbook of Environmental Chemistry*; Chandra, G. C., Ed.; Springer-Verlag: New York, 1997; Vol. 3H, Organosilicon Materials, pp 181−223.
7. Varaprath, S.; Frye, C. L.; Hamelink, J. L. Aqueous stability of permethylsiloxanes (silicones). *Environ. Toxicol. Chem.* **1996**, *15*, 1263–1265.
8. Hill, R. M.; Fey, K. C. Silicone Polymers for Foam Control. In *Silicone Surfactants, Surfactant Science Series*; Hill, R. M., Ed.; Marcel Dekker: New York, 1999; Vol. 86, pp 159−180.
9. Bluestein, B. A.; Sober H. F. Liquid Hydrocarbon Jet Fuels Containing Poly(cyanoalkyl-siloxanes) as Foam Depressors. General Electric Co. U.S. Patent 2,992,083, July 11, 1961.

10. Jarvis, N. L. Surface viscosity of polydimethylsiloxane monolayers. *J. Phys. Chem.* **1966**, *70*, 3027–3033.
11. Currie, C. C. Dow Corning Corporation. U.S. Patent 2,632,736, August 22, 1946.
12. Callaghan, I. C. Antifoams for Nonaqueous Systems in the Oil Industry. In *Defoaming: Theory and Industrial Applications, Surfactant Science Series*; Garrett, P. R., Ed.; Marcel Dekker: New York, 1993; Vol. 45, pp 119−150.
13. Ross, S. J. The Inhibition of Foaming; Bulletin No. 63; Rensselaer Polytechnic Institute: Troy, NY, 1950.
14. Everett, D. H. *Basic Principles of Colloid Science*; Royal Society of Chemistry: London, 1988.
15. LeGrand, D. G.; Gaines, G. L., Jr. Molecular weight dependence of polymer surface tension. *J. Colloid Interface Sci.* **1969**, *31*, 162–167.
16. Kanellopolous, A. G.; Owen, M. J. Adsorption of sodium dodecyl sulphate at the silicone fluid/water interface. *Trans. Faraday Soc.* **1971**, *67*, 3127–3138.
17. She, H.; Chaudhury, M. K.; Owen, M. J. Surface Properties of Thin Film Polydimethylsiloxane. In *Silicones and Silicone-Modified Materials*; Clarson, S. J., Fitzgerald, J. J., Owen, M. J., Smith, S. D., Eds.; ACS Symposium Series 729; American Chemical Society: Washington, DC, 2000; pp 322−331.
18. Chaudhury, M. K. Surface free energies of alkylsiloxane monolayers supported on elastomeric polydimethylsiloxanes. *J. Adhes. Sci. Technol.* **1993**, *7*, 669–675.
19. Garrett, P. R. The Mode of Action of Antifoams. In *Defoaming: Theory and Industrial Applications, Surfactant Science Series*; Garrett, P. R., Ed.; Marcel Dekker: New York, 1993; Vol. 45, pp 1−117.
20. Koczo, K.; Koczone, J. K.; Wasan, D. T. Mechanisms of antifoaming action in aqueous systems by hydrophobic particles and insoluble liquids. *J. Colloid Interface Sci.* **1994**, *166*, 225–238.
21. Wasan, D. T.; Koczo, K.; Nikolov, A. D. Mechanisms of Aqueous Foam Stability and Antifoaming Action with and without Oil: A Thin Film Approach. In *Foams: Fundamentals and Applications in the Petroleum Industry*; Schramm, L. L., Ed.; Advances in Chemistry Series 242; American Chemical Society: Washington, DC, 1994; pp 47−114.
22. Frye, G. C.; Berg, J. C. Antifoam action by solid particles. *J. Colloid Interface Sci.* **1989**, *127*, 222–238.
23. Lichtman, I. A.; Sinka, V. S.; Evans, D. W. *Asoc. Mex. Tec. Ind. Celul. Pap. [Bol.]* **1975**, *15*, 26.
24. Koczo, K.; Lobo, L. A.; Wasan, D. T. Effect of oil on foam stability in aqueous foams stabilized by emulsions. *J. Colloid Interface Sci.* **1992**, *150*, 492–506.
25. Wang, G.; Pelton, R.; Hrymak, A.; Shawafaty, N.; Heng, Y. M. On the role of hydrophobic particles and surfactants in defoaming. *Langmuir* **1999**, *15*, 2202–2208.
26. Bryon, K. J. Defoaming agents. *Crit. Rep. Appl. Chem.* **1990**, *30*, 133–161.
27. Frye, C. L. The environmental fate and ecological impact of organosilicon materials: A review. *Sci. Total Environ.* **1988**, *73* (1−2), 17–22.

Downloaded by PENNSYLVANIA STATE UNIV on June 23, 2012 | http://pubs.acs.org
Publication Date (Web): November 9, 2010 | doi: 10.1021/bk-2010-1051.ch020

# Subject Index

**A**

Acoustic wave traveling, 89*f*
Acrylates, 246*f*
Acrylic adhesive, 105*t*
Adhesion promoter, 183
Alumina
  silica adhesion, 187, 188*f*
  TPP adhesion, 189
Amberlyst-15, 30
Angular selectivity and holographic gratings, 254, 255*f*, 257*f*
Antifoam
  applications, 278
  components
    emulsions, 272
    formulation variables, 273
    hydrophobic solids, 272
    silicone fluids, 271
  mechanism, 274
  particle ruptures aqueous foam, 276*f*
  PDMS, 14, 276*t*
Architectural coatings and PDMS, 16
Aspartic acid, 53*f*

**B**

Biocatalytic routes to silicone, 8
Bioinspired silica, 8
Biomedical grade silica-filled PDMS elastomer, 93*t*
Biosilica, 8
BIS. *See* N,N′-methylenebisacrylamide
1,3-Bis[2-(1,2-epoxycyclohex-4-yl)ethyl]-1,1,3,3,5,5-hexamethyltrisiloxane, 246*f*
1,3-Bis[2-(1,2-epoxycyclohex-4-yl)ethyl]-1,1,3,3-tetramethyldisiloxane, 246*f*
1,3-Bis(glycidoxypropyl)-1,1,3,3,5,5-hexamethyltrisiloxane, 246*f*
1,3-Bis(3-glycidoxypropyl)-1,1,3,3-tetramethyldisiloxane, 246*f*
Bisphenol-A diglycidyl ether, 246*f*
Block copolymer
  PDHS and PDMS, 34*f*, 36*f*, 38*f*
  PDHS and PDPS, 40*f*, 42*f*
  synthesis, 30, 32*s*
Bound PDMS polymer interfacial layer and silica filler, 81*f*
Bovine pancreatic trypsin and its catalytic triad, 53*f*

**C**

Cellulose propionate, 216*f*
C-H··π interactions, 22*f*
Contact lens materials and PDMS, 17
Copolymer of polydicyclohexylsiloxane, 33*f*
Cross-linked silicone
  elastomers, 50
  formulation, 49, 50*t*
  TEOS, TES-PDMS$_{580}$, and trypsin, 51*f*
  TEOS, TES-PDMS$_{24000}$, and trypsin, 51*f*
  TES-PDMS$_{580}$, TEOS, and dibutyltin dilaurate, 51*f*
Cyclic oligomer
  ROP, 32*s*
  synthesis
    dichlorosilanes, hydrolytic condensation, 32*s*
    PDHS, 29
    PDPS, 29
Cycloaliphatic siloxanes copolymers, 27

**D**

DCF. *See* Drop cast films
Dendrimers
  Poly{*tris*-(γ-trifluoropropyl)siloxy}carbosilane (G-7.5(F)), 117
  Poly{*tris*-(γ-trifluoropropyl)siloxy}carbosilane with cyclic siloxane fragments (G-7.5(F, Si-O-Si)), 117
  physical network, 132*f*
Dibutyltin dilaurate cross-linked silicone elastomer, 52*f*
Dichlorosilanes, 32*s*
Diffraction efficiency, 250*f*
3,3-Dimethyl-1,1,1-tris(γ-trifluoropropyl)disiloxane, 113
Dipentaerythritol penta-/hexaacrylate, 246*f*
DPHA. *See* Dipentaerythritol penta-/hexaacrylate
DPHA:NVP, gratings
  angular deviation, 253*f*
  real-time diffraction efficiency, 252*f*
Drop cast films, 206
  water contact angles

Downloaded by 89.163.35.42 on June 23, 2012 | http://pubs.acs.org
Publication Date (Web): November 9, 2010 | doi: 10.1021/bk-2010-1051.ix002

Downloaded by 89.163.35.42 on June 23, 2012 | http://pubs.acs.org
Publication Date (Web): November 9, 2010 | doi: 10.1021/bk-2010-1051.ix002

**E**

Engineering silicone, network structure, 78*f*
Enzymatic synthesis
  siloxane copolyamides, 159
  siloxane copolyesters, 160*s*
Etching of silicone elastomers, 147

**F**

Fabrication of holographic gratings, 243
Filled silicone materials
  filled and unfilled systems, 82*f*
  MD simulations, 83*t*
  structural perturbations, 80*f*
Flame retardant applications and novel organo-siloxane copolymers, 157
Fluorinated POSS and 6F PFCB polymer, 198, 200*f*
Fluorine-containing dendrimers, 127*t*
Fluorine-containing derivatives
  $-[MeSiViO]_n-$, with PDMS, 130*f*
  polybutadiene, 118*s*, 126*t*
  polycarbosilanes, 120*s*, 126*t*
  polymethylvinylsiloxane, 120*s*, 126*t*
Fluorine-containing hyperbranched polymethyldiallylsilane, 116
  compression isotherm at air-water interface, 129*f*
  GPC trace, 121*f*
  $^1$H NMR spectrum, 121*f*
  reorganization, 127*s*
  TGA curves, 124*f*
Fluorine-containing hyperbranched polymethyldiundecenylsilane, 116, 130*f*
Fluorine-containing organosilicon polymers, 111
  glass transition temperature, 122*t*
Fluoroderivative of polybutadiene with 50% substitution of double bonds, 114
  compression isotherm at air-water interface, 129*f*
  $^1$H NMR spectrum, 118*f*
  synthesis, 118*s*
  TGA curves, 123*f*
Fluoroderivative of polybutadiene with 100% substitution of double bonds, 114
  GPC trace, 119*f*
  $^1$H NMR spectrum, 119*f*
  synthesis, 118*s*
  TGA curves, 123*f*
Fluoroderivatives
  polymethylvinylsiloxane, 120*f*
  synthesis, 118*s*
Fluoropolymer
  glass transition temperatures, 105*t*
  surface properties, 103*t*
Fluorosilicones, 99
  applications, 102
  characteristics, 100
  properties, 102
Foam control, 269, 274
Fox equation and glass transition temperature, 43*t*
F-PB-50. *See* Fluoroderivative of polybutadiene with 50% substitution of double bonds
F-PB-100. *See* Fluoroderivative of polybutadiene with 100% substitution of double bonds
F-PMDAS. *See* Fluorine-containing hyperbranched polymethyldiallylsilane
F-PMDUS. *See* Fluorine-containing hyperbranched polymethyldiundecenylsilane

**G**

Glass transition temperature ($T_g$)
  block copolymers, 42*f*
  fluorine-containing organosilicon polymers, 122*t*
  fluoropolymer, 105*t*
  Fox equation, 43*t*
  homopolymers, 42*f*
  PDPS, 42*f*
  random copolymers of PDHS, 42*f*

**H**

Heat release capacity of siloxane copolyimides, 163*t*
Hexamethylenetetramine, 159
  siloxane copolyamide, 162, 163*t*
High voltage insulation and PDMS, 17
Histidine, 53*f*
  and silicic acid, 54*f*
HMTA. *See* Hexamethylenetetramine
$^1$H multiple quantum nuclear magnetic resonance, 75
  multicomponent silicone materials, 78
  PDMS networks, 79*f*
  probability distributions conversion, 79*f*
$^1$H NMR spectrum
  block copolymer of PDHS and PDMS, 34*f*

Downloaded by 89.163.35.42 on June 23, 2012 | http://pubs.acs.org
Publication Date (Web): November 9, 2010 | doi: 10.1021/bk-2010-1051.ix002

  F-PB-50, 118*f*
  F-PB-100, 119*f*
  F-PMDAS, 121*f*
  PDHS homopolymers, 34*f*
  polymethylvinylsiloxane fluoroderivatives, 120*f*
  random copolymer of PDHS and PDMS, 34*f*
  siloxane copolyamide with HMTA, crosslinked products, 162*f*
Holographic gratings
  angular deviation, 253*f*
  angular selectivity, 254, 257*f*
  diffraction efficiency, 250*f*
  fabrication, 243
  formation process, 260
  FTIR spectra, 260
  morphology, 250, 255*f*, 264*f*
  photo-DSC analysis, 260, 261*f*, 262*f*
  photo-polymerization of SOE, 255
  real-time diffraction efficiency, 252*f*, 253*f*, 256*f*, 258*f*, 259*f*, 260*f*, 262*f*
  setup, 249*f*
  silicon-oxygen bonds, 243
  volume shrinkage, 251*f*
Holographic polymer dispersed liquid crystal and siloxane network formation, 257
Homopolymers
  di substituted dichlorosilane condensation, 32*s*
  PDHS, 30, 33*f*, 34*f*, 36*f*, 38*f*, 40*f*, 42*f*
  PDMS, 30
  PDPS, 30, 40*f*, 42*f*
  silicone, 5
  synthesis, 30, 32*s*
HPDLC. *See* Holographic polymer dispersed liquid crystal
Hydrophobic macrocrosslinker, chemical structure, 170*s*
Hyperbranched polymers
  F-PMDAS, 116
  F-PMDUS, 116
  PMDAS, 116
  PMDUS, 116

## I

Ion effects on trisilanolphenyl-POSS, 183
Ion exchange resin, activation, 30

## L

Langmuir trough data, 140*t*
Langmuir-Blodgett, 183
LB. *See* Langmuir-Blodgett
Linear polymers
  F-[MeSiViO]$_n$-5), 115
  F-[MeSiViO]$_n$-50), 115
  F-[MeSiViO]$_n$-100, 115
  F-PB-50, 114
  F-PB-100, 114
  -[MeSiViO]$_n$-), 115
  Polybutadiene (PB), 114

## M

Magnetic nanoparticles, 60
Magnetite magnetic nanoparticle complexes, 59
MDd. *See* Molecular dynamics
-[MeSiViO]$_n$-. *See* Polymethylvinylsiloxane
ω-Methacryloxyalkyltrialkoxysilanes, 259, 260*f*, 262*f*
Methacryloxymethyltrimethoxysilane, 248*f*
Methacryloxymethyltrimethxysilane, 248*f*
3-Methacryloxypropyltriethoxysilane, 248*f*, 262*f*
3-Methacryloxypropyltrimethoxysilane, 248*f*
MFA:NVP:E, gratings
  DPHA, 255*f*
  real-time diffraction efficiency, 253*f*
  TMPTA, 255*f*
  TPGDA, 255*f*
MH-TEOS. *See* 3-*N*-(3-Methacryloxy-2-hydroxypropyl)aminopropyltriethoxysilane
MM-TMOS. *See* Methacryloxymethyltrimethoxysilane
MM-TMS. *See* Methacryloxymethyltrimethxysilane
MM-TMS:NVP, gratings, 258*f*
MNP. *See* Magnetic nanoparticles
Molecular dynamics, 75, 83*t*
Mounted ultrasonic transducer and permeation cell, 91*f*
MPTA:MU-TEOS:NVP, gratings, 261*f*
MP-TEOS. *See* 3-Methacryloxypropyltriethoxysilane
MP-TMOS. *See* 3-Methacryloxypropyltrimethoxysilane

MQ-NMR. *See* $^1$H multiple quantum nuclear magnetic resonance
Multicomponent silicone materials, MQ NMR characterization, 78
MU-TEOS. *See* 3-*N*-(2-Methacryloxyethoxycarbonyl)aminopropyltriethoxysilane
$M_w$ and intrinsic viscosity
  fluorine-containing dendrimers, 127*t*
  polybutadiene, 126*t*
  polycarbosilanes, 126*t*
  polymethylvinylsiloxane, 126*t*

**N**

NIPAAm. *See* N-isopropylacrylamide
NIPAAm/BIS hydrogel
  compression modulus, 176*f*
  effective crosslinking density, 176*f*
  interaction parameter, 176*f*
  swelling ratio, 176*f*
NIPAAm/VTPDMS hydrogel
  compression modulus, 177*f*
  effective crosslinking density, 177*f*
  interaction parameter, 177*f*
  swelling ratio, 177*f*
N-isopropylacrylamide, 169
3-*N*-(2-Methacryloxyethoxycarbonyl)aminopropyltriethoxysilane, 248*f*, 262*f*
3-*N*-(3-Methacryloxy-2-hydroxypropyl)aminopropyltriethoxysilane, 248*f*
N,N′-methylenebisacrylamide, 168, 174*t*, 175*t*
Non-bonded interactions, 230
  silica formation, 229
    additives, 233
    electrostatic interactions, 233*f*, 235
    hydrogen bonding interactions, 233*f*, 236
    hydrophobic effect, 233*f*, 238
    structure control, 237*f*
Novel organo-siloxane copolymers, flame retardant applications, 157
NVP. *See* 1-Vinyl-2-pyrrolidone

**O**

Octaphenylcyclotetrasiloxane, polymorphs, 19, 21*f*, 23*f*, 24*f*
Organo-siloxane copolymers, 157
Oscilloscope and UTDR response, 92*f*

**P**

PALS. *See* Positron annihilation lifetime spectroscopy
PAMAMOS. *See* Poly(amidoamine-organosilicon)
PB. *See* Polybutadiene
PDHS. *See* Polydicyclohexyl siloxane
PDMS. *See* Polydimethylsiloxane
PDMS-MNP. *See* Polydimethylsiloxane stabilized magnetic nanoparticle complexes
PDPS. *See* Polydicyclopentyl siloxane
Pendant POSS PFCB copolymers
  film preparation and surface analysis, 206
  monomer synthesis, 199
  polymerization, 199
  properties, 205*t*
  random copolymer, 204*f*
Perfluorocyclobutyl aryl ether polymers, 195
Perfluoroethersiloxanes, 105
Permeation cell and mounted ultrasonic transducer, 91*f*
PET/POSS composite fibers, 214*f*
PFCB. *See* Perfluorocyclobutyl
Phenoxy resin, 218*f*
Phenoxy resin/POSS blends
  C-C FTIR stretches, 220*f*
  DMA traces, 220*f*
  DSC traces, 219*f*
  fluorescence spectra, 221*f*
  hydroxyl group shift, 222*f*
Phenyl trisilanol, 218*f*
Phenyltrimethoxysilane, biocatalyzed hydrolysis, 54*f*, 55*f*
Photo-DSC analysis, grating formation, 260, 262*f*
Photo-polymerization of SOE and holographic gratings, 255
Physical vapor deposition, 186
  alumina coating
    hydrophilic silica coated wafer, 188*f*
    TPP, 189*f*
  apparatus, 187*f*
PKFE. *See* Phenoxy resin
PMDUS. *See* Polymethyldiundecenylsilane
PMHS. *See* Polymethylhydrosiloxane
PNIPAAm. *See* Poly(N-isopropylacrylamide) hydrogels
Poly(amidoamine-organosilicon)
  applications, 141
    electronics and photonics, 142
    protective and antifouling coatings, 143

Downloaded by 89.163.35.42 on June 23, 2012 | http://pubs.acs.org
Publication Date (Web): November 9, 2010 | doi: 10.1021/bk-2010-1051.ix002

Downloaded by 89.163.35.42 on June 23, 2012 | http://pubs.acs.org
Publication Date (Web): November 9, 2010 | doi: 10.1021/bk-2010-1051.ix002

    purification and decontamination, 144
    sensors, 143
  cross-linking, 137
  dendrimers, 135
  Langmuir trough data, 140*t*
  metal ions, complexation, 139
  network coated on substrate, 142*f*
  SANS data, 142*t*
  surface activity, 138
  synthesis, 137
  XPS data, 142*t*
Polybutadiene, 114
  fluorine-containing derivatives, 118*s*, 126*t*
Polycarbonate, 218*f*
Polycarbonate/POSS blends
  DMA traces, 219*f*
  DSC traces, 218*f*
  fluorescence spectra, 221*f*
Polycarbosilanes, fluorine-containing derivatives, 120*s*, 126*t*
Polydicyclohexylsiloxane, 29
  block copolymer, 34*f*, 38*f*
  copolymer, 33*f*
  homopolymer, 30, 33*f*, 34*f*, 36*f*, 38*f*
  PDPS
    block copolymers, 40*f*
    glass transition temperature, 42*f*
    homopolymers, 40*f*
    random copolymers, 40*f*
  random copolymer, 31, 34*f*, 38*f*
Polydicyclopentylsiloxane
  cyclic oligomer, 29
  homopolymers, synthesis, 30
  random copolymer with PDMS, 31
Polydimethylsiloxane, 59, 65*f*, 66*f*, 67*f*, 69*f*
  antifoams, 14
  applications, 13
    antifoams, 14
    architectural coatings, 16
    contact lens materials, 17
    high voltage insulation, 17
    release coatings, 16
    sealants, 16
    surfactants, 15
    water-repellent coatings, 15
  block copolymer, 34*f*
  elastomers, 150*f*
  ensembles, 81*f*
  homopolymers, synthesis, 30
  local density profile, 81*f*
  networks, fillers effect, 79*f*
  properties, 14, 18*t*
  random copolymer, 34*f*
    PDHS, 31
    PDPS, 31
  regimes, 71*f*
  stabilized magnetic nanoparticle complexes, 63*f*
  stabilizer, 65*f*, 66*f*, 67*f*, 69*f*
    molecular structure, 63*f*
    regimes, 71*f*
    surface viscoelastic parameters, 68
  surface property data, 276*t*
  surface viscoelastic parameters, 68
Polydimethylsiloxane stabilized magnetic nanoparticle complexes, 65*f*, 66*f*, 67*f*, 69*f*
  regimes, 71*f*
  surface viscoelastic parameters, 68
Polyhedral oligomeric silsesquioxanes, 7, 183, 195
  side-chain functionalization to derivatize, 215*f*
  thermal instability, 215*f*
Polymer matrixes, 117
Polymer/filler composint, 80*f*
Polymethyldiallylsilane, 116
Polymethyldiundecenylsilane, 116
Polymethylhydrosiloxane, 78*f*
Polymethylvinylsiloxane, 115
  fluorine-containing derivatives, 120*s*, 126*t*
  fluoroderivatives, 120*f*
  PDMS
    compression isotherms at air-water interface, 130*f*
    fluorine-containing derivatives, 130*f*
Polymorph I of octaphenylcyclotetrasiloxane
  IR spectra, 24*f*
  ORTEP, 21*f*
  weak interactions, 23*f*
Polymorph II of octaphenylcyclotetrasiloxane
  IR spectra, 24*f*
  ORTEP, 21*f*
  weak interactions, 23*f*
Polymorph III of octaphenylcyclotetrasiloxane
  IR spectra, 24*f*
  ORTEP, 21*f*
  synthesis, 20
  weak interactions, 23*f*
Polymorphs of octaphenylcyclotetrasiloxane, 19
  C-H··π interactions, 22*f*
  polymorph I, 21*f*
  polymorph II, 21*f*
  polymorph III, 21*f*
Poly(N-isopropylacrylamide) hydrogels, 167

Downloaded by 89.163.35.42 on June 23, 2012 | http://pubs.acs.org
Publication Date (Web): November 9, 2010 | doi: 10.1021/bk-2010-1051.ix002

  BIS and VTPDMS, crosslinked, 170, 174*t*, 175*t*
    compression stress-strain curves, 172*f*
    load vs. compression curves, 171*f*
Polystyrene and alumina with TPP, adhesion, 190, 190*f*, 191*f*
Poly{tris-(γ-trifluoropropyl)siloxy}carbosilane dendrimer, 117, 121*s*
  compression isotherm at air-water interface, 132*f*
  hydrodynamic radii, 128*t*
  TGA curves, 124*f*
Poly{tris-(γ-trifluoropropyl)siloxy}carbosilane dendrimer with cyclic siloxane fragments, 117, 122*s*
  compression isotherm at air-water interface, 131*f*
  hydrodynamic radii, 128*t*
Positron annihilation lifetime spectroscopy
  PC, 222*f*
  phenoxy resin, 222*f*
POSS. *See* Polyhedral oligomeric silsesquioxanes
POSS chain terminated PFCB copolymers
  degradation analysis, 202
  monomer synthesis, 199
  polymerization, 199
  preparation, 201*f*
  properties, 203*t*
  TFVE POSS monomers, 201*f*
  thermal properties, 202
POSS PFCB polymer blends, 198, 200*f*
  $FD_8T_8$ blended into poly5, 200*f*
  $FD_8T_8$ POSS poly5 blend, 200*f*
  virgin PFCB polymer poly5, 200*f*
  water and hexadecane static contact angle, 200*f*
POSS structures, 214*f*
POSS TFVE monomer 7
  $CDCl_3$, 204*f*
  conversion, 204*f*
POSS®/polymer composite, 211
Proposed matrix formation processes, 264*s*
Psuedoemulsion film, 279*f*
PVD. *See* Physical vapor deposition

## R

Radially layered poly(amidoamine-organosilicon) dendrimers, 135
Radically polymerizable multi-functional acrylates, 246*f*
Random copolymer
  PDHS, 34*f*
  PDHS and PDMS, 34*f*, 36*f*, 38*f*
  PDHS and PDPS, 40*f*, 42*f*
  PDMS, 34*f*
  PDMS with PDHS, 31
  PDMS with PDPS, 31
  synthesis, 32*s*
Random copolymer of PDMS with PDHS
RDC. *See* Residual dipolar couplings
Real-time diffraction efficiency
  DPHA:NVP:(A - E), 252*f*
  FA:NVP:E, 253*f*
  MM-TMS:NVP, 258*f*
  siloxane-containing bis(cyclohexene oxide), 251
  siloxane-containing bis(glycidyl ether)s, 251
  SOE:TMPTA:NVP, 256*f*
  S4SU and TMPTA ratio, 256*f*
  TMPTA:ω-methacryloxyalkyltrialkoxysilane:NVP, 260*f*, 262*f*
  TMPTA:MM-TMOS, 258*f*
  TMPTA:MM-TMOS:NVP, 259*f*
Release coatings and PDMS, 16
Residual dipolar couplings, 78*f*
Ring opening polymerization, 32*s*
  monomers, 246*f*
ROP. *See* Ring opening polymerization

## S

SANS. *See* Small angle neutron scattering
SCF. *See* Spin cast films
Sealants and PDMS, 16
Serine, 53*f*
Silica, 8
  alumina, adhesion, 187
  filled PDMS elastomer
    instantaneous compaction, 95*f*
    instantaneous compaction versus transmembrane pressure, 94*f*
    instantaneous compressive strain, 95*f*
    transmembrane pressure versus instantaneous strain, 94*f*
  filled PDMS system, 77*f*
  formation
    electrostatic effect, 233*f*
    hydrogen bonding, 233*f*
    hydrophobic effect, 233*f*
    non-bonded interactions, 229
  polymerisation, 232, 236*f*
Silica and alumina, adhesion, 188*f*
Silica filler and bound PDMS polymer interfacial layer, 81*f*
Silicic acid

- histidine addition, 54*f*
- serine addition, 55*f*

Silicification, additives, 237*f*

Silicon, 8

Silicone
- applications, 13
- architecture, 5
- biocatalytic routes, 8
- characterization, 75
- copolymers, 5
- elastomers, 6
- elastomers, etching, 147, 152*f*
  - surface erosion and THF, 153*f*
  - surface profiles, 151*f*
- engineered, 78*f*
- equilibrium polymerization, 149*f*
- fluids, 6
- gels, 6
- homopolymers, 5
- modified inorganic systems, 7
- modified organic systems, 7
- nomenclature, 4
- polymers, cross-linked, 49
- properties, 13
- resins, 7
- topology, 5

Silicon-oxygen bonds, holographic gratings, fabrication, 244

Siloxane bond, 3

Siloxane copolyamides
- crosslinking with HMTA, 162*f*
- enzymatic synthesis, 160*s*
- heat release capacity, 163*t*
- hexamethylenetetramine, 162*f*
- HMTA weight percent, 163*t*
- synthesis, 159, 161*s*
- thermogravimetric analysis, 164*f*

Siloxane copolyesters, enzymatic synthesis, 160*s*

Siloxane copolymers, 164*t*

Siloxane network formation, HPDLC grating fabrication, 257

Siloxane-containing bis(cyclohexene oxide), 251, 252*f*

Siloxane-containing bis(glycidyl ether), 251, 252

Si-O bond autocorrelation function, PDMS ensembles, 81*f*

Small angle neutron scattering, poly(amidoamine-organosilicon), 142*t*

Sodiumoxy-tris(γ-trifluoropropyl)silane, 113

SOE:TMPTA:NVP, grating, real-time diffraction efficiency, 256*f*

Spin cast films and water contact angles, 207*f*

Spiroorthoesters, 247*f*

S4SU and TMPTA, real-time diffraction efficiency, 256*f*

S4SU or S4EP and TMPTA, angular selectivity, 257*f*

Surface roughness, manipulation, 147

Surfactants and PDMS, 15

**T**

TEOS and TES-PDMS, trypsin-catalyzed cross-linking, 53*f*

TES-PDMS. *See* α,ω-(Triethoxysilyl)ethyl-polydimethylsiloxane

TFVE. *See* Trifluorovinyl aryl ethers

TFVE POSS monomers, 203*f*

TGA curves
- F-PB-50, 123*f*
- F-PB-100, 123*f*
- F-PMDAS, 124*f*
- G-7.5(F), 124*f*

TMPTA. *See* Trimethylolpropane triacrylate

TMPTA:ω-methacryloxyalkyltrialkoxysilane:NVP, 262*f*

TMPTA:ω-methacryloxyalkyltriethoxysilane:NVP, 262*f*

TMPTA:MM-TMOS, gratings, 258*f*

TMPTA:MM-TMOS:NVP, gratings, 259*f*

TMPTA:MU-TEOS:NVP, gratings, 264*f*

TMPTA:NVP:E, gratings, 255*f*

TPDA. *See* Tri(propylene glycol) diacrylate

TPP. *See* Trisilanolphenyl-POSS

α,ω-(Triethoxysilyl)ethyl-polydimethylsiloxane, 49

α,ω-Triethoxysilyl-terminated polydimethylsiloxane, trypsin-catalyzed cross-linking, 47

Trifluorovinyl aryl ethers, thermal [2+2] cyclopolymerization, 197*f*

Tri(methoxysilyl)-(meth)acrylates, 248*f*

Trimethylolpropane triacrylate, 246*f*

Tri(methylsilyl)-(meth)acrylates, 248*f*

Tri(propylene glycol) diacrylate, 246*f*

Trisilanolphenyl-POSS, 184*f*
- alumina, adhesion, 188*f*, 189*f*, 190*f*
- ion effects, 183
- multilayer films, 184*f*

Trypsin
- catalyst system, 49
- catalytic triad, 53*f*
- catalyzed cross-linking

Downloaded by 89.163.35.42 on June 23, 2012 | http://pubs.acs.org
Publication Date (Web): November 9, 2010 | doi: 10.1021/bk-2010-1051.ix002

    TEOS and TES-PDMS, 53*f*
    α,ω-triethoxysilyl-terminated polydimethylsiloxane, 47
  cross-linked silicone elastomer, 52*f*
Trypsin theozyme, 55*f*
  histidine and silicic acid, 54*f*

**U**

Ultrasonic time-domain reflectometry, 88
  and oscilloscope, 92*f*
  permeation process flow loop, 90*f*
UTDR. *See* Ultrasonic time-domain reflectometry

**V**

Vinyl terminated poly(dimethyl siloxane), 168, 174*t*, 175*t*
1-Vinyl-2-pyrrolidone, 246*f*
Volume shrinkage and holographic gratings, 251*f*, 252
VTPDMS. *See* Vinyl terminated poly(dimethyl siloxane)

**W**

Water contact angles
  drop cast films, 207*f*
  POSS PFCB polymer films, 207*t*
  spin cast films, 207*f*
Water-repellent coatings and PDMS, 15

**X**

XPS. *See* X-ray photoelectron spectroscopy
X-ray photoelectron spectroscopy, PAMAMOS dendrimers, 142*t*

Downloaded by 89.163.35.42 on June 23, 2012 | http://pubs.acs.org
Publication Date (Web): November 9, 2010 | doi: 10.1021/bk-2010-1051.ix002